# Study the role of ASIC3 ion channels in pain hypersensitivities associated with the consumption of lipid rich diet

Ahmed Negm

UNIVERSITÉ CÔTE D'AZUR

ÉCOLE DOCTORALE
SCIENCES DE LA VIE ET DE LA SANTÉ

# THÈSE DE DOCTORAT

## Étude du rôle des canaux ASIC3 dans l'hypersensibilité à la douleur associée à une alimentation riche en lipides.


**Ahmed NEGM**

INSTITUT DE PHARMACOLOGIE MOLECULAIRE ET CELLULAIRE


**Présentée en vue de l'obtention du grade de docteur en** Sciences de la Vie **d'**Université Côte d'Azur

**Dirigée par:** Prof. Jacques NOËL
**Co-dirigée par:** Dr. Carole ROVERE

**Soutenue le:** 12 Juillet 2019

**Devant le jury, composé de :**
Laurent COUNILLON,
*Prof, Université de Nice Sophia Antipolis.*
Emmanuel BOURINET,
*Dr, Université de Montpellier.*
Marc LANDRY,
*Prof, Université de Bordeaux.*
Peter McNAUGHTON,
*Prof, King's College London.*
Jacques NOËL,
*Prof, Université de Nice.*
Carole ROVERE,
*Dr, Université de Nice.*

cnrs

ipmc

LABEX ICST
ION CHANNEL SCIENCE AND THERAPEUTICS

**University Côte d'Azur - URF Sciences**

**Doctoral School of Life and Health Sciences**

# THESE

Submitted to obtain the degree of

## Doctor of Philosophy in Science

By university of Côte d'Azur

Specialty: Molecular and Cellular Interactions

Presented by

**Ahmed NEGM**

Defended on 12th of July 2019 in Sophia Antipolis

# Study the role of ASIC3 ion channels in pain hypersensitivities associated with the consumption of lipid rich diet.

Thesis directed by Professor Jacques NOËL and co-directed by Dr Carole ROVERE

Members of the thesis jury :

| | |
|---|---|
| Pr Laurent COUNILLON | President |
| Dr Emmanuel BOURINET | Reviewer |
| Pr Marc LANDRY | Reviewer |
| Pr Peter McNAUGHTON | Examiner |
| Pr Jacques NOËL | Thesis director |
| Dr Carole ROVERE | Thesis co-director |

## *Remerciements & Acknowledgments*

*Tout d'abord, I want to thank Allah for giving me the power, strength and motivation that allowed me to finish this work.*

*I would like to thank all the member of the jury for my PhD viva who kindly accepted to review and evaluate my thesis. Thank you Prof. Laurent COUNILLON for being the president of the jury. Thank Prof. Marc LANDRY and Dr. Emmanuel BOURINET for accepting to review this work. Prof. Peter McNAUGHTON thank you very much for taking the effort to come from the UK to attend the viva it was an honor and a great pleasure to have to you in the jury. I want to thank you all for the very stimulating and interesting discussion we had during the viva and I would be always happy to keep our exchange and hopefully to be able to work with yours and to be able to do some collaborative work together in the near future.*

*I want to give special thanks to my ultimate mentor, the Cyclopedic, Prof. Jacques NOEL my PhD director. You inspired me and I learned many things from you, not only in research but also in life. It was amusing to discuss about experiments interpret it and quickly get new ideas for experiments. I admired your enthusiasm for research. Thank you for believing in me and for trusting me. I won't forget that although I didn't have big experience in lab work when I started my master intern because of my background as a pharmacist, nevertheless you didn't blame me for the mistakes I did but always motivated me to continue and advance. Your motivation will always guide me to advance and progress in my career. Thanks a lot Jacques for being the best supervisor; it was a fantastic and great to work with you. I will miss you a lot and I hope I would be able to work with you again and again and continue learning and get inspired by you.*

*Je tiens à remercier la codirectrice de ma thèse Dr. Carole Rovere. Ce fut un grand plaisir de travailler et d'interagir avec vous. Ce travail n'aurait jamais été possible sans votre aide pour développer le modèle de souris et l'évaluation métabolique effectuée sur celles-ci. J'ai eu le plaisir*

*de venir à votre bureau pour discuter de mes résultats et discuter beaucoup de choses différentes. J'espère que notre collaboration s'étendra dans mes travaux futurs.*

*Dr. Eric Lingueglia I am grateful to you for welcoming me in the team and for the English lab meetings also thank you very much for the very interesting ideas that helped in advancing the project. Thank you and to Labex ICST for supporting me to attend several meetings and congresses also to receive several trainings during my PhD.*

*Dr. Emmanuel Deval you are a very kind and humble person I enjoyed a lot discussing with you and exchanging ideas, I enjoyed a lot our funny conversations, your sense of humor, your advices and your kind motivation during my PhD.*

*My beloved team, I love you all and I will miss you like hell. I was astonished by your kind hospitality and how you integrated me quickly in the team from the beginning when I was a shy and quiet guy till the moment you asked me to stop talking. I enjoyed our conversations jokes laughs that brought me a lot of joy, all the parties we had together in Valerie's place, Christmas dinners and specially the sushi parties and of course the Haggen Dars. It's hard to realize that I am leaving this beautiful company and my ultimate hopes is to be able to come back to enjoy these moments again and again.*

*People from my office, Valerie queen of the team and the trouble solver I enjoyed a lot our long conversations and our jokes I will miss my little confession seat beside the window!!! I will miss walk with you and driving you to the car, I will miss you the most. I know how difficult it will be without you. My best hopes to keep in touch. Best wishes for you and your great husband Jack. Spider-woman thanks for all the toxins you gave me!!! for the motivation and discussions. Migalus I will miss our structural function discussions finally I understood some of it. Ludivine my office partner I will always remember everyone is weird, everyone needs to watch Mr Bean. Thank you for your help during writing the manuscript and for your support and motivation.*

*Anne thanks for the interesting scientific ideas and the family advices. Magda thank you very much for the great advices I will miss a lot our conversations. Clement my roommate during all the meetings we went together. We had many thoughtful moments, I will miss our scientific discussions and I wish you the best for your future. Bonnie from Yorkshire, always remember that I cleaned the patch clamp setup and it is not me who missed up your stuff, I enjoyed working with you and going to congresses together… good luck with the rest of your PhD and your viva. Jade it was short but effective many thanks to you for helping in the experiments; it was great having you in the team.*

*Jean-Louis NAHON and your team it was great and fruitful to collaborate with you. Thanks for the help you kindly gave me during many experiments. Special thanks to Katharina, working with you was stimulating I enjoyed it a lot and I believe you did too. Thanks for your help in experiments and in many tough times. Best wishes for your defense and I believe you will have a bright future after the doctorate.*

*Stephane Martin and your lovely team thank you for having me for a while and teaching me some tricks about "WB" Marie 'la mentor' merci beaucoup, Marta it was always nice to discuss with you, Gwenola thank you for letting me use your bench.*

*Massimo and your great team, it was great working side by side I enjoyed the daily conversations and thank you for sharing and lending me stuff when needed.*

*General thanks to all the people in IPMC for sharing smiles, kind conversation, ideas and things as well. Special thanks to IPMC for sponsoring travel grant to congresses, it was great to win this travel grant which allowed me to go to Boston IASP 2018.*

*Papa et Mamon I love you and I want to thank you for believing in me for supporting and motivating me before and during my PhD. Thank your kindness, your patience, for teaching me how to be persistent and productive. I look to you as ideals that I hope to reach one day. I know how tough was it to raise me but my ultimate wishes is that I made you proud. You are the best parents and I*

*love you forever. My brother and sister Islam and Reham I never realized how much we love and care about each other until we got apart, our memories and my wonderful childhood were a big motivator to go on, lets pray to God to bring us together again soon.*

*I also want to thank my beautiful wife Somaya you was and will always be a great supporter and motivator to me, without you this work would have never been completed. I thank my children Anas and Sohail for giving me a lot of joy and I am sorry for coming late from work, I will do my best to payback these hours. My family in law Magdy, Hanan, Belal and Abdulrahman thank you for all the joy, support and help you gave me from the beginning of my marriage until the end of PhD. Thank you very much and hope we enjoy many other moments together.*

## *Résumé*

L'obésité est un facteur de risque majeur pour de nombreux troubles métaboliques graves. Elle touche 13% de l'ensemble de la population adulte dans le monde, ce qui en fait un domaine de recherche important. L'obésité se caractérise par un indice de masse corporelle accru qui résulte d'un déséquilibre entre l'apport calorique et les dépenses énergétique. Cela peut être dû à une consommation accrue d'aliments riches en énergie, comme les aliments riches en graisses, qui correspondent à l'alimentation occidentale, en parallèle avec un faible niveau d'activité physique. Il est maintenant bien accepté que l'obésité induit une inflammation systémique chronique de bas grade, qui implique les adipokines et les cytokines libérées par l'intestin et le tissu adipeux. Cette inflammation de bas grade s'étend à d'autres tissus, entraînant des dysfonctionnements métaboliques systémiques. De plus, il a été démontré que l'obésité est corrélée à des douleurs chroniques, indépendamment des autres composantes du syndrome métabolique. Il n'est pas encore clairement établi comment cette douleur chronique est initiée et quels en sont les mécanismes. Notre étude s'est concentrée sur l'étude de l'effet de l'obésité sur l'activité des neurones sensoriels périphériques et la perception de la douleur, et la caractérisation des mécanismes cellulaires sous-jacents qui impliquent les canaux ioniques sensibles à l'acidose ASIC3.

### Méthodologie

Nous avons utilisé une alimentation riche en matières grasses composée essentiellement d'acides gras saturés pour induire l'obésité chez des souris juvéniles. Nous testons les seuils de perception des douleurs thermiques, mécaniques et chimiques chez les souris obèses à l'aide de tests de chaleur radiante Hargreaves, de von Frey dynamique et de formaline. Les approches électrophysiologiques, y compris les techniques de patch-clamp et l'enregistrement sur le nerf saphène, nous ont permis d'étudier l'effet l'obésité induite par un régime riche en graisses saturée sur l'excitabilité des neurones sensoriels périphériques.

### Résultats

Après 8 semaines d'alimentation riche en graisses (HFD), nous avons pu observer que les souris deviennent obèses. Ces souris sont prédiabétiques. Elles ont développé une dérégulation de l'homéostasie du glucose par rapport aux souris maigres nourries en régime standard. De plus, les souris obèses présentent une hypersensibilité thermique une fois l'obésité bien établie, alors que les autres modalités sensorielles ne sont pas affectées. Nous avons observé une surexpression des

cytokines inflammatoires chez des souris obèses non seulement dans le tissu adipeux mais aussi dans d'autres tissus impliqués dans la voie de la douleur (c'est-à-dire les ganglions radiculaires dorsaux et la moelle épinière). Le régime alimentaire riche en lipides a provoqué une dyslipidémie avec une concentration accrue de plusieurs espèces de lipides dans le sérum des souris obèses, dont le lysophosphatidylcholine. Nous montrons que le sérum de souris obèses active directement les canaux ASIC3 et potentialise les réponses à une acidification modérée (pH 7). L'obésité augmente la réponse des fibres C mechano et thermosensibles cutanées à la chaleur. L'absence des canaux ASIC3 chez les souris knockout protège ces souris de l'hyperalgésie à la chaleur.

## Conclusions

Nos expériences ont mis en lumière l'impact de l'inflammation chronique de bas grade et de la dysrégulation métabolique induite par une alimentation riche en graisses, induisant l'obésité sur le système nerveux périphérique et la douleur. Nous démontrons le rôle des canaux ASIC3 dans sur l'excitation des neurones sensorielles et l'hyperalgésie thermique. Nos résultats donnent une portée clinique intéressante et suggèrent que l'hypersensibilité thermique associée à l'obésité induite par les lipides pourrait être traitée pharmacologiquement en bloquant ASIC3.

## *Abstract*

### Aim of Investigations

Obesity is a major risk factor for many serious disorders. It affects 13% of the whole adult population worldwide making it an important field for research. Obesity is characterized by an increased body mass index resulting from an energy imbalance between caloric intake and energy expenditure. This can be caused by an increased consumption of energy-dense foods such as food rich in fat, which corresponds to occidental diet. It is now well accepted that obesity induces chronic systemic low-grade inflammation, which is mediated by Adipokines and cytokines released from the gut and adipose tissue. This low-grade inflammation extends to other tissue leading to systemic metabolic dysfunctions. In addition, obesity was shown to be correlated to chronic pain regardless of other components of the metabolic syndrome. It is not yet clear how this chronic pain is initiated and what mechanisms are involved. Our study focuses on investigating the effect of obesity on peripheral sensory neurons activity and pain perception, followed by deciphering the underlying cellular and molecular mechanisms that involve the Acid Sensing Ion Channels ASIC3.

### Methods

Mice were fed with a high-fat diet composed of saturated fatty acids to induce obesity. We used pain behavioral tests to measure the thermal, mechanical and chemical perception in obese mice using radiant heat Hargreaves test, dynamic von Frey, and formalin tests respectively. Electrophysiological approaches including patch-clamp techniques and skin-saphenous nerve recording preparation allowed us to study the effect of high-fat diet and obesity on peripheral sensory neurons excitability, while qPCR and Immunohistochemistry chemistry were used in investigating the changes in the expression of pro-inflammatory factors.

### Results

After 8 weeks of high-fat diet (HFD), we observe that mice become obese. These mice developed deregulation of glucose homeostasis compared to lean mice fed on standard regime. In addition, obese mice showed a long-lasting thermal hypersensitivity once obesity was well established, while other sensory modalities were not affected. We found an overexpression of the

inflammatory cytokines in obese mice not only in the adipose tissue but also in other tissues involved in the pain pathway (i.e. Dorsal root ganglions and spinal cord). In addition, the lipid rich diet induced dyslipidemia with increased concentration of several lipid species in the serum of obese mice. Delivering the serum from obese mice to recombinant ASIC3 channels directly activated the channels and potentiated the channels responses to moderate acidification (pH 7). Obesity led to increased firing of heat sensitive C-fibers. The genetic deletion of ASIC3 channels in ASIC3 knockout mice protected these mice from thermal hypersensitivity.

## Conclusions

Our experiments shed light on the impact of the chronic low-grade inflammation and metabolic dysregulation induced by fat-rich diet on the peripheral nervous system and pain, and on the role of ASIC3 channels in these conditions. Our results give an interesting clinical scope and suggest that the thermal hypersensitivity associated with lipid induced obesity could be treated pharmacologically by blocking ASIC3.

## *Table of content*

## *List of tables*

## *List of figures*

## *List of abbreviations*

| List of abbreviations | Serotonin |
|---|---|
| 5-HT | |
| Aα | A-alpha |
| Aβ | A-beta |
| Aδ | A-delta |
| AA | Arachidonic acid |
| ANO-1 | ANOctamin-1 |
| APETx2 | AnthoPleura Elegantissima ToXine 2 |
| ASIC | Acid Sensing Ion Channel |
| ASIC3 | Acid Sensing Ion Channel 3 |
| ASIC3ko mice | Acid Sensing Ion Channel 3 Knockout mice |
| $Ca^{2+}$ | Calcium |
| Cav | Voltage-gated $Ca^{2+}$ channel |
| CDC | Centers for Disease Control and Prevention |
| CFA | Complete Freund's Adjuvant |
| CIPP | Channel Interacting PDZ domain-containing Protein |
| CGRP | Calcitonin Gene-Related Peptide |
| COX | Cyclo-OXygenases |
| DiaComp | Diabetic complications consortium |
| DIO | Diet induced obesity |
| DEG | DEGenerins |
| DRASIC | Dorsal root acid sensing ion channels |
| DRG | Dorsal root ganglia |
| EC50 | Maximum half Effective Concentration |
| ENaC | Epithelial $Na^+$ Channel |
| FaNaC | FMRF-amide-activated $Na^+$ Channel |
| FMRF | Phenylalanine-Methionine-Arginine-Phenylalanine |
| GABA | Gamma-AminoButyric Acid |
| Glu | Glutamate |
| GMQ | 2-Guanidine-4-MethylQuinazoline |
| GPCR | G Protein Coupled Receptors |
| $H^+$ | Hydrogen |
| HFD | High Fat Diet |
| IC50 | Half maximum Inhibitory Concentration |
| ILβ | Interleukin-1 beta |
| IL6 | Interleukin 6 |
| IP | Intraperitoneal route |
| IP3 | Inositol TRI Phosphate |
| IV | Intravenous route |
| LTMR | Low threshold mechano-receptors |
| LPC | LysoPhosphatidylCholine |
| LPI | LysoPhosphatidylInositol |

| | |
|---|---|
| LPL | LysoPhosphoLipids |
| LPS | LysoPhosphatidylSerine |
| LT | LeucoTrienes |
| $Mg^{2+}$ | Magnesium |
| MitTx | Micrurus hold Toxin |
| MOP | Mu Opioid Receptor |
| mRNA | Messenger Ribonucleic acid |
| $Na^{+}$ | Sodium |
| Nav | Voltage-gated $Na^{+}$ channel |
| ND | Normal Diet |
| NGF | Nerve Growth Factor |
| NO | Nitric Oxide |
| NSAIDS | Non-Steroidal Anti-Inflammatory Drug |
| NMDA | N-methyl-D-aspartate receptor |
| P2X | ATP Ionotropic receptor |
| PCR | Polymerase Chain Reaction |
| PcTx1 | PsalmoToxin-1 |
| PDN | Peripheral diabetic neuropathy |
| PG | Prostaglandins |
| pH | Hydrogen Potential |
| PICK | Protein Interacting with C Kinase |
| PDZ domain | Post-synaptic density protein 95 (PSD-95), Drosophila disc large tumor suppressor (Dlg1) and Zona occludens 1 (ZO-1). |
| PKA | Protein Kinase A |
| PKC | Kinase C protein |
| PLA2 | PhosphoLipase A2 |
| PNS | Peripheral nervous system |
| PSD-95 | PostSynaptic Density protein 95 |
| qPCR | Quantitative Polymerase Chain Reaction |
| RA | Rapid adapting |
| SA | Slow adapting |
| SP | Substance P |
| TASK | TWIK-related Acid-Sensitive $K^{+}$ channel |
| TG | Trigeminal ganglia |
| TM | Trans Membrane |
| TNF-α | Tumor Necrosis Factor alpha |
| TRAAK | TWIK-Related Arachidonic Acid $K^{+}$ channel |
| TREK | TWIK-Related $K^{+}$ channel |
| TRESK | TWIK-Related Spinal cord $K^{+}$ channel |
| TrkA | Receiver with Tyrosine Kinase A activity |
| TRPA | Transient Receptor Potential Ankyrin |
| TRPC | Transient Receptor Potential Canonical |
| TRPM | Transient Receptor Potential Melastatin |
| TRPV | Transient Receptor Potential Vanilloid |
| TTX | Tetrodotoxin |

| | |
|---|---|
| TX | Thromboxane |
| WDR | Wide Dynamic Range |
| WHO | World Health Organization |
| WT | Wild Type |
| $Zn^{2+}$ | Zinc |

# *Introduction*

## 1. The somatosensory pathway

The somatosensory nervous system drives the sensory signals from the sensors that detect stimuli in peripheral and internal organs through a complex neuronal circuit in the spinal cord dorsal horn or brain stem and then via ascending pathways to numerous brain regions that produce reflexes, sensations and emotions. The sensory signal is processed through three main neuronal relays and five different sensory tracks. One of these pathways is uniquely responsible for the light touch and proprioception. Two other tracks are responsible for transmission of painful stimuli to inform the brain about actual or potential tissue damage. The other two pathways convey mixed signals from different body parts and for several sub modalities. The three main relays are represented in three order neurons (Basbaum and Jessell, 2013). In the first part of the introduction, I will start describing the different sensory neurons found in the periphery followed by a brief description of the modulatory processes of pain in the spinal cord and later I will describe the ascending pathways that convey sensory signals to the brain.

*Figure 1 Descartes' concept of pain transmission.*
*Descartes simply described the pain pathway and initiated the revolutionary idea that the central nervous system can influence the perception of pain. René Descartes 1641*

## 1.1. Sensory afferents

In the periphery, cell bodies of the sensory neurons are located in the dorsal root ganglia (DRG) for the body and trigeminal ganglia (TG) for the face. These neurons have a unique pseudo-unipolar morphology with a single axon that gives both a peripheral and a central axonal branch. The peripheral branch innervates the skin, internal organs, muscle or tendons. Some branches are in contact with epithelial cells, such as keratinocytes and Merkel cells. They are responsible for the generation of the neuronal sensory signals. They transduce, encode and transmit the nature and intensity of the stimulation (Kandel et al. 2013). Four distinct sensory fibers Aα, Aβ, Aδ and C-fibers are found in the periphery. These fibers are distinguished by their sensory receptors, axonal diameters and level of myelination which influence their sensory properties, conduction velocity and firing properties (Horch et al., 1977).

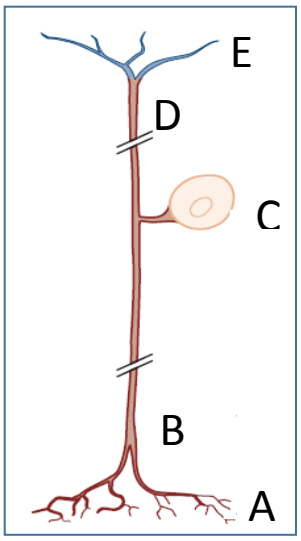


*Figure 2 Pseudo-unipolar cell. A) Free nerve terminals in the skin and muscles - transduction and AP initiation B) peripheral axons C) Cell bodies D) central axons E) Axon terminals - synaptic transmission. Source (Kandel et al., 2013)*

Aα fibers have the largest axon diameter with thick myelination. They have the highest conduction velocity due to their low internal resistance to current flow and the widely spaced nodes of Ranvier along the axon. They innervate the muscle spindle and are responsible for monitoring the velocity of muscle tension and proprioception (Lawson, 2002). Aβ fibers are myelinated with medium diameters. They innervate secondary muscle spindle endings, receptors in joint capsules, and cutaneous mechanoreceptors that respond to innocuous light touch. Aδ fibers have small diameter and low myelination. C fibers are small diameter unmyelinated axons (Dubin and Patapoutian, 2010). In the skin C-fibers compose 70% of sensory fibers while Aδ and Aβ represent 10% and 20% respectively (Millan, 1999).

*Table 1 Different sensory fibers with their myelination, cross sectional diameter (µm), and conduction velocity (m/s). Adapted from (Gardner and Johnson, 2013)*

| | Myelinated | Fiber diameter | Conduction velocity |
|---|---|---|---|
| Aα | Yes | 12–20 | 72-120 |
| Aβ | Yes | 6-12 | 36-72 |
| Aδ | Yes | 1-6 | 4–36 |
| C-fibers | No | 0.2–1.5 | 0.4–2.0 |

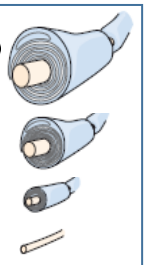

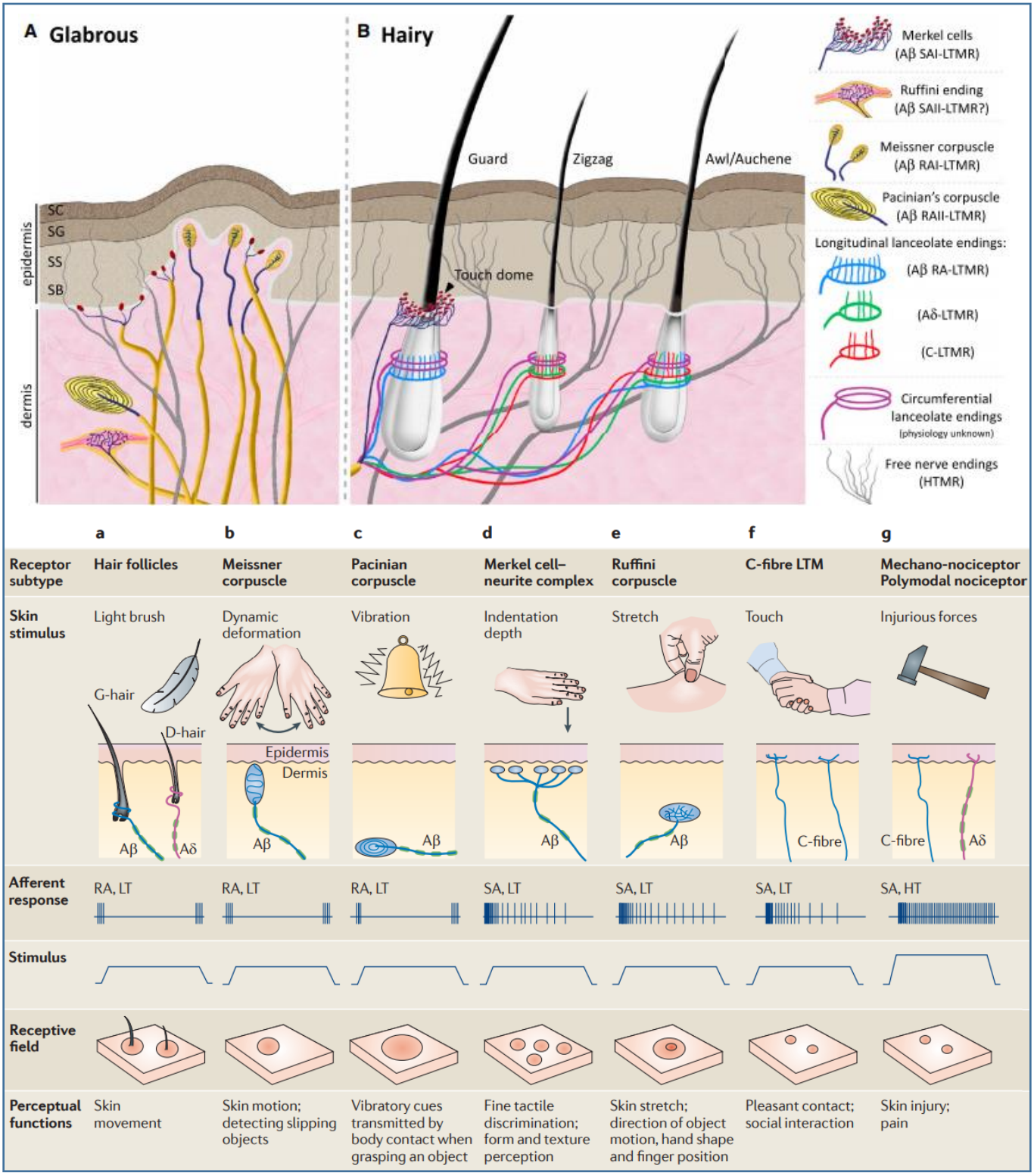


| | a | b | c | d | e | f | g |
|---|---|---|---|---|---|---|---|
| **Receptor subtype** | **Hair follicles** | **Meissner corpuscle** | **Pacinian corpuscle** | **Merkel cell–neurite complex** | **Ruffini corpuscle** | **C-fibre LTM** | **Mechano-nociceptor Polymodal nociceptor** |
| **Skin stimulus** | Light brush | Dynamic deformation | Vibration | Indentation depth | Stretch | Touch | Injurious forces |
| **Afferent response** | RA, LT | RA, LT | RA, LT | SA, LT | SA, LT | SA, LT | SA, HT |
| **Stimulus** | | | | | | | |
| **Receptive field** | | | | | | | |
| **Perceptual functions** | Skin movement | Skin motion; detecting slipping objects | Vibratory cues transmitted by body contact when grasping an object | Fine tactile discrimination; form and texture perception | Skin stretch; direction of object motion, hand shape and finger position | Pleasant contact; social interaction | Skin injury; pain |

*Figure 3 Skin receptors distribution in glabrous and hairy skin.*
*Top figures schematic representation of the mechano-receptors and free nerve terminals in glabrous and hairy skin. The color codes described on the left source (Abraira and Ginty, 2013). Lower table show distribution of different skin responses and their physiological stimulator, electric stimulation, receptive field and their perceptual function source (Delmas et al., 2011)*

## 1.2. Neurophysiological techniques

which influence their sensory properties, conduction velocity and firing properties. The differences in the conduction velocities can be measured using electric stimulation of the whole nerve. Graded increase in stimulation intensities discriminate between the different four types of fibers. Aα fibers are stimulated first because they have the lowest resistance and the highest conduction velocity. Then Aβ and Aδ fibers are activated. Finally C fibers are activated, because they are high threshold and slow conduction velocity fibers. Nerve stimulation is used in the clinic and neurophysiology laboratories to monitor defects in conductance of the peripheral nerves in relation to suspected neuropathic pain (Colloca et al., 2017; Erlanger and Blair, 1938)

## 1.3. Nociceptors

Sensory receptors that are activated by painful stimuli are called nociceptors. These nociceptors are free nerve terminals of Aδ and C fibers. They detect high intensity thermal, mechanical and chemical stimuli (Basbaum et al., 2009). In addition injured tissues release chemicals that directly activate nociceptors (i.e. ATP, $H^+$, lyso-lipids). These nociceptors can be polymodal responding to thermal, mechanical and/or chemical stimuli. It is estimated that from 35 to almost 100% of the C-fibers are polymodal (Emery and Ernfors, 2018). On the other hand, some nociceptors are unimodal responding to either mechanical, between 10 and 15% of fibers, or thermal stimuli, representing between 10 to 25% of nociceptive fibers (Dubin and Patapoutian, 2010). Experiments done with *in vivo* $Ca^{2+}$ imaging showed controversial results with 50% of pure mechanical nociceptors (M), 19% of mechanical and noxious heat (MH) nociceptors, 11% of pure noxious heat (H), and only 4% of polymodal mechanical heat and cold sensitive (MHC) nociceptors in DRGs (Emery and Ernfors, 2018; Wang et al., 2018). This controversy could be owed to the differences in the technical approaches, stimulated skin area and the thresholds used to assess responses. Because the molecular transducers expressed in the primary sensory afferents mediate their functions, efforts were done to classify them based on their molecular expression profiles. These studies revealed 3 putative categories of cold-sensitive neurons, 5 categories of mechano-heat sensitive, 4 categories of A-Low threshold mechanosensitive neurons (A-Beta), 5 for itch-mechano-heat–sensitive nociceptor types and 1 for C–low-threshold mechanoreceptor type (C-LTMR) (Emery and Ernfors, 2018). Silent nociceptors were also identified. They are inactive under

normal physiological conditions, but, they are recruited and their firing threshold is lowered under physiopathological conditions. This sensitization state can occur during inflammation, and stimulation by chemicals that are released during injury (Dubin and Patapoutian, 2010).

### *1.3.1. Aδ fiber*

Aδ fiber activation induces fast well-localized pain described as sharp and pricking. There are two classes of Aδ nociceptors. Type I high threshold mechanical nociceptors that respond to mechanical and chemical stimuli but less sensitive to heat at high temperature. Conversely, Type II Aδ nociceptors have lower temperature threshold but much higher mechanical thresholds.

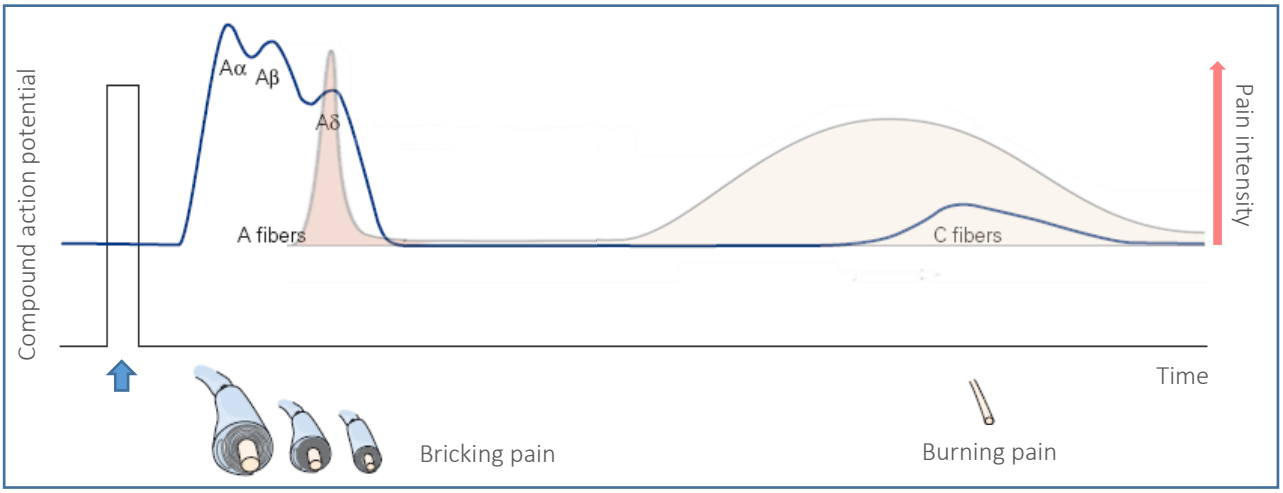


*Figure 4 Compound action potential of the sensory fibers.*
*After stimulating peripheral nerves (indicated by the arrow), several waves are generated and they are separated based on their conduction velocity. Myelinated A fibers (Aα, β and δ) appears first then the unmyelinated C fibers appear. Aδ fibers conduct cold, pressure and pain signals that produce the acute and sharp experience of pain. C fibers respond to mechanical, thermal, and chemical painful stimuli by producing a long-lasting burning sensation. Adapted from (Basbaum and Jessell, 2013).*

### *1.3.2. C-fibers*

C-fibers respond to mechanical, thermal, and chemical painful stimuli by producing a dull long-lasting burning sensation that is intolerable and poorly localized due to slow conduction speed and diffuse innervations (Basbaum and Jessell, 2013). C-fibers can be classified as peptidergic and non-peptidergic based on their expression of neuropeptides. Peptidergic neurons express substance P and calcitonin gene–related peptide (CGRP) or somatostatin (Som, SSt) (Hökfelt et al., 1975, 1976; Wiesenfeld-Hallin et al., 1984). Non-peptidergic do not express the above-described peptides but instead they bind the plant lectin Griffonia simplicifolia I-B4 (IB4). Although all non-peptidergic fibers are C-fibers(Nagy and Hunt, 1982; Silverman and Kruger, 1988), some peptidergic neurons are Aδ fibers (Lawson et al., 1996; McCarthy and Lawson, 1990). C-fibers could be mechano-heat

sensitive (C-MH), Mechano-cold sensitive (C-MC) or respond to all stimulation (C-MHC) or silent insensitive C-fibers (C-MIHI) (Dubin and Patapoutian, 2010). The mechano-, thermo- and chemo-transducers responsible for the sensory properties of the nociceptors will be described later.

## 1.4. Spinal cord modulation (or Neurotransmitters in the CNS)

Neurons that innervate the body conveyed sensory information to the dorsal horn of the spinal cord while neurons that innervate the face relay in the nucleus caudalis of trigeminal nerve in the brain stem. Central branches of DRG neurons form synapses with second order projection neurons and interneurons in one of the five dorsal laminae of the spinal cord (Basbaum et al., 2009; Peirs and Seal, 2016). The major classes of neurotransmitters released by the sensory afferents in the dorsal horn are glutamate and neuropeptides (Julius and Basbaum, 2001). Glutamate is not specific to the nociceptive sensory afferents as it is released by all sensory afferents. Neuropeptides are released as co-transmitter from peptidergic nociceptors mainly the unmyelinated C-fibers. These neuropeptides include substance P, calcitonin gene-related peptide (CGRP), somatostatin, and galanin. The two classes of neurotransmitters are stored in different vesicles allowing them to be released under different conditions of activation, and both classes act to regulate the excitability of the dorsal horn neurons (Basbaum and Jessell, 2013). Neuropeptides have a diffuse effect because they can spillover as a result they can reach to surrounding synapses compared to glutamate. This spillover happens due to the lack of adequate means for neuropeptide reuptake instead they are subject to the action of extracellular peptidases (Russo, 2017). This could explain the poor localization of several pain conditions. Substance P is particularly associated with tissue injury and upon intense stimulation of the peripheral afferents. It binds to the neurokinin receptors expressed on neurons in the dorsal horn and it potentiates the depolarization induced by glutamate on postsynaptic NMDA receptors (Cheng, 2010; Latremoliere and Woolf, 2009).

## 1.5. Spinal cord microcircuit

The integration of peripheral signals in the spinal cord is extremely complex and yet not fully characterized (Peirs and Seal, 2016). Indeed, single-cell RNA sequencing to classify sensory neurons in the mouse dorsal horn identified 15 inhibitory and 15 excitatory subtypes of neurons, equaling the complexity found in the cerebral cortex (Zeisel et al., 2018). Most Aδ and C-

nociceptive fibers form synaptic contacts in the superficial laminae I and II. Laminae II and III contain excitatory and inhibitory interneurons that receive inputs from Aδ and C-fibers. Most low-threshold proprioceptive afferents project to deeper laminae III to V. The second order projection neurons are located in laminae I, II, IV and V. Projection neurons in lamina V are called wide-dynamic-range neurons because they receive inputs from Aβ, Aδ and C fibers. Consequently, they respond to various stimuli, tactile, thermal and noxious stimuli (Moehring et al., 2018).

## 1.6. Ascending pathways

After reaching the spinal cord the somatosensory information is then conveyed to central structures through five ascending pathways that relay in the brainstem and thalamus (Willis and Westlund, 1997). The main tracks are spino-thalamic, spino-reticular, spino-mesencephalic tracks which form the Anterolateral system in addition there is the spino-limbic pathway. The Spino-thalamic track is the main track to convey the sensory components of pain and visceral signals to the ventrobasal medial and lateral areas of the thalamus. It is formed of postsynaptic neurons from laminae I, V and VII that receive their main input from Aδ and C-fibers sensory afferents. Indeed, lamina I projection neurons represent 50 % of the spino-thalamic track. WDR neurons also represent a major fraction of neurons in the spino-thalamic track. This track then projects through third order neurons to the somatosensory cortex where the perception of the location and intensity of pain occurs.

Spino-limbic projections relay in the parabrachial nucleus before projecting to the hypothalamus and amygdala, where central autonomic function, fear and anxiety are affected. Indeed, nociceptive stimuli are distributed to several brain areas that together form what is called the 'pain matrix' (Garcia-Larrea and Peyron, 2013). These brain regions helps in coding the sensory-discriminative and the emotional components of pain perception. Sensory-discriminative component of pain involve the primary and secondary somatosensory cortex, the thalamus and the cerebellum. The emotional component of pain encompass the prefrontal cortex, anterior cingular cortex, insula, amygdala, basal ganglia, periaqueductal gray area and parabrachial nucleus (Bushnell et al., 2013).

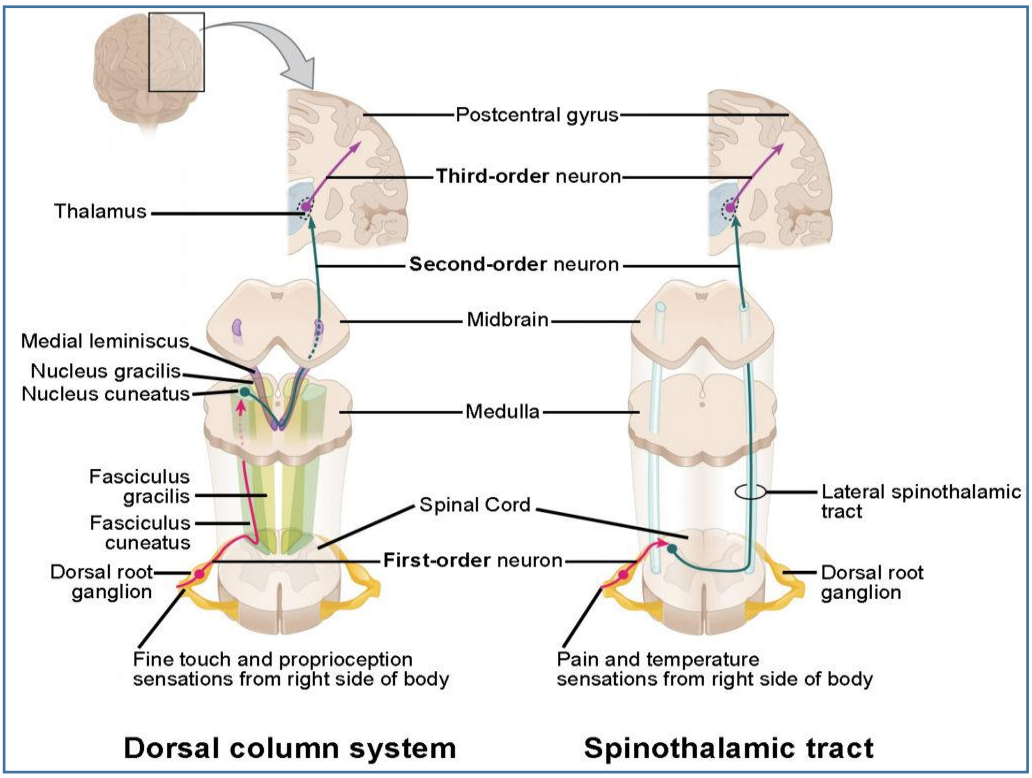


*Figure 5 the dorsal column system and spinothalamic tract.*
*They are the major ascending pathways that connect the periphery with the brain. Source (Biga et al.)*

## 1.7. Central modulation of pain; gate control theory and descending pathways

The gate control theory developed by Ronald Melzak and Patric Wall in 1965 was revolutionary in that it provided explanations to several phenomena related to pain (Melzack and Wall, 1965). The theory states that noxious signals transmitted to the spinal through Aδ, and C-fibers could be suppressed by two ways.

As described previously, in the spinal cord, the central terminals of sensory fibers that carry noxious stimuli through C and Aδ fibers and innocuous stimuli carried by Aβ fibers form synapses with projection neurons. These projection neurons can be excited by stimulation from both types of sensory afferents (noxious and innocuous). In turn, C-fibers form inhibitory synapses with inhibitory interneuron that project on the projection neurons, this lead to suppressing their inhibitory effect. On the other hand, Aβ fibers form excitatory synapses with these inhibitory interneurons where they can activate them to inhibit the activity of the projection neurons. This complex microcircuit within the spinal cord forms a gate on the transmission of the pain signals. In that sense if C-fibers are activated solely, pain signals can be transmitter to higher centers of

the brain through the projection neurons. Whereas if both C-fibers and Aβ were activated, Aβ fibers will activate the inhibitory interneurons which will decrease the activity of the projection neurons and signals passing to the higher centers of the brain will be suppressed (Basbaum and Jessell, 2013; Moayedi and Davis, 2012).

The other component of the gate control theory is the descending pathways from the amygdala and hypothalamus that project to the periaqueductal gray region (PAG). In turn neurons from PAG terminate in the nucleus locus ceruleus of the pons or the nucleus raphe Magnus in the medulla. In turn, from these two nuclei serotonergic, and noradrenergic descending neurons reach the dorsal horn of the spinal cord and terminate on central synapses of the sensory fibers, interneurons and projection neurons. These fibers induce several effect; they directly inhibit the central terminals of the sensory fibers, they activate of the inhibitory interneurons, and inhibit the projection neurons. This inhibitory effect also involve the endogenous opioid system (Bee and Dickenson, 2009; Ossipov et al., 2014).

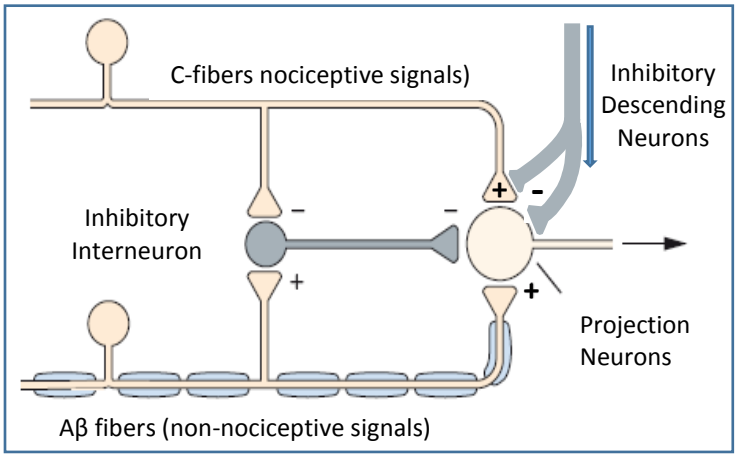


*Figure 6 Gate control theory.*
*Composed of two components first the role of non-nociceptive sensory afferents on spinal inhibitory interneurons and second role of the descending inhibitory pathways on excitatory synapses and projection neurons. Adapted from (Basbaum and Jessell, 2013)*

# 2. Pain

Pain is a specific somatosensory signal defined by the international association for the study of pain (IASP) as "an unpleasant sensory and emotional experience that is associated with actual or potential tissue damage." The sensation of pain is usually described as pricking, burning, aching, stinging, and soreness. Pain has an important function in protecting individuals. It alerts against dangerous and potentially harmful stimuli, and prompt individual's attention to alleviate, and treat the painful stimuli. Individuals lacking sensitivity to pain, as in Congenital insensitivity to pain (CIP), are usually subjected to severe injuries that can lead to permanent tissue damage. On the other hand, pain is a subjective sensory modality that is affected by several factors including emotional-aversive aspects (Basbaum and Jessell, 2013).

## 2.1. Molecular transducers for external stimuli

Peripheral nociceptors contain molecular transducers that are activated by different noxious stimulation. The classification of nociceptors is based on the expression of these molecular transduces. Molecular transduces are receptors or ion channels expressed at the plasma membrane of the nociceptors, where upon their activation or inactivation they depolarize the nociceptors to the threshold of firing action potentials (Bautista et al., 2008; Basbaum et al., 2009).

## 2.2. Thermo-sensation

Four different types of thermal sensation can be distinguished: noxious cold, cool, warm and noxious heat. The normal skin temperature is at 32 °C. Although we can sense sudden changes in temperature, if the same change in temperature were gradual, we would be unaware of this change within a range from 31°C to 36°C (Basbaum and Jessell, 2013). Above 36°C the sensation progresses from warm to hot then it becomes painful above 42°C. Below 31°C, the sensation proceeds from cool to cold and becomes painful below 17°C. These thermo-receptors transmit signals in a linear way in respect to rising temperature until it reach saturation. Thermal sensation is generated by the activation of various temperature sensitive ion channels.

TRPM8 and TRPA1 are activated by different ranges of cold temperatures (McKemy et al., 2002; Story et al., 2003). TRPM8 respond to cool temperatures below 25°C. It is expressed in high and low threshold cold receptor terminals (McKemy et al., 2002).

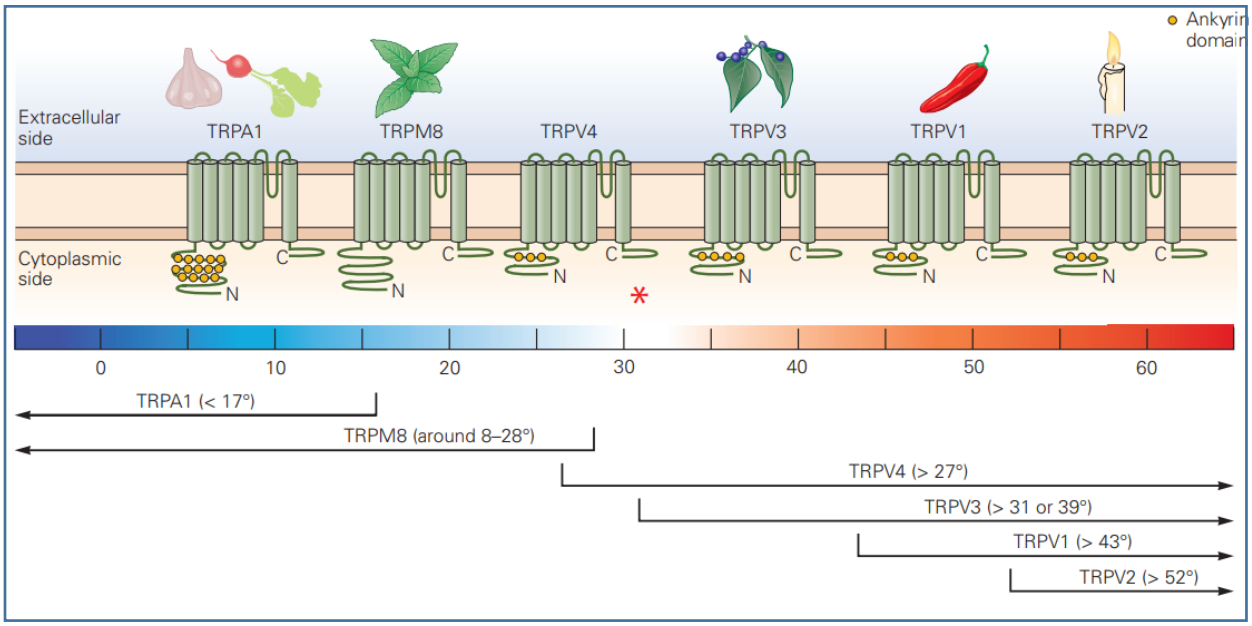


*Figure 7 Transient receptor potential ion channels (TRP).*
*Molecules that activate different TRP channels and the rage of temperatures that activate these channels. Source (Kandel et al., 2013)*

TRPA1 respond to cold temperatures below 17°C and they are only expressed in the high threshold cold receptor terminals (Story et al., 2003). The role of TRPA1 in cold temperature sensitivity is still debatable (Sexton et al., 2014). Nav1.8 and Nav1.9 have also been implicated in cold perception (Lolignier et al., 2015; Zimmermann et al., 2007). On the other hand, different ranges of hot temperatures can activate six type of heat sensitive channels including TRPV1, TRPV2, TRPV3, TRPV4, TRPM2, TRPM3 and ORAI (Caterina et al., 1997, 1999; Cho et al., 2012; Facer et al., 2007; Smith et al., 2002; Tan and McNaughton, 2016; Vriens et al., 2011). TRPM2 responds to non-noxious warmness (Tan and McNaughton, 2016). TRPV4 responds to normal skin temperatures above 27°C (Facer et al., 2007). TRPV3 respond to warm temperatures above 35°C (Smith et al., 2002). TRPV1 respond to hot temperatures above 45°C (Caterina et al., 1997). Finally, TRPV2 respond to extreme temperature above 52°C (Caterina et al., 1999). TRPM3 knockout mice showed reduced heat sensitivity (Vriens et al., 2011). TRPV1 knockout mice showed only minor deficits in the acute noxious heat perception (Caterina et al., 2000; Davis et al., 2000). On the other hand, complete deletion of all sensory fibers expressing TRPV1 neurons resulted in complete loss of heat sensation (Mishra et al., 2011). TRPV1 expressing neurons represent about 35 to 50% of the DRG and TG neurons (Fukuoka et al., 2002; Kobayashi et al., 2005). Interestingly, a recent study showed that heat responses involve the co-activation of three different TRP channels, TRPV1,

TRPA1, and TRPM3. Triple knockout mice, lacking the genes of these three channels, showed dramatic loss of acute withdrawal responses to noxious stimuli. This severe loss of thermal sensation led to injuries in these transgenic mice (Vandewauw et al., 2018).

### 2.3. Mechano-sensation

Mechanical nociceptors respond to strong mechanical pressure applied to the skin while, the Low threshold mechanoreceptors (LTMR) innervating the skin are responsible for proprioception and sensing light touch (Koltzenburg and Lewin, 1997). LTMR are innervated by Aβ sensory afferents. Mechanoreceptors are activated upon physical deformation of their surrounding tissue. These modifications could be in term of pressure applied on the skin, stretching, or vibration which will lead to the activation of mechano-sensitive ion channels in the mechanoreceptors (Delmas et al., 2011). Innocuous tactile sensitivity is essentially dependent on the expression of Piezo2 channel in LTMRs (Coste et al., 2010, 2012; Ranade et al., 2014). Other candidate ion channels have been proposed including the DEG/ENaC/ASIC Ion Channels or TACAN (Ranade et al., 2015). In turn, the activated ion channels will depolarize the nerve and action potentials are generated. The nerve terminals of the Mechanoreceptors are surrounded by nonneuronal end organs (Meissner corpuscles, Merkel cells, Pacinian corpuscles, and Ruffini endings) with which they interact to achieve mechano-perception (Ranade et al., 2015).

### 2.4. Pain intensity

Pathological pain is a modification in the perception of pain. This modification can be a decrease of the perception of pain referred as hypoalgesia, or it can be an increase in pain perception that is referred as allodynia and hyperalgesia. Allodynia is the perception of pain in response to non-painful stimuli, while hyperalgesia is an exaggerated pain response to a painful stimulation. These alterations in the pain perception occur due to nociceptive or neuropathic conditions (Baumgärtner et al., 2002; Basbaum et al., 2009).

### 2.5. Normal and Pathological pain conditions

Pain could be acute, persistent or chronic. Acute and persistent pain are beneficial as it promotes seeking treatment. On the other hand, pain can last longer than necessary and become chronic when it last more than three months (Verhaak et al., 1998). Indeed, pain symptoms persisting long

after an initial insult can be considered a disease. They can be neuropathic or inflammatory in etiology. Indeed, both pain states are thought to involve nervous system plasticity that alters basic transcriptional and post-transcriptional responses leading to persistent hyperexcitability and ectopic discharge of nociceptors (Schaible, 2007).

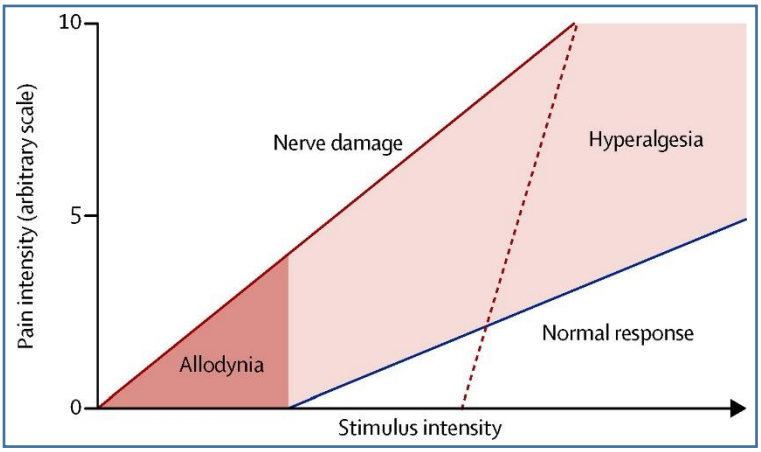


*Figure 8 Pain perception intensity in response to stimulus in normal and in pathological conditions.*

### 2.5.1. Neuropathic pain

The International Association for the Study of Pain (IASP) defined Neuropathic pain, as pain caused by a lesion or disease of the somatosensory nervous system. It can be triggered by trauma in peripheral nerves or central pain pathways, post-stroke, viral infection and diabetes. This type of pain is usually described as burning or electric sensation. Diabetic neuropathic pain will be described later in section 4.

### 2.5.2. Inflammatory pain

Inflammatory pain could be acute or chronic. Acute inflammation is an immune response that prompt survival during infection or injury. It is characterized by the four cardinal signs of inflammation: rubor et tumor cum calore et dolore (redness and swelling with heat and pain) (Medzhitov, 2010). On the other hand, chronic inflammatory pain is thought to be the consequence of an underlying inflammatory responses related to tissue pathology that occurs during several disorders including arthritis, gastritis, dermatitis, and repetitive strain injuries (Aley et al., 2000).

During tissue inflammation, nociceptors are sensitized and their threshold of activation is lowered inducing a state of hyperalgesia and allodynia (Basbaum and Jessell, 2013). This sensitization is moderated by chemicals released from damaged tissue and immune cells (Pinho-Ribeiro et al., 2017). These cells release several inflammatory mediators including cytokines (i.e. IL-1b, IL-6, TNFa, IL-17A, and IL-5), chemokines (e.g. CCL2, CX3CL1), growth factors (e.g. NGF, BDNF, CSF-1), neurotransmitters such as (5HT, ATP), histamine, bradykinin, prostanoids and pro-inflammatory lipids (including prostaglandins, prostacyclins, thromboxane, Leukotriene B4, arachidonic acid, lysophospho-lipids, and sphingosine-1-phosphate), and protons (Woolf et al., 1997; Shubayev and Myers, 2001; Gao and Ji, 2010; Aich et al., 2015; Pinho-Ribeiro et al., 2017). These inflammatory mediators interact directly and indirectly with ion channels and receptors expressed on peripheral nociceptors (Chiu et al., 2016; Pinho-Ribeiro et al., 2017). In addition, several signaling pathways were shown to be activated during inflammation. The activated signaling pathways induce changes in ion channels expression and activity leading to the increased excitability and enhanced nociceptive responses (Huang et al., 2006). For short-term hyperalgesia, the cAMP-PKA pathway is dominant, while the prolonged hyperalgesia could be regulated by PKCε-dependent or -independent pathways (Aley and Levine, 1999; Khasar et al., 1999a, 1999b; Aley et al., 2000; Huang et al., 2015). Among excitatory ion channels that are significantly affected by the inflammatory mediators are voltage dependent sodium channels (NaV1.7, 1.8 and 1.9), TRPV1, TRPA1, P2X3, and channels of the Acid Sensing Ion Channel family, ASIC3, ASIC1a (Jarvis et al., 2002; Mamet et al., 2002; Pinho-Ribeiro et al., 2017; Wood et al., 2004). The complex interactions between the different inflammatory mediators and ion channels with receptors on the nociceptors are reviewed in (Huang et al., 2006; Basbaum et al., 2009; Pinho-Ribeiro et al., 2017). Some of these interactions will be described below.

Histamine released from mast cells after tissue damage directly activates C-fibers (Koppert et al., 2001). Also endothelial cells and platelets release ATP, acetylcholine, and serotonin, in turn, these chemicals further increase the production and release of prostaglandin and bradykinin (Basbaum and Jessell, 2013). Prostaglandin and bradykinin sensitize Aδ and C-fibers directly through acting on their prostaglandin, and bradykinin receptors respectively (Pinho-Ribeiro et al., 2017). NGF act on TrkA receptors expressed on nociceptors, and stimulate the induction of signaling pathways (Basbaum et al., 2009). In addition, neuropeptides, substance P and CGRP, released from

peripheral terminals of C-fibers spillover and reach adjacent sensory fibers, to sensitize them and further enhance the pathological state.

Bradykinin generate vasodilatation and plasma extravasation (plasma effusion in interstitial tissues causing edema). Bradykinin directly interacts with its transmembrane G-protein-coupled receptors B1 and B2 (Levy and Zochodne, 2000). B1 receptors are mainly expressed during inflammation and they were shown to be involved in the heat evoked currents in DRG neurons (Huang et al., 2006). The activation of B1 receptors initiate several signal transduction pathways leading to $Ca^{2+}$ mobilization and activation of PKC signaling pathway (Couture et al., 2001; Petersen et al., 1998). TRPA1 and Nav channels activities are potentiated by Bradykinin (Bandell et al., 2004; Chahine et al., 2005). On the contrary, Bradykinin inhibits Kv7 (KCNQ), which will facilitate the neuronal excitability (Delmas and Brown, 2005).

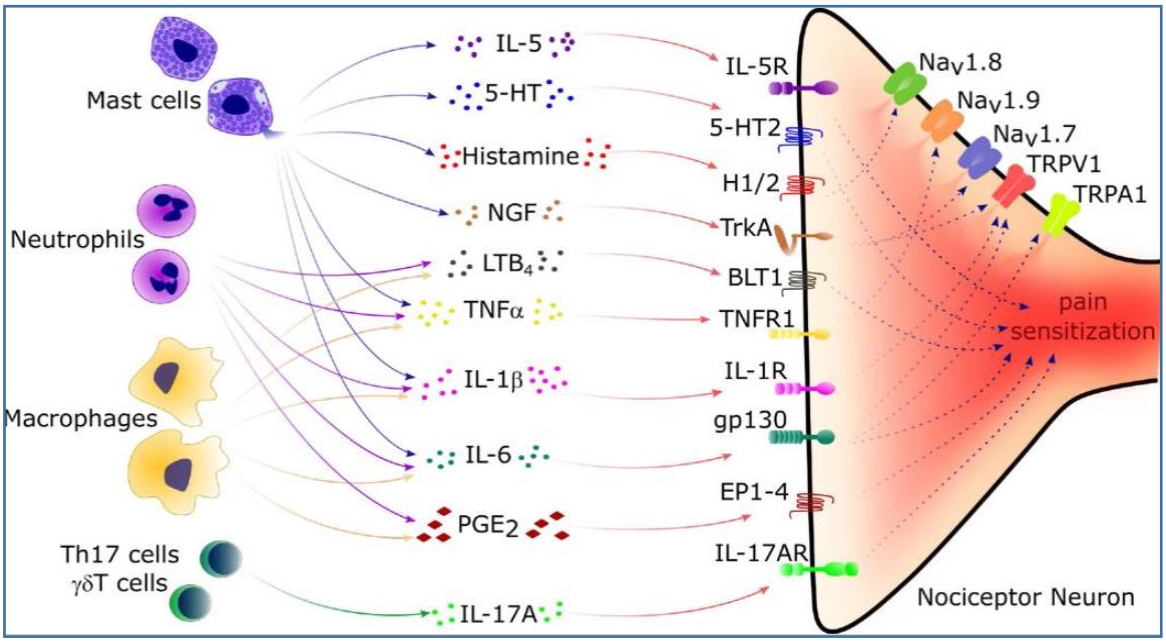


*Figure 9 Nociceptor Sensitization during inflammation.*
*During inflammation, tissue resident and recruited immune cells secrete inflammatory mediators that act on the peripheral nerve terminals of nociceptors to induce pain sensitization. In these neurons, specific cytokine, lipid, and growth factor receptor initiate intracellular signaling pathways lead to phosphorylation and/or change in gating of ion channels including Nav1.7, Nav1.8, Nav1.9, TRPV1 and TRPA1, leading to increased action potential generation and pain sensitivity. Mast cells release Interleukin 5 (IL-5), serotonin (5-HT), histamine and nerve growth factor (NGF) that act on IL-5R, 5-HT2, histamine receptor 2 (H2), TrkA, expressed on nociceptive neurons, respectively, resulting in pain sensitization. Tumor necrosis factor alpha (TNFα), IL-1ß and IL-6 produced by mast cells, macrophages, and neutrophils also sensitize nociceptors. TNFα receptor 1 (TNFR1) activation leads to the phosphorylation of Nav1.9 channels. Activation of IL-1 receptor 1 (IL-1R1) increases TRPV1 expression in nociceptors, while IL-6 binds gp130 on nociceptors and this increases expression of both TRPV1 and TRPA1, enhancing responsiveness to heat and reactive chemicals. Prostaglandin E2 (PGE2) released by macrophages and other innate immune cells also sensitize nociceptor neurons through PGE2 receptors 1–4 (EP1-4). Th17 cells and γδT cells can also sensitize nociceptor neurons through IL-17A release and neuronal IL-17RA signaling. Source (Pinho-Ribeiro et al., 2017)*

Prostaglandins are produced upon the cleavage of arachidonic acid by cyclooxygenase enzyme (Basbaum et al., 2009). Prostaglandin E2 acts on its receptors EP1 to sensitize TRPV1, and EP3 to sensitize P2X3 (Huang et al., 2006). In addition, protons activate the proton sensitive GPCR T-cell death-associated gene 8 (TDAG8) in turn, this can sensitize TRPV1 (Dai et al., 2017). On the other hand, 5-HT enhances the function of TRPV1, possibly through 5-HT2 and 5-HT7 receptors (Ohta et al., 2006). 5-HT also enhances the acid activation of ASIC3 and potentiates its role in nociception (Wang et al., 2013).

Studies showed that the sensitization of these ion channels contributes specifically toward location and determination of the type of stimulation. ASIC1a was shown to mainly participate in the primary mechanical hyperalgesia induced by muscle inflammation, while, ASIC3 may play an important role in the secondary mechanical hyperalgesia (Walder et al., 2010). On the other hand TRPV1 is implicated in both thermal and mechanical hyperalgesia associated with inflammation (Huang et al., 2006).

At the central terminals of the nociceptors, intense and/ or prolonged noxious stimulation lead to the integration of NMDA receptors in the synapse (Basbaum et al., 2009). This increases the intracellular concentration of $Ca^{2+}$ in postsynaptic neurons, and in turn, activates $Ca^{2+}$ dependent intracellular signaling pathways leading to synaptic plasticity and the establishment of central sensitization, leading to the establishment and maintenance of chronic pain.

This type of inflammation differs from the inflammation triggered by metabolic stress during obesity which will be described below in section 3.

# 3. Bioactive lipids and pain

Tissue inflammation and tissue damage causes the degradation of the plasma membranes, which generates various pro- and anti-inflammatory lipids. Membrane phospholipids (phosphatidyl-choline, -ethanolamine , -serine and -inositol) are degraded to release pro-inflammatory fatty acids in particular AA, lysophosphatidyl (-ethanolamine [LPE], -serine [LPS] -inositol [LPI], and -choline [LPC]), and lysophosphatidic acid [LPA] (Chiurchiù et al., 2018). Some effects of these lipids are direct modulation of nociceptors activity through actions on ion channels and GPCRs. Other lipids serve as substrate for the synthesis of eicosanoids like prostaglandins and leukotrienes (Smith et al., 2000; Kihara et al., 2014; Chiurchiù et al., 2018).

## 3.1. Lysophospholipids (LPL)

LPL are subdivided into two large groups that include those that possess a sphingosine backbone (lysosphingolipids) and those that contain a glycerol backbone (lyso-glycero-phospholipids) (Chiurchiù et al., 2018). LPL are particularly interesting because they possess pro- and anti-inflammatory properties and can be generated by two completely different pathways. Either they are produce by the activity of phospholipases A2 or they are produced by different reactive oxygen species (ROS) that are generated in significant amounts under inflammatory conditions (Fuchs et al., 2012). LPLs are particularly considered as important signaling molecules in different pathologies such as infertility, cancer, atherosclerosis or inflammatory diseases.

### *3.1.1. Lysophosphatidylcholine (LPC)*

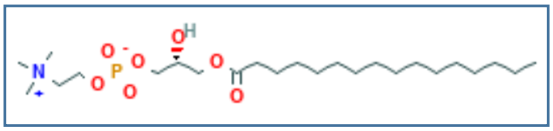

*Figure 10 LPC(16:0)*

LPC is the most abundant LPL (Daniels et al., 2009). It is produced by the hydrolysis of phosphatidylcholine in the plasma membrane by removing the fatty acid on the second carbon of the glycerol by means of the phospholipase A2 enzyme.

LPC affects the curvature of the plasma membrane, in addition it act as a signaling molecule that has proinflammatory properties and it is involved in cell growth and death (Kooijman et al., 2003;

Escribá et al., 2008; Shindou et al., 2013). High levels of LPC were reported in several chronic inflammatory conditions, atherosclerotic lesions, type 2 diabetes, cancers, besides, it can prompt demyelination (Lee et al., 2002; Moreno-Navarrete et al., 2012; Sevastou et al., 2013; Heimerl et al., 2014; Matsuoka et al., 2018; Rivera and Chun, 2008). LPC induces demyelination and mechanical hyperalgesia in rats (Bhangoo et al., 2007). LPC promotes inflammatory skin responses in humans (K. Ryborg, B. Deleuran, H. Søgaard, 2000) . LPC interacts with GPCR and ion channels where it serves as an agonist of G protein-coupled receptor 4 (GPR4) and as an antagonist of G2A (Zhu et al., 2001; Murakami et al., 2004). LPC binding to GPR4 lead to the activation MAPK signaling pathway, while LPC binding to G2A lead to a reduction in it's proton dependent activation.

The role of LPC in regulating the function of TRP channels involved in pain has been studied (Morales-Lázaro et al., 2016). LPC was not reported to interact with TRPV1 or TRPA1 (a polymodal noxious chemo-sensor). Indeed, it was shown that LPC does not affect the temperature activation of TRPV1 channel reconstituted in liposomes (Cao et al., 2013). This excludes a direct effect of LPC on TRPV1 but the possibility of an indirect effect through a metabolic pathway is possible. LPC activates TRPM8 when expressed in heterologous systems. LPC, produced from iPLA2 activity, opens TRPM8 channel and triggers $Ca^{2+}$ influx through the channel at normal body temperature (37°C), a temperature at which the channel is not usually active (Andersson et al., 2007; Gentry et al., 2010). Injection of LPC in mice hind paw potentiates cold sensitivity at 10°C. The cold hypersensitivity induced by high concentration of LPC is absent in TRPM8 knockout mice but conserved in TRPA1 knockout mice (Gentry et al., 2010). Interestingly, Gentry and his colleges also observed that pro-inflammatory poly-unsaturated fatty-acid, including AA, are strong inhibitors of TRPM8.

TRPV2 is expressed in low-threshold mechanosensitive myelinated DRG neurons and was proposed to be involved in mechano-sensation (Martinac, 2014). However, its role in pain is still unclear since knockout mice have normal thermal and mechanical nociception (Park et al., 2011). It is also expressed in CNS astrocytes. In astrocytes, LPC was reported to activate TRPV2 (Shibasaki et al., 2013). LPC and LPI stimulate TRPV2 and enhance the channel's translocation to the plasma membrane in prostate cancer cell (Monet et al., 2009). However, the activation of TRPV2 by LPC

and LPI in these cells is indirect since it requires intracellular signaling through Gi/Go and PI3,4K pathways.

LPLs modulate the activity of $K^+$ channels involved in pain sensing. The background $K^+$ channels of the TREK and TRAAK family are activated by LPLs with long hydrophobic acyl chains and large polar heads, such as LPC and platelet-activating factor. However, these lipids do not have a direct effect on TREK and TRAAK channels since they require cell integrity. They are not effective in the excised membrane recording configuration of patch-clamp or when they are applied on the intracellular side of the membrane (Lesage et al., 2000; Maingret et al., 2000).

LPC was also shown to activate ASIC3 channels (Marra et al., 2016) and this study have great relevance to my project therefore it will be described later in ASIC3 and pain section.

### *3.1.2. Lysophosphatidic acid (LPA)*

lyso-phosphatidylcholine is a precursor of LPA where it is produced intracellularly from LPC by the action of lyso-phospholipase D, and extracellularly by autotaxin (ENPP2) (Federico et al., 2008). In addition, it is also produced from phosphatidic acid by phospholipases A1 or A2 (PLA1/2). Therefore, LPC and LPA conserve a fatty-acyl chain of 16 to 22 carbons that can be saturated, mono-unsaturated or poly-unsaturated (Block et al., 2010). The nature of the fatty acid chain may also has a functional role.

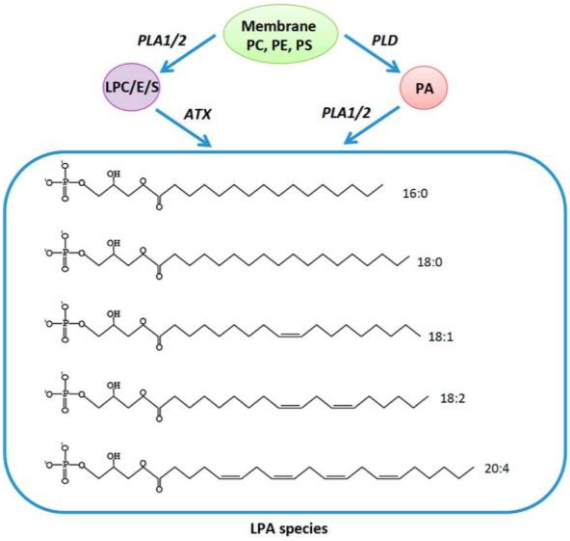


*Figure 11 LPA biosynthesis (Riaz et al., 2016)*

LPA has several biological effects including cell growth, differentiation, proliferation, survival, motility, and pain. LPA actions are mainly mediated by six specific GPCRs, LPA1−6. These GPCRs initiate different signaling pathways through Gα proteins (Gi, Gq, G12, and Gs) inducing different tissue responses (Riaz et al., 2016). In the nervous system, LPA signaling has been shown to play important role in neuronal development and myelination (Yung et al., 2015). LPA was shown to modulate pain signals where intrathecal injection of LPA induce neuropathic like behaviors, mechanical allodynia and thermal hyperalgesia, that lasted for 7 to 8 days (Inoue et al., 2004). Another study reported that wild-type mice injected with LPC intrathecally also showed neuropathic pain like behavior with mechanical and thermal hyperalgesia (Inoue et al., 2008a). This neuropathy is lost in mice lacking the LPA receptor LPA1 suggesting that the effect of LPC on pain is mediated through its degradation to LPA. In addition, partial attenuation of autotaxin, the enzyme responsible for converting LPC to LPA, in heterozygous mutant mice lowered the neuropathy induced by the intrathecal injection of LPC (Inoue et al., 2008b). Altogether, these data show that the injected LPC was converted to LPA by autotaxin, and in turn, LPA activates LPA1 receptor expressed in the DRG neurons to induce neuropathic like pain.

LPA could be involved in C-fiber retraction associated with some types of neuropathy (Ueda, 2008). These effects were shown to be mediated through activation of LPA1 receptors that initiate downstream signaling pathways and possibly interacting directly or indirectly with several ion channels including TRPV1, TRPA1, Nav, K2P, and Cav leading to the modulation of their activity.

TRPV1 was found to be directly targeted by LPA and the pain induced by LPA is reduced in TRPV1 knockout mice (Nieto-Posadas et al., 2011). This interaction was shown to be mediated through a direct interaction with the C-terminus of the channel. LPA also interact with TRPA1, another member of the TRP channels. However, this activation induced itch behavior rather than pain when LPA was injected in mice (Kittaka et al., 2017).

Nav1.7-1.9 are expressed in small DRG neurons and they are important in the initiation and the propagation of pain signals in nociceptors (Theile and Cummins, 2011). LPA enhances Nav1.8 and Nav1.9 currents in small DRG neurons (Seung Lee et al., 2005). In addition, the expression of Nav1.8 and LPA1 receptors is upregulated in rat DRG neurons after LPA injection, and this upregulation is blocked by LPA1 receptor antagonist (Pan et al., 2016). In a model of pain induced

by bone cancer, LPA1 receptors and Nav1.8 expression are elevated and by blocking LPA1 receptors the expression of Nav1.8 is reduced and the associated hyperalgesia is partially attenuated. Further experiments confirmed that the interaction between the LPA1 receptors and Nav1.8 is mediated by PKCε (Pan et al., 2016). Beside these channels, several K2p channels were reported to be activated by LPA. TRESK channel is involved in the neuronal excitability and mice lacking it's gene needed less current to elicit action potentials (Cohen et al., 2009), while overexpressing this channel reduced neuronal responses to capsaicin (Guo and Cao, 2014). TRESK expression is co-localized with LPA2 receptors in small diameter DRG neurons (Kollert et al., 2015). In cells co-expressing TRESK and LPA2 receptor, the application of LPA increases basal potassium currents, an effect dependent on the LPA2 receptors. This indicates that LPA can induce opposite effects on DRG neurons excitability through activation of either TRPV1 or TRESK channels. Yet it is unclear under which condition LPA induces rather than inhibits pain. Other members of K2P channels including TREK1, TREK2 and TRAAK, were also shown to be positively regulated by LPA. The mechanism behind this regulation is still unknown but it was suggested that the effect of LPA on the membrane curvature open the machano-sensitive TREK-TRAAK channels (Chemin et al., 2005).

Voltage gated calcium channels are implicated in the pain pathway as they play an important role in releasing excitatory neurotransmitters and/or neuropeptides at the central synapses of the nociceptors (Sekiguchi et al., 2018; Zamponi et al., 2009). When the action potentials reaches the central terminals of primary neurons, the depolarization trigger the activation of Cav channels. Cav channels are modulated by accessory subunits (Dolphin, 2016). It was reported that intrathecal injection of LPA triggered upregulation in the expression of α2δ1 subunit of HVA calcium (Cav2.2) in DRG neurons, producing neuropathic pain similar of nerve injury (Inoue et al., 2004). Indeed, this up regulation was lost in LPA1 receptor knockout mice, indicating that it was mediated by LPA1 receptor activation. In addition, Cav3.2, which is expressed in nociceptors, was also shown to be positively regulated by LPA enhancing its currents in native rat DRG neurons (Iftinca et al., 2007; Rose et al., 2013).

## 3.2. Sphinoglipids

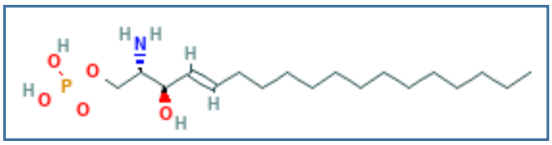

*Figure 12 Sphingosine 1-phosphate*

Members of the sphinoglipids including ceramides and their byproducts (sphingosine-1 phosphate) participate in several inflammatory processes in addition to controlling intracellular trafficking and signaling, cell growth, adhesion, vascularization, survival, and apoptosis (El Alwani et al., 2006). Increased ceramide signaling was linked to inflammation in the adipose tissue and insulin resistance leading to obesity and type 2 diabetes through over activating the immune cells including macrophages and B cells (Haus et al., 2009; Błachnio-Zabielska et al., 2012; Chaurasia and Summers, 2015). A causal link between sphingolipids and neuropathic pain has been found in many studies in rodents. In addition, some mutations in the genes SPTLC1 and SPTLC2, which encode serine palmitoyl-transferase, an enzyme that in turn drives sphingolipids synthesis, lead to neuropathic pain in humans because of the production of a neurotoxic sphingoid metabolite (Emery and Wood, 2018).

## 3.3. Eicosanoids

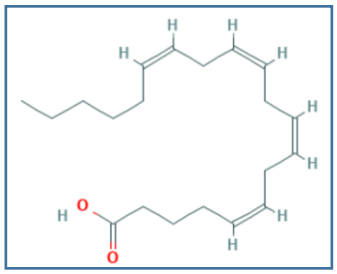

*Figure 13 Arachidonic acid*

Eicosanoids are a group of bioactive lipids that produce prostaglandins (PGs), prostacyclins, thromboxanes (TXs), leukotrienes (LTs), hydroxyeicosatetraenoids (HETEs), and lipoxins (LX) HETEs and epoxyeicosatrienoids (Dennis and Norris, 2015). These molecules share the same precursor, arachidonic acid originated from ω-6 polyunsaturated fatty acid. Several enzymes use AA as substrate to produce the different types of Eicosanoids. Cyclooxygenases 1 and 2 (cox -1/2)

produce PGs, prostacyclins, and TXs. lipoxygenases (LOX) produce LTs, HETEs, and LX, while P450 epoxygenase generates HETEs and epoxyeicosatrienoids.

This family of biolipids is involved in several functions including control of vascular tone, platelet aggregation, ovulation, and embryo implantation, in addition to pain perception (Chiurchiù et al., 2018). Prostaglandins specially PGD2, PGE2, PGI2, and PGF2α are well known for their contribution in the initiation of acute inflammation, and the most widely used anti-inflammatory drugs, nonsteroidal anti-inflammatory drugs NSAID, exhibit there effect mainly through inhibiting COX1/2 leading to suppression of the production of these prostaglandins. In addition to their contribution in acute inflammation, recent studies described their possible contribution in chronic inflammation as they prompt the transition to chronic inflammation, reviewed in (Vane, 2002). LTs also play an important role in acute inflammation, where they help in the induction of edema, and neutrophil influx associated with acute inflammation (Dennis and Norris, 2015).

In addition, they can enhance the inflammatory signals leading to the tissue damage associated with several chronic inflammatory diseases. Recently, several studies showed that genetic variations in genes that lead to changes in eicosanoids biosynthesis or those affecting the functioning of their receptors can increase the susceptibility to chronic inflammatory disorders including Crohn's disease, asthma, multiple sclerosis, inflammatory bowel disease, psoriasis, and rheumatoid arthritis (Lee et al., 2015; Fredman et al., 2016), for review (Chiurchiù et al., 2018).

### 3.4. Specialized pro-resolving lipid mediators

Specialized pro-resolving lipid mediators (SPM) is a group of newly discovered bioactive lipids that serves as anti-inflammatory, opposing the effect Eicosanoids. They act as "immune-resolvents", leading to a shortened 'inflammation resolution time' by activating endogenous resolution programs, promoting tissue regeneration and healing (Serhan, 2014). They exhibit these effects through reducing the infiltration of leukocyte, recruiting and stimulating of non-phlogistic mononuclear cells, enhancing the killing and clearance of pathogens, macrophage-mediated phagocytosis of apoptotic granulocytes and inhibition of pro-inflammatory cytokines while increasing the production of anti-inflammatory mediators (Buckley et al., 2014). They are produced during the peak of acute inflammation from ω-6, AA and ω-3 polyunsaturated fatty

acids, PUFA, by the same enzymes involved in the production of eicosanoids (COXs, LOXs, and P450) (Chiurchiù et al., 2018).

## 3.5. Endocannabinoids

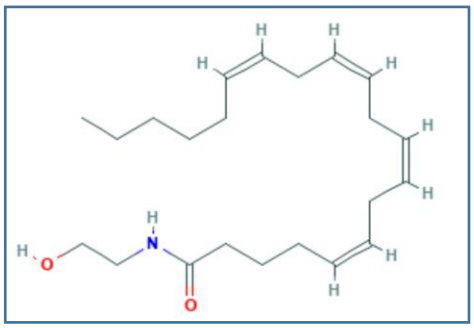

*Figure 14 Anandamide*

Endocannabinoids are a group of endogenous bioactive lipids that are produced in most tissues and immune cells (Maccarrone et al., 2014). They include Arachidonoyl-ethanolamide (anandamide, AEA) and 2-arachidonoylglycerol (2-AG). They activate the cannabinoid receptors type-1 and type-2 (CB1 and CB2) (Lu and Mackie, 2016). On the other hand, endocannabinoids can also bind to six TRP channels (TRPV1, TRPV2, TRPV3, TRPV4, TRPA1, and TRPM8), and GPCRs (Zygmunt et al., 1999; Muller et al., 2018). However, endocannabinoids may have opposite effects on TRP channels. AEA is an endogenous agonist of TRPV1, but it is also an antagonist of TRPM8. Endocannabinoids can regulate the activity of several immune cells, and they exhibit anti-inflammatory effects (Chiurchiù et al., 2018). Malfunctioning in the endocannabinoids system was found in several chronic inflammatory diseases including cancer, metabolic and gastrointestinal diseases, autoimmune and neuro-inflammatory disorders.

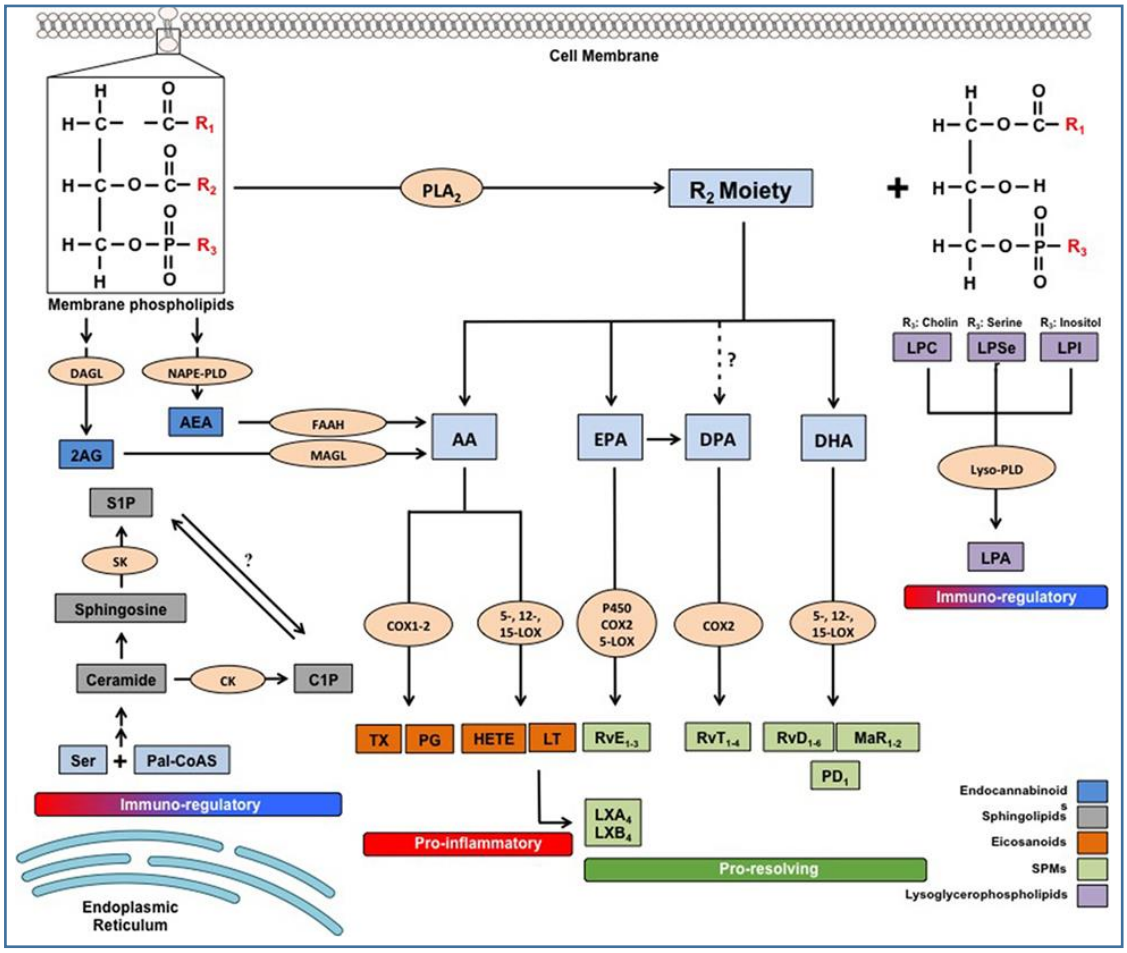


*Figure 15 Bio-synthesis of bioactive lipids.*
*Source (Chiurchiù et al., 2018)*

## 4. Ion channels

Ion channels are pore-forming transmembrane proteins that allow the flow of ions across membranes. They are responsible for the rapid signaling in the nervous system. They induce rapid changes in the transmembrane electric potential. This leads to action potentials generation that travel along the axons.

There are several families of ion channels where each family respond to specific type of electrical, mechanical or chemical signals. Upon activation, the ion channels undergo conformational changes in their structure forming a transmembrane pore, where ions can pass through it to cross the membrane down their electric and chemical gradients (Barker et al., 2017). Malfunctioning of ion channels therefore can lead to many neurological diseases and disorders including cardiac and skeletal muscles diseases.

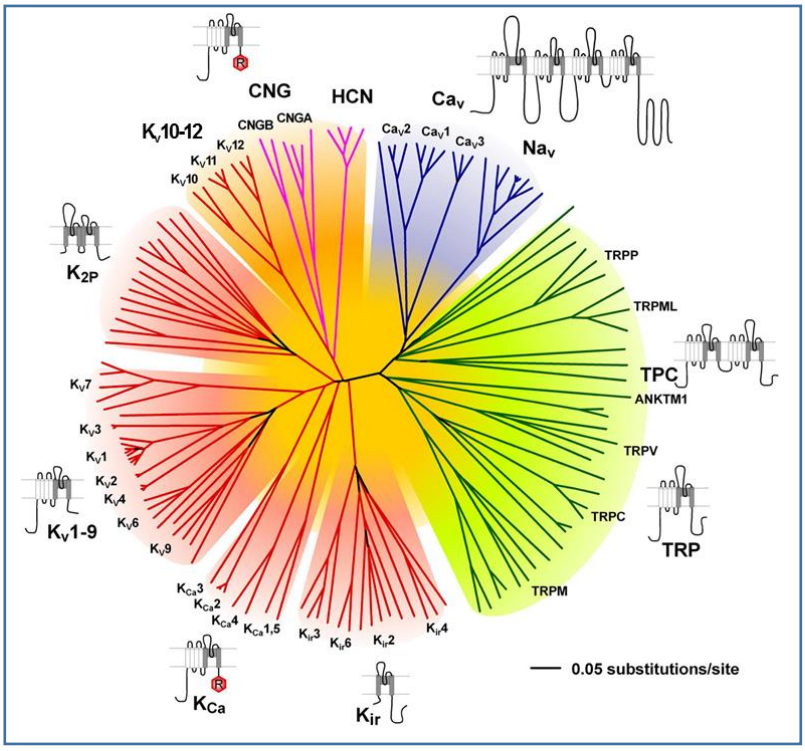


*Figure 16 Voltage gated and voltage gated-like ion channels.*
*Voltage gated ion channels include Na, K, Ca and some Cl channels. Voltage-gated-like (VGL) channels share several structural similarities (e.g., K, Na, Ca, HCN and TRP channels). voltage-insensitive ion channels gated by second messengers and other intracellular and/or extracellular mediators (such as certain K and Cl channels, TRP channels, ryanodine receptors and IP3 receptors). Source (Harding et al., 2018).*

## 4.1. Ion channels implicated in pain

### *4.1.1. Voltage gated sodium channels*

Navs are formed of six transmembrane α-helical segments, from S1–S6. Both C and N termini are intracellular. Several interact with the α-subunit. The β-subunits play an important role in modulating Navs activity and expression. Segments S5 and S6 are connected by the P-loop that form the ion pore. They are selectively permeable to $Na^+$ ions (Barker et al., 2017). Navs are voltage-gated channels that opens upon depolarization of the membrane potential. Upon the opening of the channel, the influx of $Na^+$ ions to the neurons allow further depolarization, which is responsible for the rapid uprising phase of the action potential (Catterall, 2017). There are 10 α-subunit isoforms for Nav, Nav1.1–1.9 in addition to Nax. Besides there are four β-subunits (β1–4). These channels are further classified based on their sensitivity to the puffer-fish toxin tetrodotoxin (TTX). TTX-sensitive channels include Nav1.1 to 1.4, 1.6, and 1.7 while Nav1.5, 1.8, and 1.9 are resistant to TTX. Nav1.1, Nav1.6, Nav1.7, Nav1.8, and Nav1.9 are expressed in the PNS. Nav1.7, 1.8 and 1.9 are specific to the PNS (Catterall, 2017). Alterations in the function of Navs are associated with several diseases and disorders including pain (Dib-Hajj et al., 2010; Bennett and Woods, 2014).

Nav1.3 is not initially expressed in the DRGs but it's expression is upregulated upon peripheral nerve injury and spinal cord injury. This expression upregulation could be involved in the increased pain hypersensitivity associated with these conditions (Black et al., 1999; Hains et al., 2003). Gain of function mutation of Nav1.8 was identified in patients suffering from painful small fiber neuropathy (Faber et al., 2012), while the deletion of the channel in mice led to the attenuation to noxious mechanical and thermal stimuli and insensitivity to noxious cold stimuli (Akopian et al., 1999; Zimmermann et al., 2007). Nav1.9 was shown to be upregulated in inflammatory disorders and diabetic neuropathy (Priest et al., 2005; Amaya et al., 2006; Lolignier et al., 2015). Mutations in Nav1.7 that lead to loss of function was found in patients suffering from congenital indifference to pain (CIP) (Goldberg et al., 2007). These patients were unable to recognize painful stimuli. On the other hand, patients with severe pain disorders including inherited erythromelalgia and paroxysmal extreme pain disorder were shown to have gain of function mutations in the Nav1.7 (Habib et al., 2015).

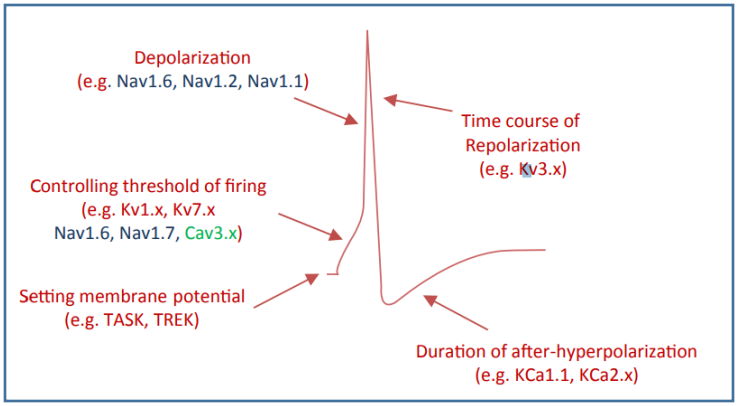


*Figure 17 Ion channels involved in action potential generation.*
*Source (Barker et al., 2017)*

### 4.1.2. $K^+$ Channels

$K^+$ Channel family forms a large super family of hyperpolarizing ion channels with more than 80 gens coding for $K^+$ channels in human (Coetzee et al., 1999). They play a crucial role in controlling resting membrane potential. They allow selectively the follow of $K^+$ ions across the plasma membrane usually leading to the efflux of $K^+$ ions out of the cells inducing hyperpolarization. They respond to a variety of stimuli including variation in the voltage, pH, intracellular calcium concentration, and lipids (Maingret et al., 1999, 2000; Lesage et al., 2000). $K^+$ Channel family could be sub-classified into four main families: inward rectifying (Kir), voltage-gated (Kv), $Ca^{2+}$-activated (KCa), and two-pore domain background $K^+$ channels (K2P). Members of this family are involved in controlling the resting membrane potential, action potential threshold, and the repolarization phase of the action potential (Busserolles et al., 2016). $K^+$ channels from all four families are expressed in DRG neurons and numerous studies have associated $K^+$ channels activity to acute and chronic pain conditions (Tsantoulas and McMahon, 2014; Flegel et al., 2015). We have described the regulation of the K2P channels TRESK and TREK-TRAAK channels by lipids. These channels are largely expressed in DRG neurons (Alloui et al., 2006; Kang et al., 2005). TREK-TRAAK channels are mechano and thermo-activated channels (Kang et al., 2005). They have been involved in the control of temperature perception threshold and mechanical sensitivity of mice (Alloui et al., 2006; Noël et al., 2009, 2011; Acosta et al., 2014). Knockout mice for TREK and TRAAK channels show mechanical allodynia. These channels are also involved in inflammatory pain perception. It has been proposed that TREK-TRAAK channels oppose nociceptors activation by other temperature sensitive excitatory channels like thermo-TRP channels. They prevent the activation of nociceptive

neurons at moderate temperatures (between 18°C and 42°C) that should not be perceived as noxious. TRESK is modulated by changes in membrane tension and mice lacking TRESK show mechanical allodynia (Callejo et al., 2013). TRESK has been involved in the regulation of nociceptive neuronal excitability after nerve injury (Tulleuda et al., 2011). A dominant-negative mutation in TRESK was associated with familial migraine with aura (Lafrenière et al., 2010; Liu et al., 2013). TRESK mutation produces a non-functional channel and a second protein fragment that co-assembles with and inhibits TREK1 and TREK2 channels. This down-regulation of TRESK, TREK1 and TREK2 increases trigeminal sensory neuron excitability leading to a migraine-like phenotype in rodents (Royal et al., 2019).

### *4.1.3. Calcium channels*

The intracellular concentration of $Ca^{2+}$ has high importance as it perform several functions from gene expression and translation, muscle contraction, neurotransmitter release, cell signaling, apoptosis, learning and memory (Berridge et al., 2000; Bourinet et al., 2014). Calcium channels are permeable selectively to $Ca^{2+}$ ions. As the concentration of the intracellular $Ca^{2+}$ is very low compared to the extracellular, the opening of the $Ca^{2+}$ channels lead to $Ca^{2+}$ influx. $Ca^{2+}$ channels shares a similar common structure despite the big variability in their function and pattern of activation. $Ca^{2+}$ channels respond to changes in membrane potentials, where they could be classified as high voltage activated (HVA) or low voltage activated (LVA) (Barker et al., 2017). Among the HVA are the L-type calcium channel (Long-Lasting, dihydropyridin receptor) or Cav1.1-1.4, the P/Q-type calcium channel (P for Purkinje) or Cav2.1, and the N-type calcium channel (Neuronal) or Cav2.2. The R-type calcium channel (Residual) or Cav2.3 is intermediate voltage activated. The LVA are the T-type calcium channel (Transient) or Cav3.1-3.3 (Bourinet et al., 2014).

Calcium channels involved in pain include Cav2.2, which is widely expressed in the central terminals of the peptidergic C-fibers. Its expression is elevated in response to nerve injury and tissue inflammation (Lee, 2013). Genetic deletion of CaV3.2 channels lead to reduced acute mechanical, thermal and chemical pain without affecting mice responses toward neuropathic pain induced by spinal nerve ligation (Lee, 2013). In addition, α2δ an auxiliary subunit of the HVA $Ca^{2+}$ channels was found to be overexpressed in DRG neurons of neuropathic animal models. Gabapentin, a drug that is used to treat epilepsy, and neuropathic pain, was proposed as GABA

receptor agonist. later it was found that this drug binds to the auxiliary subunit of the HVA $Ca^{2+}$ channels, α2δ-1 and α2δ-2 decreasing the trafficking of the channels to the membrane and reducing the generated $Ca^{2+}$ currents (Barker et al., 2017). Cav3.2 is expressed in nociceptors and the downregulation of these channels by intrathecal injection of antisense oligodeoxynucleotides significantly attenuated acute noxious thermal and mechanical perception of rats (Bourinet et al., 2005). In addition, the downregulation of Cav3.2 was able to alleviating thermal and mechanical hyperalgesia associated with a model of neuropathy, chronic constriction injury (Bourinet et al., 2005). Colonic nociceptive fibers are responsible for the exaggerated pain perception associated with a model of irritable bowel syndrome IBS. These fibers express Cav3.2 where the genetic inhibition and pharmacological blockade of this channel attenuated IBS-like painful symptoms (Marger et al., 2011).

### *4.1.4. Transient Receptor Potential Channels (TRP)*

TRP channels are nonselective cation channels that are permeable to $Na^{+}$ and $Ca^{2+}$. These channels can be activated by a variety of stimuli including changes in temperature described earlier in the thermos-sensation. They are activated by pH, change in pressure, lipids, and natural compounds while their activation is affected by membrane potential. Upon activation, these channels tend to depolarize the neurons through influx of cations (Nilius et al., 2005). This family of receptors is divided into six subfamilies including TRPV (vanilloid), TRPA (ankyrin), TRPM (melastatin), TRPC (canonical), TRPML (Mucolipin), and TRPP (Polycystin) (Barker et al., 2017). A numerous amount of studies have shown the role of TRP channels in acute, inflammatory and neuropathic pain reviewed in (Sexton et al., 2014).

TRPV1 expressed in peptidergic small and medium neurons. It does not contribute significantly to the acute thermal perception but it is involved in the thermal hyperalgesia associated with inflammation (Caterina et al., 1997). On the contrary, TRPV1+ neurons was found to be the main sensory afferents responsible for conveying thermal sensation (Mishra et al., 2011). TRPV2 is also expressed in peptidergic small and medium neurons and was shown to be upregulated in the DRG neurons in response to inflammatory insult (Caterina et al., 1999). TRPV3 is expressed in a subset of TRPV1 expressing neurons. Studies suggested that this channel contribute to the acute thermal perception (Smith et al., 2002). TRPV4 is involved in Inflammatory mechanical and thermal

hyperalgesia (Facer et al., 2007). TRPC1 and TRPC6 are expressed in peripheral sensory neurons and they were found to be involved in the mechanical hyperalgesia induced by inflammatory and neuropathic insults (Elg et al., 2007; Alessandri-Haber et al., 2009)

*Table 2 TRP channels distribution and the associated types of pain.*

| TRP | Peripheral sensory neuron expression | Possible role in pain | References |
|---|---|---|---|
| TRPV1 | Peptidergic small- and medium-diameter sensory neurons | Inflammatory hyperalgesia- Acute thermal - perception acute noxious pain. | (Caterina et al., 1997; Mishra et al., 2011; Vandewauw et al., 2018) |
| TRPV2 | Peptidergic small-diameter and mediumdiameter fibres | Appears to be upregulated in DRG in certain models of inflammatory pain, though functional significance unclear. | (Caterina et al., 1999) |
| TRPV3 | Peptidergic small- and medium-diameter sensory neurons (in a subset of TRPV1+ neurons) and keratinocytes | Acute noxious heat. | (Peier et al., 2002a, 2002b; Smith et al., 2002) |
| TRPV4 | Small- and medium-diameter sensory neurons | Inflammatory mechanical and thermal hyperalgesia. | (Facer et al., 2007) |
| TRPA1 | Peptidergic small- and medium-diameter sensory neurons (co-expressed with TRPV1) | Acute noxious cold mechanosensation – acute noxious pain. | (Story et al., 2003; Vandewauw et al., 2018) |
| TRPM3 | Large subset of small-diameter sensory neurons from dorsal root and trigeminal ganglia. | noxious heat and in the development of inflammatory heat hyperalgesia | (Vriens et al., 2011; Vandewauw et al., 2018) |
| TRPM8 | Small-diameter, capsaicin-insensitive neurons (higher expression in TG than DRG) | Innocuous cold, noxious cold activated by temperatures 8 –28 °C. | (McKemy et al., 2002) |
| TRPC1 | Peripheral sensory neurons. Co-expressed with TRPV4 and TRPC6 | Mechanical hyperalgesia | (Elg et al., 2007; Alessandri-Haber et al., 2009) |
| TRPC6 | Most peripheral sensory neurons co-expressed with TRPV4 and TRPC1 in peripheral sensory neurons | (Mechanical hyperalgesia | (Alessandri-Haber et al., 2009; Quick et al., 2012) |

TRPV1 is selectively activated by capsaicin, where its application to DRG depolarizes the neuron and triggers action potentials. A study showed that the $Ca^{2+}$ activated chloride channel Anoctamin-1 (ANO1, TMEME16A) is co-expressed with TRPV1 in DRG neurons and contribute to the response of neurons to capsaicin. Inactivation of ANO1 inhibits the action potentials generated by neurons

in response to the application of capsaicin. This show that the coupling of these two channels are important for the triggering of action potentials associated with capsaicin application (Takayama et al., 2015). Another recent study showed that behavioral responses to heat involve the co-activation of three different TRP channels, TRPV1, TRPA1, and TRPM3. Triple knockout mice, lacking genes of these three channels, showed severe impaired acute withdrawal responses to noxious stimuli (Vandewauw et al., 2018).

### *4.1.5. Hyperpolarization-activated cyclic nucleotide–gated (HCN)*

HCNs are particular ion channels that are activated in response to hyperpolarization within the range of -60 to -90 mV. They are constitutively opened at voltages near the resting membrane potentials. This mode of activation differs to all other voltage gated ion channels that are activated upon membrane depolarization (Tsantoulas et al., 2017). These channels are permeable to $Na^+$ and $K^+$ ions (Benarroch, 2013). Four HCN isoforms were identified in the sensory neurons HCN 1-4. HCN4 is expressed in the heart. HCN2 is highly expressed in small fibers. HCN3 is expressed in all sensory neurons. Large diameter neurons express HCN1. HCN are well-known for their important contribution in the pacemaker potential of the heart nevertheless their role in different pathological pain conditions including inflammatory and neuropathic is significantly emerging (Emery et al., 2012).

Increased levels of intracellular cAMP reduce the threshold for HCN2 and HCN4 activation by depolarization where more positive membrane voltages activate the channels leading to the generation of depolarizing currents. As described earlier, during pathological conditions like inflammation PGE2 and bradykinin are released by various cells, in turn, they increase the activity of adenylate cyclase leading to a rise in the intracellular cAMP concentration. High levels of cAMP interact with HCN2 leading to increased spontaneous action potentials firing (Emery et al., 2011). The role of HCN2 in pain models of diabetic neuropathy will be described later in section 4.

Acid sensing ion channels are the focus of this study therefore they will be described in a separate section.

# 5. Acid Sensing Ion Channels

The extracellular physiological pH in most tissues is maintained around 7.4. This pH can vary under certain physiological and pathological conditions including infection, inflammation, ischemia, tissue damage, and tumors (Reeh and Steen, 1996; Immke and McCleskey, 2001; Dubé et al., 2009). For instance, lactate acid and $CO_2$ can accumulate in muscles following exercise or due to modification in tissue metabolism and perfusion leading to changes in the extracellular pH. Protons can be directly released from lysed cells, activated immune cells, voltage-gated proton channels and excessive synaptic vesicle release. This lead to the lowering of the extracellular pH (Wang and Xu, 2011; Zeng et al., 2015; Rash, 2017a). In 1980 Krishtal and Pidoplichko showed that the application of low pH to isolated DRG and TG neurons induces cationic currents, highlighting the existence of a proton gated channel with a probable role in nociception (Krishtal and Pidoplichko, 1980). Later it was discovered that acid sensing ion channels are responsible for these depolarizing currents (Price et al., 1996; Waldmann et al., 1996).

ASIC channels belong to the family of degenerin/epithelial sodium channels (ENaC). They include six members (ASIC1a/b, ASIC2a/b, ASIC3, and ASIC4). These subunits can combine forming functional homomerics or heteromerics channels except for ASIC2b homomeric coupling do not form a functional channels (Deval et al., 2010). ASIC4 are not activated by low pH and its function is not known yet (Lin et al., 2015a). The homomerics or heteromerics channels have different pH sensitivity, activation and inactivation kinetics and pharmacological properties (Hesselager et al., 2004; Cristofori-Armstrong and Rash, 2017).

## 5.1. Structural and biophysical properties

ASICs exhibit a relatively simple topology compared to voltage-gated channels. It is composed of 500-560 amino acids and each subunit has two transmembrane domains (Saugstad et al., 2004). A functional channel is formed by the herteromerization of three subunits, resulting in a large extracellular domain, a small transmembrane region, and an intracellular N- and C-termini. The extracellular domain contains an acidic pocket that allows the binding of proton (Deval et al., 2010). The binding of a proton induces conformational changes allowing the opening of the channel and the flow of ions (Ramaswamy et al., 2013).

ASICs are more permeable to $Na^+$ ions with 10 folds higher than its permeability to $Ca^{2+}$. The activation of ASICs lead to rapid influx of the ions leading to a peak current that inactivates relatively rapid depending on the subunits forming the channel. ASIC3 and ASIC1 are more sensitive to moderate acidification compared to ASIC1a/ASIC2a heteromers with half activation $pH_{50}$ at 6.5-6.7, 6.4-6.6, and 4.8-5.4 respectively (Gründer and Pusch, 2015). After the peak current the homo and heteromeric channels containing ASIC3 and the herteromerics channels containing ASIC2b do not inactivate completely, forming a plateau current that is sustained as long as the acidification is maintained (Gründer and Pusch, 2015). ASIC3 sustained currents result from two different mechanisms based on the level of acidification. Shifting to moderate acidification (pH6.5) from pH7.4, produce sustained current resulting from window current that is formed due to the overlap of the activation and inactivation curves. On the other hand, strong acidification below pH6 induces sustained current by a different gating mechanism (Salinas et al., 2009). In primary neuronal cultures, the activation of ASICs lead to depolarization that can trigger action potentials in the presence of inflammatory signals (Mamet et al., 2002). In addition, ASIC3 window currents is potentiated by inflammatory signals and this was proposed to be responsible for the non-adapting pain associated with tissue acidosis (Deval et al., 2008, 2010).

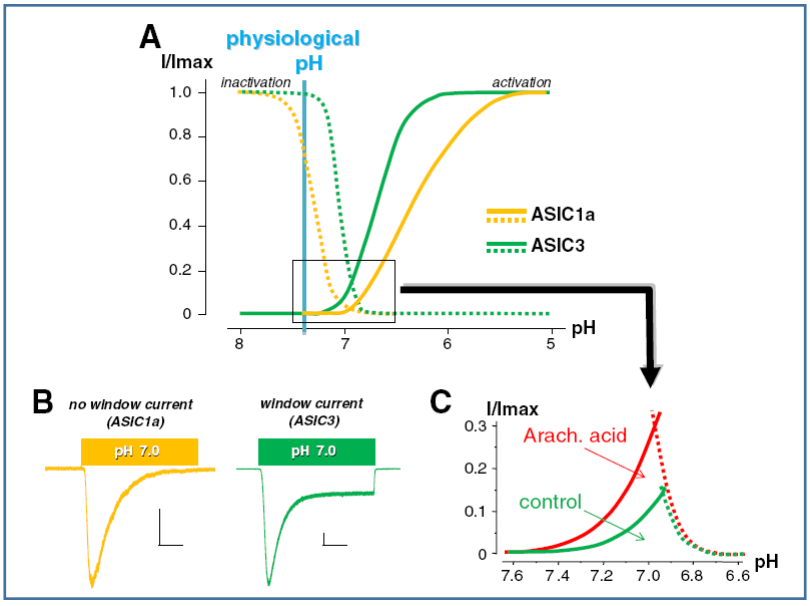


*Figure 18 Shape of ASIC currents.*
*A) pH-dependent activation and inactivation curves of ASIC1a and ASIC3 currents. B) Traces of currents evoked by extracellular acidification (voltage clamp configuration) for ASIC1a (left) and ASIC3 (right) C) The window current seen in ASIC3 channels is potentiated by arachidonic acid. Source (Deval et al., 2010).*

## 5.2. Distribution of ASICs

ASICs are expressed in neuronal and non-neuronal cells. In the CNS ASIC1a, ASIC2 and ASIC4 are the dominant subunits while in the PNS the expression of ASIC1b and ASIC3 seems to be dominant (Waldmann et al., 1996; García-Añoveros et al., 1997; Lingueglia et al., 1997; Waldmann et al., 1997a, 1997b; Baron et al., 2002a; Wemmie et al., 2002, 2003; Wu et al., 2004; Baron et al., 2008). There are controversy data regarding the expression of ASIC3 as it was initially suggested to be expressed only in the peripheral neuron (Waldmann et al., 1997b), yet some studies described its expression in both peripheral and central nervous system (Babinski et al., 1999; Wu et al., 2010; Wang et al., 2014). ASIC1a and ASIC3 channels are co-localized in sensory neurons (Rosa et al., 2002; Voilley et al., 2001). In the CNS ASIC1a is expressed in the amygdala and it can elicit fear (Ziemann et al., 2009), while its expression in the brain stem can control respiration (Huda et al., 2012). ASIC4 are widely expressed in the pituitary gland (Akopian et al., 2000; Gründer et al., 2000). in the PNS ASICs are expressed in the dorsal root and trigeminal ganglia, retina, cochlear hair cells, taste receptors, and vagal afferents (Rash, 2017b). ASICs are also expressed in non-neuronal cells like central and peripheral immune cells (e.g., astrocytes, microglia, macrophages, leukocytes, etc.), bone cells (osteoclasts and osteoblasts), adipose cells, and vascular endothelial cells (Kellenberger and Schild, 2015; Lin et al., 2015b). Within sensory fibers, ASIC3 is expressed in most peptidergic neurons expressing TRPV1. Also it is expressed in Low mechano receptors, A fibers, figure 19 (Emery and Ernfors, 2018).

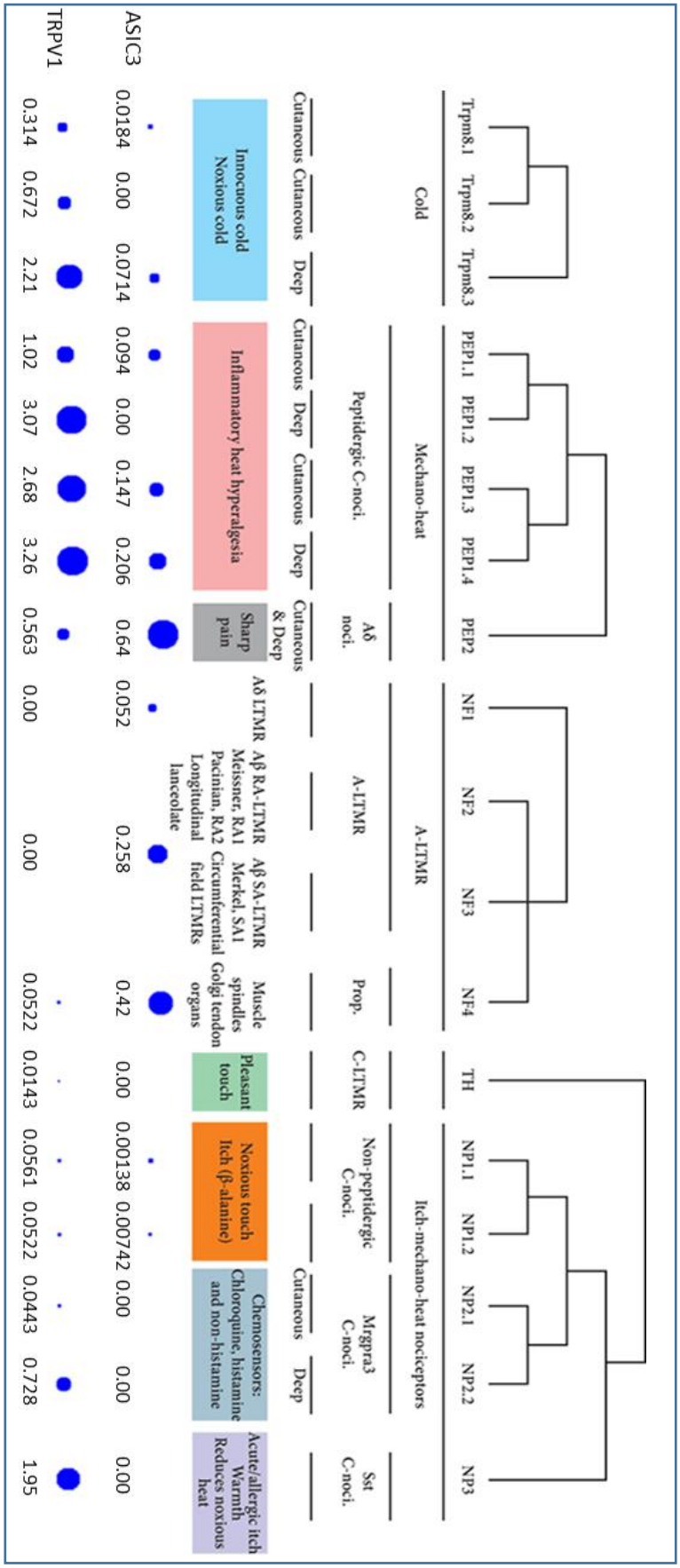


*Figure 19 ASIC3 and TRPV1 level of mRNA expression within the different sensory afferents. adapted from http://mousebrain.org/ (Zeisel et al., 2018)*

## 5.3. Pharmacology and modulators

### *5.3.1. Pharmacological blockers and activators*

The further characterization of ASICs and the study of their functions were possible due to several pharmacological tools that can activate or inhibit them. The first described inhibitor of ASICs was amiloride that blocks all homomeric ASIC channels with an IC50 of 10-30µM. Nevertheless high concentrations of amiloride above 200µM is able to potentiate ASIC3 sustained currents (Waldmann et al., 1996, 1997a, 1997b). It has poor selectively to ASICs as it act on members of ENaC family and it induce potassium sparing effect for which it was used primarily as a diuretic (Canessa et al., 1994).

PcTx1 a peptide extracted from tarantula venom can inhibit homomeric ASIC1a, and the heteromeric ASIC1a/ASIC2 channels (Escoubas et al., 2000; Sherwood et al., 2011; Joeres et al., 2016). On the other hand, PcTx1 tends to potentiate homomeric ASIC1b (Chen et al., 2006). The intrathecal and intracerebro-venticular injections of PcTx1 induced analgesia (Duan et al., 2007; Mazzuca et al., 2007). Mambalgin is a peptide extracted from the venom of the black mamba snake. It was discovered in our team by Sylvie Diochot. Mambalgin can potently block ASIC1 containing channels with IC50 of less than 10nM (Diochot et al., 2012). The peptide APeTx2 extracted from the sea anemone Anthopleura was also discovered by Sylvie Diochot. Among the ASIC family APETx2 selectively blocks homomeric and heteromeric channels containing ASIC3 with IC50 between 37 and 2000nM (Diochot et al., 2004). Beside its affinity to ASIC3 channels, APETx2 was shown to block some members of the voltage gated sodium channels (Nav1.2, Nav1.8) in addition to hERG (Blanchard et al., 2012; Jensen et al., 2012; Peigneur et al., 2012). Peripheral injection of APETx2 induce analgesic effect (Deval et al., 2008).

Non-steroidal anti-inflammatory drugs were also shown to block ASICs. Ibuprofen inhibits ASIC1a, whereas salicylic acid, aspirin, and diclofenac can inhibit the sustained currents of ASIC3 (Voilley et al., 2001). Micro-molar concentrations of Zinc can uniquely potentiate homomeric and heteromeric ASIC2a, while at nano-molar concentrations, it can inhibit ASIC1a containing homomeric and hetermeric channels (Baron et al., 2001; Gao et al., 2004). ASIC3 can be potentiated by agmatine and GMQ (2-guanidine-4-methylquinazoline) (Rash, 2017b). GMQ achieve this effect by shifting the pH activation curve of ASIC3 to more alkaline values while shifting

the inactivation curve to more acidic values, thus allowing the formation of a large window current at the neutral pH 7.4 (Yu et al., 2010; Alijevic and Kellenberger, 2012).

### 5.3.2. *Inflammatory mediators and ASICs*

Several studies addressed the involvement of ASICs in inflammatory states, with their substantial activation and modulation by intracellular signaling pathways. The expression of several ASIC subunits including ASIC1a, ASIC3, and ASIC2b are increased by (6- to 15-folds) two days after inflammation induced by the application of CFA. The number of ASIC1a expressing neurons were also increased, especially in the peptidergic neurons, after inflammation. Interestingly this overexpression of ASIC channels was reduced upon the application of steroidal and non-steroidal anti-inflammatory drugs (Voilley et al., 2001). Several inflammatory molecules released during inflammation could be responsible for the overexpression in the ASIC channels during inflammation. NGF, serotonin, interleukin-1 and bradykinin elevate the expression of ASIC1a, -1b, -2b, and -3 by 3-10 fold, without having an effect on TRPV1 channels (Mamet et al., 2002). In addition, the application of an inflammatory cocktail containing NGF, serotonin, interleukin-1, and bradykinin, in concentrations relative to those measured during inflammatory states, increased the number of neurons expressing ASIC currents. This increased number of neurons was found to be in the neurons expressing TRPV1 channels. ASIC1a and ASIC3 evoked currents by acidification (pH5) in the neurons treated with the inflammatory cocktail were increased. Interestingly the application of pH 6 in neurons expressing ASIC3-like currents could not trigger action potentials unless it was pre-incubated with the inflammatory cocktail. These effects were accomplished without affecting the resting potential of the neurons (Mamet et al., 2002). This indicates that the application of the inflammatory cocktail increased the expression of ASIC3 channels in the DRG and this led to increase the channel's proton-evoked currents resulting in an increased neuronal excitability.

Nitric oxide is an important reactive species that is also increased during inflammation. This increase results from the upregulation of the enzyme inducible nitric oxide synthetase (iNOS) responsible for NO synthesis (Chu and Xiong, 2013). NO was shown to enhance ASIC currents evoked by acidification in rat DRG neurons. This potentiation effect was seen in recombinant ASIC1a for pH between 6.9 and 6.6. NO directly interact with ASICs and does not involve protein

kinase G, which is knows to be activated by NO. The effect of NO on ASIC currents causes a significant increase in the pain induced by iontophoresis of acidic solution in the skin of human volunteers in the presence of nitric oxide donner. Thermal and mechanical pain thresholds were unaffected by the sole application of the NO donner, indicating that NO specifically was able to enhance acid evoked pain (Cadiou et al., 2007).

### 5.3.3. *Activation of ASICs by neuropeptides*

FMRFamide and structurally related neuropeptides were shown to modulate pain response (Askwith et al., 2000). Neuropeptide FF was found to be increased in inflammation. The expression of these neuropeptides were found in the CNS including NPFF and NPSF while NPFF were also found in the DRGs. Based on the location of injection, FMRF-amide and related neuropeptides can exhibit opposite effect. If they are injected in the intra-cerebro-ventricular space, they induce hyperalgesia while intrathecal injection of these neuropeptides induces analgesic effect (Askwith et al., 2000). Due to structure similarity between ASICs and FMRFamide-activated $Na^+$ channel, it was hypothesized that these peptides may interact with ASIC channels. Indeed , Askwith et coll. showed that these neuropeptides are able to enhance ASIC ( ASIC1a, ASIC3) responses to protons when the neuropeptides are applied before the pH drop (Askwith et al., 2000). The peptides do not show direct activation of the ASIC channels. On the contrary, these neuropeptides are able to enhance the peak currents in ASIC1a and ASIC3, while it dramatically enhanced the sustained current that characterizes ASIC3 channels in response to acidification (Askwith et al., 2000; Deval et al., 2003). Based on these findings the interaction between ASICs and FMRF amides could play a role in the enhanced neuronal excitability and the hyperalgesia associated with inflammation. Other endogenous neuropeptides found to interact with ASICs are bignorphins and Dynorphin A that were found to potentiate ASIC1a and ASIC1b currents (Deval et al., 2010).

### 5.3.4. *Modulation of ASICs with external stimuli*

In addition, external stimuli can affect ASIC activity where it was shown that temperature could modulate the activity of ASICs. Cold can decrease the inactivation of the channels, while warmth can increase it (Askwith et al., 2001; Neelands et al., 2010).

### 5.3.5. Modulation of ASICs by lipids

Arachidonic acid (AA) is a polyunsaturated fatty acid that exists in all cell membranes. It was shown that AA enhance the $H^+$ evoked ASIC currents recorded from cerebellar Purkinje cells (Allen and Attwell, 2002). The enhancement was shown in the peak currents of ASICs. Regarding the sustained currents, AA was able to induce sustained currents in 70% of the neurons that did not show them in the control recordings, while in neurons expressing sustained currents, AA was able to enhance it in 77% of the neurons. These effects were suggested to mediated by the ability of AA to integrate in the plasma membrane leading to its stretching and subsequently activating ASIC channels (Allen and Attwell, 2002). Smith et al, studied the effect of AA on ASIC channels expressed in peripheral sensory neurons. They showed that in rat DRG neurons, AA at 10 µM potentiates the peak and the sustained currents of ASICs evoked by lowering the pH. This effect was observed in ASIC1a, ASIC2a, and ASIC3. The potentiation induced by AA did not involve AA metabolites as the potentiation effect was not reduced in the presence of inhibitors of AA metabolism. In contrast to the previously suggested mechanism of AA on ASIC channels, this study shows that AA is able to potentiate ASIC currents directly and not through stretching the membrane. AA exhibit its effect when it is applied on both sides of the membrane in excised patch. The key factor that mediates the potentiation of ASIC currents by lipids is the number of double bond existing in the lipid tail (Smith et al., 2007).

Lysophosphatidyl-choline (LPC) is another lipid that activates and potentiates ASIC3. This was shown by our team in 2016 (Marra et al., 2016). They tested the effect of inflammatory exudates collected from patients suffering from joint pain. The exudates significantly activated human ASIC3 expressed in heterologous systems, inducing a sustained inward current that was not seen in ASIC1a expressing cells. The ASIC3 current was significantly reduced upon chelating the lipids or by the application of the ASIC3 blocker, APeTx2. Lipid analysis of the exudates revealed the presence of high concentrations of AA 148 ± 42 µM and several species of LPC with 113 ± 14, 26 ± 3, 47 ± 6 and 14 ± 1 µM for LPC16:0, LPC18:1, LPC18:0, and LPC20:4, respectively. AA, LPC16:0, LPC18:0, and LPC18:1 each at 10 µM activate ASIC3 channels at neutral pH, while free fatty acids and other species of lysophospholipids failed to produce the same effect. Co-application of AA and LPC16:0 has a synergistic effect on the currents produced by recombinant ASIC3 channels. Co-

application of AA and LPC16:0 induces depolarizing currents in DRG neurons that are blocked by amiloride. This synergistic effect results in increased firing of the peripheral C-fibers, and pain behaviors in animals injected locally in their hind paws with both AA and LPC16:0 (Marra et al., 2016).

### 5.3.6. *Interaction of ASICs with other receptors and ion channels*

Oxytocin is a neuropeptide composed of nine amino acids, synthesized in the hypothalamus then transported to the pituitary gland to be released in the blood stream (Sofroniew, 1983; Viero et al., 2010). Oxytocin plays important roles in several behaviors including orgasm, social recognition, pair bonding, anxiety, and maternal behaviors (Viero et al., 2010). Oxytocin induces an analgesic effect upon its central administration in the brain and the spinal cord (Yu et al., 2003). Peripheral administration of oxytocin induces analgesia that is linked to its ability to inhibit ASIC channels through activating vasopressin V1A receptors (Qiu et al., 2014). Indeed, peripheral administration of oxytocin is able to reduce the number of flinches raised after an intra-planter injection of acetic acid, while this analgesia is lost in mice lacking vasopressin V1A. *In vitro* experiments done in DRGs collected from rats showed that oxytocin application, or an activator of the vasopressin V1A receptor, reduces ASIC currents evoked by acidification at pH 6.5 and 5. This inhibitory effect is reversed upon the co-application of oxytocin with vasopressin V1A receptor antagonist. In addition, Oxytocin is able to reduce the number of action potentials evoked by acidification (Qiu et al., 2014). This study shows that ASIC channels can be functionally associated with other receptors or ion channels and this association can lead to direct or indirect modulation of ASIC channels activity.

Another example for an interaction between ASIC channels and other receptors was reported by Fang Qiu et al in 2012 (Qiu et al., 2012). They studied a possible interaction between ASIC channels and 5HT2 receptors. 5HT levels are elevated during inflammation and this result in sensitizing the nociceptors and induce hyperalgesia. 5HT exhibits its effect by activating serotonin receptors including 5HT2. 5HT2 receptor is expressed in the rat sensory neurons, and it's activation was shown to be responsible for the hyperalgesia associated with 5HT (Tokunaga et al., 1998; Lin et al., 2011). Native ASIC currents recorded from rat DRG neurons is potentiated by 5HT2 agonist and it is inhibited by PKC signaling pathway inhibitors. This potentiation results in increased excitability

of the DRG neurons represented by increased amplitude of depolarization, and number of evoked action potentials after co application of 5HT2 agonist and acidification. This modulatory interaction between ASICs and 5HT2 was also shown to increase nociceptive behaviors in vivo in response to intra-plantar injection of acetic acid when the rats were pretreated with 5HT2 agonist.

P2X5 co-localize with ASIC3 in sensory neurons. It was suggested that both can form a molecular complex. Indeed, ATP modestly activates neurons expressing ASIC3 channels. ATP (1 µM) induces a long lasting potentiation of ASIC3 currents evoked by acidification through enhancing the acid sensitivity of the channels. In heterologous expression systems, $H^+$ gated ASIC3 currents were only potentiated in the presence of P2X2/4/5, and was independent on any intracellular signaling that could be mediated by P2X activation. Forster resonance energy transfer (FRET) experiments confirmed that P2X and ASIC3 channels are directly coupled (Birdsong et al., 2010). All together ASIC channels activity can be modulated by activation of other receptors or channels including the vasopressin 1A, 5HT2, and P2X.

### 5.3.7. *Modulation o ASICs by signaling pathways (kinases)*

ASIC1a, -2a, and 2b structure contain a site on their C-terminus allowing the binding of PDZ domain (Baron et al., 2002b; Deval et al., 2004; Duggan et al., 2002; Hruska-Hageman et al., 2002). The PDZ domain found in the Protein Interacting with C Kinase 1 (PICK1) can bind to these channels allowing the PKC to phosphorylate these channels. This interaction enhances ASIC2a currents in response to acidification by increasing the channel's opening probability (Baron et al., 2002b).

PICK1 and PKC do not interact directly with ASIC3, since ASIC3 does not have the compatible PDZ binding domain (Deval et al., 2004). However, the dimerization of ASIC3 with ASIC2b allows the phosphorylation of ASIC3 by PKC. The phosphorylation of ASIC3 occurred through ASIC2b that binds to PICK1, which allows the binding of PKC and the close association with ASIC3. This positive regulation of the heteromeric channels by PKC signaling leads to the enhancement of ASIC3 proton gated currents, in heterologous expression systems. Because both ASIC3 and ASIC2b are co-expressed in the peripheral nervous system the possible regulation of the hetermerized ASIC3 and ASIC2b channels was tested in native DRG neurons (Deval et al., 2004). Indeed, PKC activation enhanced the neuronal excitability suggesting a role of ASICs in pain enhancement during pathologies that lead to the activation of the PKC signaling pathway.

ASIC3 sequence contains a binding site for another PDZ domain that can bind the protein CIPP. Co-expression of both proteins increased ASIC3 currents evoked by acidification to five folds. This enhancement was a result of alkaline shift in the activation curve of ASIC3 in the presence of CIPP (Anzai et al., 2002).

ASIC1a, but not ASIC2 expression was enhanced by PKA signaling pathway. The interaction was achieved through the ability of PKA to phosphorylate ASIC1a leading to the disruption of PICK1 binding to ASIC1a and altering its localization (Leonard et al., 2003).

During ischemia NR2B-containing (NMDARs) is activated. In turn, it activate calcium/calmodulin-dependent protein kinase II which phosphorylate ASIC1a. The channel become sensitized and the produced currents in response to acidification are potentiated leading to cell death (Gao et al., 2005).

## 5.4. Functional role of ASICs

ASICs were shown to contribute to several physiological and pathological processes including mechano-sensation, taste, synaptic plasticity, learning and memory, neurodegeneration, and nociception for review (Deval and Lingueglia, 2015; Deval et al., 2010).

### *5.4.1. Description of ASIC knockout mice*

ASICs are expected to have a role in nociception because functional ASICs are widely expressed in small and medium diameter neurons that convey nociceptive signals in DRG and TG. Their expression was found in the peripheral terminals, and cell bodies, but not in the central terminals of the sensory afferents (Deval et al., 2010). Their expected role in acute nociception was contradicted by the early description of ASIC knockout mice. It was shown that ASIC1a knockout mice have enhanced mechano-sensitivity of mechanoreceptors in colon and gastroesophageal tract without affecting the cutaneous mechanoreceptors (Page et al., 2004).

The loss of ASIC3 channels in knockout DRG neurons reduced their responses to low acidification at pH6.5 also led to slowed the proton evoked currents inactivation, without affecting the percentage of neurons responding to low pH. This indicated that ASIC3 is not the only pH sensor in the DRG neurons. Besides, it was shown that the number of action potentials evoked by the

application of pH to the receptive field of polymodal C-fibers was reduced in ASIC3 ko mice. Also recording the activity of the mechano-heat sensitive fibers by skin nerve preparation showed a reduced by 29% in ASIC3 ko mice upon heating the skin to 52°C (Price et al., 2001). On the contrary, in vivo experiments done on ASIC3 KO mice did not show significant difference to wild-type mice toward acute thermal pain, and thermal hyperalgesia associated with carrageenan induced inflammation. The pain mediated by local injection of acidic solution of pH3 was not altered in ASIC3 knockout mice compared to wild-type mice. Nevertheless some aspects of mechano-sensation were affected in ASIC3 ko mice (Price et al., 2001).

Another group described different phenotypes in ASIC3 ko mice, where the knockout mice were more sensitive to acute acidic pain, thermal pain, mechanical pain at high intensity stimuli, with no contribution in inflammatory pain models (Chen et al., 2002). In addition, the use of dominant negative ASIC3 mutant channels reduced the peak currents associated with heteromeric channels containing ASIC3 in homologous systems (Mogil et al., 2005). DRG neurons expressing this dominant negative mutant did not show any peak response to strong acidification (pH5). The dominant negative mice did not show significant difference compared to WT on hot plate test, tail flick, paw withdrawal in Hargreaves test. The transgenic mice showed hypersensitivity to mechanical stimuli on von Frey, tail clip, and inflammatory stimuli including formalin, abdominal acidification with acetic acid (writing test) (Mogil et al., 2005).

### 5.5. Involvement of ASICs pain

Experiments done in humans showed strong contribution of ASICs in acidic pain. One study showed that direct infusion of moderate acidic solution (pH6) in the skin induces pain that was blocked by non-specific ASIC blocker amiloride, but not by capsazipine, a blocker of TRPV1 (Ugawa et al., 2002). Pain induced by more acidic solution (pH5) was partially blocked by amiloride. Blocking TRPV1 with capsazepine at this pH5 reduced the pain. This indicates that activation of ASICs contribute to pain associated with moderate acidification while strong acidification induce the activation of both ASICs and TRPV1 (Ugawa et al., 2002). Another study delivered acidic solution to human skin by iontophoresis and this induced pain that desensitize within minutes (Jones et al., 2004). Several applications of the acidic solution desensitize the skin and results in reduction in the described pain. Capsaicin also sensitized the skin and its co-injection with acid

increased the evoked pain. Pain associated with Acid application is not affected by desensitized or non-desensitized skin with capsaicin indicating that the pain evoked by acid follow a different pathway. Blockers of ASICs, including diclofenac and ibuprofen, reduce the pain associated with acid application but not the one associated with capsaicin. Amiloride also inhibited the pain associated with the acidic injection (Jones et al., 2004). These studies confirmed that the pain associated with moderate acidosis is mainly mediated by ASICs and not by other channels activated by protons like TRPV1.

The use of pharmacological inhibitors and activators of ASICs in rodents contributed to clarify their roles in nociception. One study done on rats showed that injecting the hind paw with serotonin, capsaicin or formalin at acidic pH (5.8) enhanced the pain response in rats compared to their injection at neutral pH indicating that pain response to these irritant molecules are potentiated by acidity. Amiloride injection improved the pain responses to these irritant molecules (Rocha-González et al., 2009). A-317567 a compound that blocks ASIC currents in homologous and heterologous systems was able to reduce thermal pain associated with inflammatory insult (CFA model) and improved the weight bearing responses after post-operative model of pain in mice (Dubé et al., 2005). Furthermore, venom obtained from the Texas coral snake, which induces a very painful bite, was shown to contain two active toxins called MitTx (Bohlen et al., 2011). Local injection of MitTx in the mice paw produce robust pain responses. MitTx injection increased c-fos staining in the superficial laminae of the spinal cord, corresponding to increased nociceptive input. In vitro experiments showed that MitTx can activate ASICs with high affinity toward ASIC1a and ASIC1b, more than ASIC3. The currents induced by the toxin were large and sustained currents with amplitudes similar to the transient currents produced by activating the channels by acidification but without inactivation. These currents were inhibited by amiloride. The direct effect of MitTx on ASIC2a was small but the toxin induced large potentiation in their currents produced by acidic solutions. The toxin did not show significant effect toward other potential target channels or other channels involved in pain transduction. MitTx sensitive neurons encompass peptidergic and non-peptidergic neurons, but the pain elicited by the toxin was mainly mediated by TRPV1 positive neurons (Bohlen et al., 2011).

## 5.6. Role of ASIC 1&2 in pain

Several studies were able to highlight the involvement of ASIC1 and 2 channels in nociception using genetic, pharmacological and RNA silencing approaches. Mazzuca and coll., in the IPMC in 2007, showed that blocking homomeric ASIC1a expressed in the central nervous system by PCTx1 reduces acute thermal and chemical pain and the thermal and mechanical pain associated with neuropathic pain (Mazzuca et al., 2007). This effect was shown to be mediated through increasing the met-enkephalin release. Another study showed an over expression of ASIC1a channels in the ipsilateral side of the spinal cord after CFA injection (Duan et al., 2007). This increase in the cannel expression did not overlap with CGRP or IB4 staining most likely indicating ASIC1a expression in the spinal interneurons. Intrathecal injection of PcTX1 or ASIC1a antisense oligonucleotide did not affect normal nociception but they were able to reduce the thermal hyperalgesia associated with CFA injection (Duan et al., 2007). Also, Pctx1 application didn't affect the windup in the WDR neurons of naive rats but it decreased the WDR activity toward brushing and pinching after inflammatory insult with CFA (Duan et al., 2007). Mambalgin can inhibit ASIC1 and 2 containing channels (Diochot et al., 2012). Peripheral injection in the paw induces analgesic effect toward acute thermal pain and thermal pain associated with inflammation through blocking ASIC1b. Central administration of Mambalgin reduces acute thermal pain associated with inflammatory insult through blocking central ASIC1a and ASIC2a (Diochot et al., 2012). The central effect of Mambalgin was resistant to naloxone treatment indicating that it is not mediated though opioid pathway as it the case for PCTx1.

## 5.7. Role of ASIC3 in pain

In 2008, Deval et coll. showed that the application of APeTx2 reduced C-fibers firing in response to mild acidification (pH 6.9) (Deval et al., 2008). The application of the same acidic solution pH 6.9 to the skin of hind paw increased pain responses in rats, represented by an increased number of flinches. This study also showed that arachidonic acid and hypertonicity potentiate ASIC3 currents toward acidification in vitro. In agreement, co-injection of AA and/or hypertonic solution increased the pain responses to moderate acidic solution in animals. These increased pain responses were reversed by application of ASIC3 blocker APeTx2 or by down regulating of ASIC3 channels through intrathecal injection of the ASIC3 antisense RNA. This illustrated that several

factors can modulate ASIC3 channels in a synergistic manner and co-application of several activators potentiate the effect (Deval et al., 2008). ASIC3 channels showed a role in postoperative pain. ASIC3 expression in small DRG neurons was elevated after surgical incisions (Deval et al., 2011). Local injection of APeTx2 or the use of silencing RNA improved the thermal hyperalgesia and weight bearing scores following these incisions.

In mirror, the use of ASIC3 activators enhanced pain. An example to this is GMQ a molecule that activates ASIC3 channels at the physiological pH 7.4 and increase its sustained currents (Yu et al., 2010). Local injection of GMQ in the hind paw o mice induced pain expressed as increased time of paw licking in WT mice but not ASIC3 knockout mice (Yu et al., 2010). Serotonin is another molecule shown to potentiate the sustained current of ASIC3 in a dose dependent manner (Wang et al., 2013). Serotonin, but not substance P, bradykinin, PGE2, or histamine, directly interact with homomeric and heteromeric ASIC3 containing channels. This interaction between ASIC3 and serotonin is through a non-proton site. It is independent of 5HT receptors or signaling pathways as the potentiation effect was seen in single channel recording. In addition, serotonin increases the depolarization induced by application of acidic pH in DRGs of wild-type but not ASIC3 knockout mice. Co-injection of acetic acid and serotonin enhances pain in WT mice. This pain potentiation was blocked by amiloride in WT, and was not seen in ASIC3 ko mice (Wang et al., 2013). This indicate that elevated level of serotonin seen during inflammation can lead to the potentiation of ASIC3 current directly through interacting with the ASIC3 channels or indirectly through activating 5HT2 receptors (Qiu et al., 2012; Wang et al., 2013).

Emphasizing the role of ASIC3 in inflammatory pain, Yen and colleagues showed that inactivating ASIC3 channels does not affect the basal thermal and mechanical nociception in mice (Yen et al., 2009). In contrary, thermal and mechanical hyperalgesia associated with inflammatory pain induced by carrageenan injection were improved in the ASIC3 knockout mice. This contribution of ASIC3 could involve Nav1.9 and Nav1.8, since Nav1.9 was upregulated two days after carrageenan injection in WT but not in ASIC3 knockout mice. In addition, Nav1.8 currents were enhanced two days after carrageenan injection in the WT mice and not in ASIC3 knockout mice. The absence of ASIC3 reduced the infiltration of inflammatory cells after repeated injections of the inflammatory molecules in the muscles (Yen et al., 2009).

These studies which focused on the contribution of ASIC3 in pathological pain condition confirm that ASIC3 does not participate in the basal thermal or mechanical acute pain but that it is involved in pain during pathological conditions of inflammatory, neuropathic or post-operative origins. It is interesting to note that ASIC currents can have different modes of activation based on the activator and that these currents can be potentiated synergistically when several potentiators are co-applied together.

These group of studies highlighted the important role of ASICs in enhancing pain signals and that blocking native ASICs expressed in the central and peripheral nervous system reduce acute, inflammatory, and neuropathic pain, while activating these native channels enhance dramatically the pain perception.

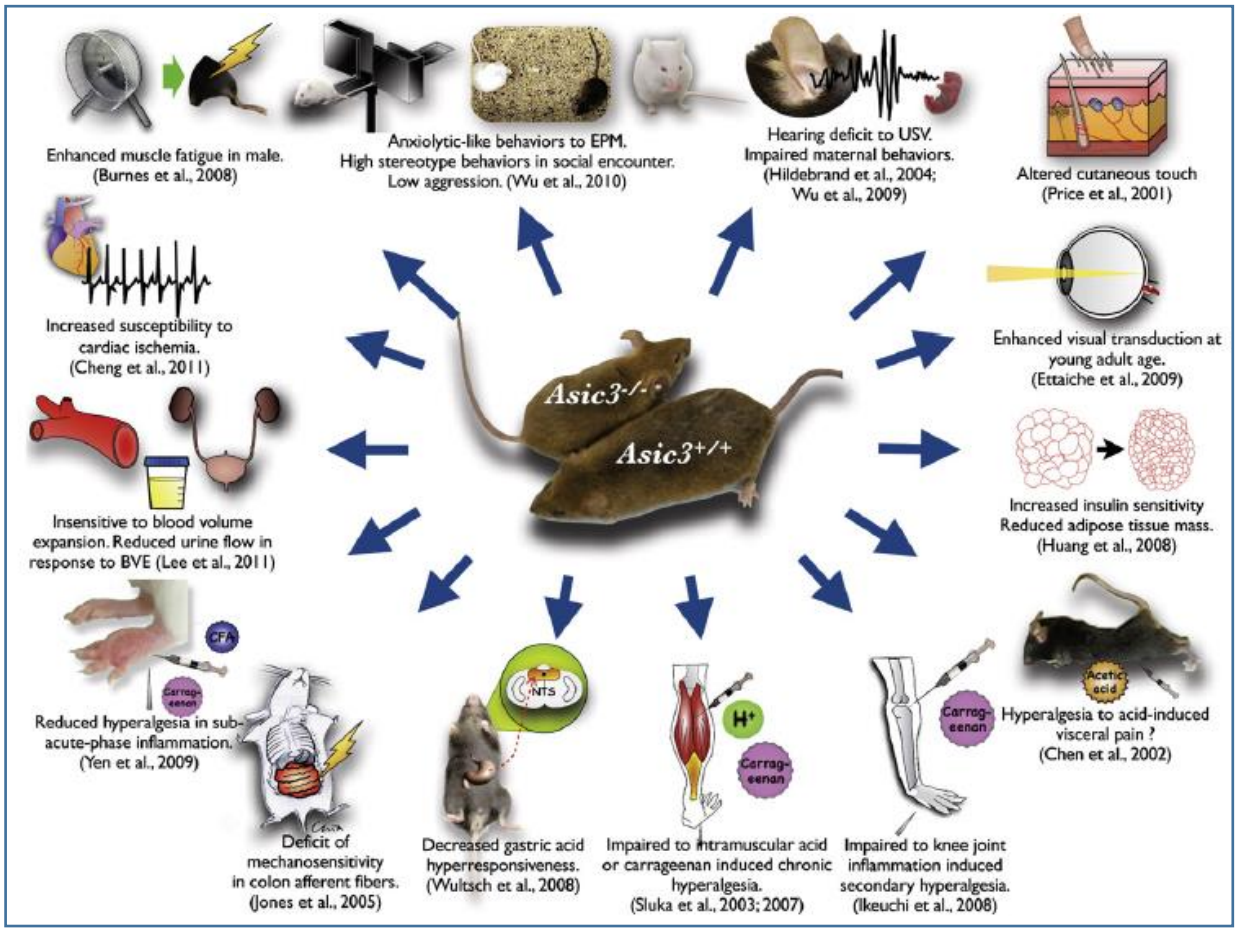


*Figure 20 Role ASIC3 channels in different models of pain and pathologies (Wu et al., 2012)*

# 6. Obesity

## 6.1. Definition and assessment

The world health organization (WHO) defines obesity as abnormal or excessive fat accumulation that presents a risk to health (WHO - Obesity).

The main assessment of obesity is based on the body mass index BMI, which is calculated by dividing the body weight in kilograms by individual's height in squared meter. Indeed, this simple calculation does not give an idea about the body composition in term of the mass of body organs and bones, amount of fats in respect to proteins, neither consider the distribution of fats in the body. Of course, the latter two parameters are very important factors that can lead to huge health risks (Pouliot et al., 1992; Björntorp, 1993; Fujimoto et al., 1994). For that, other parameters should be considered when assessing obesity including the waist circumference and fat mass found in the central region of the body (intra-abdominal and subcutaneous) and in the peripheral region (hip) (Kahn et al., 2001).

The distribution of fat in the body can greatly affect health, where in human, total adiposity and truncal subcutaneous fat accumulation during adolescence, is positively associated with atherosclerosis at age 36 (Ferreira et al., 2004). In addition, the accumulation of fat in the central region of the body is associated with insulin resistance, while the body fat found in more peripheral regions were found to have less impact on metabolic parameters (Kahn et al., 2001). Furthermore, it is debatable which pattern of distribution within the central region would affect more the insulin resistance whether it is the visceral and intra-abdominal fat or is it the subcutaneous fat. For that another method which consider the measurements of hip circumference and height are used to assess obesity. This method is called the body adiposity index (BAI) (Bergman et al., 2011). Indeed, this assessment was significantly correlated with the levels of leptin in a study included 1770 patients (Melmer et al., 2013). Although, other studies suggested other methods of assessment may be better than the BMI and BAI in assessing of obesity and show more correlation with pathologies (Bennasar-Veny et al., 2013), the widely accepted assessment by researchers and health care professionally is the BMI.

The BMI index classify individuals into five classes; normal between 18.5-24.9 kg/m$^2$, overweight 25-29.9 kg/m$^2$, class-1 obesity 30-34.9 kg/m$^2$, class-2 obesity 35-39.9 kg/m$^2$, class-3 obesity equal or greater than 40 kg/m$^2$. There is a great risk of morbidity and related co-morbidities associated with class-2 and class-3 obesity (Dixon et al., 2011; Ashwell et al., 2014).

## 6.2. Prevalence of obesity

In 2016, 39% of the whole adult world population was overweight and 13% suffered from obesity, with 11% for men and 15% for women (WHO - obesity). This prevalence of obesity was almost one third of its value in 1975. Indeed, obesity is now considered as a worldwide health problem. A meta-analysis based on 1769 studies conducted in 104 centers confirmed the considerable increase in the prevalence of obesity between 1980 and 2013. The proportion of adults having BMI equal or greater than 25 kg/m$^2$ increased from 29% to 37% of the population (Ng et al., 2014). Moreover, since 1985, the prevalence of obesity within each classes increased from 5.1% to 13.1% for class-1, 0.8% to 3.6% for class-2, and from 0.3% to 1.6% for class-3 (Twells et al., 2014). It is expected that in 2019, the prevalence of obesity within the Canadians in the classes 1, 2 and 3 will reach 14.8%, 4.4% and 2.0% respectively (Twells et al., 2014). In the USA it is expected that almost 86% of adult population to be overweight or obese by 2030 (Ginter and Simko, 2014a). The prevalence of obesity in children was also found to be higher than 20% in sixteen countries including developed and developing ones (Bibiloni et al., 2013). Overweight children often become overweight adolescents and adults where, children or adolescent with a high BMI have a high risk of being overweight or obese at the age of 35 (Guo et al., 2002).

## 6.3. Causes of obesity

Obesity is not a consequence of one simple issue, indeed to be able to fully understand the body weight regulation it is important to consider several factors and the interaction between them. These factors include environmental, socioeconomic, and genetic factors, while personal behaviors in response to these conditions have a dominant role in affecting the outcome on “obesity” for review (Wyatt et al., 2006; Hruby and Hu, 2015; Xu and Xue, 2016).

### 6.3.1. Genetic factors affecting obesity

Although over 60 genetic markers have been linked to increased susceptibility to obesity, the consequence of these genetic variants on obesity does not justify the dramatic rise in global obesity in the whole population over the last half-century. Indeed, the top 32 genetic factors that can induce obesity only increase the overall inter-individual variation in BMI by less than 1.5% (Speliotes et al., 2010). Besides if these 32 genetic variants were combined together, they would increase the BMI with just 2.7 kg/m$^2$; 7 kg for 1.6 meter individual, compared to individuals with low genetic risk factors. Nevertheless considering the interaction between genetic and environmental factors could be useful in the sense that genetic risks can enhance individual's responses toward these environmental factors. To support this hypothesis, a meta-analysis for 45 studies that included adults and children, showed that in individuals having the strongest known susceptibility locus for obesity, FTO gene, obesity were attenuated by 27% in physically active adults (Kilpeläinen et al., 2011).

On the other hand, monogenic obesity caused by a mutation in a single gene that is not affected by environmental factors is special and rare (Zhao et al., 2014). Among the mutated genes proopiomelanocortin (POMC), leptin receptor (LEPR), leptin (LEP), proconvertase 1 (PC1), and melanocortin 4 receptor (MC4R), have been confirmed as the casual genes to the onset of monogenic obesity (Zhao et al., 2014). Leptin pathway is one of the well studies pathways that cause obesity and it is reviewed in (Tartaglia, 1997).

Leptin is an adipokine hormone secreted from the adipocytes after meals to control appetite and satiety. As other hormones Leptin can reach the blood and its levels in the serum reflects the amount of the energy stored in adipose tissue (Considine et al., 1996). In turn, it binds to its membrane receptor (ObR) that is distributed in various tissue and it is strongly expressed in the hypothalamus. Several factors stimulate the release of leptin including excess energy stored as fat (obesity), overfeeding, glucose, insulin, estrogen, and proinflammatory cytokines (TNF-α, IL-6). Other factors that reduce leptin release are low energy states with decreased fat stores (leanness; lipoatrophy), fasting, cold exposure, thyroid hormone, and testosterone (Moon et al., 2013). The activation of leptin receptors in the hypothalamus stimulate the release of several neuropeptides and activate several signal transduction pathways for review (Kelesidis et al., 2010). In turn, this

decrease food intake, regulate neuroendocrine function, energy intake and expenditure (Mantzoros, 1999). Administrating large quantities of leptin reduce body fat stores in rats (Chen et al., 1996). During obesity levels of circulating leptin are increased but these individuals develop what is called "leptin resistance" (Park and Ahima, 2015). on the other hand, defects in leptin functioning due to mutations in its gene results in hyperphagia, early-onset obesity and various endocrine disturbances in both rodents and humans (Coleman, 1978; Montague et al., 1997; Clément et al., 1998; Strobel et al., 1998). The ob/ob and db/db mice are two transgenic mice that have mutation in the leptin gene and its receptor respectively. These mice show severe early-onset of obesity and insulin resistance, hyperphagia, reduced energy expenditure, infertility, and decreased linear growth (Carroll et al., 2004).

On the other hand, several factors were shown to increase risk of off-spring obesity, including famine exposure, parental obesity, smoking, endocrine-disruption and some chemicals, in addition to parental weight gain during gestation and gestational diabetes (Hruby and Hu, 2015). These effects on off-springs could be mediated by fetal programing mechanisms involving epigenetic modifications (Dabelea and Harrod, 2013).

### *6.3.2. Individual Behaviors that affect obesity*

The diet composition is a very important factor in obesity. Indeed many recent studies focused on diet and the impact of the individual behavior on obesity. This is justified by the fact that in the USA, 15% of deaths in 2000 were linked to obesity resulting from poor quality diet (rich in lipids) and low physical activity (Mokdad et al., 2004). To further emphasize the importance of diet in obesity, the most popular and effective approache for weight-management nowadays is the caloric restriction method (Hruby and Hu, 2015).

The energy balance equation, represented as the long term balance between energy intake and expenditure, is mainly affected by individual behaviors in addition to genetic and environmental factors. The concept of energy balance is simply addressed as that stored energy will increase if the energy intake exceeds the total body energy expenditure. Energy expenditure takes into account the level of physical activity, basal metabolism, and adaptive thermogenesis. Physical activity is referred to voluntary movements, while basal metabolism activity is the total biochemical processes that maintain survival, while adaptive thermogenesis is referred to the

energy converted to heat in response to environmental changes. With this equation, individuals can control the two main factors of the energy balance equation, i.e. the energy intake and the energy expenditure through physical activity (Spiegelman and Flier, 2001).

## 6.4. Meta-flammation

The excess consumption of nutrients, not only leads to obesity but it also induces inflammation in specialized metabolic cells such as adipocytes (Gregor and Hotamisligil, 2011). This type of inflammation differs from the classical one triggered by tissue injury or infection in several aspects. These aspects include the origin of the insult, the mediator of inflammation, the consequences, and the duration of inflammation. For this, inflammation induced by metabolic insult is referred as meta-flammation (Gregor and Hotamisligil, 2011).

Meta-flammation is characterized by being generated in response to metabolic and nutritional insult. It is initiated and maintained within the metabolic tissue. The expression level of inflammatory mediators induced by stress sensors such as IKK and JNK, is considered moderate to low-grade compared to acute inflammation induced by infection, trauma or acute immune response. Another feature of meta-flammation is that the expression of inflammatory cytokine and immune cell infiltration appear to occur gradually and to stay unresolved over time. This is in contrary to acute inflammation where resolution occur at the site of injury, and take place relatively faster, within days or weeks (Gregor and Hotamisligil, 2011).

The initiators of inflammation within the metabolic tissue after over feeding or the consumption of high energy fat diet is not yet clear. Traditional inflammatory responses is triggered when a pathogens like molecules from a microbe, parasite, foreign body, or injured tissue engage a cell signaling pathway (either in the host cells or sentinel immune cells) leading to initiation o an immune response. In meta-flammation the situation is different as the initiation factor (pathogen) is not fully known, yet it is proposed that it activates signaling pathways in specialized metabolic cells, e.g., the adipocyte, hepatocyte, or myocyte. In turn, the defensive mechanisms of these nonimmune cells are activated. These mechanisms include inflammasome and TLR activation, JNK and NF-κB signaling, and production of inflammatory cytokines (Gregor and Hotamisligil, 2011).

Several theories explaining the induction of meta-flammation were proposed. First theory hypothesized that nutrients themselves are naturally inflammatory, and upon their consumption, digestion and metabolism slight inflammation is elicited that is reversed quickly under normal condition by the effect of anti-inflammatory signaling (Wellen et al., 2007). On the contrary, during obesity, these anti-inflammatory mechanisms are impaired leading to an uncontrolled inflammatory state after the consumption and digestion of food (Wellen et al., 2007).

Another hypothesis proposed that nutrients by themselves are not inflammatory but their abundance can activate the immune response pathways. This is could be considered as the ''mistaken identity theory'' where the system is tricked into thinking that these abundant nutrients are pathogens. For instance, some of the pathogen-sensing receptors TLRs, of the innate immune system, are expressed in adipose tissue like TLR4 and TLR2. These pathogen sensors could mistakenly recognize the structural similarities of certain molecules like lipids with pathogens, especially when the concentration of these nutrients is high. A study done in mice showed that adipose TLR4 are activated by infusion of saturated fatty acids leading insulin resistance (Shi et al., 2006). In addition, TLR4 expression is increased when the system has high levels of fatty acids after HFD feeding. The genetic loss of TLR4 in these conditions may ameliorate insulin resistance (Saberi et al., 2009).

A third hypothesis is that after feeding there is an increase in the permeability of the intestine to allow the maximum passage of nutrients, during which inflammatory molecules also can pass the gut barrier. To support this hypothesis, studies showed that after feeding the levels of LPS in the serum are increased in rodents and humans. After feeding termination these high levels of LPS are reduced (Cani et al., 2007; Erridge et al., 2007). Levels of serum LPS are maintained high in obese subjects, indicating that either the mechanisms responsible for the resolution of these inflammatory molecules are impaired in obesity or that the intestine permeability of obese subjects is permanently compromised, leading to high levels of inflammatory molecules in the serum (Cani et al., 2007; Erridge et al., 2007).

Either one of these hypothesis or a combination of all of them is the cause of meta-flammation induction, meta-flammation leads to the activation of several kinases and their downstream signaling cascades. The activation of c-jun N-terminal kinase (JNK), inhibitor of κ kinase (IKK), and

protein kinase R (PKR) was observed in obese tissues such as adipose tissue and liver. Studies that used genetic deletion of these kinases showed attenuation of the inflammation related to obesity (Hirosumi et al., 2002; Cai et al., 2005; Nakamura et al., 2010).

As mentioned above the immune sensors known as the inflammasome and the Toll-like receptors (TLRs) including NLRP3 and TLR4 were found to be activated in obese tissues compared with lean control animals (Shi et al., 2006; Song et al., 2006; Schroder et al., 2010). Several signaling pathways within the metabolic cells can be activated in response to excess nutrition leading to the stimulation of inflammatory response for review (Gregor and Hotamisligil, 2011).

Furthermore, obesity is associated with increased infiltration of immune cells into the metabolic tissues. A study showed that the macrophage population is increased in the adipose tissue of obese mice or mice that receive a high-fat diet (HFD) compared with lean mice fed normal chow (Weisberg et al., 2003; Xu et al., 2003). This contributes to increase in cytokines expression. Obesity leads to an increase in the population of activated macrophages and induces a shift to the pro-inflammatory M1 population of macrophages with respect to the anti-inflammatory M2 macrophages (Olefsky and Glass, 2010). This state of activation in the immune cells is also found to be extended to mast cells and natural killer T (NKT) cells, which are found to be increase in obese adipose tissue compared to lean tissue. The activation of the immune cells may have a role in establishing inflammation and contribute to the metabolic dysfunction associated with obesity (Liu et al., 2009; Ohmura et al., 2010).

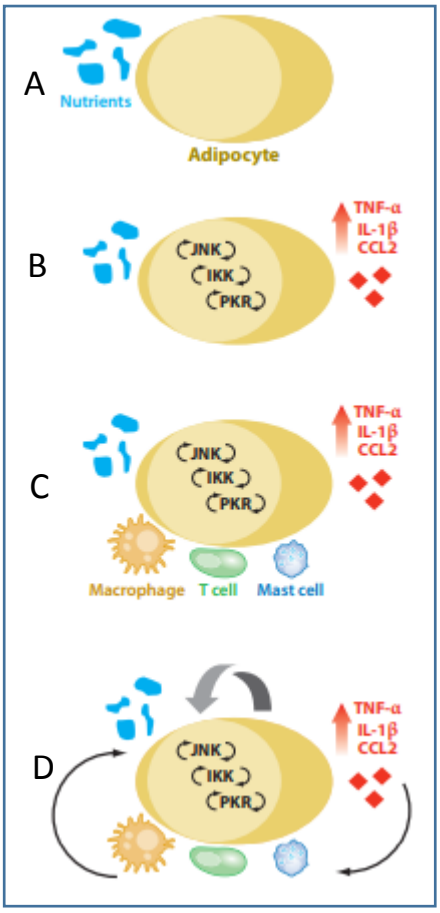


*Figure 21 Establishment of the Meta-flammation. A) The metabolic insult: Meta-flammation originate in metabolic tissue after excess nutrients. B) Induction: Metabolic stress engage inflammatory pathways induce low-level release of inflammatory cytokines. C) Immune cells infilteration: Metabolic tissue is reconstructed with immune cell infiltration. D) Maintained: Well-establishment of a chronic and unresolved inflammatory state. Adapted from (Gregor and Hotamisligil, 2011)*

Thus, induction of inflammatory signaling pathways increases infiltration of the immune cells within the metabolic tissue. In turn this lead to elevated levels of inflammatory cytokine such as TNF-α, interleukin (IL)-6, IL-1β, CCL2 for the most important

ones (Berg and Scherer, 2005; Shoelson et al., 2006). Although the increase in inflammatory cytokines after obesity is predominant in the adipose tissue, several studies reported that other tissues are also affected including the liver, pancreas, brain, and even muscles (Saghizadeh et al., 1996; Cai et al., 2005; De Souza et al., 2005; Ehses et al., 2007). This state of inflammation represented as elevation in the cytokines upon obesity was found to be extended systemically (Shoelson et al., 2006). The difference in the inflammatory state between obese and lean animals was also seen in humans.

### 6.5. Consequence of meta-flammation

The increased inflammatory mediators in adipose tissue can cause insulin resistance in adipocytes. This effect was found to be mediated by several factors. For example, adipocytes treated with TNFα show decreased insulin signaling and decreased glucose uptake (Hotamisligil et al., 1994). Excess nutrient or inflammatory signals result in activation of JNK and/or IKK. In turn, they phosphorylate insulin receptor substrate 1 (IRS-1), leading to the inhibition of insulin receptor signaling cascade. The impact of meta-flammation on insulin resistance was confirmed in vivo by genetic inactivation of several inflammatory mediators like TNF-α, TNFR1/2, JNK, TLR2, and IKKε. The results showed beneficial metabolic effects when these mediators were inactivated in the context of metabolic insult by exposure to HFD (Gregor and Hotamisligil, 2011). An example for that, obese TNFα knockout mice show decreased blood glucose and insulin levels in addition to improved glucose and insulin sensitivity, compared with obese control wild-type mice (Uysal et al., 1997).

## 7. Peripheral Diabetic Neuropathy PDN

Neuropathic pain is caused by a lesion or disease affecting the somatosensory pathway (Finnerup et al., 2016). For this, neuropathic pain defers from inflammatory and idiopathic pain in which the sensory neuroaxis is intact (Jensen and Finnerup, 2014). The damage in the somatosensory pathway leads to a paradoxical state of sensory loss and pain that is accompanied with or without hyperalgesia in one or more sensory modalities (Feldman et al., 2017). The prevalence of the neuropathic pain is enormous affecting 8% of the general population in the USA and Europe, and type II diabetes is the main cause for this neuropathy (Gregg et al., 2004). It is estimated that 60 to 70% of diabetic patients will develop Peripheral diabetic neuropathy (PDN) (Todorovic, 2016). This prevalence increases with the duration of diabetes mellitus.

The main cause of diabetic neuropathy is the long exposure of neurons to hyperglycemia associated with metabolic dysregulations, which lead to the activation of the polyol flux, accumulation of the advanced glycation end products like methyglyoxal, oxidative stress and dyslipidemia (Oates, 2008; Tesfaye et al., 2010). Several signaling pathways are activated during inflammation mentioned in the previous chapter ''obesity and inflammation'' (Tesfaye et al., 2010). As for diabetic retinopathy and nephropathy, damage in nerves could also be caused by the alterations in the micro-vascularity.

Diabetic neuropathy is complex and heterogeneous in several aspects including symptoms, affected neurons, risks, pathologic alterations, and underlying mechanisms, for review (Feldman et al., 2017). Indeed not all patients suffering from severe neuropathy will develop pain and the relation between the severity of neuropathy and poor glycemic control with both the risk and intensity of neuropathic pain is not a linear relation (Themistocleous et al., 2016). An example to highlight the diversity and complexity of the disease, type I, II diabetes both lead to significant hyperglycemia in human and in animal models. Yet a Cochrane review collecting data from all clinical studies done between 1983 and 2010 showed that well maintained glucose levels in diabetic patients decreases the incidence of diabetic neuropathy in type I patients but has very little protective effect in T2DM patients (Callaghan et al., 2012a). This finding support that diabetic neuropathy in type I and type II diabetic patients could has similar symptoms but the underlining pathophysiological mechanisms are different (Callaghan et al., 2012b, 2012a). Indeed, this also

emphasizes that not only the present symptoms and manifestations should be considered in order to describe and classify diseases but also the origins of the disease should be taken into account. Surprisingly, although there has been a huge effort on research conducted to understand and decipher the pathogeneses of DN in the last two decades, all the clinical trials conducted in the USA aiming to control the progress of the disease failed (Pop-Busui et al., 2017). This indicate that the clues and aspects of the disease are not all discovered, promoting that basic research should be directed on finding new targets and mediators for understanding the etiology of the disease.

### 7.1. Typical diabetic peripheral neuropathy

This subclass of neuropathy is the most common type that is characterized by its chronicity. The damage affects peripheral neurons of both sides of the body in a length dependent manner that is termed as 'length-dependent sensorimotor polyneuropathy' (Feldman et al., 2017). The damage starts with the longest fibers innervating the toes, feet, and legs. Later, in the course of the disease the shorter fibers in hands and face are affected. Studies showed that the unmyelinated C fibers are firstly affected leading to degeneration / regeneration processes resulting in pain (Green et al., 2010). By time, the degeneration predominates and results in the loss of C-fibers and loss of sensation (Ziegler et al., 2009). Later the myelinated sensory fibers are affected too and finally motor nerves leading to motor deficit (Malik et al., 2005). The reason behind this pattern of progression is unknown but it could be owed to that, myelinated fibers are protected by Schwann cells compared to the unmyelinated C-fibers. This protection is lost over time and degeneration of the myelinated fibers take place (Mizisin, 2014). Sensory neurons especially those of the DRGs are more vulnerable to damage compared to motor nerves because they lack the protection of the blood nerve barrier (Feldman et al., 2017). The blood nerve barrier protects neurons against systemic metabolic cytotoxic metabolites. The described symptoms could be decreased sensation, numbness, pricking, stabbing, burning or aching pain (Tesfaye et al., 2010).

### 7.2. Atypical DPN or Painful DPN

This type differs from the typical DPN in several features; symptoms, onset, and mechanisms. It is estimated that 25% of the diabetic patients might experience painful DPN (Tesfaye et al., 2010). Some studies suggested that symptoms of painful DPN may be improved by the increase in the sensory loss. The associated symptoms are distal, symmetrical, and described as prickling, deep

aching, sharp, like an electric shock, and burning accompanied with hyperalgesia and allodynia to thermal and mechanical stimulation (Apfel et al., 2001; Boulton et al., 2004). The predisposition of painful DPN could be due to the involvement of ion channels that could be directly activated, modulated or have a genetic predisposition (Feldman et al., 2017). The involvement of some of these ion channels will be described in a following section.

## 7.1. Mice models of DPN

In response to the increasing epidemic of DPN, and the lack of effective treatment for it, the National institute of health formed a consortium named diabetic complications consortium (DiaComp). The main aim of this consortium is to identify and characterize novel models of diabetic complication. In addition, it provides phenotyping protocols and set criteria to define the complications associated with diabetes in order to minimize inter-investigator variability and increase the gain from new studies, for review (O'Brien et al., 2014).

Similar to the clinical diagnostic in patients, DPN phenotyping in mice include; measuring nerve conduction velocity, anatomical assessment of the intra-epidermal nerve fiber densities (IENFDs) and assessing changes in the level of myelination. In addition, the impact on the sensory mechanical and thermal modalities can be assessed for allodynia, hyperalgesia, or hypoalgesia (DiaComp). Thermal sensitivity can be assessed by the tail-flick and hind paw withdrawal tests (Hargreaves or paw flick), while the Von Frey filaments is used for assessing mechanical sensitivity (Chaplan et al., 1994). Usually the early phase of DPN is associated with thermal hypersensitivity and tactile allodynia, whereas the late course of the disease is associated with hyposensitivity and reduced responses (O'Brien et al., 2014). Furthermore, assessing levels of oxidative stress, inflammatory infiltrates, and impaired angiogenesis within peripheral nerve tissue can be assessed by immunohistochemistry (Kusano et al., 2004; Vareniuk et al., 2007; Dauch et al., 2013).

Besides, metabolic phenotyping for the mice completes the characterization of DPN models. The assessment includes monitoring of body weight, fasting blood glucose, and impaired glucose hemostasis. Diabetes is determined when the fasting glycaemia exceeds 150 mg/dL (Sullivan et al., 2007). One of the associated disorders to diabetes is dyslipidemia, for that it is important to characterize the serum lipid profiles of mice (Vincent et al., 2009a, 2009b). More extensive

investigations can be done by measuring the ratios of cholesterol and triglycerides, and plasma insulin.

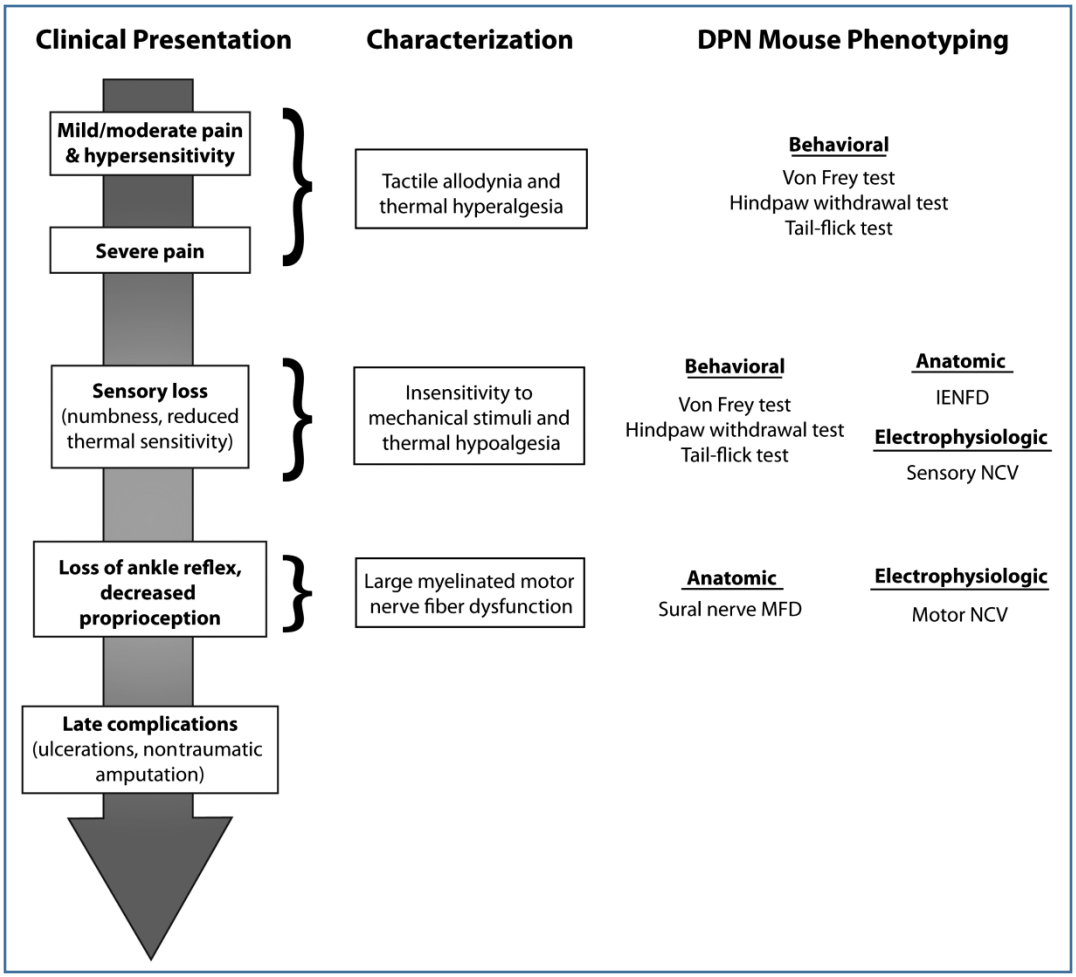


*Figure 22 evolution of PDN symptoms with the appropriate assessments.*
*Source (O'Brien et al., 2014)*

### 7.1.1. DPN phenotyping in Diet induced obesity mouse model

Type II diabetes accounts for 95% of all diabetic patients, besides there is high prevalence of diabetes within obese subjects (CDC, 2011). As presented previously, the main cause of obesity is the imbalance between energy intake and energy expenditure resulting in excessive caloric intake, increase of fat mass, obesity and insulin resistance. The incidence of insulin resistance starts as an impaired glucose tolerance in prediabetes then later develops to hyperglycemia and diabetes mellitus (O'Brien et al., 2014). In addition, type II diabetes is a component of the metabolic syndrome that includes obesity, high blood pressure and dyslipidemia where all can contribute to the DPN associated with type II diabetes.

Several mice models are used to study DPN induced by type II diabetes including the genetically modified mice ob/ob and db/db mice. Although ob/ob and db/db mice share several aspects of type II diabetes, several reports described contradicting phenotypes that could be related to the genetic background of the mice and the used type diet, reviewed in (O'Brien et al., 2014).

The advantage of using high fat diet (HFD) in studying type II diabetes and the associated DPN, is that HFD induces gradual increase in obesity, moderate hyperinsulinemia and impaired glucose tolerance without having hyperglycemia (Obrosova et al., 2007; Vincent et al., 2009a; Coppey et al., 2011; Guilford et al., 2011). A study showed that feeding the mice with 58% of food calories coming from fat induced signs of prediabetes like weight gain, impaired glucose tolerance and normal levels of fasting glucose after 16 weeks of diet (Obrosova et al., 2007). These mice also showed neuropathy described as decreased motor and sensory nerve conductance velocities, mechanical allydonia and thermal hypoalgesia. These mice did not show signs of intra-epidermal nerve fiber loss or axonal atrophy. Interestingly switching these mice from HFD to normal chow for 6 weeks corrected the sensory phenotypes (Obrosova et al., 2007). Other studies using high fat diet showed opposite results with nerve dysfunction and the presence of diabetes (table 3). The differences in the amplitude of the neuropathy between these studies could be due to difference in the neuropathy phenotyping approaches. In addition, differences in sex and age, in addition to, differences in the starting age and duration of HFD feeding (Vincent et al., 2009a; Guilford et al., 2011), of course, the source, composition and percentage of fat content in the diet have high impact on the developed symptoms (Ikemoto et al., 1996; Wang et al., 2002a).

| Chow | | | Mice | | Paradigm | | | Neuropathy phenotype[a] | | | Reference |
|---|---|---|---|---|---|---|---|---|---|---|---|
| **Fat** | **Chow supplier** | **Primary fat source** | **Strain** | **Sex** | **HFD initiation, wks** | **HFD duration, wks** | **Final age, wks** | **Behavior** | **NCV** | **Anatomy** | |
| **45%** | Research Diets D12451 | Lard | C57BL/6 | Male | 3 | 34 | 38 | Thermal hypoalgesia (12 wks) | ↓ MNCV (12 wks)<br>↓ SNCV | ↓ IENFD | (1) |
| | | | C57BL/6 | Male | 12 | 12 | 24 | Thermal hypoalgesia (6 wks) | ↓ SNCV<br>Ns Δ MNCV (6 wks) | ↓ IENFD | (2) |
| | | | C57BL/6 | Male | 12 | 12 | 24 | Thermal hypoalgesia | ↓ SNCV<br>Ns Δ MNCV | ↓ IENFD | (3) |
| **54%** | Harlan Teklad TD.07011 | Vegetable oil | C57BL/6 | Male | 7 | 8 | 15 | Tactile allodynia<br>Absent thermal hypoalgesia | ↓ MNCV<br>Ns Δ SNCV | Ns Δ IENFD | (4) |
| **58%** | Research Diets D12330 | Coconut oil | C57BL/6 | Male | — | 16 | — | Mechanical hypoalgesia<br>Thermal hypoalgesia | ↓ MNCV<br>↓ SNCV | — | (5) |
| | | | C57BL/6 | Male | — | 23 | — | Mechanical hypoalgesia (16 wks)<br>Thermal hypoalgesia (16 wks)<br>Tactile allodynia (16 wks) | ↓ MNCV<br>↓ SNCV | — | (6) |
| | | | C57BL/6 | Female | — | 16 | — | Tactile allodynia<br>Thermal hypoalgesia | ↓ MNCV<br>↓ SNCV | Ns Δ IENFD | (7) |
| | | | C57BL/6 | Female | — | 16 | — | Tactile allodynia<br>Thermal hypoalgesia | ↓ MNCV<br>↓ SNCV | — | (8) |

*Table 3 Phenotyping of Neuropathy in models of DIO.*
*References are placed in order 1-8 (Vincent et al., 2009a; Coppey et al., 2011, 2012; Guilford et al., 2011; Lupachyk et al., 2013; Watcho et al., 2010; Stavniichuk et al., 2010; Obrosova et al., 2007) Adapted from (O'Brien et al., 2014)*

A recent study tested the effect of high fat diet in inflammatory pain model in two different strains of rats (Song et al., 2017). First, they found that the consumption of high fat diet for eight weeks induced obesity, and increased body fat in a strain-dependent manner (Long-Evans and Sprague-Dawley rats). The basal mechanical and cold responses were unaltered between rats fed with low fat or high fat diet in both strains. In turn, they studied the impact of six weeks of high fat diet on pain responses in two models of inflammatory pain; DRG inflammation by intrathecal injection of zymosan, and peripheral inflammation by injection of CFA in the rat hind paw. Low concentrations of both inflammatory compounds were used to avoid ceiling effect. These low doses of inflammatory compounds induced moderate effects in rats fed with the normal chow, and showed fast recovery. On the contrary, rats fed the high fat diet showed mechanical and cold allodynia in addition to increased guarding behavior compared to control rats. Interestingly, this enhanced pain associated with the inflammatory molecules was found in both rat strains fed the high fat diet regardless of the state of obesity (Song et al., 2017). This argues that high fat diet can induce pain even in the absence of obesity. In search of the underlining mechanisms behind enhanced pain responses in both strains, the contribution of insulin, leptin and inflammatory cytokines could be excluded as they were elevated in the obese rats but not in the lean rats fed with the high fat diet.

On the other hand, there was an increased density of macrophages in the DRGs of both strains of rats after inflammation suggesting that the enhanced pain responses could be mediated through this effect. The mechanism behind the enhanced pain could be owed to that obesity and local inflammation can downregulate the anti-inflammatory receptor peroxisome proliferator-activated receptor-α (PPARα), which can directly sense fatty acids and lipid-derived substrates in many tissues (Song et al., 2017). Altogether, the consumption of high fat diet induced enhanced pain responses in inflammatory models regardless of the state of obesity and the strain of rats. Conversely, the establishment of obesity was highly affected by the strain of rats. This Highlight the important role of the high fat diet in inducing pain and the less importance of the state of obesity in the pain process.

## 7.2. Ion channels in PDN

As discussed previously, ion channels drive the excitability of sensory fibers. Their role in PDN has been investigated in many studies.

A study tested the contribution of Hyperpolarization-activated cyclic nucleotide–gated (HCN) in mouse models of PDN, where they showed that 88% of mice injected with streptozocin (STZ) developed hyperglycemia while 80% developed hyperalgesia (Tsantoulas et al., 2017). In this model of type I diabetes, mice developed mechanical hypersensitivity in a progressive manner that started at 2 weeks post STZ injection to reach a plateau at 8 weeks and lasted for 18 weeks. Diabetic mice developed thermal hyposensitivity 6 to 8 weeks post-injection. Pharmacological blockade and genetic deletion of the HCN2 channel in nociceptive neurons improved the mechanical hypersensitivity in these diabetic mice, while no effect was seen on the diabetic thermal hypoalgesia (Tsantoulas et al., 2017). The blockade of HCN did not affect acute mechanical or thermal pain. Using the db/db mouse model of type II diabetes, mice developed obesity, hyperglycemia, and diabetes. These diabetic mice also developed mechanical hypersensitivity that was corrected by a non-selective blocker of HCN channels. The study hypothesized that HCN2 channels could be sensitized by the elevated intracellular cAMP levels, and become active at more depolarized membrane potentials leading to increased noxious perception. This was accompanied by increased C-fos$^{+}$ neurons in the first and second lamina of the dorsal horn which were less numerous in animals treated with HCN blocker or by genetic deletion of HCN2. Electrophysiology and immunohistochemistry argue against any change in HCN2 channel expression or properties of HCN currents in small diameter DRG neurons. Nevertheless levels of cAMP was found to be higher in diabetic mice that showed pain, and this increase in cAMP was able to shift the activation of HCN2 channels to more positive membrane voltage (Tsantoulas et al., 2017).

Voltage gated sodium channels are responsible for the generation and propagation of action potentials along axons of DRG neurons. Nav1.7, 1.8 and 1.9 are predominantly expressed in DRG neurons (Barker et al., 2017). They are subject of important post-translational modifications that affect the excitability of the DRG neurons (Rizzo et al., 1994). Indeed, dysregulations in their functionality and expression were linked to painful diabetic neuropathy. Studies showed that Nav1.8 is overexpressed in painful diabetic neuropathy, and its currents are enhanced. This

enhancement in Nav1.8 currents leads to a facilitation of triggering action potentials in the sensory neurons resulting in pain hyperalgesia (Sun et al., 2012).

Several mutations in the Navs were found to be associated with increased risk and severity of painful diabetic neuropathy. For example, a gain of function mutation found in Nav1.7 leads to hyper-excitability of DRG neurons. This effect could be mediated by Nav1.7 amplifying the depolarization induced by external stimuli to a level close to the threshold of Nav1.8 activation (Hoeijmakers et al., 2014; Li et al., 2015).

Nav1.8 channels expressed in the nociceptors are the main channel responsible for triggering action potentials in these neurons and drive their excitability. Methylglyoxal is a highly reactive metabolite of glucose, where a study showed that methylglyoxal production is increased after hyperglycemia (Bierhaus et al., 2012). In addition, the expression of the enzyme responsible for metabolizing methylglyoxal to lactate is reduced during diabetes. High concentration of this active metabolite was found in patients with PDN. The same high concentration of methylglyoxal can depolarization sensory neurons through a post-translational modification of Nav1.8 that increases the channel activity. Methylglyoxal also slows the inactivation of Nav1.7 (Bierhaus et al., 2012). Behavior experiments show that naïve mice treated with methylglyoxal have similar features of painful diabetic neuropathy seen in mice suffering from type I diabetes 8 weeks after STZ injection. These mice have thermal and mechanical hyperalgesia in addition to reduction in nerve conduction velocity (Bierhaus et al., 2012). Injection of methylglyoxal in Nav1.8 knockout mice did not induce any pain phenotype. Interestingly this study highlighted the role of Nav1.8 in the painful diabetic neuropathy regardless the degenerative or regenerative changes in sensory nerves, a finding that can confirm the importance of ion channels in the induction and maintenance of painful PDN. Later another study failed to find a significant co-relation between the concentration of methylglyoxal, with either cardiovascular autonomic neuropathy, diabetic peripheral neuropathy or painful diabetic neuropathy in well-treated patients suffering from short-term diabetes (Hansen et al., 2015).

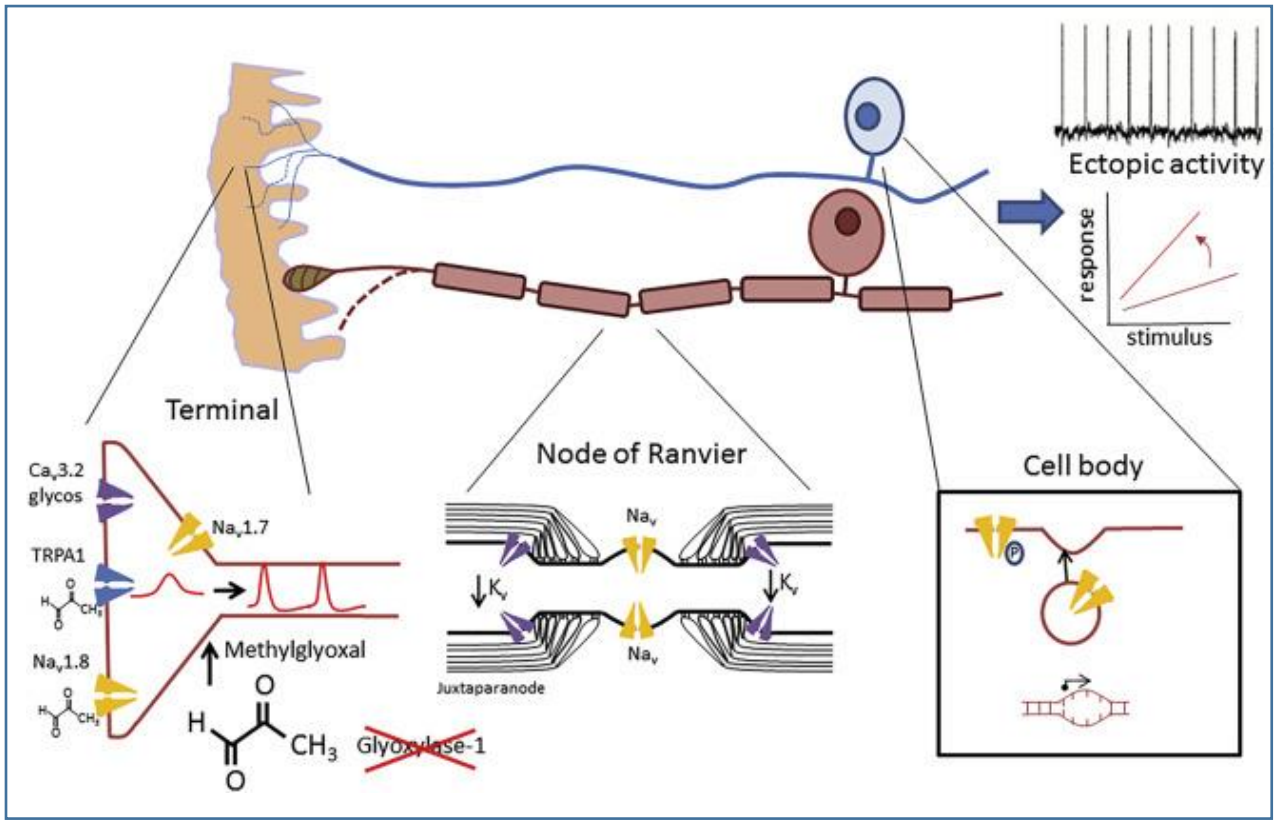


*Figure 23 ion channels in PDN.*

*Unmyelinated C-fibers (blue) and myelinated axons (brown) undergo length-dependent degeneration and retraction (dotted lines). Ion channels expressed on the nociceptors, can be activated or potentiated by post-translational modifications, for example, increased methylglyoxal and enhanced glycosylation increase activity of several ion channels. In myelinated axons, the distribution of voltage-gated ion channels at the node of Ranvier changes with reduced expression of shaker-type Kv at the juxtaparanode, leading to hyper-excitability. All these changes lead to a state of hyper-excitability of the sensory afferents and may lead to ectopic activity. Source* (Feldman et al., 2017).

Another ion channel shown to be contributing to the pathogenesis of painful diabetic neuropathy is TRPA1. Methyglyoxal activates TRPA1 leading to neuronal hyper-excitability (Andersson et al., 2013). During diabetes, several reactive oxygen species (ROS) are increased. ROS deteriorate pancreatic β-cell function and increase insulin resistance. In addition, ROS are also involved in the development of atherosclerosis, which is often observed under diabetic conditions. These ROS can produce $H_2o_2$ and hydroxynonenal, which can directly activate TRPA1, and indirectly they can potentiate the effect of methyglyoxal on TRPA1 (Andersson et al., 2008, 2013). Indeed, pharmacological blockage of TRPA1 attenuates the mechanical hypersensitivity in a model of type 1 diabetes obtained by STZ injection in rats (Wei et al., 2009). However, in this study, diabetes did not affect the acute thermal sensitivity neither the administration of the TRPA1 antagonist.

Several studies found that in models of diabetic neuropathy, an extracellular arginin residue of T-type $Ca^{2+}$ channels is glycosylated leading to modification in the activation kinetics of the channel, increased current densities, and increased surface expression (Orestes et al., 2013). Because these channels plays an important role in regulating the sub-threshold excitability of the nociceptors, these effects lead to hyper-excitability of DRG neurons. Interestingly the downregulation of the Cav3.2 T-type Calcium channel reduces the pain hypersensitivity in STZ rats (Messinger et al., 2009).

# Materials & Methods

In this section I will describe materials and methods that is not described in the Article in the results section.

## 1. Diet composition

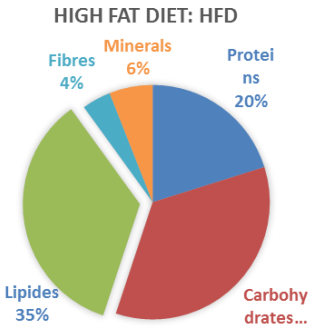


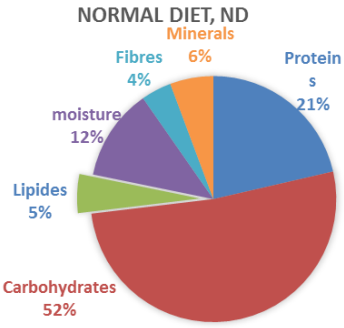


*Table 4 Diet composition*

| | Normal diet | High Fat Diet |
|---|---|---|
| Energy Kcal/Kg | 3.2 | 5.283 |
| Percentage of energy provided by lipids | 13.6 | 60 |
| Total lipid % | 5% | 36% |
| Saturated Fatty acid/ Unsaturated Fatty acid % | 23 / 77 | 70 / 30 |
| Ratio ω-6/ ω-3 | 8 (51/8) | 8 (6/1) |
| Lipid composition % in diet (mg/Kg) | | |
| *Palmatic acid C16:0* | 1% (7600) | 11%( 110471) |
| *Stearic acid C 18:0* | 0.005% (1500) | 4% (37134) |
| *Oleic acid C 18:1* | 0.01% (10000) | 7% (63883) |
| *Linoleic Acid C18:2* | 3% (25000) | 2% (16894) |
| *Arachidonic acid C20:4* | 0.01% | 0.036% (340) |
| Protein | 21% | 19% |
| Carbohydrates | 52% | 32% |

## 2. Formalin test

The formalin test developed by (Dubuisson and Dennis, 1977). Animals were removed from their home cage to record their body weight and mark them. The marked animals were placed separately into the formalin test chamber fitted with mirrors behind and beside the container to ensure that hind paws can be seen from all angles. Animals were acclimated for 15 to 30 min. Then animals were injected with 10 µl of 5% formalin into the dorsal surface of the paw using 50-µl Hamilton syringes equipped with 30-G needle. Immediately returned to the containers, and time spent mice showing nocifensive behaviors during 5 min interval over 60 minutes were recorded.

## 3. RNA extraction and qPCR

Protocol of RNA Extraction: According Chomczinski via FastPrep® : Total RNA extraction from tissue of animal were done according to (Chomczynski and Sacchi, 2006) protocol: For each sample of 20 to 200 mg: add 1ml mixture "Solution D + ß Mercaptoethanol" in a tube FastPrep for "Lysing Matrix D 'green cap (in kit fastRNA® Pro Green Kit (Q-BIOgene)) and keep in ice. Add in the tube containing "solution D + ß-Me," the tissue sample. Place tubes in FastPrep® for 40s at 6.0 speed. Remove the tubes and centrifuge 5min - 14000rpm - 4 ° C. Transfer the liquid into another clean 2 ml tube being careful not to disturb the beads (~ 600 to 700µl). Incubate 5min samples transferred into the ice (or at 4° C). Add to this tube: 1/10 volume of 2M NaOAc pH 4 agitate / mix good, 1 volume of phenol saturated with water at pH 4.5-5 shake / mix well, 1/5 volume of Sevag (chloroform-49; isoamyl alcohol-1) agitate for at least 10s. Incubate at least 15 minutes in the ice. Centrifuge tubes 15min - 14000rpm - 4 ° C. Transfer the upper phase (without disturbing the interphase) into a 1.5 ml tube. If part of the interphase is transferred, repeat the centrifugation the upper phase and transfer the new upper phase to a clean tube. Add 1 volume of cold isopropanol (in a freezer at -20 ° C); mixed by inversion 5 times and incubate at least 1 hour at -20 ° C. Centrifuge 20min - 14000rpm - 4 ° C and remove the supernatant. Wash the pellet once with 75% ethanol 500µl cold (-20 ° C freezer) vortex. Centrifuge 5min - 14000rpm - 4 ° C. Remove ethanol, let air dry for 10 to 15 minutes at RT ° (do not let the RNA pellets completely dry). Resuspend in an appropriate volume of $H_2O$ milliQ tissue: 20-50µl fabric <50mg and 100 .mu.l fabric> 50mg (25µl for ½ hypothalamus; 50 .mu.l for ½ cortex). Incubate 10 min at 65 ° C and the

RNA stored at -20 ° C. Determine the concentration of RNA by Nanodrop. Calculate RNA concentration in mcg / ml using the formula: (OD $_{260)}$ * (40µg / ml / per OD) * 100 (dilution factor) = ug RNA / ml. The integrity of the RNA was analyzed visually by loading 1 .mu.g RNA per well in a 1% agarose gel + Agilent Bioanalyzer. RT-qPCR : Quantitative real-time PCR. composition of the reaction 12,5µl or 8 µ l SybrGreen ROCHE (2x) 2,5µl or 1.6 µ l of mix oligos S (or M) + AS (or R) 5µl or 3.4 µ l water 5µl or 3 µ l of diluted RT ed products 1/5. Prepare the mixture of SybrGreen, of oligos S + AS and water for the number of wells to be tested. Add 13 µl of the mixture into each well to electronic pipette. Depositing 3 µ l of RT products from the sample in duplicate (2 wells per test sample) by changing the pipette tip between each well. Seal the plate using transparent adhesive plastic film are being careful to leave any fingerprints. Vortex and centrifuge 1min - 1000rpm - RT °

Sequence of oligo-nucleotides used for PCR

| Gene | Reverse or Forward | Sequence (5'-3') | Concentration to use |
|---|---|---|---|
| GADPH | R | CCA-GTG-AGC-TTC-CCG-TTC-A | 300nM |
| GAPDH | F | GAA-CAT-CAT-CCC-TGC-ATC-C | 300nM |
| IL-1ß | F | TGGTGTGTGACGTTCCCATT | 500 or 600nM |
| IL-1ß | R | CGACAGCACGAGGCTTTTTT | 500 or 600nM |
| IL-6 | F | CCCAATTTCCAATGCTCTCCT | 500 or 600nM |
| IL-6 | R | GAATTGGATGGTCTTGGTCC | 500 or 600nM |
| TNF-α | F | GGTGACCAGGCTGTCGCTAC | 500 or 600nM |
| TNF-α | R | AGGGCAATTACAGTCACGGC | 500 or 600nM |
| MCP1 | F | CCAACTCTCACTGAAGCCAGC | 300nM |
| MCP1 | R | CAGGCCCAGAAGCATGACA | 300nM |
| RANTES | F | ACACCACTCCCTGCTGCTTT | 300nM |
| RANTES | R | AAATACTCCTTGACGTGGGCA | 300nM |
| ASIC1a | F | GCCCTGCTCAACAACAGGTA | 300nM |
| ASIC1a | R | TACGGAAGTTGGCCTTGTCC | 300nM |

| | | | |
|---|---|---|---|
| ASIC1b | F | cgcacgtgactttgctagat | 300nM |
| ASIC1b | R | gaaggtgacagctgggaaga | 300nM |
| ASIC2a | F | AAGTTCAAGGGGCAGGAGTG | 300nM |
| ASIC2a | R | TGTCCAGCATGATCTCCAGC | 300nM |
| ASIC2b | F | CCCGCACAACTTCTCCTCAG | 300nM |
| ASIC2b | R | TGTCCAGCATGATCTCCAGC | 300nM |
| ASIC3 | F | cacccaatgacttgcactgg | 300nM |
| ASIC3 | R | taggcagcatgttcagcagg | 300nM |

Steps of qPCR Launch of the PCR: PCR program Initial denaturation: *95 ° C - 5min; Ramp Rate = 4.4 ° C / s*. Amplification: 45 cycles. *95 ° C - 10s - Ramp Rate 4.4 ° C / s. 60 ° C - 10s - Ramp Rate 2.2 ° C / s. 72 ° C - 10s - Ramp Rate 4.4 ° C / s* Melting Curve: *95 ° C - 5s - Ramp Rate 4.4 ° C / s. 65 ° C - 1min - Ramp Rate 2.2 ° C / s. 97 ° C - Ramp Rate 0.11 ° C / s*. Cooling:. *40 ° C - 10 s - Ramp Rate 1.5 ° C / s. Data are expressed as fold increase with reference to GAPDH.*

## 4. Immunohistochemistry

For intra-cardiac perfusion of PFA 4%, animals were Perfused with 10 mL of cold PB 0.1M. (Speed = 3.5mL/min) then Perfused with 20-30 mL of PFA 4% + cold PB 0.1M. (Speed = 3.5m/min). Spinal cord was collected and post-fixed in PFA 4% + PB 0.1M at 4°C for 4 hours.

Staining protocol: Slice using vibratome at 30 micron. Wash 3 X 5 min in PBS 1x then agitate the slices in PBS 1X + 0.1% Triton + 1% BSA at room temperature for 30 minutes (mn). Incubate with the primary antibody overnight in the cold room (4°C) or at room temperature for 4 hours. Wash twice for 5-10mn. Incubate with the appropriate secondary antibody. Rinse twice for 5-10mn in PB 0.1M at room temperature. Apply DAPI 0.01% (diluted in PBS 1X) at room temperature for 5mn. Rinse twice for 5-10mn in PB 0.1M at room temperature. Mount the slices between slide and cover with Mowiol mounting medium. Antibodies rabbit anti-IBa1 290A,B Biocare, rabbit anti-GFAP Z0334 Dako both at 1/400. Secondary antibody Alexa 488 A-21207 Invitrogen.

# Results

## 1. Lipid-rich diet consumption induce thermal pain through the activation of ASIC3 channels.

NEGM A.[1], STOBBE K. [2], DEVAL E. [1], LINGUEGLIA E. [1], ROVERE C. [2], and NOEL J.[1,2].

[1] Université Côte d'Azur, CNRS, IPMC, France; LabEx Ion Channel Science and Therapeutics, IPMC, France.

[2] Université Côte d'Azur, CNRS, IPMC, France.

## 1.1. Introduction

Obesity is considered a worldwide health problem affecting 13% of the overall world's adult population (WHO-Obesity). Moreover, the increasing prevalence of obesity during the last two decades encourages to further study the causes and consequences of this metabolic disorder (Ginter and Simko, 2014b; Hruby and Hu, 2015; Twells et al., 2014). 90% of causes of obesity is not related to hormonal or genetic factors but rather owed to behavior and environmental factors that lead to increased energy intake (Le Thuc et al., 2017; Xu and Xue, 2016). This increase is caused by consumption of high caloric food intake accompanied by low physical activity (Spiegelman and Flier, 2001). The burdens of obesity is not only it's effect on the physical appearance and the fitness of individuals, but it is a major risk factor for several disorders including metabolic syndrome; diabetes type II, dyslipidemia, increase blood pressure, and cardiovascular disorders in addition to pain (Hruby and Hu, 2015; Okifuji and Hare, 2015).

Several studies showed that the consumption of lipid rich diet could lead to diabetic neuropathic pain. Nevertheless the features and the severity of the symptoms varies dramatically based on the experimental design, species, sex, differences in the starting age, duration of HFD feeding(Guilford et al., 2011; Vincent et al., 2009a), and quality and quantity of the fat content(Ikemoto et al., 1996; O'Brien et al., 2014; Wang et al., 2002b). While several reports focused on the contribution of several ion channels in the context of diabetic neuropathic pain associated with models of type I or type II diabetes generated by genetic intervention, less is known about the contribution of ion channels in models of lipid rich diet(Bierhaus et al., 2012; Tsantoulas et al., 2017).

Acid sensing ion channels (ASIC) are cationic ion channels that belong to the family of degenerin/ epithelial sodium channels (ENaC)(Deval et al., 2010; Kellenberger and Schild, 2002). Six members of this sub-family were discovered. Their expression is found in neuronal and non-neuronal cells with different patterns, and in a species dependent manner (Chen et al., 1998; Deval and Lingueglia, 2015; Deval et al., 2010; García-Añoveros et al., 1997; Waldmann et al., 1997a). Clinical experiments showed that ASICs are responsible for the acidic pain (Jones et al., 2004; Ugawa et al., 2002). Among this family is ASIC3 subunit formally named DRASIC as it's expression is almost restricted to the peripheral nervous system(Price et al., 2001; Xie et al., 2002). Early studies showed that ASIC3 channels have relatively low contribution to the acute pain(Chen et al., 2002;

Mogil et al., 2005; Price et al., 2001). Nevertheless, the activation of ASIC3 by local injection in mouse paw of 2-guanidine4-methylquinazoline, GMQ, induced pain behaviors, while knocking down the expression of ASIC3 in rodents attenuated the inflammation-induced heat hyperalgesia(Deval et al., 2008; Yen et al., 2009; Yu et al., 2010). Other Studies also showed the positive involvement of ASIC3 channels in postoperative pain and more recently in joint pain(Deval et al., 2011; Marra et al., 2016).

In addition, several agents were shown to enhance ASIC3 channels activity and currents, including divalent and polyvalent cations, proteases, kinases, and lipids (Vullo and Kellenberger, 2019). Among these lipids, Arachidonic acid which was shown to enhance ASIC3 currents evoked by acidification(Deval et al., 2008; Smith et al., 2007). Lysophosphatidylcholine LPC is a species of lipids found to interact with ASIC3 channels not only potentiating its responses toward acidification but also directly activating the channel at physiological pH 7.4, leading to a depolarization and increased C-fibers firing(Marra et al., 2016). Indeed, the co-injection of AA and LPC in mice increased pain behaviors in naïve but not ASIC3 knockout mice(Marra et al., 2016).

Therefore, we hypothesized that a lipid rich diet which induces dyslipidemia and upregulation of several species of lipids in the blood of mice may interact with ASIC3 channels expressed in the distal terminals and cell bodies of sensory neurons. In turn this will result in hypersensitivity toward some pain phenotypes.

## *1.2.* Materials and Methods

### *1.2.1. Animals*

Experiments were performed on male C57Black6J wild-type mice (Janvier labs) and ASIC3 knockout mice raised on C57Black6j genetic background(Wultsch et al., 2008). Animals were housed in a 12 hours reversed light-dark cycle with food and water ad libitum. Lights intensity in the housing room was set at 2000 lux. Mice were acclimated to housing and husbandry conditions for at least 1 week before experiments. Animal procedures were approved by the Institutional Local Ethical Committee and authorized by the French Ministry of Research according to the European Union regulations and the Directive 2010/63/EU and was in agreement with the guidelines of the Committee for Research and Ethical Issues of the International Association for the Study of Pain(Zimmermann, 1983). (Agreement 02677.01). Animals were sacrificed at experimental end points by CO2 euthanasia.

### *1.2.2. Mice diet*

Four weeks-old mice 15-18 g were weight-matched between groups and used for the Feeding experiments. Mice were distributed equally into two groups of 8 to 10 mice and were housed separately. One group received normal standard diet (ND) and the other received high fat diet (HFD). The amount of food are calculated where each mice receive 4g of food per day, this is ad libitum amount. The weight of the mice, the amount of food and water consumed were measured 3 times a week. The two diets are obtained from Scientific Animal Food and Engineering Company (SAFE®). (“SAFE”)

The ND is a normal standard breeding diet given to the control mice. The caloric intake of the ND diet is 3200 kcal/kg, mainly through protein and fibers (25.4% of total nutritional composition) and with only 5.1% of Kcal from lipids. Lipids in ND food is an equilibrated balance between polyunsaturated (linoleic acid, omega 6, and linolenic acid, omega 3), mono-unsaturated (oleic acid) and saturated fatty acid (palmitic acid). The high fat diet HFD contain high concentration of lipids, 36% in diet, which is destined to increase total body weight and adipose body mass, with diabetogenic effect. The high fat diet is used to produce obese mice (Diet Induced Obesity or DIO). HF diet caloric intake is 5 283 kcal/kg, mainly from saturated fatty acids from anhydrous butter.

35.5% of fat content comes from saturated fatty acids (palmitic and stearic acids) and less than 1% of fat content from omega 3 poly-unsaturated fatty acids (linolenic acid). HFD brings 61 % of the food energy from fats.

### *1.2.3. Behavioral assays*

- Thermal pain sensitivity *thresholds tests*

For nociceptive behavior experiments, mice were placed individually in an observation chamber (8 x 8 cm) where they were acclimated for at least 20 min before measures. The thermal pain thresholds were measured with the plantar Hargreaves' radiant heat test (Analgesia Meter, Bioseb) as described previously(Verkest et al., 2018). Mice were placed individually in plastic enclosures on an elevated transparent plastic floor. A radiant infrared heat source was then focused under one animal's hind paw and maintained until the mice lifted its paw. Reaction scores were the results of two measures on both hind paws, with a minimum of 5 min interval between measures. For injections mice were restrained gently while APETx2 (0.23µg/g), were administered intraperitoneal using a 26-gauge needle connected to a 100-ml Hamilton syringe.

The tail immersion test was done by immersing the tail of the mice in a temperature-controlled water bath adjusted at 48°C until withdrawal was observed (cutoff time, 30 seconds). Mice were habituated to manipulation and moderate contention for two days and the measurements were done on the third day. The latency of tail withdrawal was calculated by averaging three responses separated by at least 1 minute.

- *Mechanical sensitivity*

The mechanical sensitivity of the mice was evaluated with a dynamic plantar aesthesiometer (Bioseb). Mice were placed in individual plastic boxes on top of a wire grid surface. The mice hind paw was subjected to a force ramped up to 7.5 g during 10 seconds. The paw withdrawal force threshold (g) was measured in duplicate for each paw, and the mean force was calculated(Verkest et al., 2018).

- *Motor activity and anxiety tests*

The rotarod (Bioseb, Chaville, France) was used to measure the motor coordination, and balance of the mice(Jones and Roberts, 1968). Mice were placed on the Rotarod at an accelerating speed from 4 to 40 rpm for 300 seconds. The mean latency to fall off the Rotarod during the trials was recorded and used in subsequent analysis. Measures were repeated with 15 min between each of the three trials performed.

Open field experiments were done by placing the mice in the open field boxes (40 x 40 x 30 cm) with illumination and video tracking above the boxes. The behavior of mice was analyzed by ANY-maze tracking software (Anymaze, Stoelting, USA). The time spent in the central zone and the total traveled distance within 10 min trial was scored.

- *Glucose homeostasis*

For glucose tolerance test, the mice were fasted for 16 h with free access to water. Mice were injected intraperitoneal with glucose (1.5 g/kg in phosphate buffer saline). Blood plasma glucose concentrations were measured from tail vein samplings at various times using an AccuChek Performa glucometer (Roche Diagnostic, Saint-Egreve, France).

- *Chemicals*

APETx2 was synthesized by Synprosis/Provepep (France). Lipids were purchase from Sigma and/or Avanti (Coger, France). All lipids were prepared as stock solutions in either saline, DMSO, or EtOH, stored at −20°C, and diluted to the final concentration into the proper control solution just before the experiments.

### *1.2.4. Serum preparation and delipidization*

The blood of the mice were collected in (micro tube 1.1 ml sarstedt) and kept on ice all time. Then it was centrifuged at 10000g for 10 min at 4°C to separate the serum. **Protocol of serum delipidation**: the protocol was adapted from(Renaud et al., 1982) where the serum density was adjusted by NaBr to be 1.215 g/ml using Radding-Steinberg formula. Following serum was ultra-centrifuged at 223000g for 24 hours and the lower phase containing the delipidized serum was collected in new tubes this step was repeated 3 times. The delipidized serum was then dialyzed in

Slide-A-Lyzer® Dialysis Thermo scientific 5 times against control bath solution containing (in mM) the following: 145 NaCl, 5 KCl, 2 MgCl2, 2 CaCl2, and 10 HEPES (pH 7.4 with NaoH).

### *1.2.5. Lipidomic analysis*

**Sample Preparation Reagents:** Acetonitrile (ACN) and isopropropanol (IPA) were purchased from (Carlo Erba). Chloroform (ChCl3) from Merck. These solvents were LC-MS grade. Methanol (MeOH) was from VWR. Formic acid Optima LC-MS quality was purchased from ThermoFisher. Ultrapure water was from purelab flex (Veolia Water), and formate ammonium (99%) was from Acros Organics.

**Lipids extraction:** Lipids were extracted according to a modified Bligh and Dyer protocol(Bligh and Dyer, 1959). Lipid extraction was performed in 1.5 ml solvent-resistent plastic Eppendorf tubes and 5 ml glass hemolyse tubes to avoid contamination. Methanol, chloroform and water were at 4°C. 120 µL of serum was collected in a 1.5 ml Eppendorf tube and 300 µl of methanol was added. After vortexing (30s), the sample was frozen for 20 min at -20°C. The sample was transferred in a glass tube and 100 µL of chloroform was added. The mixture was vortexed for 30s and centrifuged (2500 rpm, at 4°C for 10 min). After centrifugation, the supernatant was collected in a new glass tube and 150 µL of chloroform and 150 µL of water were added. The sample was vortexed for 30s and centrifuged (2500 rpm, 4°C, and 10 min). 150 µL of the non-polar phase was collected, added in a new glass tube and dried under a stream of nitrogen. The dried extract was re-suspended in 60 µL of methanol/chloroform 1:1 (v/v) and transferred in an injection vial before liquid chromatography and mass spectrometry analysis. **Instruments and methods:** Reverse phase liquid chromatography was selected for separation with an Ultra Performance Liquid Chromatography UPLC system (Ultimate 3000, ThermoFisher). Lipid extracts of serum from mice were separated on an Accucore C18 150x2.1, 2.5µm column (ThermoFisher) operated at 400 µl/min flow rate. The injection volume was 3 µl of diluted lipid extract. Eluent solutions were ACN/H2O 50/50 (V/V) containing 10mM ammonium formate and 0.1% formic acid (solvent A) and IPA/ACN/H2O 88/10/2 (V/V) containing 2mM ammonium formate and 0.02% formic acid (solvent B). The used step gradient was : 0 min 35% B, 0.0–4.0 min 35 to 60% B, 4.0–8.0 min 60 to 70% B, 8.0–16.0 min 70 to 85% B, 16.0-25 min 85 to 97% B, 25-25.1 min 97 to 100% B, 25.1-31 min 100% B and finally the column was reconditioned at 35% B for 4.0 min. The UPLC system was coupled with a Q-exactive

orbitrap Mass Spectrometer (thermofisher, CA); equipped with a heated electrospray ionization (HESI) probe. This spectrometer was controlled by the Xcalibur software and was operated in electrospray positive mode. MS spectra were acquired at a resolution of 70 000 (200 m/z) in a mass range of 250–1200 m/z with an AGC target 1e6 value and a maximum injection time of 250 ms. 15 most intense precursor ions were selected and isolated with a window of 1 m/z and fragmented by HCD (Higher energy C-Trap Dissociation) with normalized collision energy (NCE) of 25 and 30 eV. MS/MS spectra were acquired in the ion trap with an AGC target 1e5 value, in a mass range of 200-2000 m/z, the resolution was set at 35 000 at 200 m/z combined with an injection time of 80 ms. Data were reprocessed using Lipid Search 4.1.16 (Thermo Fisher). In this study, the product search mode was used and the identification was based on the accurate mass of precursor ions and MS2 spectral pattern. Mass tolerance for precursor and fragments was set to 5 ppm and 8 ppm respectively. m-score threshold was selected at 5 and ID quality filter was fixed at grades A, B and C. $[M+H]^+$, $[M+Na]^+$ and $[M+NH4]^+$ adducts were searched.

LPC quantification was done using a standard calibration curve. For that, we used three LPC standards: LPC (16:0), LPC (18:0) and LPC (18:1). Each standards was analyzed with seven different concentration (5, 10, 25, 40, 50, 70 and 100 µM). Each concentration was injected 4 times for technical replicates with the same UPLC-HRMS method used for serum analysis. The measures given in arbitrary unit (area under the peak) were fitted against their corresponding standard concentrations by linear regression.

### *1.2.6. Primary culture of DRG neurons*

DRG neurons were prepared from male C57Bl6J mice (6–14 weeks old) based on previous study (Francois et al., 2013). After isoflurane anesthesia, animals were killed by decapitation and lumbar DRG were collected on cold HBSS. Mouse DRGs were enzymatically digested at 37°C for 40min with collagenase II (Biochrom, 2mg/ml, 235U/mg) and dispase II (Gibco, 5mg/ml, 1,76U/mg). Gentle mechanical dissociation was done with a 1ml syringe and several needles with progressive decreasing diameter tips (18G, 21G and 26G) to obtain a single cell suspension. Neurons were then plated on collagen-coated 35 mm Petri dishes (Biocoat) and maintained in culture at 37°C (95% air/5% $CO_2$) with the following medium: Neurobasal-A (Gibco) completed with L-glutamine (Lonza, 2mM final), B27 supplement (Gibco, 1X) and 1% penicillin/streptomycin. One day after

plating, culture medium was carefully changed to remove cellular debris and replaced with complete culture medium. The following additional growth factors were used: Nerve Growth Factor (NGF, Sigma) 100ng/ml, retinoic acid 100nM (Sigma), Glial Derived Neurotrophic Factor (GDNF) 2ng/ml, Brain Derived Neurotrophic Factor (BDNF) 10ng/ml and Neurotrophin 3 (NT3) 10ng/ml (all three from Peprotech). Patch-clamp recording were done 1-4 days after plating on both small (capacitance <40pF) and large (>40pF) diameter neurons. The average capacitance of the used DRGs was 37.2 +/- 1.53 pF that correspond to small to medium diameter neurons (bardoni etal, 2014) and the average resting potential was -58.8 +/- 0.82 mV. No significant difference was found in these 2 parameters between the different conditions.

### *1.2.7. HEK293 cell cultures and transfection*

HEK293 cell lines were grown as described previously(Marra et al., 2016). One day after plating, cells were transfected with 0.5µg of DNA per dish of one of the following pIRES2-mASIC3-EGFP or pIRES2-rASIC1a-EGFP vectors using the JetPEI reagent according to the supplier's protocol (Polyplus transfection SA, Illkirch, France). Fluorescent cells expressing GFP were used for patch-clamp recordings 2–4 days after transfection.

### *1.2.8. Patch-clamp experiments*

Patch-clamp whole-cell configuration technique was used to measure membrane currents and voltages under voltage clamp and current clamp configurations respectively. Recordings were performed using an axopatch 200B amplifier (Axon Instruments) with a 2 kHz low-pass filter at room temperature. The data sampling was done at 10 kHz, digitized by a Digidata 1440 A-D/D-A converter (Axon Instruments) and recorded on a hard disk using pClamp software (version 10; Axon Instruments). For whole-cell experiments, the patch pipettes (2–8 MΩ) contained (in mM): 135 KCl, 2.5 $Na_2$-ATP, 2 $MgCl_2$, 2.1 $CaCl_2$, 5 EGTA, and 10 HEPES (pH 7.25 with KOH). The control bath solution contained (in mM) the following: 145 NaCl, 5 KCl, 2 $MgCl_2$, 2 $CaCl_2$, 10 HEPES, and 10 glucose for neurons (pH 7.4 with N-methyl-D-glucamine or NaOH). ASIC currents were activated by shifting one out of eight outlets of the microperfusion system from a holding control solution (i.e., pH 7.4) to an acidic test solution.

### *1.2.9. Nerve-skin preparation and single fiber recordings*

Single C-fiber recording technique from the isolated skin-saphenous nerve preparation were used as described previously(Marra et al., 2016). After euthanasia of the mice, the hind paw skin of 12-16 week-old male mice was dissected with the saphenous nerve. The skin was pinned corium side up in an organ chamber perfused with warm (~30-31°C) synthetic interstitial fluid (SIF), in mM : 120 NaCl, 3.48 KCl, 5 $NaHCO_3$, 1.67 $NaH_2PO_4$, 2 $CaCl_2$, 0.69 $MgSO_4$, 9.64 Na-gluconate, 5.5 glucose, 7.6 sucrose, and 10 HEPES, pH adjusted to 7.4 with NaOH, saturated with O2/CO2—95%/5%. The nerve end was placed in a recording chamber fielded with paraffin oil, dissociated with fine forceps. Few fibers were placed on the gold recording electrode connected to a DAM-80 AC differential amplifier (WPI), Digidata 1322A (Axon Instruments) and Spike2 software (CED) to record extracellular potentials. The receptive field of an identified C-fiber was searched by mechanical probing of the skin while recording action potential. The mechano-sensitivity of the fiber was further characterized with calibrated von Frey filaments. This protocol implies that all C-fibers were mechano-sensitive. The conduction velocity (CV) was measured by electric stimulation with bipolar electrode placed in the middle of the receptive field. C-fibers were classified with CV below 1.3 m/s. C-fibers' receptive fields were isolated with a stainless steel ring 0.8 cm diameter (internal volume of 800 µl). Solutions were applied in the ring through local perfusion pipes of a CL-100 bipolar temperature controller (Warner instrument). Electrical recordings were amplified (x10 000), band-pass filtered between 10 Hz and 10 kHz and stored on computer at 20 kHz with pClamp 9 software (Axon Instrument). The action potentials were detected and analyzed offline with the principal component analysis extension of the Spike2 software (Cambridge Electronic Design). Data analysis was performed using GraphPad Prism 6 software.

Statistical and data analysis was performed using Origin 8.5 and GraphPad Prism 6 softwares. Data are presented as mean ± s.e.m. and statistical differences between sets of data were assessed using either parametric or nonparametric tests followed by *post-hoc* tests, when appropriate.

## 1.3. Results

In order to investigate the impact of lipid rich diet on sensory modalities, we used a model of diet-induced obesity (DIO). Two groups of male C57black6J mice of four weeks old were fed with normal standard diet (ND) or high fat diet (HFD). Both groups had the same weight of 16.8 +/- 0.27, and 16.91 +/- 0.29 g at the beginning of the feeding period. Mice fed the HFD gained significantly more weight after three to five weeks of diet compared to mice fed the normal diet (ND) (fig.1a). Mice became obese and after seventeen weeks of regime, the weight of mice on HFD was 36.7% more than the mice on ND (37.3 +/- 1.9 g and 27.3+/- 0.9 g respectively; p = 0.001 Mann Whitney test). The total area under the curve, AUC, over the seventeen weeks of the feeding period showed highly significant difference between groups. HFD mice had higher AUC compared to the ND mice with averages 240.6+/-3.2 and 145+/-2.6 respectively. Monitoring water and food consumption showed that mice fed with HFD mice drink and eat less than mice fed with ND, however, the average energy consumption in kcal/week is higher by 16.1% (fig. 1b). DIO is a model of type 2 diabetes in mice; we therefore tested the glucose homeostasis in HFD mice by measures the fasting plasma glucose concentration and performing the glucose tolerance test (GTT)(Stino and Smith, 2017) at 4, 8, 12 and 16 weeks of diet (fig 1c). We observed that fasting glucose concentration in plasma of mice was not significantly different between both groups of mice at 4, 8 and 12 weeks of regime. After 16 weeks of diet, the HFD mice had fasting plasma glucose concentration significantly higher than that for ND mice (164.3 +/- 9.7 and 97.8 +/-4 mg/dl respectively p >0.001 Multiple t test of Two-way ANOVA). The group of mice on HFD showed differences in plasma glucose regulation compared to mice fed with ND after only four weeks of regime. However, plasma glucose concentrations were not significantly different between both groups after 2 hours of GTT (fig S1a). This showed only a moderate impairment of glucose tolerance at this early stage of obesity. The plasma glucose concentration was higher in HFD mice at 8, 12 and 16 weeks of diet (fig 1d), data not shown for 12 and 16 weeks. After 8 weeks of HFD, the mice showed significant impaired plasma glucose regulation compared to the group of mice on ND (AUC, 17553.9 ± 1151.4, and 2339.6 ± 1362.6 for ND and HFD respectively). At this stage, the maximum glucose concentration in the serum of obese mice fed with HFD was higher than in the serum of mice with ND (at 30 min post glucose, 407 +/- 21.9 mg/dl and 353.0 +/- 9.8 mg/dl respectively; p = 0.01, Multiple t-test).

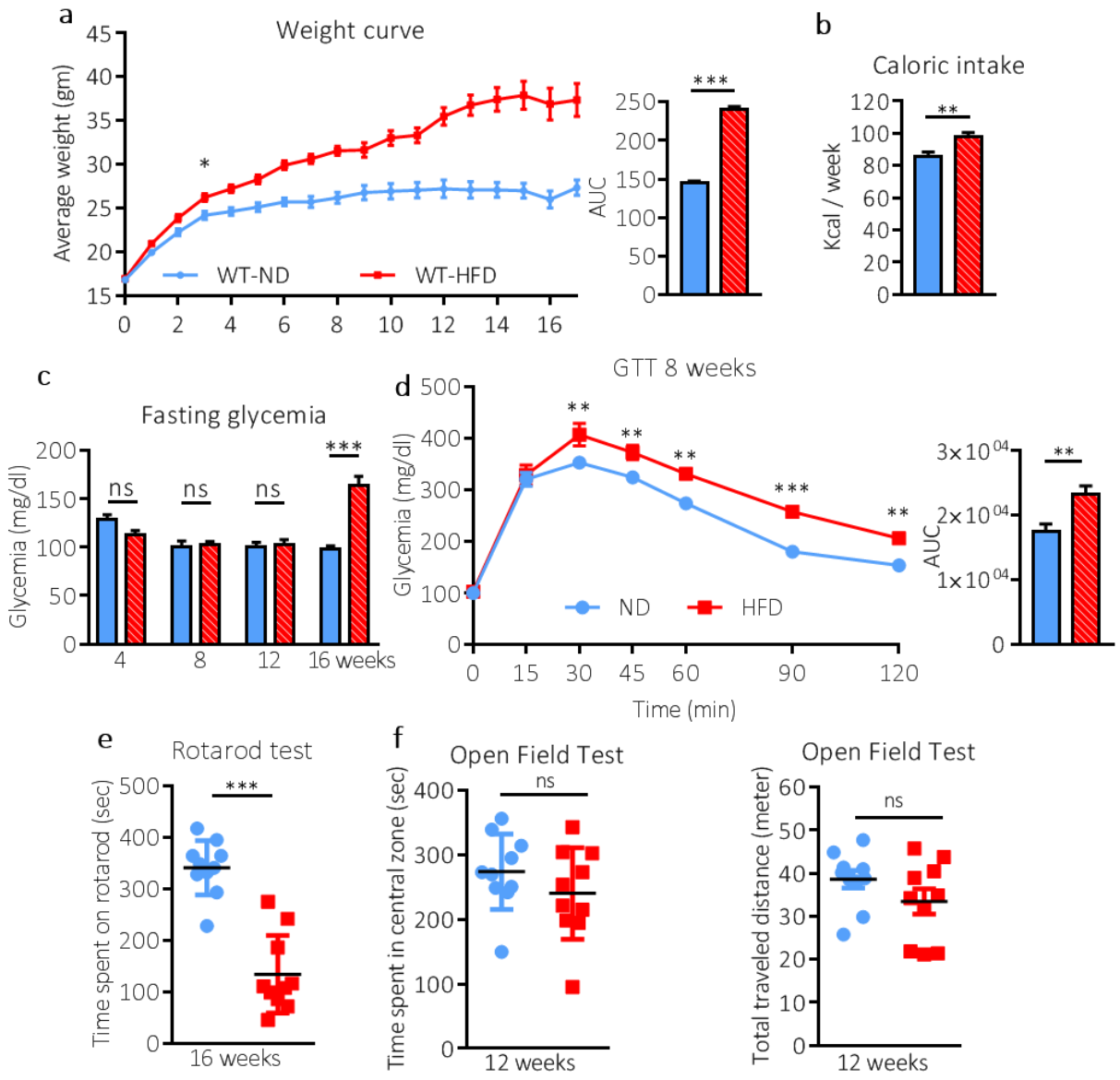


*Figure 1 Lipid rich diet induce obesity, hyperglycemia, and motor impairment without affecting stress. (a) Weight gain over weeks for ND and HFD mice, n=30-10. Right panel area under the curve (AUC) of the total weight during the whole period of feeding for mice fed high fat diet (HFD) red, control mice fed the normal diet (ND) (blue). Color codes will be maintained over all the figures. (b) Caloric intake of ND and the HFD. (c) Fasting plasma glucose concentrations at different time points for the ND (blue) and the HFD (red) mice. (d) Glucose tolerance test (GTT) after 8 weeks of diet for ND and HFD mice. n=10 mice for both groups. Right panel, the AUC of the GTT at 8 weeks of diet. (e) Time spent on the Rotarod by ND and HFD mice. (f) Open field experiment. Left panel, time spent by the mice in the central zone of the boxes, and, right panel, total walking distance of HFD (red) and ND (bleu) mice. Data are presented as mean ± SEM. * for $p < 0.05$, ** for $p \leq 0.01$, *** for $p \leq 0.001$. Mann-Whitney test unless indicated. n=10-10 mice per group unless indicated.*

Importantly, obese mice did not fully recover to pre-test glucose; the plasma glucose concentration after 2 hours of GTT for the mice at 16 weeks of HFD was above 200 mg/dl. GTT and fasting plasma glucose concentration show that between 8 and 12 weeks of diet, obese HFD mice

have prediabetes. After 16 weeks of diet, HFD mice may be at an early stage of type 2 diabetes, however, this require further testing. Obesity and prediabetes are accompanied by motor deficit. We next tested the locomotor activity of obese mice with the rotarod and the open field tests. The later was also used to test anxiety. Mice fed with HFD spent less time on the rotarod compared to the ND mice (134.1+/-25.1 and 341+/-17.6 seconds respectively Fig 1e; p = 0.001, Mann Whitney test). This showed that HFD mice might have some impairments in motor coordination. On the other hand both groups of mice behaved similarly in the open field test, measured as the time spent by mice in the central zone of the open field boxes (Fig 1f) (274 +/- 19.5 sec, and 240.3 +/- 23.7 sec for ND and HFD mice respectively; p = 0.3 Mann Whitney). The total distance traveled by both groups was also not significantly different (38.6 +/-2.1 and 33.4 +/-3.0 meter respectively; p = 0.2, Mann-Whitney test). This indicated that HFD mice did not show alterations in anxiety levels and their activity was similar to ND mice.

We then investigated whether obese mice on HFD had sensory disfunction. We tested the mice for their sensitivity to mechanical and thermal stimuli over the period where the mice showed progressive impairment of glucose homeostasis. To test the mechanical perception of the mice, we performed the dynamic von Frey test at 8, 12, and 16 weeks of diet (Fig 2a). Both groups of mice, ND and HFD, did not show any significant difference in the mechanical forces that induced paw withdrawal at whatever the duration of the diet. The forces that induced the paw withdrawal were 4.0 +/- 0.3 g and 4.2 +/- 0.5 g at 8 weeks, 3.7 +/- 0.2 g and 3.9 +/- 0.5 g at 12 weeks, and 3.5 +/- 0.3 and 3.7 +/- 0.4 at 16 weeks for ND and HFD mice respectively. We then performed the Hargreaves' test to evaluate heat perception of mice. There was no difference between both groups of mice at 4 weeks of diet (paw withdrawal latencies, PWL, were 9.5 +/- 0.5 sec and 8.1 +/- 0.4 sec for the ND and the HFD mice, Fig. 2b). However, after 8 weeks of diet, HFD mice showed significant thermal hypersensitivity compared to control ND mice. The hyperalgesia of HFD mice was still observed at 20 weeks of diet, while, over the same period, the perception of heat by ND mice did not change. ND mice, PWL were 9.0 +/- 0.4 sec, 9.4 +/- 0.7 sec, 8.6 +/- 0.4 sec, and 10.4 +/- 1.9 sec at 8, 12 , 16 and 20 weeks of diet; while for HFD mice PWL were 6.0 +/- 0.3 sec, 5.5 +/- 0.4 sec, 4.4 +/- 0.3 sec, and 4.3 +/- 0.5 sec at 8, 12, 16 and 20 weeks of diet)(Fig 2b).

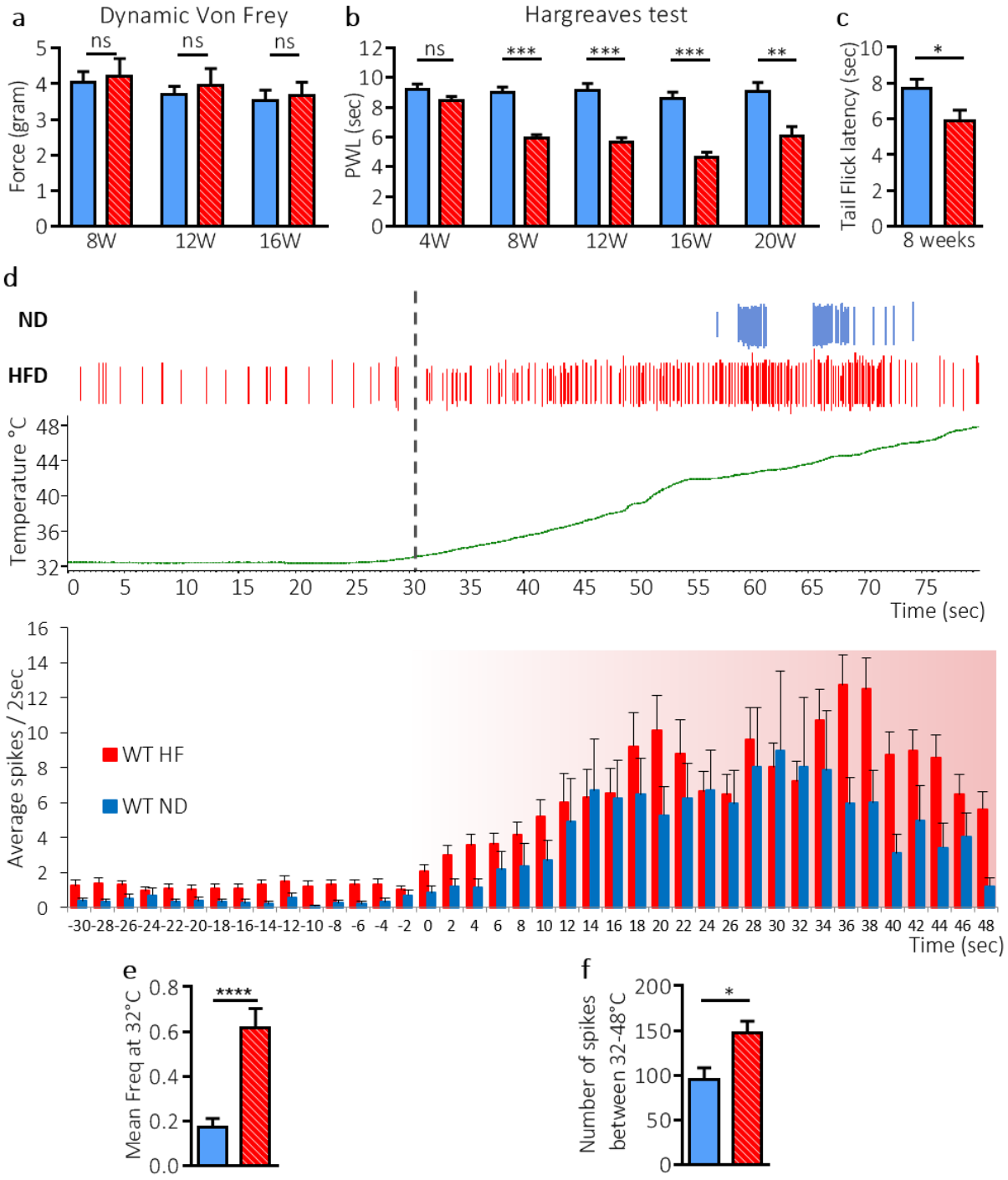


*Figure 2 Pain perception and peripheral nociceptive fibers activity in obese HFD and control ND mice. (a) Estimation of mechanical perception by paw withdrawal latencies (PWL) with the dynamic von Frey test of obese HFD mice and control ND mice. n= 10-8 at 8, 12 and 16 weeks of diets. Kruskal-Wallis test. (b) Hargreaves' test with HFD and ND mice at 4, 8, 12, 16, and 20 weeks of diet. n=58-10 mice. Kruskal-Wallis test. (c) Tail flick experiment performed at 8 weeks of diet on ND and HFD mice, n=10-10. (d) Nerve-skin recording of mechano and heat-sensitive C-fibers from ND and HFD mice. Top panel shows 2 exemplar traces of the spike firing activity of single C-fibers recording from saphenous nerve of ND (blue) and HFD mice (red) at normal temperature of the skin (32°) and during warming the skin from 32°C to 48°C in 50 sec. Each vertical line represent an action potential. The ramp of temperature is shown under the traces. Lower panel shows the cumulative activity of the heat sensitive C-fibers of skins from control lean ND and obese HFD mice represented as the number of spikes during 2 seconds periods plotted against the corresponding temperature in °C. 23 - 48 fibers from n=4-6 mice.. (e) Left panel shows the mean basal frequency (Hz) of heat sensitive C-fibers of the ND and HFD mice at 32°C recorded during 30 seconds. (f) Shows the average total number of action potentials of heat sensitive C-fibers during the heat ramp from 33°C up to 48°C. Data are presented as mean ± SEM. *p < 0.05, **p ≤ 0.01, ***p ≤ 0.001. Mann-Whitney test unless indicated.*

The tail immersion test confirmed the thermal hypersensitivity of the HFD mice after 8 weeks of regime (Fig 2c) (tail flick latencies of 7.7 +/- 0.6 sec and 5.9 +/- 0.7 seconds for ND and HFD mice respectively p= 0.02 Mann Whitney test). This indicates that HFD induced a long lasting thermal hypersensitivity in mice, starting from 8 weeks of diet, but it did not have any impact on the mechanical perception of the mice. Heat-hyperalgesia could result from sensitization of peripheral sensory fibers. We thus recorded single C-fiber's activity using the *ex-vivo* skin-saphenous nerve preparation on skin dissected from ND and HFD mice (Fig 2d). We observed that C-fibers from HFD mice had significantly higher spontaneous activity at normal skin temperature (31 - 32°C) than fibers from ND mice (0.2 +/- 0.04 Hz and 0.6 +/- 0.1 Hz for ND and HFD mice respectively) (Fig. 2e).

The high basal activity could reflect increased excitability of C-fiber in obese mice. We next measured the sensitivity of C-fibers to heat by increasing the temperature of the perfusion solution on the fibers receptive field in the skin from 31-32°C to 48-50°C during 50 seconds. Heat-sensitive C-fibers responded to warming by firing action potentials. After excluding the basal activity of the fiber, heat-sensitive C-fibers from HFD mice fired significantly more action potentials during the heat ramp than C-fibers from ND mice (averaged total number of spikes of 95 +/- 13.8, and 148 +/- 12.9 for ND and HFD skin respectively p=0.01 Mann Whitney test) (Fig. 2f). The increased activity of C-fiber in response to heat corroborated the observation that HFD increased the heat sensation in mice. This suggested that obesity affects the detection of heat by increasing the excitability of cutaneous nociceptive C-fibers.

DRG neurons and sensory fibers, especially those from unmyelinated C-fibers, are not protected by the blood brain barrier(Feldman et al., 2017) which support that molecules within the blood could reach and interact with ion channels and receptors expressed on these neurons. We next wanted to investigate candidate ion channels that could be involved in the pain hyperalgesia of obese HFD mice. Indeed, the composition of serum of the mice is highly affected by the diet, therefore to test this hypothesis we first studied the changes in the serum of HFD then translated these changes to test them by *in vitro* approaches. The HFD contains high concentration of saturated lipids, so to further characterize the metabolic state of the obese mice we assessed the serum lipid profile of obese mice compared to ND mice by using lipidomic mass spectrometry analysis. Phosphatidylcholine and lysophosphatidylcholine were the most concentrated phospholipids in the serum of obese HFD mice (Fig 3a). The difference were most significant for

Lysophosphatidylcholine (LPC), including LPC16:0, LPC18:0, LPC18:1, and LPC18:2. These elevated levels of PC and LPC species were significantly reduced upon the delipidization of the serum, to levels similar to their concentrations in the serum of the ND mice (Fig 3a). We then tested the effect of HFD serum on native DRG neurons with patch-clamp recordings in the current clamp configuration. Delivering serum from HFD mice to WT DRG neurons in cultures immediately induced depolarizing currents in all recorded neurons (average depolarization of 6.9 +/- 1.2 mV, n = 10 Fig3b). This depolarization was able to induce action potentials firing in 3 out of 10 recorded neurons. The speed of the depolarization without delay caused by the application of HFD serum suggested a possible direct effect on depolarizing ion channels. Among ion channels modulated by lipids is ASIC3 channel. Indeed, ASIC3 were shown to be potentiated by Lysophosphatidylcholine (LPC), that was increased in the serum of HFD mice (Marra et al., 2016). Therefore we wanted to investigate the contribution of ASIC3 channel in the evoked depolarization induced by the HFD serum on WT DRGs. APeTx2 is a peptide shown to block ASIC3 channel with high potency (Diochot et al., 2004). For that, we compared the levels of depolarization evoked by applying the HFD serum alone to those evoked by perfusing the neurons with APeTx2 at (2 µM) for 1 min and then co-applying it with the HFD serum Fig 3c. The application of APeTx2 significantly reduced the amplitude of depolarization evoked by HFD serum, with a mean reduction of -29 % (6.9 +/- 1.2 mV with HFD serum; 4.12 +/- 0.8 mV for HFD serum and APeTx2 p=0.002 Wilcoxon matched-pairs signed rank test) (Fig 3c). The effect of APeTx2 in reducing the depolarization may have been underestimated because the concentration of the toxin may have been submaximal owing to the viscous nature of the serum and also the possibility that part of the concentration of the toxin was buffered or degraded by the effect of proteins found in the serum. It was not possible to increase the toxin concentration in the serum because at higher concentrations, the toxin may lose its specificity for ASIC3 and inhibit Nav1.8 (Rash, 2017b).

We also wanted to know whether the HFD serum would be able to affect the excitability of the DRG neurons by changing the rheobase required to trigger action potentials. For that, we used a protocol of increasing steps of injecting currents in patch-clamp at current clamp configuration and we compared the amplitude of current injected in the cell through the recording pipette required to trigger the first action potential before and during the application of the serum (Fig

3d). In order to avoid the variability in the resting membrane potential between the different neurons and to exclude the direct depolarizing effect of the serum, we unified the starting basal resting potential of the neurons at -55 mV. The application of the ND serum on WT DRGs did not affect significantly the rheobase required to trigger action potential (Fig 3d). On the contrary, the application of the HFD serum significantly lowered the rheobase of the WT DRG neurons (Fig 3d). The fold change in the rheobase after applying the ND and HFD serum compared to before the application of serum was 1.07 +/- 0.08 and 0.67 +/-0.1 for ND and HFD serum respectively. Earlier we showed that ASIC3 contribute to the depolarization of DRG neurons by HFD serum, we then measured the effect of the HD serum on the rheobase of DRG neurons from ASIC3 knockout mice (ASIC3 KO). Interestingly, the application of HFD serum did not affect the rheobase of DRG neurons from ASIC3 KO mice (fold change with HFD serum was 1.03 +/- 0.07). Delivering the HFD serum did not affect significantly the action potential threshold of firing when compared to the control trace (p=0.2402 Wilcoxon test).

Several ion channels including the voltage gated sodium and potassium channels are involved in triggering action potentials, and could possibly be responsible for the depolarizing excitatory effect of HFD serum. Therefore, we tested the HFD serum on whole-cell currents of DRG neurons in the whole-cell voltage-clamp recording configuration at a holding potential of -80 mV. This membrane potential is the reversal potential of $K^+$ channels and well below the activation thresholds of $Na^+$ channels. We could therefore exclude the contribution of $K^+$ channels and minimize the participation of Nav channels.

*Figure 3 Effect of HFD and ND serum on DRG neurons membrane currents and excitability. (a) Histogram comparing the sum of quantitative responses (peak area signals) of different LPC species in serum collected from lean ND and obese HFD mice. Obese mice had higher levels of LPC 16:0, 18:0, 18:1 and 18:2 compared to lean ND mice. Delipidification of the HF serum reduced the amount of all LPC species. n = 3/each. (b) Exemplar recording of a WT DRG neuron in whole-cell current-clamp configuration. Perfusion of HFD serum on wild-type DRG neurons triggered action potential in 3 out of 10 neurons. (c) Left panel shows traces of recordings in current-clamp configuration of WT DRGs, during the application of HFD serum alone (red) or with APETx2 2µM. The mean amplitude of depolarization induced by both conditions are represented in the right panel. n=10. (d) Effect of serum on the rheobase of WT DRG neurons. The membrane potential DRG neurons were at -55 mV and steps of increasing current intensities were injected in the cell until the first action potential was triggered. Control traces in black, recordings in the presence of ND serum in blue and red traces for HFD serum. Right panel, the fold change in the rheobase obtained with perfusing ND or HDF serum compared to their own controls. Blue and red bars represent ND and HFD serums perfused on WT DRG neurons respectively, black bar represent the change in rheobase upon perfusing the HFD serum on DRG neurons from ASIC3 knockout mice. n= 15-8. Kruskal-Wallis test. (e) Voltage clamp recordings of wild-type DRG neurons. Left panel, exemplar traces of whole-cell currents of DRG neurons upon application of HFD serum on WT DRG neurons (red) or DRG neurons from ASIC3 knockout mice (black). Right panel shows the calculated current densities of whole cell currents evoked by the application of ND serum on WT DRG neurons (blue), HFD serum on WT DRG neurons (red), ASIC3 knockout DRG neurons (black), and delipidized HFD serum (HFDd) on WT DRGs (green). n per each condition is indicated under each bars. Kruskal-Wallis test. Data are presented as mean ± SEM. *p < 0.05, **p ≤ 0.01, ***p ≤ 0.001.*

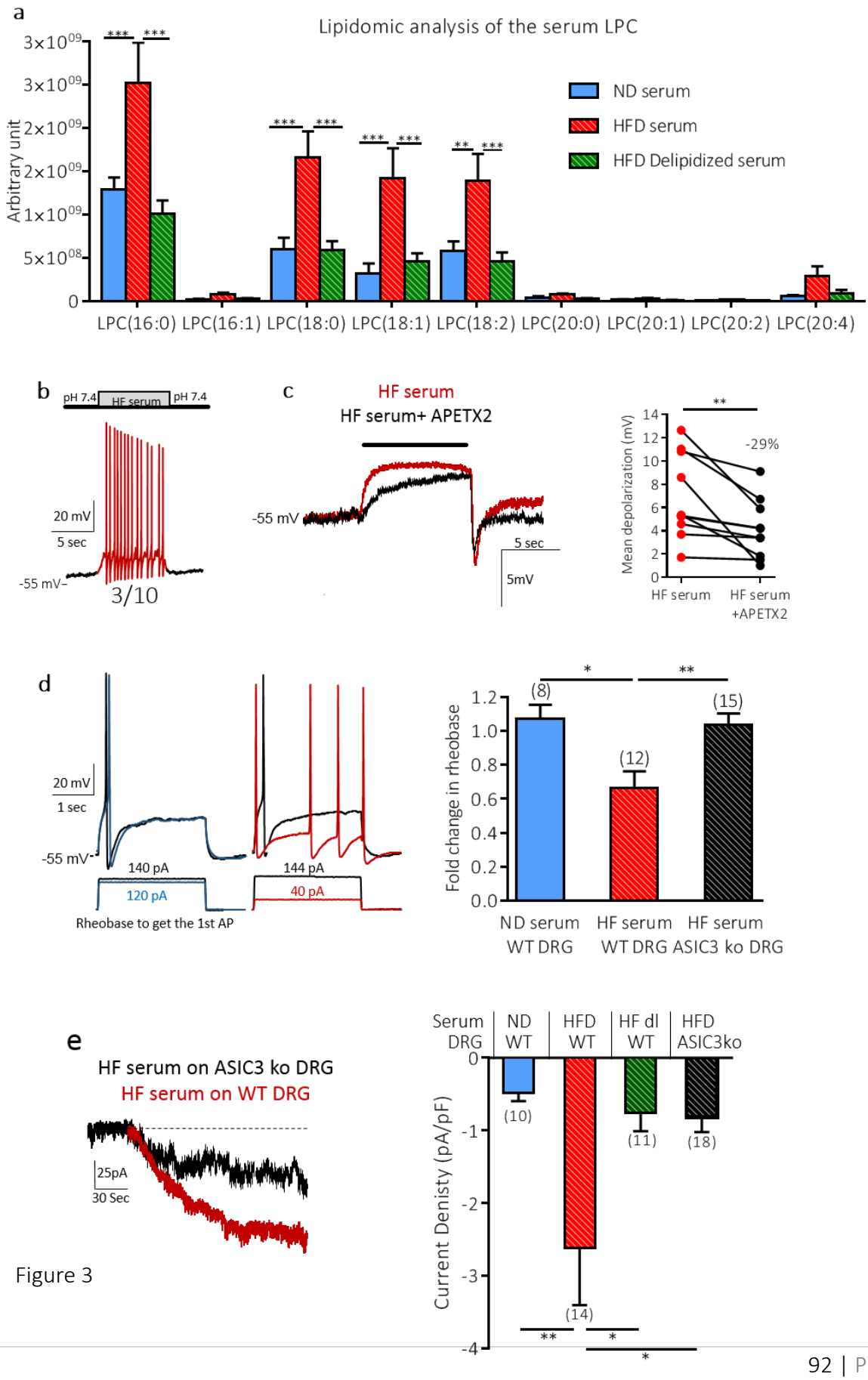
a
Lipidomic analysis of the serum LPC
Arbitrary unit
ND serum
HFD serum
HFD Delipidized serum
LPC(16:0) LPC(16:1) LPC(18:0) LPC(18:1) LPC(18:2) LPC(20:0) LPC(20:1) LPC(20:2) LPC(20:4)
b
pH 7.4
HF serum
pH 7.4
20 mV
5 sec
-55 mV
3/10
c
HF serum
HF serum+ APETX2
-55 mV
5 sec
5mV
Mean depolarization (mV)
-29%
HF serum
HF serum +APETX2
d
20 mV
1 sec
-55 mV
140 pA
120 pA
144 pA
40 pA
Rheobase to get the 1st AP
Fold change in rheobase
ND serum WT DRG
HF serum WT DRG
HF serum ASIC3 ko DRG
e
HF serum on ASIC3 ko DRG
HF serum on WT DRG
25pA
30 Sec
Serum
DRG
ND WT
HFD WT
HF dl WT
HFD ASIC3ko
Current Denisty (pA/pF)

Figure 3

The application of HFD serum on WT DRG neurons evoked inward currents that was significantly higher than currents evoked by perfusing the ND serum (current densities were -2.62 +/- 0.8 pA/pF and -0.48 +/- 0.1 pA/pF for HFD and ND serum respectively)(Fig 3e). Moreover, application of the delipidized HFD serum (HF dl) to WT DRG neurons evoked currents that were not different from the ND serum and significantly lower than that with the HFD serum (current density -0.75 +/- 0.2 pA/pF). Interestingly the inward currents evoked by delivering HFD serum on WT DRGs was not reproduced in DRG neurons from ASIC3 KO mice (current densities on DRGs from ASIC3 KO were -0.82 +/- 0.2 pA/pF)(Fig 3e). These experiments show that HFD serum contain molecules that act on DRG neurons to activate depolarizing conductance, and that ASIC3 channel is one of the main mediator of the excitatory effect of these compounds.

To test whether the excitatory effect of the HFD serum was mediated through a direct interaction with ASIC3 channel or through an indirect pathway through it's previously described interaction with ion channels or receptors (Birdsong et al., 2010; Qiu et al., 2012, 2014). Therefore, we measured the effect of HFD and ND serum on ASIC3 channel expressed in HEK293 cells, with voltage-clamp whole-cell configuration (holding potential -80 mV) (Fig. 4a). The expression of ASIC3 was confirmed with a brief pulse of 10 sec of low pH 6.6 solution. HFD serum induced a significantly larger inward current on ASIC3 expressing cells compared to serum from ND mice (current densities were -1.3 +/- 0.3 pA/pF, and -4.5 +/- 0.5 pA/pF for the ND and HFD serum respectively)(Fig. 4a). The effect was immediate, maintained as long as the serum was applied and reversible (Fig. 4a). The effect of the HFD serum on ASIC3 was not observed on ASIC1a channel (current density amplitude -1.5 +/- 0.3 pA/pF). The delipidized HFD serum (HFdl) reduced the activation of ASIC3 channel to a level that was significantly lower than current densities obtained with the HFD serum, and not different from ND serum (-1.2 +/- 0.3 pA/pF). Interestingly supplementing the delipidized HFD serum with a cocktail of LPC species with concentrations corresponding to what we found in the HFD serum (LPC16:0 40 µM, LPC18:0 20µM, LPC 18:1 20µM) significantly rescued the lost activation of ASIC3 due to delipidized, (current density amplitude -3.7 +/- 0.9 pA/pF) (Fig. 4a). ASIC3 currents produced by the application of extracellular solution at pH 7 were significantly potentiated by a short pre-incubation of 1 minute with the HFD serum (Fig. 4b). On the contrary, the pre-incubation with the ND serum failed to induce any significant potentiation of the ASIC3 current at pH 7. The fold change in the pH 7 evoked ASIC3

currents after pre-incubation with the serum compared to the control pH 7 currents were 1.1 +/- 0.1 and 1.6 +/- 0.1 for the ND and HFD serum respectively (Fig. 4b, right panel).

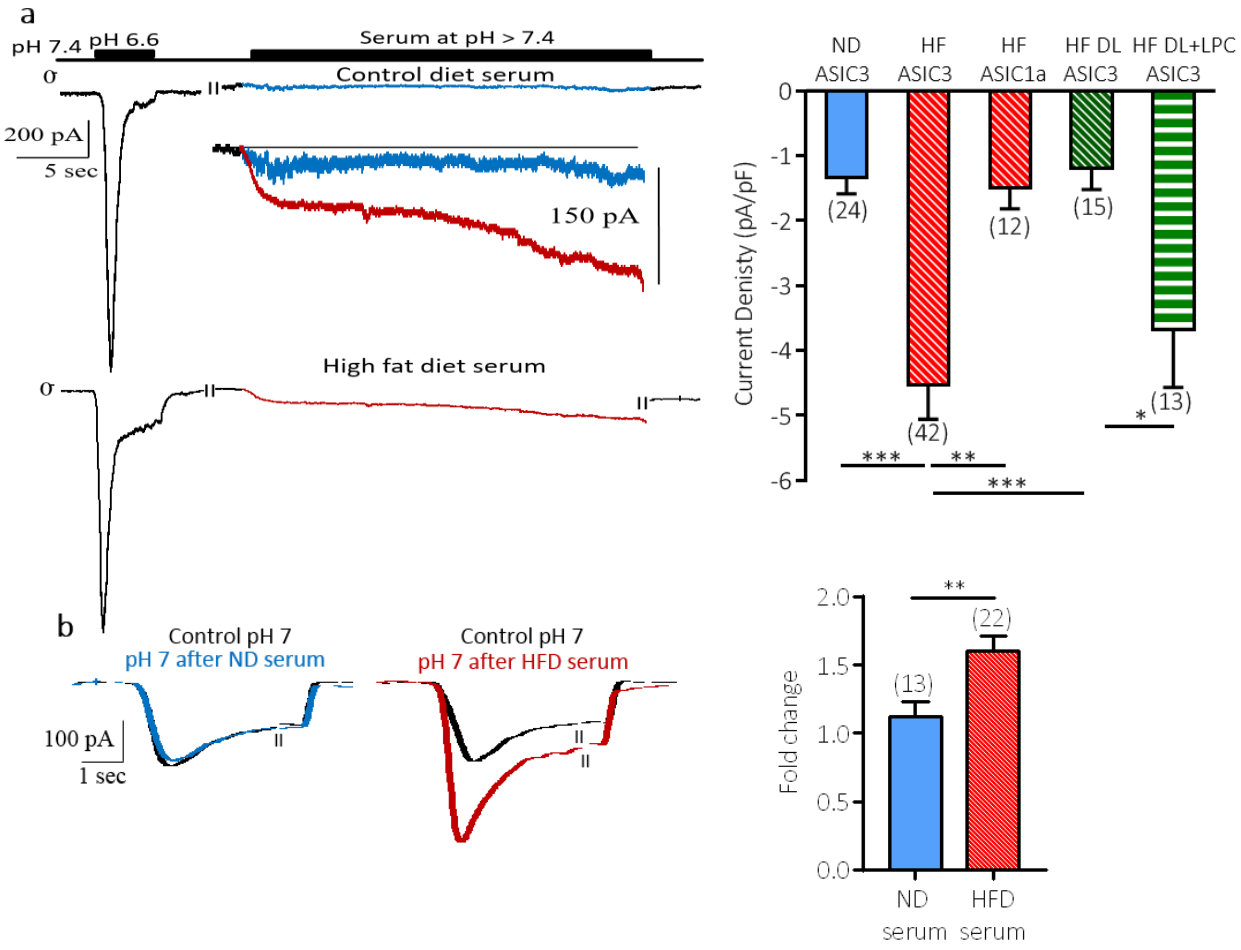


*Figure 4 Effect of lipid rich diet on recombinant ASIC3 channels activation. (a) Left panel shows exemplar traces of patch-clamp recordings in voltage-clamp configuration of HEK 293 cells transfected with mouse ASIC3 channel. The bars above the recording traces shows the protocol. A brief application of extracellular solution at pH 6 evoked ASIC3 currents with characteristic peak and sustained plateau phases. Application of Normal diet (ND) or high fat diet (HF) serum. The ASIC3 currents were significantly larger in the presence of HFD serum than ND serum. Right panel shows the averaged current densities (pA/pF) upon serum applications in different conditions: ND serum on ASIC3 (blue), HFD serum on ASIC3 (red), HFD serum on ASIC1a (red), HFD serum delipidized (HF dl) on ASIC3, HF dl supplemented with LPC cocktail on ASIC3 expressing HEK 293 cells. Kruskal-Wallis test. (b) Left panel shows traces of patch-clamp recordings of the effect of serum application on ASIC3 currents at pH7. Superimposed traces of pH 7 evoked ASIC3 currents before (black) and after 1 min application of the serum (ND serum, blue trace; HFD serum, red trace). The right panel shows the fold change of pH 7 evoked ASIC3 currents in the presence of serum. Data are presented as mean ± SEM. *p < 0.05, **p ≤ 0.01, ***p ≤ 0.001.*

Based on these findings we hypothesized that the pain phenotypes described as thermal hyperalgesia seen in HFD obese mice could be a consequence of the activation of ASIC3 channels by the high concentration of LPC found in their serum. To test this hypothesis, we fed 2 groups of ASIC3 KO mice with ND and HFD. The ASIC3 KO mice fed with HFD gained significantly more weight than ASIC3 KO mice fed with ND. Indeed, the weight gain by ASIC3 KO mice was not different from WT mice fed with HFD (fig S1b). Furthermore, fasting glucose plasma concentration and GTT were not different between ASIC3 KO and WT mice (data not shown). ASIC3 KO mice were obese after 5 weeks of HFD and were prediabetic after 8 weeks of HFD. We then measured the thermal perception of ASIC3 KO mice by performing the Hargreaves' test on the two groups of ASIC3 KO mice fed the ND or the HFD for 4, 8, 12, 16, 20, and 25 weeks of diet(Fig 5a). At all-time points, both groups showed no difference in thermal perception. The mean PWL over all the time points were 8.8 +/- 0.9 sec and 8.1 +/- 0.9 sec for the ASIC3 KO ND, and the ASIC3 KO HFD. These results indicated that ASIC3 KO mice fed the HFD did not develop the thermal hyperalgesia.

*Figure 5 Effect of ASIC3 channels blockage in-vivo on the thermal hyperalgesia induced by lipid rich diet. (a) The graph show the PWL for the Hargreaves test performed on ASIC3 knockout mice (ASIC3ko) that received the normal diet compared to those that received the high fat diet. The PWL for the ASIC3 KO fed the ND (white) at 4, 8, 12, 16, 20, and 25 weeks of diet were 8.4 +/- 0.9 sec, 8.6 +/- 1.2 sec, 10 +/- 0.9 sec, 8.4 +/- 1.1 sec, 8.1 +/- 0.7 sec, and 9.5 +/- 0.9 sec respectively. The PWLs of the ASIC3 KO fed the HFD (black) were 8.3 +/- 1.2 sec, 7.8 +/- 0.8 sec, 9.0 +/- 0.7 sec, 7.3 +/- 0.4 sec, 7.3 +/- 1.0 sec, and 9.1 +/- 1.2 sec for the same sequence. The thermal perception was not significantly affected in both groups. P=0.5 Kruskal-Wallis test n= 14-5 (b) PWL measurements of WT mice that received the ND and the HFD, these mice received 7 intraperitoneal injections with an ASIC3 channel blocker, APETx2, at 0.23 mg/kg. A single injection was delivered every other day for 2 weeks starting from the 7th week of diet. At 4 and 7 weeks of diet before starting the injections both groups did not show any significant differences in the PWL in the Hargreaves' test. At 8 and 9 weeks during the period of injection, the PWL was not different, showing that blocking ASIC3 channel can delay the onset of the thermal hyperalgesia induced by the lipid rich diet. 3 weeks after stopping the injections, at 12 weeks of diet, there were a tendency of decrease in the PWL in the obese mice compared to lean mice, while after 4 weeks of stopping the ASIC3 blocker at 13 weeks of diet obese HFD mice showed a significant reduction in the PWL compared to the lean ND mice. This reduction was maintained up to 16 weeks. n=8. P=0.02, Kruskal-Wallis test. (c) PWL on Hargreaves' tested of WT mice that received ND and the HFD. These mice received APETx2 injections using the same protocol used in previously, starting from 12 weeks over two weeks. At 4 weeks, both groups had no significant difference in the PWL (PWL of 7.4 +/- 0.7 sec and 7.7 +/- 0.6 sec for the ND and the HFD mice). At 8 and 12 weeks, obese HFD mice showed significantly increased heat perception compared to lean ND mice. At 13 weeks; after 4 injection, obese mice did not show any more a significant reduction in the PWL. The effect of the injected ASIC3 blocker was confirmed at 13 weeks and 14 weeks too. n=8 for both groups.*

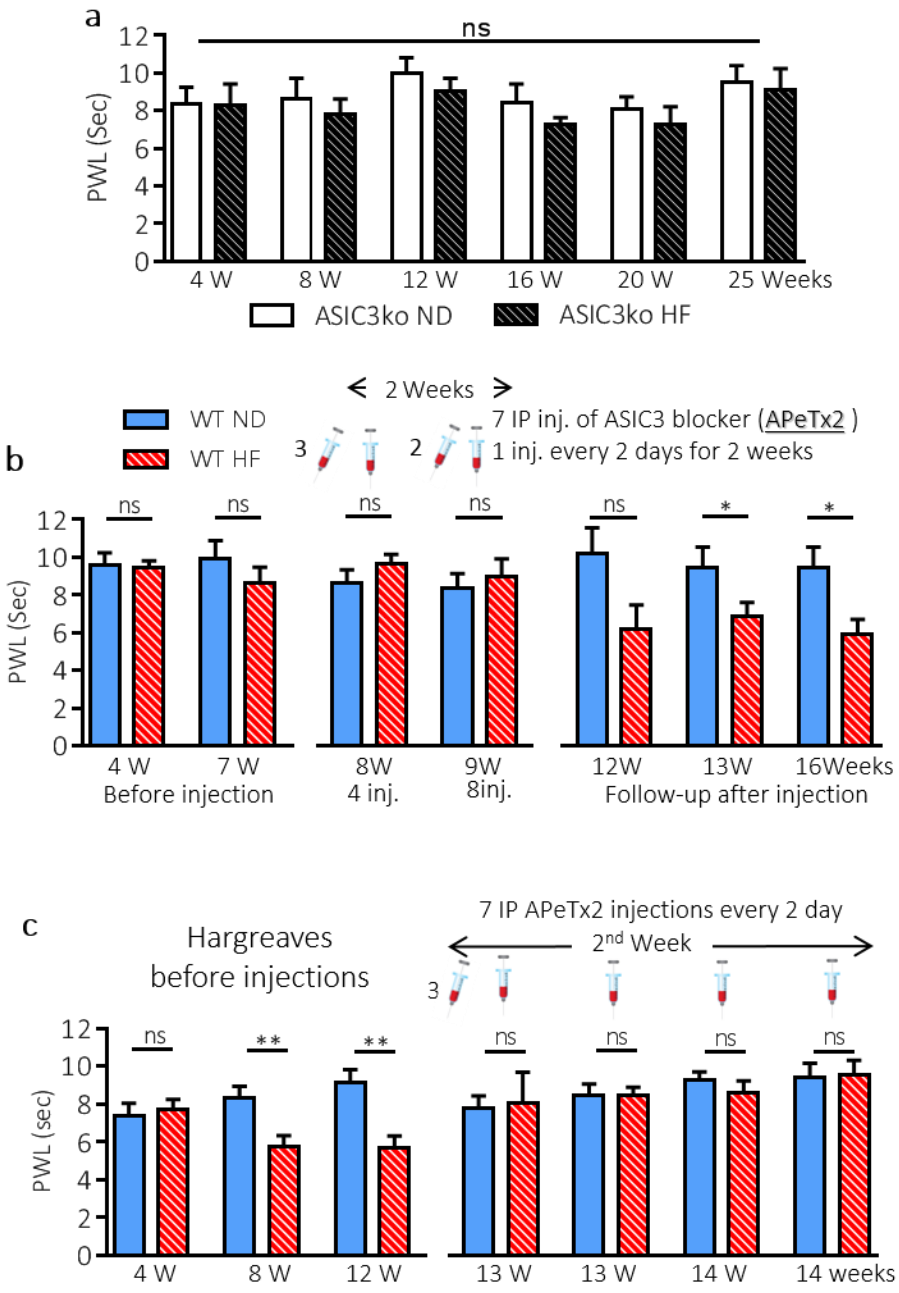


Figure 5

The genetic deletion of ASIC3 channel could be subject to compensatory mechanisms that could affect the mice behaviors. For that, we wanted to test if pharmacological inhibition of native ASIC3 channel *in vivo* would correct the thermal hyperalgesia that was seen in mice consumed the HFD. To address this question we took advantage of an ASIC3 blocker, APETx2, and we performed a chronic intraperitoneal injection of APeTx2 in mice (1 injection every other day over two weeks, at 0.23 mg/kg in PBS) (Fig 5b). For these injections, we used WT mice that received the ND or the HFD, and we monitored their thermal perception at 4, 7, 8, 9, 12, 13 and 16 weeks of diet with

Hargreaves test. At 4 and 7 weeks of diet, before starting the injections, both groups of mice did not show any significant differences in their thermal perception. The PWL were 9.6 +/-0.7 sec and 9.4 +/- 0.4 seconds at 4 weeks of diet and at 7 weeks, they were 10 +/- 1 sec and 8.6 +/- 0.9 sec for the ND and HFD mice respectively.

The chronic injections of APeTx2 started from the 7th week of diet. Hargreaves test performed on the 8th week of diet, after four injections of ApeTx2, did not show significant difference in the thermal perception of both groups with PWL of 8.7 +/- 0.7 sec and 9.6 +/- 0.6 sec ($p > 0.9$, Kruskal-Wallis test). Hargreaves test performed on the 9th week of diet, and after seven APETx2 injections again did not show significant differences in PWL of both groups (7.9 +/- 0.9 sec and 9.0 +/- 1.0 seconds for ND and HFD; $p > 0.9$, Kruskal-Wallis test). After stopping the injections, we followed up the thermal perception of the mice, at 12, 13 and 16 weeks of diet. We found that the mice fed the HFD started to show the thermal hyperalgesia starting from the 13th week of diet, after 3 weeks of stopping the injections (PWL of 9.5 +/- 1.2 sec and 6.8 +/- 0.8 sec for ND and HFD mice). This showed that blocking native ASIC3 can delay the onset of the thermal hyperalgesia associated with HFD.

Then we wanted to investigate if blocking native ASIC3 can reverse the HFD induced thermal hyperalgesia. To address this question, we performed the same protocol of chronic APETx2 injections, as in the previous set of experiments, on two groups of WT mice fed the ND and the HFD. At 4 weeks, both groups did not show significant differences at their thermal perception. However, at 8 and 12 weeks of diet, the HFD mice showed heat hyperalgesia compared to the ND mice. The chronic injections started at the 12th week. Hargreaves test performed at 7, 9, 11, and 13 days post injection did not show significant differences between the two injected groups of mice. The PWLs at 7 days post-injection were 7.8 +/- 0.7, and 8.1 +/- 1.7, at 9 days post-injection it were 8.4 +/- 0.7, and 8.4 +/- 0.5, while at 11 days it were 9.2 +/- 0.5, and 8.6 +/- 0.7, and finally at 13 days post-injections were 9.4 +/- 0.8, and 9.5 +/- 0.8 (Fig 5c). This results show that blocking ASIC3 can correct the thermal hyperalgesia associated with the consumption of the HFD.

## 1.4. Discussion

The dyslipidemia and obesity associated with HFD induce metabolic stress leading to the induction of several inflammatory signaling pathways within the metabolic tissue specially the adipose tissue(Gregor and Hotamisligil, 2011). These signaling pathways elevate the release of several inflammatory cytokines, which decrease insulin signaling and affect glucose homeostasis(Hirosumi et al., 2002; Uysal et al., 1998). This well documented role of lipids in the metabolic tissues should be extended to other organs that could be affected with it. The sensory pathway is one of the tissues that are dramatically affected by dysregulations in metabolic parameters(Feldman et al., 2017). Indeed peripheral neuropathies (PDN) associated with diabetes can cause pain disorders. Nevertheless, the etiologies of pain associated with diabetic neuropathies are not well characterized. The importance of categorizing diabetic models, was highlighted by several clinical trials showing that although these models manifest permanent hyperglycemia, good glycemic control can improve symptoms of diabetic neuropathy only in type I diabetic patients but not in patients having type II diabetes(Callaghan et al., 2012b).

The research on DNP often used the streptozocin model that induce robust and effective ablation of pancreatic β cells resulting in insulinopenia and systemic hyperglycemia(O'Brien et al., 2014). This model mimics type 1 diabetes, typically presents in childhood or adolescence, that represent 5% of the diabetic population([CSL STYLE ERROR: reference with no printed form.]). Other studies on type II diabetes used genetic models, such as ob/ob or db/db mice, obtained by interrupting leptin-signaling pathway resulting in hyperphagia, obesity, and insulin resistance. Genetic predispositions contribute to less than 10% of the causes of obesity, which is far from representing the huge population that suffer from obesity and its consequences(Le Thuc et al., 2017; Xu and Xue, 2016). The use of lipid rich diet in models of DIO gives a strong advantage in being closer to the physiological causes of obesity in human, but some of the disadvantages of the DIO models used in PDN research are the severity of the diet needed to optimize the progression of obesity, boost its consequences and reduce inter-individual variability(O'Brien et al., 2014). This later feature should be considered before interpretation of our data.

The work presented here shows that consumption of lipid rich diet has harmful impacts on health; increased the mice body weight, and induced obesity in a few weeks of diet. Although, the HFD

mice showed impaired glucose tolerance, their fasting glucose did not exceed 150mg/dl(O'Brien et al., 2014; Obrosova et al., 2007) indicating a state of prediabetes. The lipid rich diet induced dyslipidemia with increased concentration of several lipid species in the serum of obese mice. Delivering the serum from mice fed with HFD onto recombinant ASIC3 channels activated the channel at neutral physiological pH 7.4 with no delay, probably indicating a direct activation of the channel. The HFD serum potentiated the ASIC3 channel response toward acidification. This effect required the presence of lipid in the serum because Delipidizing the serum strongly reduced the effect of the serum on ASIC3 channel. Although several species of lipids were increased in the serum of mice fed with HFD, we investigated the role of LPC in the serum because LPC, together with PC, are the most concentrated phospholipids in serum of obese HFD mice. High LPC concentrations have been reported in inflammatory conditions(Marra et al., 2016) on the contrary its concentration is low in lean mice fed with ND. Importantly, LPC was reported to activate ASIC3(Marra et al., 2016). Supplementing the delipidized HFD serum with a cocktail of LPC within their concentration in the HFD serum partially restored the activity of the HFD serum on ASIC3 channel. These experiments strongly suggest that LPC found at high concentration in the serum of HFD mice is a direct activator of ASIC3 channels. The activation of ASIC3 by the lipids present in HFD serum was also observed in native DRG neurons. The inward current evoked by HFD serum was lost in DRG neurons collected from ASIC3 knockout mice indicating that the serum exhibit its depolarizing effect through activating ASIC3 channels. In addition, the excitatory effects of HFD serum on cultured DRG neurons (activation of inward depolarizing currents and diminution of the rheobase) were reduced upon ASIC3 inhibition by genetic intervention or the use of its inhibitory toxin, APeTx2. This effect could be mediated through a mechanism similarly to what was previously described with the effect of inflammatory mediators on ASIC3 channels(Mamet et al., 2002) or through the described modulation of Nav1.8 and Nav1.9 by ASIC3 channels (Yen et al., 2009).

We confirmed *in vivo* the pro-excitatory role of ASIC3 channel expressed in DRG neurons in the heat-hyperalgesia that we observed in obese mice fed with HFD. Indeed the activation of ASIC3 led to pain phenotypes. The nociceptive C fibers that innervate the skin of HFD mice had increased firing in response to heat between 32°C and 50°C compared to C fibers of mice fed with ND. This show that the detection of heat is increased in the skin of HFD mice. This was confirmed by the

observation that HFD mice have thermal heat hypersensitivity phenotypes in the Hargreaves' and tail flick tests. Again, the role of ASIC3 was confirmed with the observation that ASIC3 knockout mice fed with HFD were obese and showed glucose homeostasis deregulation similar to WT mice on the same diet, but that ASIC3 knockout mice fed with HFD were protected from thermal heat-hypersensitivity. Interestingly, pharmacological inhibition of ASIC3 channel with APeTx2 delayed the onset of the thermal hypersensitivity and reversed the hypersensitivity when it was established in wild type mice. The later results give an interesting scope as they suggest that ASIC3 is involved in the continuous expression of the thermal hyperalgesia phenotype and that its inhibition can reverse the hypersensitivity of mice fed with HFD. Of course more work is needed to confirm the role of ASIC3 in pain disorders associated with metabolic syndromes in obese patients but this may have some implication in the clinic as it suggests that inhibition of ASIC3 may have less unwanted effects of inhibiting heat sensitive ion channels from the TRP family. This could be a great advantage to avoid the harmful consequences of blocking TRP channels like the hyperthermia and the alteration in the basal thermal sensitivity that lead to severe burn injuries seen in clinical studies used these blockers (Gram et al., 2017; Moran and Szallasi, 2018).

In the described HFD model, obese mice did not develop the previously described mechanical hypersensitivity associated with diabetic neuropathy(Bierhaus et al., 2012; Tsantoulas et al., 2017). This could be owed to the differences in the diet composition (e.g. the quantity and quality of lipids in the diet such as saturated v/s unsaturated lipids, the presence of LPC species…), duration, and the age of the mice at the beginning of the feeding period. Indeed the mechanical hypersensitivity is thought to be mediated through neuropathy associated with A-Beta fibers while we show that the thermal hypersensitivity is associated with the sensitization of unmyelinated nociceptive C-fiber(Baron and Maier, 1995; Khan et al., 2002). Although both types of fibers express ASIC3 channels(Emery and Ernfors, 2018; Usoskin et al., 2015), those channels expressed in the A-Beta fibers could be more protected by myelin sheet from the increased metabolic components in the blood following HFD, especially LPC, and limiting the access of these components from reaching the channels. In addition, the differential expression of ASIC3 channels within the two sub-types of fibers could also justify the expression of thermal pain but not mechanical pain. To solve this unclear issue, further experimentations should be conducted. Of

course, it would be interesting to measure the activity of myelinated A-beta and A-delta fibers after prolonged periods of diet and the full development of type 2 diabetes.

Our observations are in agreement with previously described role of LPC in pain for neuropathic like model(Inoue et al., 2008b) and joint pain(Marra et al., 2016) nevertheless, the underlining mechanisms were found to be different. The first study owed the pain to LPC being metabolized to LPA that activates its receptors in the DRG neurons leading to the induction of inflammatory signaling pathways and pain. The second paper suggested a direct interaction of LPC with ASIC3 channels leading to sensitizing the neurons expressing these channels. Our results fits with the second report owing to the fact that LPA concentration in the serum of the HFD mice is much lower than the concentration of LPC and that LPA has no activity on the ASIC3 channel(Marra et al., 2016). In addition, ASIC3 KO mice did not have heat hypersensitivity associated with the lipid rich diet. Indeed further investigation could be done to investigate if genetic deletion of ASIC3 channel could affect the expression or the activity of LPA receptors.

Our data support the growing role of ASIC3 channel in different models of inflammatory pain, where several signals including inflammatory cytokines, lipids, and divalent ions can modify the expression and the activity of this quiescent channel and recruit its activity in pathophysiological conditions. The activity of ASIC3 channel sensitizes the DRG neurons in a state that is similar to priming, thus leading to lowering the current intensity needed to trigger action potentials, potentially inducing pain phenotypes. Further investigations are needed to find more specific and clinically relevant drugs that are effective in blocking ASIC3 to test their possible use in decreasing pain phenotypes associated with obesity and metabolic syndromes, as well as other pain conditions such as inflammatory or neuropathy.

## 1.5. References

Baron, R., & Maier, C. (1995). Painful neuropathy: C-nociceptor activity may not be necessary to maintain central mechanisms accounting for dynamic mechanical allodynia. *The Clinical Journal of Pain*, *11*(1), 63–69.

Bierhaus, A., Fleming, T., Stoyanov, S., Leffler, A., Babes, A., Neacsu, C., … Nawroth, P. P. (2012). Methylglyoxal modification of Nav1.8 facilitates nociceptive neuron firing and causes hyperalgesia in diabetic neuropathy. *Nature Medicine*, *18*(6), 926–933. https://doi.org/10.1038/nm.2750

Birdsong, W. T., Fierro, L., Williams, F. G., Spelta, V., Naves, L. A., Knowles, M., … McCleskey, E. W. (2010). Sensing Muscle Ischemia: Coincident Detection of Acid and ATP via Interplay of Two Ion Channels. *Neuron*, *68*(4), 739–749. https://doi.org/10.1016/j.neuron.2010.09.029

Bligh, E. G., & Dyer, W. J. (1959). A rapid method of total lipid extraction and purification. *Canadian Journal of Biochemistry and Physiology*, *37*(8), 911–917. https://doi.org/10.1139/o59-099

Callaghan, B. C., Hur, J., & Feldman, E. L. (2012). Diabetic Neuropathy: One disease or two? *Current Opinion in Neurology*, *25*(5), 536–541. https://doi.org/10.1097/WCO.0b013e328357a797

Chen, C.-C., England, S., Akopian, A. N., & Wood, J. N. (1998). A sensory neuron-specific, proton-gated ion channel. *Proceedings of the National Academy of Sciences*, *95*(17), 10240–10245. https://doi.org/10.1073/pnas.95.17.10240

Chen, C.-C., Zimmer, A., Sun, W.-H., Hall, J., Brownstein, M. J., & Zimmer, A. (2002). A role for ASIC3 in the modulation of high-intensity pain stimuli. *Proceedings of the National Academy of Sciences*, *99*(13), 8992–8997. https://doi.org/10.1073/pnas.122245999

Deval, E., Gasull, X., Noël, J., Salinas, M., Baron, A., Diochot, S., & Lingueglia, E. (2010). Acid-sensing ion channels (ASICs): Pharmacology and implication in pain. *Pharmacology & Therapeutics*, *128*(3), 549–558. https://doi.org/10.1016/j.pharmthera.2010.08.006

Deval, E., & Lingueglia, E. (2015). Acid-Sensing Ion Channels and nociception in the peripheral and central nervous systems. *Neuropharmacology*, *94*, 49–57. https://doi.org/10.1016/j.neuropharm.2015.02.009

Deval, E., Noël, J., Gasull, X., Delaunay, A., Alloui, A., Friend, V., … Lingueglia, E. (2011). Acid-sensing ion channels in postoperative pain. *The Journal of Neuroscience: The Official Journal of the Society for Neuroscience*, *31*(16), 6059–6066. https://doi.org/10.1523/JNEUROSCI.5266-10.2011

Deval, E., Noël, J., Lay, N., Alloui, A., Diochot, S., Friend, V., … Lingueglia, E. (2008). ASIC3, a sensor of acidic and primary inflammatory pain. *The EMBO Journal*, *27*(22), 3047–3055. https://doi.org/10.1038/emboj.2008.213

Diochot, S., Baron, A., Rash, L. D., Deval, E., Escoubas, P., Scarzello, S., … Lazdunski, M. (2004). A new sea anemone peptide, APETx2, inhibits ASIC3, a major acid-sensitive channel in sensory neurons. *The EMBO Journal*, *23*(7), 1516–1525. https://doi.org/10.1038/sj.emboj.7600177

Emery, E. C., & Ernfors, P. (2018). Dorsal Root Ganglion Neuron Types and Their Functional Specialization. *The Oxford Handbook of the Neurobiology of Pain*. https://doi.org/10.1093/oxfordhb/9780190860509.013.4

Feldman, E. L., Nave, K.-A., Jensen, T. S., & Bennett, D. L. H. (2017). New Horizons in Diabetic Neuropathy: Mechanisms, Bioenergetics, and Pain. *Neuron*, *93*(6), 1296–1313. https://doi.org/10.1016/j.neuron.2017.02.005

Francois, A., Kerckhove, N., Meleine, M., Alloui, A., Barrere, C., Gelot, A., … Bourinet, E. (2013). State-dependent properties of a new T-type calcium channel blocker enhance Ca(V)3.2 selectivity and support analgesic effects. *Pain*, *154*(2), 283–293. https://doi.org/10.1016/j.pain.2012.10.023

García-Añoveros, J., Derfler, B., Neville-Golden, J., Hyman, B. T., & Corey, D. P. (1997). BNaC1 and BNaC2 constitute a new family of human neuronal sodium channels related to degenerins and epithelial sodium channels. *Proceedings of the National Academy of Sciences of the United States of America*, *94*(4), 1459–1464. https://doi.org/10.1073/pnas.94.4.1459

Ginter, E., & Simko, V. (2014). Recent data on obesity research: β-aminoisobutyric acid. *Bratislavske Lekarske Listy*, *115*(8), 492–493.

Gram, D. X., Holst, J. J., & Szallasi, A. (2017). TRPV1: A Potential Therapeutic Target in Type 2 Diabetes and Comorbidities? *Trends in Molecular Medicine*, *23*(11), 1002–1013. https://doi.org/10.1016/j.molmed.2017.09.005

Gregor, M. F., & Hotamisligil, G. S. (2011). Inflammatory Mechanisms in Obesity. *Annual Review of Immunology*, *29*(1), 415–445. https://doi.org/10.1146/annurev-immunol-031210-101322

Guilford, B. L., Ryals, J. M., & Wright, D. E. (2011). Phenotypic changes in diabetic neuropathy induced by a high-fat diet in diabetic C57BL/6 mice. *Experimental Diabetes Research*, *2011*, 848307. https://doi.org/10.1155/2011/848307

Hirosumi, J., Tuncman, G., Chang, L., Görgün, C. Z., Uysal, K. T., Maeda, K., … Hotamisligil, G. S. (2002). A central role for JNK in obesity and insulin resistance. *Nature*, *420*(6913), 333–336. https://doi.org/10.1038/nature01137

Hruby, A., & Hu, F. B. (2015). The Epidemiology of Obesity: A Big Picture. *PharmacoEconomics*, *33*(7), 673–689. https://doi.org/10.1007/s40273-014-0243-x

Ikemoto, S., Takahashi, M., Tsunoda, N., Maruyama, K., Itakura, H., & Ezaki, O. (1996). High-fat diet-induced hyperglycemia and obesity in mice: Differential effects of dietary oils. *Metabolism: Clinical and Experimental*, *45*(12), 1539–1546.

Inoue, M., Xie, W., Matsushita, Y., Chun, J., Aoki, J., & Ueda, H. (2008). Lysophosphatidylcholine induces neuropathic pain through an action of autotaxin to generate lysophosphatidic acid. *Neuroscience*, *152*(2), 296–298. https://doi.org/10.1016/j.neuroscience.2007.12.041

Jones, B. J., & Roberts, D. J. (1968). The quantitative measurement of motor inco-ordination in naive mice using an accelerating rotarod. *Journal of Pharmacy and Pharmacology*, *20*(4), 302–304. https://doi.org/10.1111/j.2042-7158.1968.tb09743.x

Jones, N. G., Slater, R., Cadiou, H., McNaughton, P., & McMahon, S. B. (2004). Acid-Induced Pain and Its Modulation in Humans. *Journal of Neuroscience*, *24*(48), 10974–10979. https://doi.org/10.1523/JNEUROSCI.2619-04.2004

Kellenberger, S., & Schild, L. (2002). Epithelial sodium channel/degenerin family of ion channels: A variety of functions for a shared structure. *Physiological Reviews*, *82*(3), 735–767. https://doi.org/10.1152/physrev.00007.2002

Khan, G. M., Chen, S.-R., & Pan, H.-L. (2002). Role of primary afferent nerves in allodynia caused by diabetic neuropathy in rats. *Neuroscience*, *114*(2), 291–299. https://doi.org/10.1016/S0306-4522(02)00372-X

Le Thuc, O., Stobbe, K., Cansell, C., Nahon, J.-L., Blondeau, N., & Rovère, C. (2017). Hypothalamic Inflammation and Energy Balance Disruptions: Spotlight on Chemokines. *Frontiers in Endocrinology*, *8*, 197. https://doi.org/10.3389/fendo.2017.00197

Mamet, J., Baron, A., Lazdunski, M., & Voilley, N. (2002). ProInflammatory Mediators, Stimulators of Sensory Neuron Excitability via the Expression of Acid-Sensing Ion Channels. *The Journal of Neuroscience*, *22*(24), 10662–10670. https://doi.org/10.1523/JNEUROSCI.22-24-10662.2002

Marra, S., Ferru-Clément, R., Breuil, V., Delaunay, A., Christin, M., Friend, V., … Deval, E. (2016). Non-acidic activation of pain-related Acid-Sensing Ion Channel 3 by lipids. *The EMBO Journal*, *35*(4), 414–428. https://doi.org/10.15252/embj.201592335

Mogil, J. S., Breese, N. M., Witty, M.-F., Ritchie, J., Rainville, M.-L., Ase, A., … Séguéla, P. (2005). Transgenic Expression of a Dominant-Negative ASIC3 Subunit Leads to Increased Sensitivity to Mechanical and Inflammatory Stimuli. *Journal of Neuroscience*, *25*(43), 9893–9901. https://doi.org/10.1523/JNEUROSCI.2019-05.2005

Moran, M. M., & Szallasi, A. (2018). Targeting nociceptive transient receptor potential channels to treat chronic pain: Current state of the field. *British Journal of Pharmacology*, *175*(12), 2185–2203. https://doi.org/10.1111/bph.14044

*National Diabetes Fact Sheet, 2011*. (n.d.). 12.

O'Brien, P. D., Sakowski, S. A., & Feldman, E. L. (2014). Mouse models of diabetic neuropathy. *ILAR Journal / National Research Council, Institute of Laboratory Animal Resources*, *54*(3), 259–272. https://doi.org/10.1093/ilar/ilt052

Obrosova, I. G., Ilnytska, O., Lyzogubov, V. V., Pavlov, I. A., Mashtalir, N., Nadler, J. L., & Drel, V. R. (2007). High-Fat Diet–Induced Neuropathy of Pre-Diabetes and Obesity: Effects of "Healthy" Diet and Aldose Reductase Inhibition. *Diabetes*, *56*(10), 2598–2608. https://doi.org/10.2337/db06-1176

Okifuji, A., & Hare, B. D. (2015). The association between chronic pain and obesity. *Journal of Pain Research*, *8*, 399–408. https://doi.org/10.2147/JPR.S55598

Price, M. P., McIlwrath, S. L., Xie, J., Cheng, C., Qiao, J., Tarr, D. E., … Welsh, M. J. (2001). The DRASIC Cation Channel Contributes to the Detection of Cutaneous Touch and Acid Stimuli in Mice. *Neuron*, *32*(6), 1071–1083. https://doi.org/10.1016/S0896-6273(01)00547-5

Qiu, F., Qiu, C.-Y., Cai, H., Liu, T.-T., Qu, Z.-W., Yang, Z., … Hu, W.-P. (2014). Oxytocin inhibits the activity of acid-sensing ion channels through the vasopressin, V1A receptor in primary sensory neurons. *British Journal of Pharmacology*, *171*(12), 3065–3076. https://doi.org/10.1111/bph.12635

Qiu, F., Qiu, C.-Y., Liu, Y.-Q., Wu, D., Li, J.-D., & Hu, W.-P. (2012). Potentiation of acid-sensing ion channel activity by the activation of 5-HT2 receptors in rat dorsal root ganglion neurons. *Neuropharmacology*, *63*(3), 494–500. https://doi.org/10.1016/j.neuropharm.2012.04.034

Rash, L. D. (2017). Acid-Sensing Ion Channel Pharmacology, Past, Present, and Future …. In *Advances in Pharmacology* (Vol. 79, pp. 35–66). https://doi.org/10.1016/bs.apha.2017.02.001

Renaud, J. F., Scanu, A. M., Kazazoglou, T., Lombet, A., Romey, G., & Lazdunski, M. (1982). Normal serum and lipoprotein-deficient serum give different expressions of excitability, corresponding to different stages of differentiation, in chicken cardiac cells in culture. *Proceedings of the National Academy of Sciences*, *79*(24), 7768–7772. https://doi.org/10.1073/pnas.79.24.7768

SAFE. (n.d.). Retrieved October 30, 2015, from http://www.safe-diets.com/eng/

Smith, E. S., Cadiou, H., & McNaughton, P. A. (2007). Arachidonic acid potentiates acid-sensing ion channels in rat sensory neurons by a direct action. *Neuroscience*, *145*(2), 686–698. https://doi.org/10.1016/j.neuroscience.2006.12.024

Spiegelman, B. M., & Flier, J. S. (2001). Obesity and the regulation of energy balance. *Cell*, *104*(4), 531–543.

Stino, A. M., & Smith, A. G. (2017). Peripheral neuropathy in prediabetes and the metabolic syndrome. *Journal of Diabetes Investigation*, *8*(5), 646–655. https://doi.org/10.1111/jdi.12650

Tsantoulas, C., Laínez, S., Wong, S., Mehta, I., Vilar, B., & McNaughton, P. A. (2017). Hyperpolarization-activated cyclic nucleotide-gated 2 (HCN2) ion channels drive pain in mouse models of diabetic neuropathy. *Science Translational Medicine*, *9*(409), eaam6072. https://doi.org/10.1126/scitranslmed.aam6072

Twells, L. K., Gregory, D. M., Reddigan, J., & Midodzi, W. K. (2014). Current and predicted prevalence of obesity in Canada: A trend analysis. *CMAJ Open*, *2*(1), E18-26. https://doi.org/10.9778/cmajo.20130016

Ugawa, S., Ueda, T., Ishida, Y., Nishigaki, M., Shibata, Y., & Shimada, S. (2002). Amiloride-blockable acid-sensing ion channels are leading acid sensors expressed in human nociceptors. *The Journal of Clinical Investigation*, *110*(8), 1185–1190. https://doi.org/10.1172/JCI15709

Usoskin, D., Furlan, A., Islam, S., Abdo, H., Lönnerberg, P., Lou, D., … Ernfors, P. (2015). Unbiased classification of sensory neuron types by large-scale single-cell RNA sequencing. *Nature Neuroscience*, *18*(1), 145–153. https://doi.org/10.1038/nn.3881

Uysal, K. T., Wiesbrock, S. M., & Hotamisligil, G. S. (1998). Functional analysis of tumor necrosis factor (TNF) receptors in TNF-alpha-mediated insulin resistance in genetic obesity. *Endocrinology*, *139*(12), 4832–4838. https://doi.org/10.1210/endo.139.12.6337

Verkest, C., Piquet, E., Diochot, S., Dauvois, M., Lanteri-Minet, M., Lingueglia, E., & Baron, A. (2018). Effects of systemic inhibitors of acid-sensing ion channels 1 (ASIC1) against acute and chronic mechanical allodynia in a rodent model of migraine. *British Journal of Pharmacology*, *175*(21), 4154–4166. https://doi.org/10.1111/bph.14462

Vincent, A. M., Hayes, J. M., McLean, L. L., Vivekanandan-Giri, A., Pennathur, S., & Feldman, E. L. (2009). Dyslipidemia-Induced Neuropathy in Mice. *Diabetes*, *58*(10), 2376–2385. https://doi.org/10.2337/db09-0047

Vullo, S., & Kellenberger, S. (2019). A molecular view of the function and pharmacology of acid-sensing ion channels. *Pharmacological Research*. https://doi.org/10.1016/j.phrs.2019.02.005

Waldmann, R., Champigny, G., Bassilana, F., Heurteaux, C., & Lazdunski, M. (1997). A proton-gated cation channel involved in acid-sensing. *Nature*, *386*(6621), 173–177. https://doi.org/10.1038/386173a0

Wang, Y., Miura, Y., Kaneko, T., Li, J., Qin, L.-Q., Wang, P.-Y., … Sato, A. (2002). Glucose intolerance induced by a high-fat/low-carbohydrate diet in rats effects of nonesterified fatty acids. *Endocrine*, *17*(3), 185–191. https://doi.org/10.1385/ENDO:17:3:185

WHO | Obesity. (n.d.). Retrieved May 15, 2019, from WHO website: https://www.who.int/topics/obesity/en/

Wultsch, T., Painsipp, E., Shahbazian, A., Mitrovic, M., Edelsbrunner, M., Waldmann, R., … Holzer, P. (2008). Deletion of the acid-sensing ion channel ASIC3 prevents gastritis-induced acid hyperresponsiveness of the stomach – brainstem axis. *Pain*, *134*(3), 245–253. https://doi.org/10.1016/j.pain.2007.04.025

Xie, J., Price, M. P., Berger, A. L., & Welsh, M. J. (2002). DRASIC contributes to pH-gated currents in large dorsal root ganglion sensory neurons by forming heteromultimeric channels. *Journal of Neurophysiology*, *87*(6), 2835–2843. https://doi.org/10.1152/jn.2002.87.6.2835

Xu, S., & Xue, Y. (2016). Pediatric obesity: Causes, symptoms, prevention and treatment. *Experimental and Therapeutic Medicine*, *11*(1), 15–20. https://doi.org/10.3892/etm.2015.2853

Yen, Y.-T., Tu, P.-H., Chen, C.-J., Lin, Y.-W., Hsieh, S.-T., & Chen, C.-C. (2009). Role of acid-sensing ion channel 3 in sub-acute-phase inflammation. *Molecular Pain*, *5*, 1. https://doi.org/10.1186/1744-8069-5-1

Yu, Y., Chen, Z., Li, W.-G., Cao, H., Feng, E.-G., Yu, F., … Xu, T.-L. (2010). A Nonproton Ligand Sensor in the Acid-Sensing Ion Channel. *Neuron*, *68*(1), 61–72. https://doi.org/10.1016/j.neuron.2010.09.001

Zimmermann, M. (1983). Ethical guidelines for investigations of experimental pain in conscious animals. *PAIN*, *16*(2), 109. https://doi.org/10.1016/0304-3959(83)90201-4

## 1.6. Supplementary data

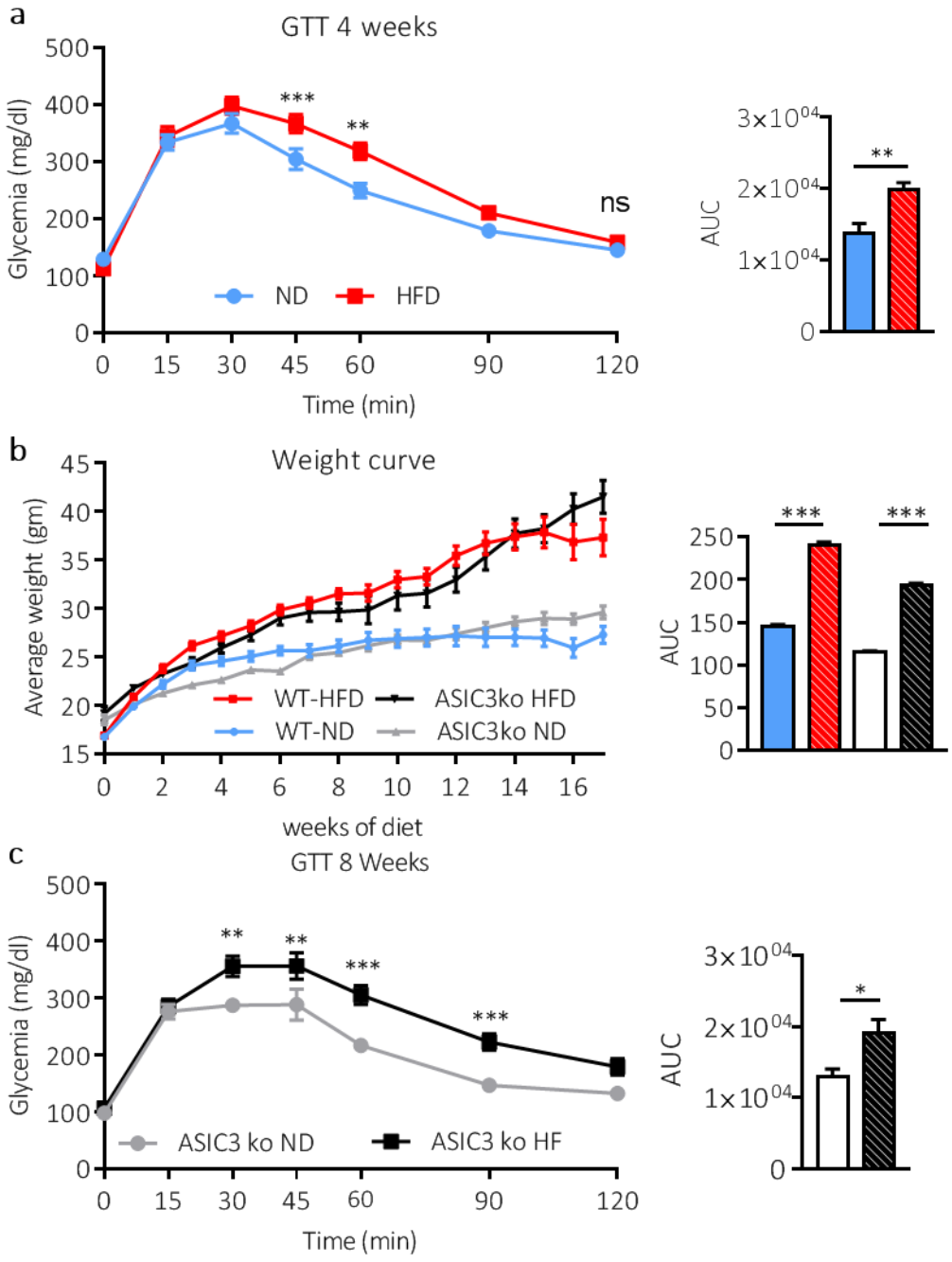


*Figure S 1: Feeding ASIC3 knockout mice induce significant obesity and glucose intolerance*

*(a) GTT for the WT mice at 4 weeks of diet. n=10-10 Multiple t tests (b)Average weight in gram of the (ASIC3 knockout mice fed the normal grey, and the high fat diet black) and (WT fed the ND blue and the HFD red).The right panel show the area under the curve. n=7-6. (c) Glucose tolerance test performed at 8 weeks of diet for of the ASIC3ko mice fed the ND and the HFD Multiple t tests. The right panel show the AUC. n=7-6.*

## 2. Glucose tolerance test GTT

To evaluate the progression in the development of glucose intolerance in mice fed the high fat diet, we performed the glucose tolerance test (GTT) at several time points' Fig24. We measured the basal glycaemia after 16 hours of fasting the mice to evaluate the fasting glycemia and this point was also considered the control point for the GTT. Fasting blood glucose is important to evaluate the incidence of diabetes where if it exceeds 150mg/dl this is considered as a diabetic state. The last measurement, 2 hours after glucose injection, in the GTT experiment also comprise an important indicator of dysregulation in the glucose hemostasis. The fasting glucose of WT and the GTT for WT at 4 and 8 weeks of diet are described in the paper but I reinserted them in this figure to facilitate the comparison with other time points described here. The fasting blood glucose was not significantly different in wild type (WT) mice fed the ND and the HFD at 4, 8 and 12 weeks of diet. The HFD mice had significantly higher fasting blood glucose at 16 weeks of diet (data described in the paper Fig 1). After 4 weeks of diet, the intraperitoneal injection of glucose in WT mice fed the ND and the HFD increased blood glucose that almost recovered to the pre-injection levels in 2 hours. The difference in glycaemia 2 hours post injection was insignificant in both groups the ND and the HFD at 4 weeks of diet Fig24A. Starting from 8 weeks of diet mice fed the HFD developed dysregulation in the glucose hemostasis indicated as significant higher level of glycaemia after 2 hours post injection of glucose compared to the control mice (data described in paper). The dysregulation in the glucose hemostasis found in the HFD mice at 8 weeks persisted up to 12 and 16 weeks with 2 hour post-injection glycaemia of 251.4 +/- 19.3 265 +/- 26.5 mg/dl at 12 and 16 weeks compared to the ND mice with 143.3 +/- 4.9 and 134.1 +/- 6.4 mg/dl for the 2 time points respectively Fig 24 C-D. The AUC of the glucose tolerance test experiments done on the WT mice fed the ND and the HFD at the different time points show that HFD mice had significantly higher glycaemia at all the tested time points starting from 4 weeks of diet Fig 24E. The genetic deletion of the ASIC3 channels in the knockout mice did not alter the development of dysregulations in the glucose hemostasis after consuming the HFD. The glucose tolerance test was performed on ASIC3ko and the WT mice both received the HFD at 4, 8, and 12 weeks of diet in Fig24 F, G and H respectively. The 2 hours post glucose injection point and the AUC (Fig 24I) were not significantly different in both groups at 4, 8, and 12 weeks of diet.

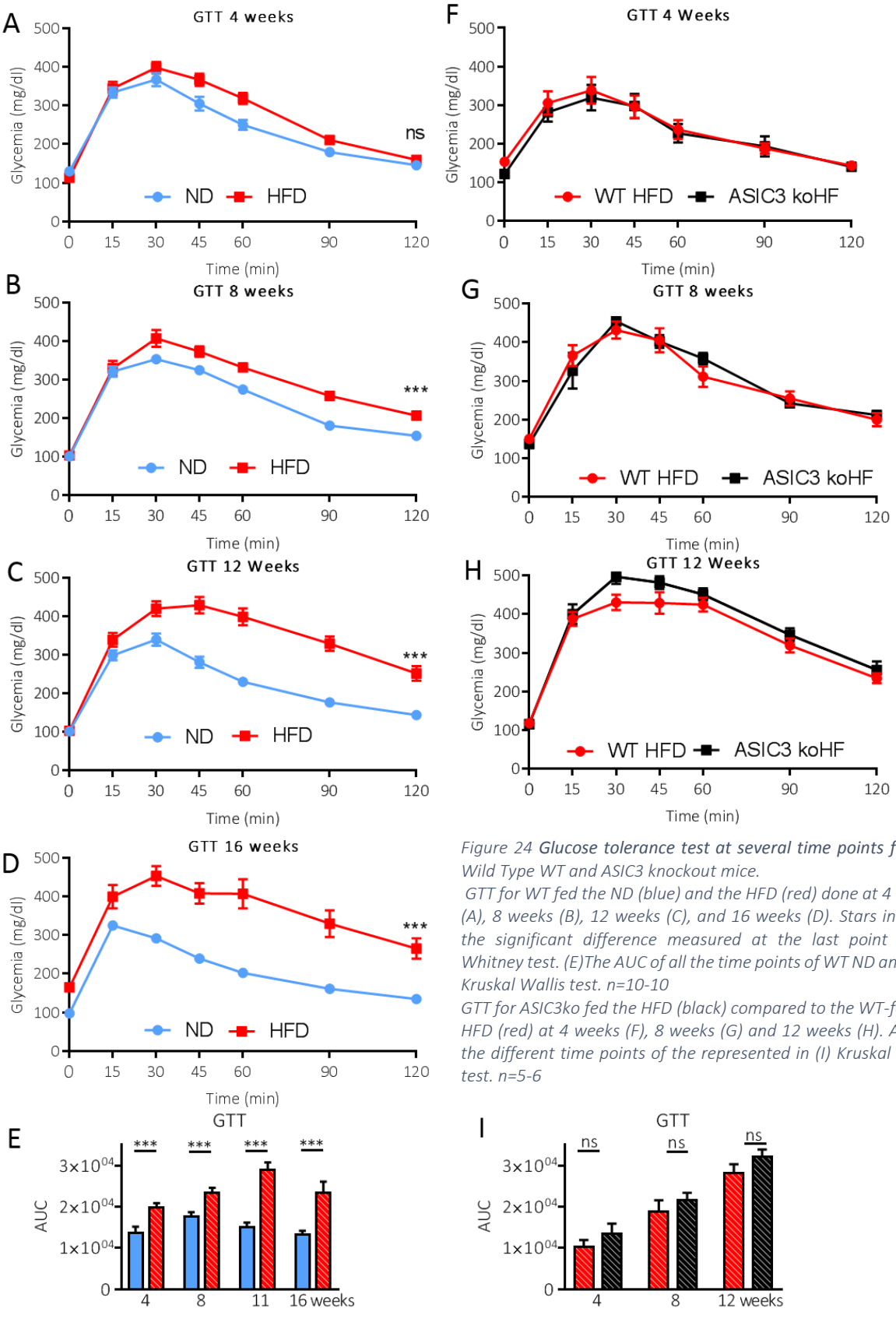


*Figure 24* ***Glucose tolerance test at several time points for the*** *Wild Type WT and ASIC3 knockout mice.*

*GTT for WT fed the ND (blue) and the HFD (red) done at 4 weeks (A), 8 weeks (B), 12 weeks (C), and 16 weeks (D). Stars indicate the significant difference measured at the last point Mann Whitney test. (E)The AUC of all the time points of WT ND and HFD Kruskal Wallis test. n=10-10*

*GTT for ASIC3ko fed the HFD (black) compared to the WT-fed the HFD (red) at 4 weeks (F), 8 weeks (G) and 12 weeks (H). AUC of the different time points of the represented in (I) Kruskal Wallis test. n=5-6*

## 3. Food and water

Wild type mice fed the HFD consumed significantly less water and food compared to the control mice fed the ND and the average water consumption per mouse was 31.9+/-0.89 and 21.82 +/- 0.64 gm/week for ND and HFD respectively Fig 25A. The food consumption was 26.75 +/- 0.88 and 18.61 +/- 0.46 gm/ week for the ND and the HFD respectively Fig 25B. On the other hand, upon calculating the average caloric intake of the mice, we found that the HFD mice consumed more calories with 85.61 +/- 2.8 and 98.2 +/- 2.4 Kcal/week/mouse for the ND and the HFD respectively Fig 25C.

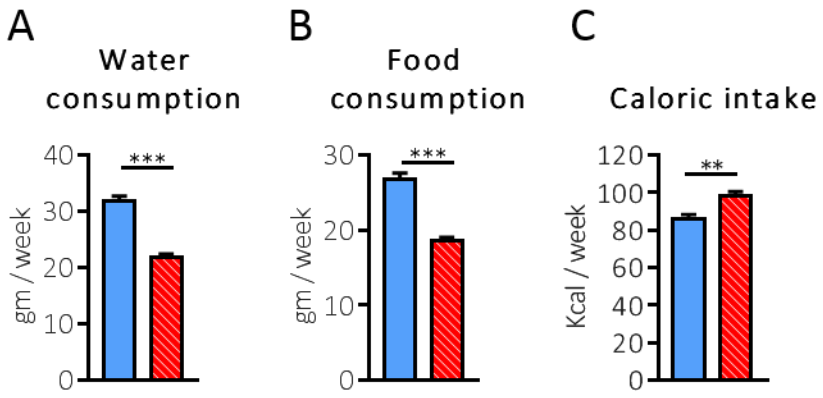


*Figure 25 average food and water consumption of WT mice.*
*The average weekly consumption of water (A), food (B) and caloric intake (C) for the wild type mice fed the ND (blue) and the HFD (red) n=10-10 Mann Whitney test.*

## 4. Formalin test

Intra-planter injection of formalin induce a biphasic pain behavior where the pain seen during the first 5 minutes is due to peripheral activation of the nociceptors. The pain seen between 5 and 15 minutes is mediated by both peripheral and central component of the pain pathway and finally the pain seen 15 minutes post-injection is mainly due to central activation of the pain pathway. To assess the chemical pain sensitivity of mice the ND and the HFD we performed the formalin test after 12 weeks. Indeed, both groups of mice developed the biphasic pain behaviors in response to the intra-planter injection of formalin Fig 26A. The total time mice spent showing pain behaviors during the 60 minutes of the experiment were not significantly different between the two wild

type groups of mice fed the ND and HFD Fig 26B. In addition, we compared the time spent showing pain behaviors of the HFD and ND mice during the first 5 minutes, 5-15, and between 15 and 60 minutes Fig 26 C-D. Both groups did not show significant difference in the time spent showing pain during the first 5 minutes neither between 5-15 nor between 15-60 minutes. This indicate that the consumption of the HFD did not affect significantly the mice pain responses toward a chemical insult.

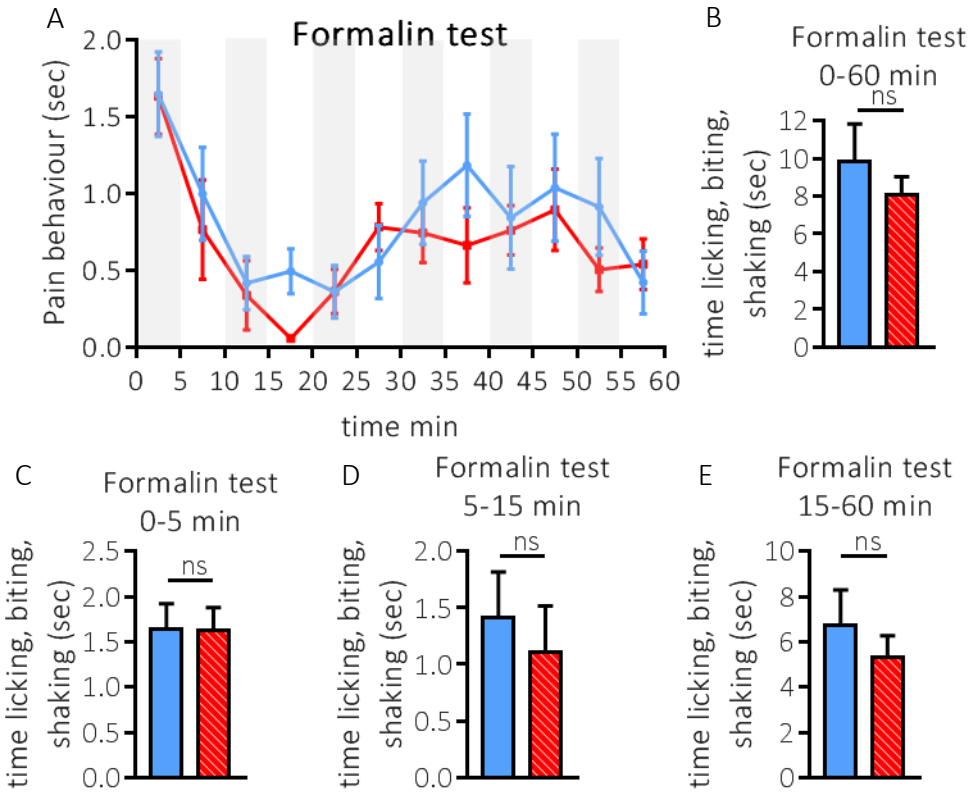


*Figure 26 Formalin test done on WT mice.*
*Mice fed the ND (blue) and the HFD (red) Pain responses during 60 minutes (B) n= 9-8. Time mice showing nociceptive behavior during the first 5 min (C), between 5 and 15 min (D), and between 15-60 min (E). Mann Whitney*

## 5. Lipidomic

In addition to the results found with the lipidomic analysis for LPC described in the paper, we found that several species of lipids were increased in the serum of mice fed the HFD compared to the serum of those fed the ND. Delipidizing the HFD serum reduced the amount of lipids within several lipid species. Because the protocol of de-lipidization require a final step of dialyzing the serum with a 3.5 KDalton cutoff cassettes, we performed the dialysis step on a part of the HFD serum without performing the centrifugation steps required in the protocol to separate the lipid phase. Indeed, dialyzing the HFD serum reduced the amount of some lipids in the serum, but this reduction was not as efficient as the whole protocol of delipidization. To note, the excitatory effect of the HFD serum on HEK cells transfected with recombinant ASIC3 subunit was lost after dialyzing the serum, data not shown. The collective amount of lipids within each lipid species is represented in Fig 27A while the amount of each member within these lipid species are represented in Fig 27 B-M.

*Figure 27* ***Analysis of the serum lipids.***
*The collective amount of lipids within each species of lipids in the ND (blue), HFD (red), HFD delipidized (green) and HFD dialyzed (white with black strips) n= 3 for each. Levels of the different subtypes of lipids within each family of lipids indicated in (B-M) Lipid species name indicated in the title and the name lipids within these lipid species indicated on the X axis. n=3 for each condition.*

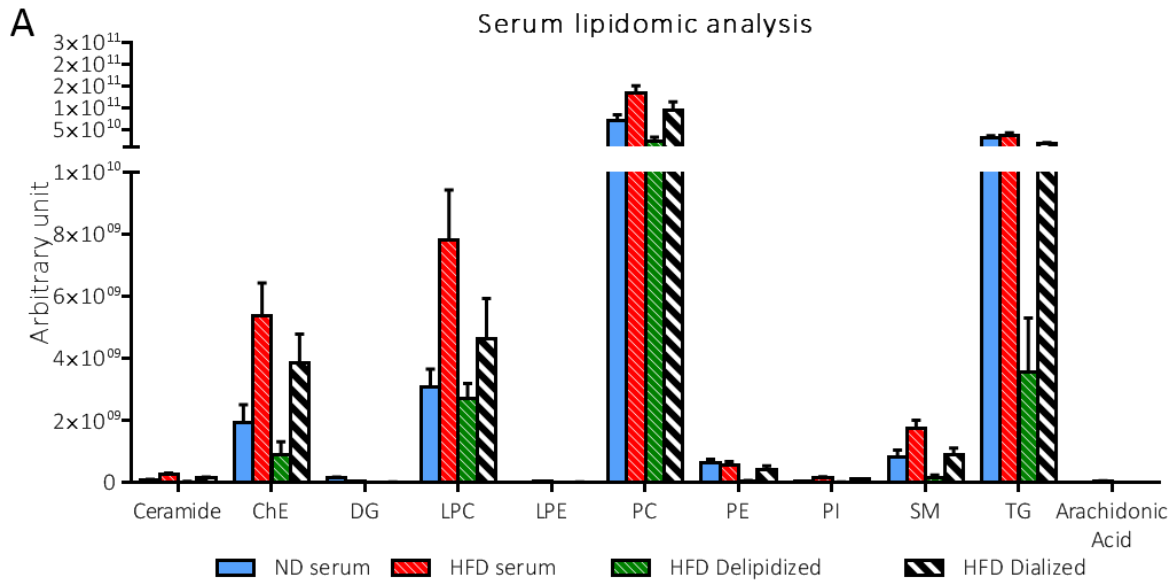

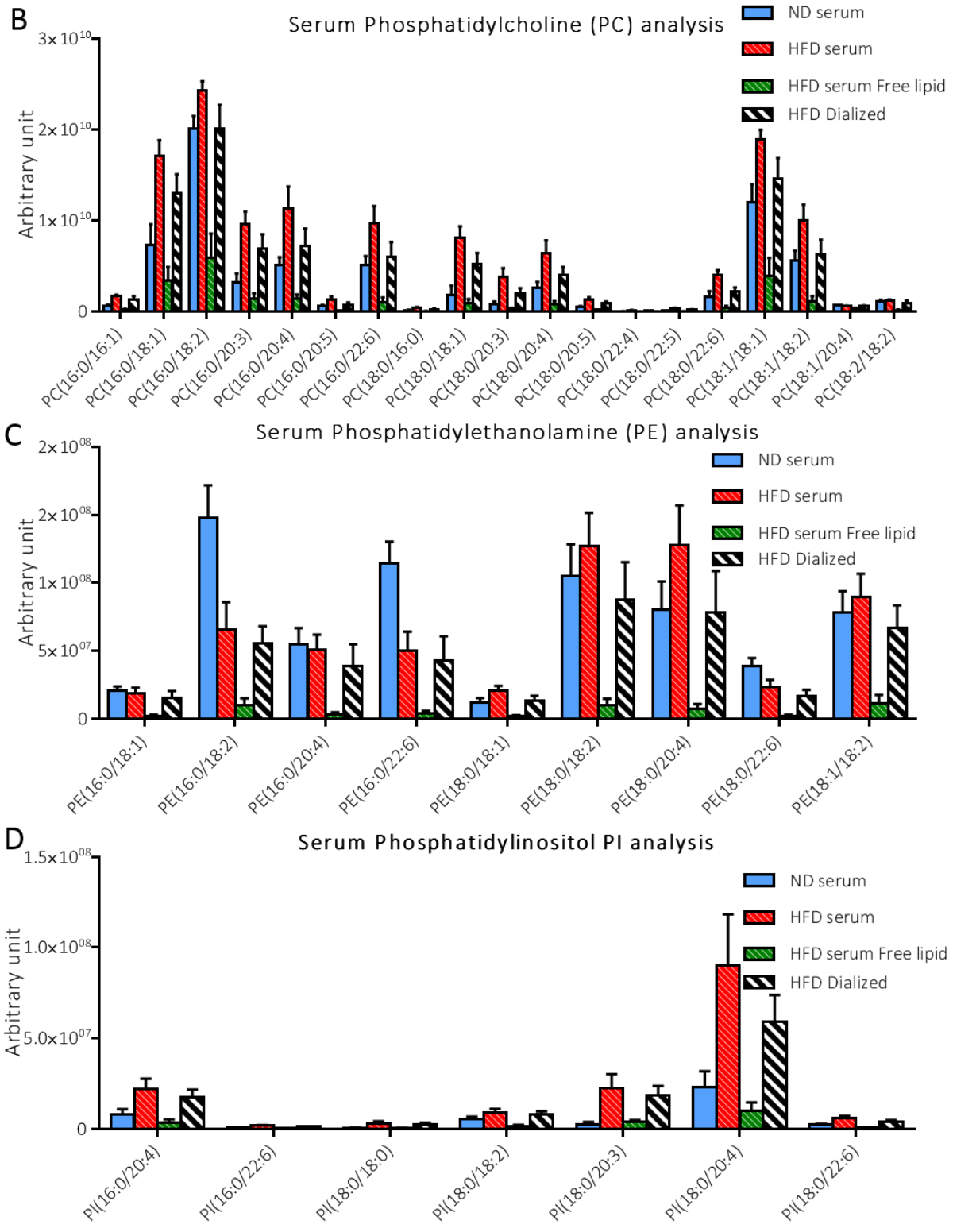
B
Serum Phosphatidylcholine (PC) analysis
ND serum
HFD serum
HFD serum Free lipid
HFD Dialized
Arbitrary unit
3x10^10
2x10^10
1x10^10
0
PC(16:0/16:1)
PC(16:0/18:1)
PC(16:0/18:2)
PC(16:0/20:3)
PC(16:0/20:4)
PC(16:0/20:5)
PC(16:0/22:6)
PC(18:0/16:0)
PC(18:0/18:1)
PC(18:0/20:3)
PC(18:0/20:4)
PC(18:0/20:5)
PC(18:0/22:4)
PC(18:0/22:5)
PC(18:0/22:6)
PC(18:1/18:1)
PC(18:1/18:2)
PC(18:1/20:4)
PC(18:2/18:2)
C
Serum Phosphatidylethanolamine (PE) analysis
ND serum
HFD serum
HFD serum Free lipid
HFD Dialized
Arbitrary unit
2x10^08
2x10^08
1x10^08
5x10^07
0
PE(16:0/18:1)
PE(16:0/18:2)
PE(16:0/20:4)
PE(16:0/22:6)
PE(18:0/18:1)
PE(18:0/18:2)
PE(18:0/20:4)
PE(18:0/22:6)
PE(18:1/18:2)
D
Serum Phosphatidylinositol PI analysis
ND serum
HFD serum
HFD serum Free lipid
HFD Dialized
Arbitrary unit
1.5x10^08
1.0x10^08
5.0x10^07
0
PI(16:0/20:4)
PI(16:0/22:6)
PI(18:0/18:0)
PI(18:0/18:2)
PI(18:0/20:3)
PI(18:0/20:4)
PI(18:0/22:6)

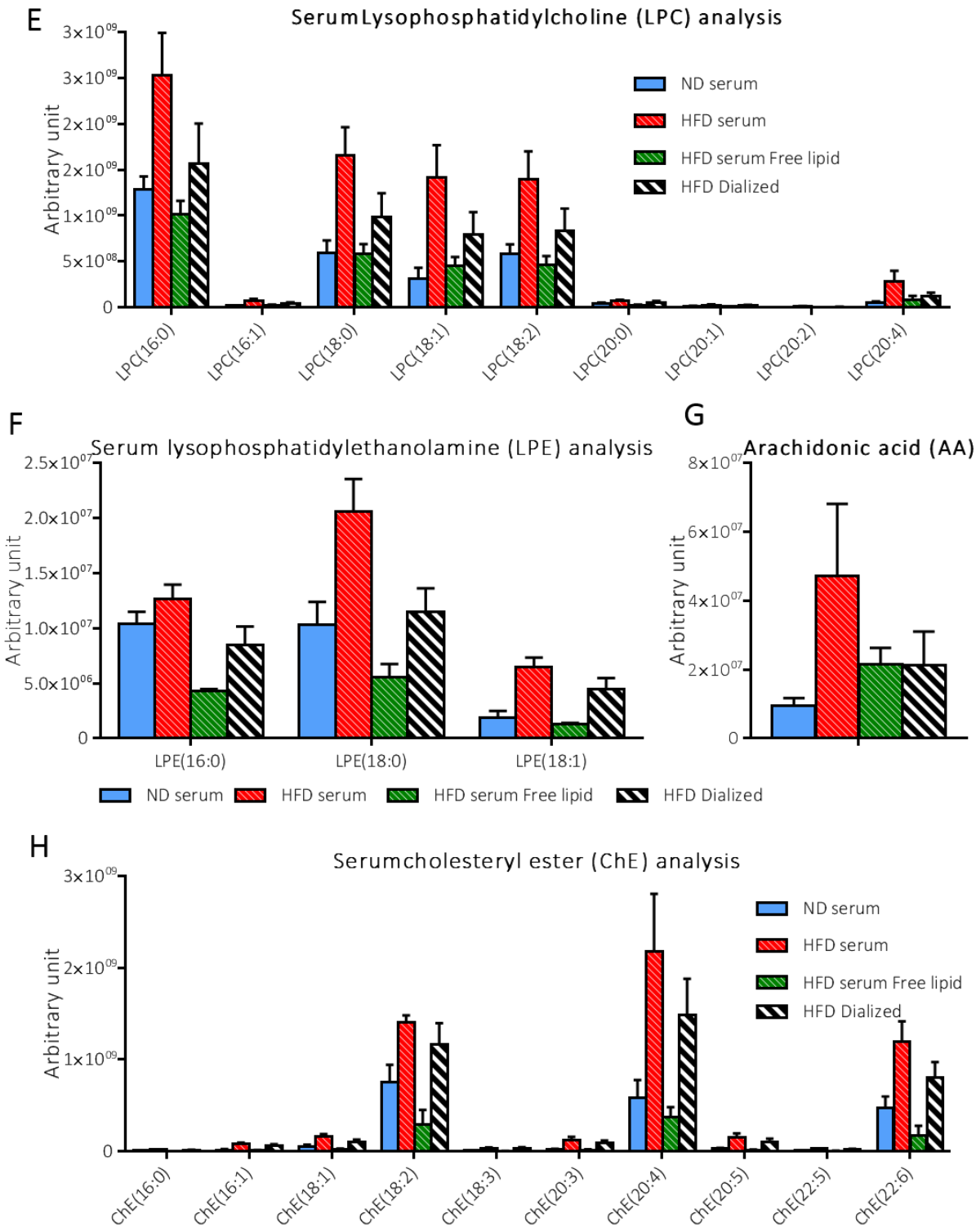
E
Serum Lysophosphatidylcholine (LPC) analysis
Arbitrary unit
3x10^09
3x10^09
2x10^09
2x10^09
1x10^09
5x10^08
0
ND serum
HFD serum
HFD serum Free lipid
HFD Dialized
LPC(16:0)
LPC(16:1)
LPC(18:0)
LPC(18:1)
LPC(18:2)
LPC(20:0)
LPC(20:1)
LPC(20:2)
LPC(20:4)
F
Serum lysophosphatidylethanolamine (LPE) analysis
Arbitrary unit
2.5x10^07
2.0x10^07
1.5x10^07
1.0x10^07
5.0x10^06
0
LPE(16:0)
LPE(18:0)
LPE(18:1)
ND serum
HFD serum
HFD serum Free lipid
HFD Dialized
G
Arachidonic acid (AA)
Arbitrary unit
8x10^07
6x10^07
4x10^07
2x10^07
0
H
Serum cholesteryl ester (ChE) analysis
Arbitrary unit
3x10^09
2x10^09
1x10^09
0
ND serum
HFD serum
HFD serum Free lipid
HFD Dialized
ChE(16:0)
ChE(16:1)
ChE(18:1)
ChE(18:2)
ChE(18:3)
ChE(20:3)
ChE(20:4)
ChE(20:5)
ChE(22:5)
ChE(22:6)

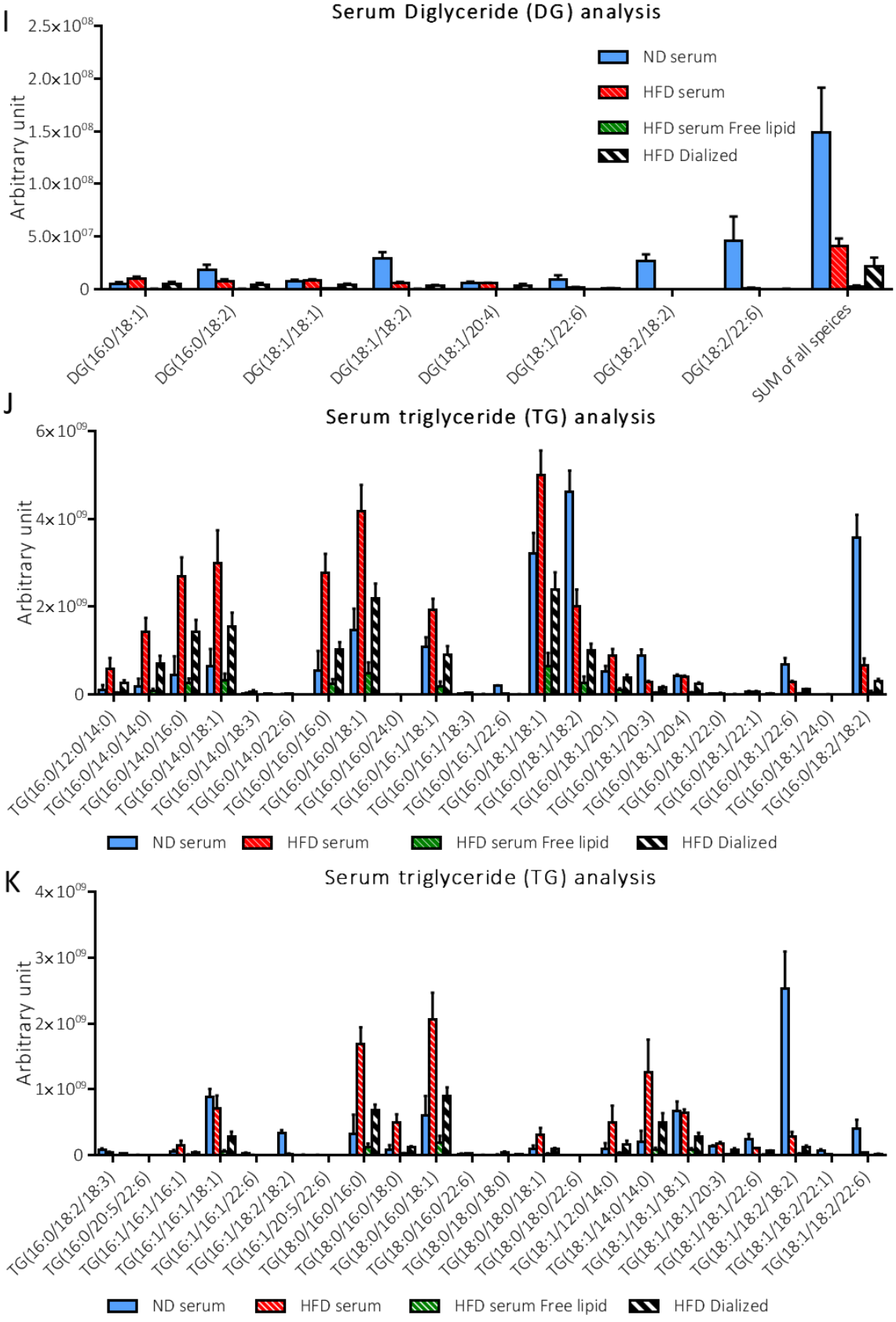
I
Serum Diglyceride (DG) analysis
Arbitrary unit
2.5x10^08
2.0x10^08
1.5x10^08
1.0x10^08
5.0x10^07
0
ND serum
HFD serum
HFD serum Free lipid
HFD Dialized
DG(16:0/18:1)
DG(16:0/18:2)
DG(18:1/18:1)
DG(18:1/18:2)
DG(18:1/20:4)
DG(18:1/22:6)
DG(18:2/18:2)
DG(18:2/22:6)
SUM of all speices
J
Serum triglyceride (TG) analysis
Arbitrary unit
6x10^09
4x10^09
2x10^09
0
TG(16:0/12:0/14:0)
TG(16:0/14:0/14:0)
TG(16:0/14:0/16:0)
TG(16:0/14:0/18:1)
TG(16:0/14:0/18:3)
TG(16:0/14:0/22:6)
TG(16:0/16:0/16:0)
TG(16:0/16:0/18:1)
TG(16:0/16:0/24:0)
TG(16:0/16:1/18:1)
TG(16:0/16:1/18:3)
TG(16:0/16:1/22:6)
TG(16:0/18:1/18:1)
TG(16:0/18:1/18:2)
TG(16:0/18:1/20:1)
TG(16:0/18:1/20:3)
TG(16:0/18:1/20:4)
TG(16:0/18:1/22:0)
TG(16:0/18:1/22:1)
TG(16:0/18:1/22:6)
TG(16:0/18:1/24:0)
TG(16:0/18:2/18:2)
ND serum
HFD serum
HFD serum Free lipid
HFD Dialized
K
Serum triglyceride (TG) analysis
Arbitrary unit
4x10^09
3x10^09
2x10^09
1x10^09
0
TG(16:0/18:2/18:3)
TG(16:0/20:5/22:6)
TG(16:1/16:1/16:1)
TG(16:1/16:1/18:1)
TG(16:1/16:1/22:6)
TG(16:1/18:2/18:2)
TG(16:1/20:5/22:6)
TG(18:0/16:0/16:0)
TG(18:0/16:0/18:0)
TG(18:0/16:0/18:1)
TG(18:0/16:0/22:6)
TG(18:0/18:0/18:0)
TG(18:0/18:0/18:1)
TG(18:0/18:0/22:6)
TG(18:1/12:0/14:0)
TG(18:1/14:0/14:0)
TG(18:1/18:1/18:1)
TG(18:1/18:1/20:3)
TG(18:1/18:1/22:6)
TG(18:1/18:2/18:2)
TG(18:1/18:2/22:1)
TG(18:1/18:2/22:6)
ND serum
HFD serum
HFD serum Free lipid
HFD Dialized

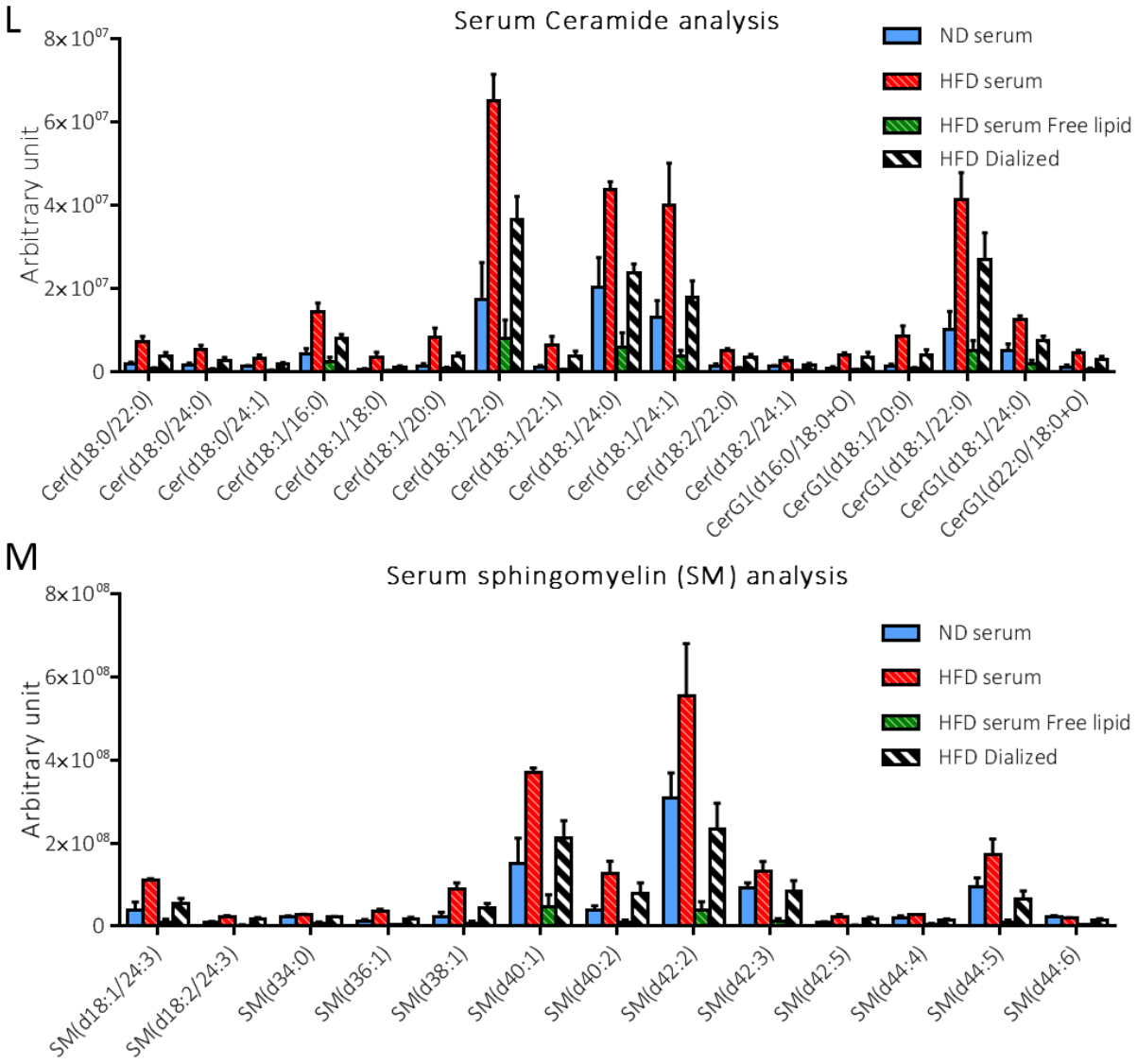
L
Serum Ceramide analysis
Arbitrary unit
8x10^07
6x10^07
4x10^07
2x10^07
0
ND serum
HFD serum
HFD serum Free lipid
HFD Dialized
Cer(d18:0/22:0)
Cer(d18:0/24:0)
Cer(d18:0/24:1)
Cer(d18:1/16:0)
Cer(d18:1/18:0)
Cer(d18:1/20:0)
Cer(d18:1/22:0)
Cer(d18:1/22:1)
Cer(d18:1/24:0)
Cer(d18:1/24:1)
Cer(d18:2/22:0)
Cer(d18:2/24:1)
CerG1(d16:0/18:0+O)
CerG1(d18:1/20:0)
CerG1(d18:1/22:0)
CerG1(d18:1/24:0)
CerG1(d22:0/18:0+O)
M
Serum sphingomyelin (SM) analysis
Arbitrary unit
8x10^08
6x10^08
4x10^08
2x10^08
0
ND serum
HFD serum
HFD serum Free lipid
HFD Dialized
SM(d18:1/24:3)
SM(d18:2/24:3)
SM(d34:0)
SM(d36:1)
SM(d38:1)
SM(d40:1)
SM(d40:2)
SM(d42:2)
SM(d42:3)
SM(d42:5)
SM(d44:4)
SM(d44:5)
SM(d44:6)

## 6. Quantitative PCR qPCR

Several reports described the induction of inflammatory signaling pathway in the adipose tissue in response to metabolic stress. In turn, several inflammatory cytokines including TNF-α, interleukin (IL)-6, IL-1β are elevated in the adipose tissue and are extended to other metabolic tissue indicating a state of low grade inflammation **(Gregor and Hotamisligil, 2011)**. We wanted to test if this state of low grade inflammation was extended to tissues involved in pain transmission. Therefore, we performed qPCR at 8 weeks of diet to check mRNA levels of cytokines considered as inflammatory markers TNF-α, IL-6, and IL-1β in the DRGs and the spinal cord of ND and HFD mice. In the HFD DRGs we found that mRNA levels of TNF-α were significantly elevated compared to the ND mice with a $2^{-\Delta\Delta CT}$ 0.8 +/- 0.09 and 3.2 +/- 0.6 for the ND and the HFD respectively p=0.02 Mann Whitney Fig28A. In the spinal cord, we found IL-1β to be significantly elevated in the HFD mice with 1.1 +/- 0.15 and 2.4 +/- 0.3 for $2^{-\Delta\Delta CT}$ in the ND and the HFD respectively p= 0.01 Mann Whitney Fig 28B. This indicate that the HFD mice suffer from a state of low grade inflammation. In addition, we checked the mRNA levels of ASIC3 channel in two groups of mice fed the ND and the HFD at 8 weeks of diet In the DRG. We found that mRNA levels of ASIC3 was not significantly different in both groups Fig 28C.

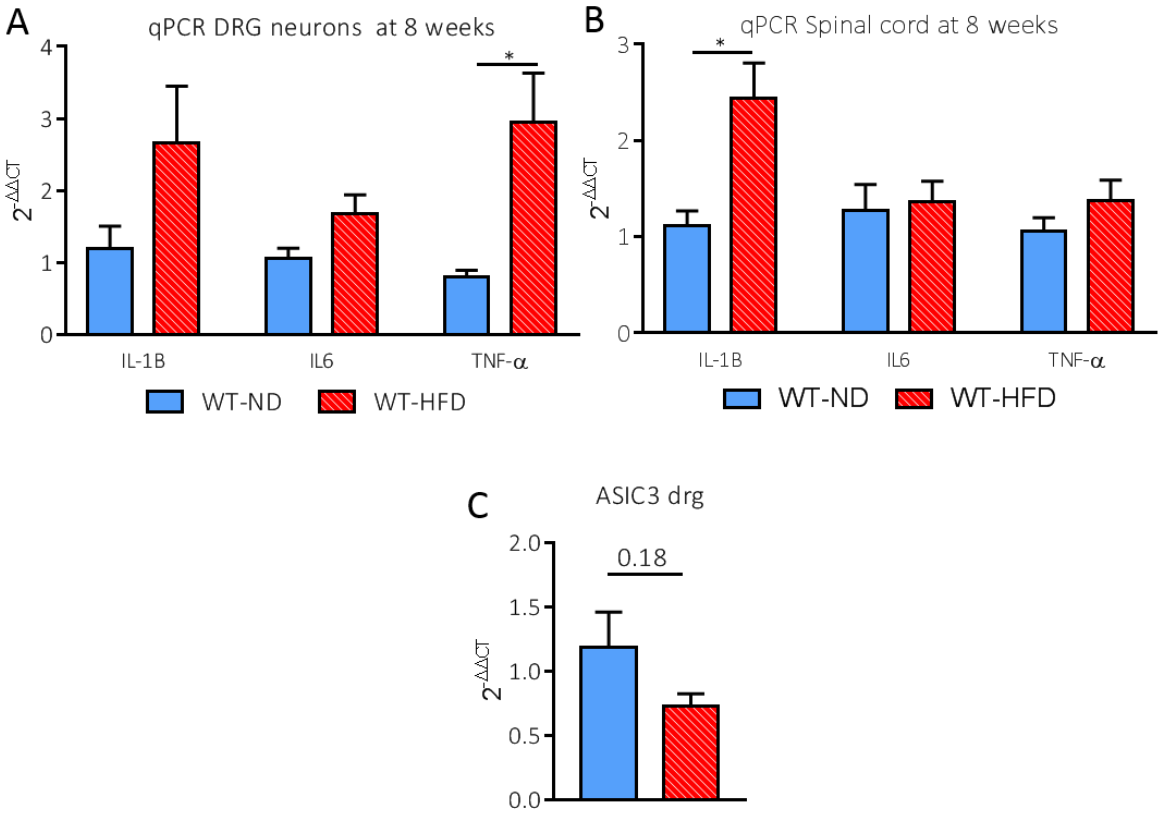


*Figure 28 The mRNA levels of the inflammatory cytokines.*
*mRNA found in the DRG represented in (A) and spinal cord in (B) of the ND (blue) and the HFD mice (red). (C) The mRNA levels of ASIC3 subunits in the DRG neurons of ND and the HFD n=10-10. Mann Whitney.*

## 7. IHC

Astrocytes are glia cells found in the CNS and they provide structural and functional support for neurons. They have the ability to release gliotransmitters that modulate synaptic activity **(Perea et al., 2009)**. Moreover, microglia another type of glia cells plays an important role in neuroprotection and neurotoxicity **(Kim and de Vellis, 2005)**. Both types of glia cells contribute to immune and inflammatory responses in the CNS **(Farina et al., 2007; Kim and de Vellis, 2005; Sofroniew and Vinters, 2010)**. They can release pro and anti-inflammatory cytokines/chemokines upon their activation by CNS infection, injury, cellular debris, abnormal protein aggregation, excessive neuroinflammation or immune stimuli **(Allan and Rothwell, 2003; Jang et al., 2013; Markiewicz and Lukomska, 2006)**. Therefore, we wanted to know if the state of low-grade inflammation could be associated with increased activation of astrocytes and microglia found in the spinal cord. Therefore, we performed immune-histochemistry at 12 weeks of diet on spinal cord slices from the lumber region of ND and HFD mice. We used GFAP to stain astrocyte and IBa1 to marker of microglia. We then evaluated the percentage of total surface area stained with GFAP within a square of 400$\mu M^2$ drawn in the superficial laminae of the dorsal horn of the spinal cord. We found that GFAP staining was significantly increased in the spinal cord of the HFD compared to the ND mice with 19.9 +/- 1 to 23.5 +/- 1.4% for the ND and the HFD respectively p=0.04 t.test Fig 29A. The skeleton of the astrocytes was also increase in the HFD with 9.7+/- 0.6 to 12.1 +/- 0.7 for the ND and HFD respectively p=0.01 t.test. We did the same with microglia and we found that the total staining of the IBa1 was increased in the dorsal horn of the spinal cord of the HFD mice compared to the control with a percentage of surface area stained 15 +/- 1.7 and 21.1 +/- 1.7 for the ND and the HFD respectively p=0.04 Mann Whitney test. The surface area stained with the skeleton of the microglia was 8.7 +/-0.7 and 12.5+/-1.1 for both conditions respectively. This indicate that there is a substantial activation of astrocytes and microglia.

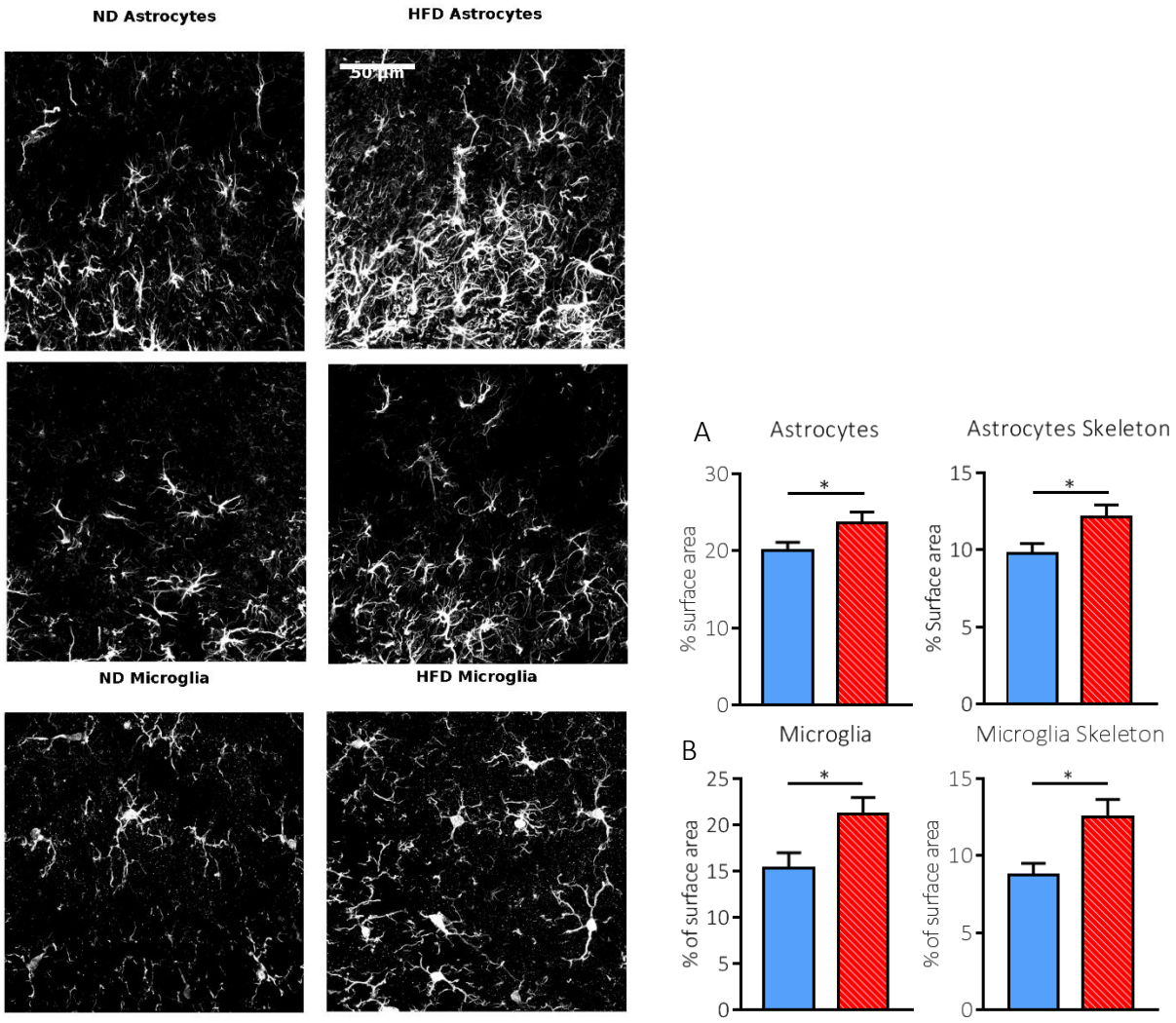


*Figure 29* ***IHC on spinal cord slices.***
***GFAP staining ND (left) HFD right and the total surface area and astrocytes skeleton are presented (A) n= 25-27 slices from 3-4 animals. Representative figure for IBa1 staining of microglia in ND left and HFD. (B) The averaged total area stained with IBa1 and the*** *microglia Skelton*. ***8-7 slices from 3-4 animals.***

## 8. LPS injection

We wanted to know if the described state of the low-grade inflammation could affect the thermal perception of the mice and make them prone to inflammatory sensitization. From the previous described results, we know that HFD mice develop thermal hypersensitivity after 8 weeks of diet. Therefore, we used mice that were adapted to the ND and the HFD for 5 weeks and measured their basal thermal sensitivity by tail flick experiment. At this time point the thermal sensitivity of both groups of mice were not significantly different. In turn, we injected both groups of mice with a low dose of LPS (0,1 µg/20g mouse) intraperitoneal and found that at 6 and 24 hours post injection there were no significant difference in the tail flick latencies between both groups the ND and the HFD. Interestingly, we found that 48 hours post LPS injection the HFD mice showed reduced tail flick latencies that were significantly different with 7.66 +/- 0.6 sec, and 5.5 +/- 0.34 sec for ND and HFD respectively Fig 30 p=0.008 2way ANOVA. This reduction in the latencies were persistent when we measured the thermal sensitivity of the mice 9 days after the LPS injection with tail flick latencies of 8.38 +/- 0.47 and 6.28 +/- 0.42 seconds for the ND and the HFD respectively p= 0.01 2way ANOVA test. This raised the possibility that mice fed the HFD could be more prone toward mild inflammation because of the already established state of low-grade inflammation and this buildup of inflammation led to pain hypersensitivities.

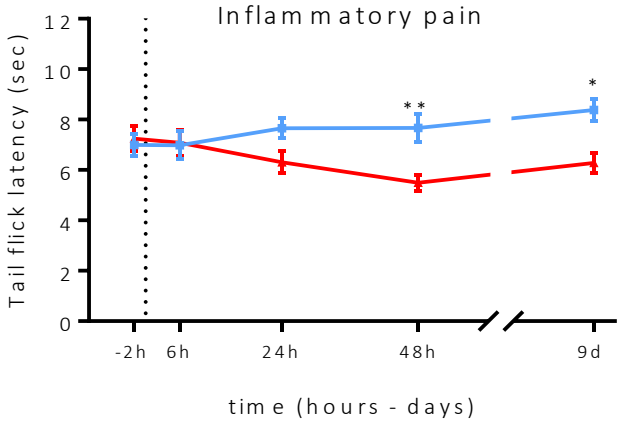


*Figure 30* ***Tail flick test after LPS injection.***
*Tail flick test done on mice fed the ND and the HFD for 5 weeks. Basal tail flick latency measured 2hours pre injection. Time of injection indicated by the dotted line. H (hours) D (days) n=10-10 2way ANOVA test*

# Discussion

The HFD contains high concentrations of saturated fatty acids that led to an increase in the caloric intake. Feeding the mice with this HFD led to an increase in the body weight and obesity, estimated as more than 25% of weight above normal diet mice, as expected and previously described by other reports for review (Heydemann, 2016; Primeaux et al., 2008; Winzell and Ahrén, 2004, 2004). A study showed that when rats were given simultaneous access to HFD and low fat diets they obtained 38% of the total calories from the HFD on the first day. This high caloric intake through the HFD decreased to 5% on the subsequent days showing that rats developed a rejection to the HFD and a decreased food consumption (Warwick, 1996). Our data is in agreement with this observation as we found that long-term consumption of the HFD was associated with decreased food and water consumptions. Nevertheless, due to the high caloric input of the HFD the overall caloric food intake was higher in the HFD group compared to the control group.

To determine whether the mice developed diabetes, it is well accepted to assess the fasting blood glucose where Diabetes is defined when its levels surpasses 150mg/dl (Sullivan et al., 2007; O'Brien et al., 2014). Besides it is important to evaluate the glucose intolerance to determine if the mice could be considered as a prediabetes state (Stino and Smith, 2017). Our data shows that HFD did not affect the fasting blood glucose until 16 weeks of diet but caused slight glucose intolerance at 4 weeks that progressively increased at 8 weeks of diet. This indicates that our model mice should be characterized as prediabetes state. The onset of diabetes at 16 weeks occurred long after the well establishment of the pain phenotypes of heat hyperalgesia, promoting the idea that it is most likely independent to previously described diabetic neuropathy. Late onset of diabetes is in agreement with previous studies that used the HFD as a model showing a gradual onset of metabolic dysregulation with moderate hyperinsulinemia, and glucose intolerance without elevated fasting plasma blood glucose (Coppey et al., 2011; Guilford et al., 2011; Obrosova et al., 2007; Vincent et al., 2009a). The onset of diabetes occurring long after the induction of the pain phenotype suggests an independent process led to its development.

HFD is also associated with dyslipidemia (Vincent et al., 2009a, 2009b). Hyperlipidemia was characterized as risk factor associated with neuropathy in prediabetic patients suffering from obesity (Singleton et al., 2005; Smith and Singleton, 2008; Stino and Smith, 2017). It is thus important to well characterize the lipid profiles associated with models of diabetic neuropathy.

Most studies that evaluated the lipid profile of mice with DIO models focused on plasma cholesterol and triglycerides as they are considered as great risk factor for the development of diabetic neuropathy (Syvänne and Taskinen, 1997). Nevertheless several other types of lipids were found to be associated with enhanced pain sensitivity including prostanoids, ceramides (Salvemini et al., 2013), arachidonic acid (Smith, 2006), LPA (Juárez-Contreras et al., 2018; Ueda, 2011; Yung et al., 2015), and LPC (Inoue et al., 2008b, 2008a; Marra et al., 2016) for review (Malan and Porreca, 2005; Piomelli et al., 2014). These lipids can directly sensitize nociceptive afferents and directly activate ion channels involved in the pain pathway. Our data confirm that several families of lipids were enhanced upon the consumption of the HFD compared to control mice. Among those lipids is LPC that was found to be significantly increased in the HFD serum compared to serum from the control mice on low lipid diet. LPC is increasingly recognized as a lipid messenger involved in inflammation and peripheral neuropathy. High concentrations of LPC induce demyelination of the sciatic nerve and neuropathy (Nagai et al., 2010). LPC together with AA were increased in the painful exudates of patients suffering from joint pain (Marra et al., 2016). These two lipids can directly activate human and rat ASIC3 channels and behavioral experiments confirmed that LPC activation of ASIC3 lead to pain phenotypes that were lost in ASIC3 knockout mice. In our model of DIO, the levels of LPC in the serum of obese mice was comparable to those found in the study of Marra et al, while the levels of AA were much lower. All the experiments done in the later paper used human and rat recombinant ASIC3 subunits and DRG neurons from rats so the effect of LPC was never tested on mouse ASIC3 subunit. We focused our study on the mouse ASIC3 subunit as all of our experiments where done in mice WT and ASIC3 knockout mice. We observed similar effects of LPC on the mouse ASIC3 subunits, compared to the rat and human subunits. Another study showed that intrathecal LPC injection induced neuropathic pain with mechanical allodynia and thermal hyperalgesia that lasted for 7 days. The effect was abolished in LPA1 receptor gene knockout mice and the authors concluded that the neuropathic effect of LPC was mediated through the enzymatic hydrolysis of LPC to LPA by autotaxin (Inoue et al., 2008b). This is unlikely to be the same mechanism that led to the pain phenotype in our model as the thermal pain phenotype seen in our model was lost in the ASIC3 knockout mice and ASIC3 in not activated by LPA (Marra et al., 2016). Indeed further experiments should be conducted to

absolutely exclude the contribution of the LPA1 receptor in our model first by controlling the expression of LPA1 receptor in ASIC3 knockout mice to be sure that the expression of this receptor was not affected by knocking out ASIC3. In addition, our lipidomic analysis did not show increased levels of LPA as it was not detected in the lipid profiling. The reason of the low detection of AA and LPA could be owed to limitations in the extraction methods or the detection protocols used or due to their low expression in the serum of our mice. Indeed, in human healthy individuals, serum concentration of LPA was measure between 0.5 and 1 µM, while LPC concentration was about 200 µM (Sevastou et al., 2013). It will be important to exclude these possibilities to be able to properly interpret our observations.

To translate our model from the *in vivo* to the *in vitro* was a great challenge, nevertheless we managed to use the serum that is dramatically affected by changes in the quality and the quantity of the food intake. The limitation was the reduced quantities of serum that could be collected from a single mouse. For that, we took advantage of a pressure puff system that allowed us to deliver small quantities of the serum directly onto cells. Using the puff system during patch-clamp recording was a great advantage. This showed that the serum from HFD mice was able to rapidly activate recombinant mouse ASIC3 channels, significantly more than the serum collected from the control mice. This effect of the serum was greatly reduced upon delipidization of the HFD serum to a level that was not different from the serum obtained from control mice. Interestingly LPC was one of the lipid families that was most significantly reduced by the process of delipidization. Of course, other compounds could also be reduced significantly during the delipidization procedure. This process includes a step of dialysis of the serum, with a cut-off at 3.5 kDa, to eliminate the excess salts added to the serum to increase the density of the serum and form a differential centrifugation that allow the separation of lipids from the serum. This step of dialysis raised the possibility that the reduction in the effect of the HFD serum after delipidization could be due to the loss of small molecules, other than lipids, that have a molecular weight below 3.5 kDalton. The observation that dialysis of the serum without centrifugation led to the reduction of several families of lipids among which LPC, and reduction of the effect of the dialyzed serum on ASIC3 channels seemed to indicate that the loss of small size molecules could be responsible for this. For example, serotonin (5-HT), a pro-inflammatory mediator, was shown to enhance the proton-

evoked sustained, but not transient, ASIC3 mediated currents in DRG neurons. The effect of 5-HT on ASIC3 channels did not involve 5-HT receptors, but was mediated through a direct interaction of 5-HT on ASIC3 channels (Wang et al., 2013). Co-application of 5-HT and acidic solution significantly increased pain behavior in mice. There were several controls that could be envisaged like testing protein free serum or the use of concentrators that allow the retention of proteins with certain molecular weight. However, besides involving severe manipulation to the serum, these approaches have their own limitations that could make the interpretation of the effect uncertain. Of course, we cannot at this stage exclude the contribution of a yet non-identified small signaling molecule but to bypass this issue we supplemented the delipidized serum with a cocktail of LPC. Interestingly this approach rescued partially, but significantly, the activation of ASIC3 by the serum, thus confirming that the effect of the HFD serum was mainly mediated by the increased concentration of LPC. The serum from HFD mice was not acidic (pH between 7.4 and 7.5) but it is interesting to note that the HFD serum was able to potentiate ASIC3 responses to moderate acidification at pH 7. This could increase the activity of DRG neurons in response to mild tissue acidosis associated with inflammatory insults.

The recordings of native DRG neurons to test the effect of the HFD was important to allow us to test the effect of HFD closer to physiological conditions. We found that amplitude of the membrane inward currents activated by the application of the HFD on WT DRG neurons was significantly higher than the amplitude of the currents activated by ND serum. This was thus in coherence with the effects observed in recombinant ASIC3 expressing HEK cells. Of note, the amplitudes of the currents activated upon application of the HFD serum in native DRG neurons were less compared to those measured in the transfected HEK cells. This could be due to different expression levels of ASIC3 in both types of cells. As described previously, the subset of DRG neurons expressing proton evoked ASIC3 currents was less in mice (Leffler et al., 2006). Mild acidification at pH7 and pH6.6 induced larger currents in cells line expressing recombinant ASIC3 channels than in native mice DRG neurons (deval 2010). We used the same range of pH to characterize native ASIC3 currents to avoid the activation of the TRPV1 channels that is widely expressed in nociceptors. TRPV1 is activated with strong acidification below pH6 (leffler2006, Tominaga et al, 1998; Lingueglia, 2007). Indeed some neurons showed ASIC3 like currents at this

mild acidification but the percentage of neurons was much less compared with what was described previously (Cadiou et al., 2007; Deval et al., 2008; Mamet et al., 2002; Voilley et al., 2001). It would have been better to use stronger acidification like pH5 to be able to reveal the real proportion of neurons that express ASIC3 and to further characterize them by the kinetics of currents and their sensitivity to toxins. Nevertheless, the important contribution of ASIC3 channels in the depolarizing currents produced by the HFD serum was confirmed by recordings from DRG neurons from ASIC3 knockout mice. The amplitude of the currents activated by HFD serum was reduced significantly in the absence of ASIC3. This showed that a large proportion of the inward current activated by the serum from HFD mice in DRG neurons is mediated through ASIC3 channels.

Action potentials are generated and affected by the activity of several ion channels. Among these ion channels is ASIC3 channel that was shown to affect the excitability of DRG neurons in the presence of lipid modulators like AA or LPC, and during inflammation (Allen and Attwell, 2002; Deval et al., 2008; Mamet et al., 2002; Marra et al., 2016; Smith, 2006). Thus, we tested the effect of the HFD serum on the excitability of the DRG neurons. In current clamp configuration, the HFD serum induced depolarization in all recorded neurons that reached the threshold for triggering action potentials in 30% of the neurons (3/10). We then uses the well characterized ASIC3 blocker toxin APeTx2 (Diochot et al., 2004) to block ASIC3 in the presence of HFD serum. The presence of the APeTx2 toxin (2 µM) reduced the amplitude of depolarization when delivered with the HFD serum. This again argues that ASIC3 contributes to the depolarization of the DRG neurons by the HFD serum. The amplitude of the reduction was less than expected but this could be owed to the amount of toxin buffered by proteins found in the serum or due to the high viscosity of the serum compared to the normal control solutions. This high viscosity can affect the amount of toxin reaching the channels. Of course, in native conditions, we cannot fully exclude the contribution of other ion channels to the membrane depolarization by HFD serum.

The HFD serum was also able to increase the excitability of the WT DRG neurons by lowering the rheobase to trigger action potential firing. Importantly, the reduction of the rheobase by HFD serum was not seen with ND serum and was lost in DRG neurons from ASIC3 knockout. This again confirmed that the effect of the HFD serum needed the functional expression of ASIC3. Because

neurons do not have the same resting potential and the HFD serum was able to induce depolarization of the membrane, currents were injected to adjust/ compensate the resting potential to -55 mV before starting the protocol of injecting increasing steps of current through the recording pipette. This allowed us to compare the different conditions recorded in different cells.

The mechanism behind how the HFD serum lowered the rheobase of DRG neurons is unknown. Similar effect was previously described by others (Mamet et al., 2002), where a drop in pH from 7.4 to 6 triggered action potential firing in neurons expressing ASIC3-like currents only in the presence of cocktail of inflammatory mediators containing NGF, serotonin, interleukin-1, and Bradykinin. Similarly, the effect of the inflammatory cocktail was not mediated through affecting the resting potential of these neurons. Another study described the upregulation of Nav1.9 expression in a model of inflammatory pain that was lost in ASIC3 knockout mice. In addition, Nav1.8 currents recorded from DRG neurons were enhanced and again this effect was lost in the ASIC3 knockout mice (Yen et al., 2009). These studies suggested that ASIC3 channels expressed in DRG neurons could affect the rheobase through an indirect mechanism, possibly through affecting the currents and expressions of Nav channels. We cannot exclude the possibility that ASIC3 activation can directly sensitize the neurons and prim them to further excitation. This would be a state similar to nociceptors priming. Of course, further investigations will clarify this and reveal the role of ASIC3 channels and other channels in the neuronal excitability associated with obesity and HFD.

The behavior experiments done on wild type mice showed that the thermal perception of mice fed the HFD was significantly affected and showed a long lasting heat hyperalgesia that started after only 8 weeks of diet. Other sensory modalities tested were not significantly affected including the mechanical perception, and the chemical sensitivity. The reason for the difference in the affected modalities is not known. TRPV1 expressing neurons are responsible for conveying thermal pain (Mishra et al., 2011). The molecular classification of DRG neurons showed that ASIC3 is expressed in the TRPV1 expressing neurons and this can explain the thermal sensitivity in response to ASIC3 activation (Zeisel et al., 2018). On the other hand, ASIC3 is mildly or not expressed in the non-peptidergic neurons responsible for mechanical pain giving to some extent a justification to

the absence of mechanical pain in our DIO model (Zeisel et al., 2018). Nevertheless, mechanical sensitivity is mainly mediated by A-beta fibers and neuropathies in these fibers lead to mechanical allodynia, as seen in diabetic neuropathy, yet these fibers express ASIC3 channels (Baron and Maier, 1995; Emery and Ernfors, 2018; Khan et al., 2002). An argument for that is ASIC3 channels expressed in the free nerve terminals of peptidergic C-fibers responsible for conveying heat signals are more vulnerable to metabolic changes compared to myelinated fibers responsible for mechanical perception. Indeed Schwann cells supply nutrients and provide protection to the latter fibers against toxic metabolites (Feldman et al., 2017; Wang et al., 2012). This issue remain unclear why in our DIO model, HFD obese mice develop thermal but not mechanical hypersensitivity and further investigations will still be required to decipher this issue.

C-fibers compose the majority (70%) of peripheral sensory fibers (Millan, 1999) and nearly half of them convey thermal heat perception (Wang et al., 2018). We focused on heat sensitive C-fibers activity by performing the skin-saphenous nerve preparation. These recordings revealed that the basal activity of C-fibers was significantly increased in the skin of HFD obese mice. In addition, the response to heat was also higher in the skin of the HFD obese mice. These observations confirmed the phenotype of heat hyperalgesia observed with the HFD mice. It showed that the hyperalgesia of obese mice resulted from higher sensitivity to heat in peripheral nociceptive C-fibers, a large fraction of which express ASIC3. It was possible to record these differences because the nerve-skin preparation used fresh isolated skin within less than 2 hours after the dissection. This gives a significant advantage for this approach over recording from DRG primary cultures, which are subjected to severe enzymatic and mechanical manipulations required to dissociate the cells, and maintained in culture conditions with growth factors for 1 to 2 days. This could be one of the reasons why we could not observe any differences between ND and HFD DRG neurons recorded 1-2 days after plating. The time in culture may have masked the differences between the two conditions. Nevertheless, it could be interesting to test the acutely dissociated DRG neurons plated in absence of growth factors that may alter the expression or/and the activity of the neurons.

The availability of ASIC3 knockout mice gave the advantage of testing the thermal sensitivity of these mice fed with the HFD. Interestingly ASIC3 KO mice fed with the HFD gained weight with similar rate as WT mice, and were obese after a few weeks of regime. Fasting glucose level and

glucose tolerance test showed that ASIC3 KO mice are in a state of prediabetes, not different from WT, at 8 and 12 weeks of diet. Obese ASIC3 KO mice did not develop thermal hypersensitivity confirming that ASIC3 channels were essential for its occurrence. Because ASIC3 KO mice fed the HFD developed obesity and glucose intolerance, we can exclude the hypothesis that ASIC3 could be mediating its sensory effects through affecting the metabolic parameters of the mice. In contrast, a study showed that ASIC3 channels were expressed in the adipose tissue and that the knockout mice were protected from age-dependent glucose intolerance and improved insulin sensitivity (Huang et al., 2008). It should be noted that in this study, mice aged 11 weeks and have normal fasting glucose concentration and glucose tolerance. The apparent controversy, in the results with our study could be due to the difference in diets as they used only the normal diet and the glucose intolerance was developed by the effect of aging.

As discussed above APETx2 was able to reduce the depolarization induced by the HFD serum in native neurons so we were interested in investigating whether pharmacological blockage of ASIC3 by this toxin would affect the developed thermal hyperalgesia seen in WT HFD mice. The intraperitoneal injection of APeTx2 revealed that blocking ASIC3 *in vivo* delayed the onset of the thermal hypersensitivity. Interestingly, APeTx2 was also able to reverse heat hyperalgesia after it was well established. This argues that ASIC3 channels contribute to the establishment and the maintenance of the heat hyperalgesia. Altogether, we show that the consumption of HFD caused obesity, glycose intolerance, and dyslipidemia. The dyslipidemia was associated with increased levels of LPC that activate ASIC3 channels. In turn, ASIC3 sensitized DRG neurons and heat sensitive C-fibers resulting in thermal hyperalgesia.

Several channels were involved in the acute thermal sensitivity including TRPV1, TRPA1 and TRPM3 (Sexton et al., 2014; Vandewauw et al., 2018). It is not clear in our study if they contribute along with ASIC3 to heat hyperalgesia associated with HFD and obesity.

Several clinical trials aimed at blocking TRPV1 failed to get approval for phase 3 clinical studies because these drugs caused transient increase in body temperature referred as febrile reaction. In addition, the long exposure to TRPV1 antagonists led to compromised noxious heat sensation that resulted in burn injuries (Gram et al., 2017; Moran and Szallasi, 2018). Our study shows that

ASIC3 is an interesting target to study the alteration of the sensory modalities associated with obesity, prediabetes, and other pathologies leading to thermal hypersensitivities.

The effect of HFD and diabetes on sensory modalities was investigated in several studies, but the results were inconsistent, reviewed in (O'Brien et al., 2014). The differences were seen in the affected modalities, with hypo or hypersensitivity to thermal or mechanical stimuli. Some studies reported that these modalities were affected while other showed no effect. The onset period of the hypo/hyperalgesia also varied between the different studies ranging from 6 to 16 weeks after starting the diet. Some of these experiments measured the motor nerve conductance velocity and the intra-epidermal nerve fiber density, which are important parameters that can indicate the development of neuropathy. The results from these two parameters were also variable or were not affected in these studies. These controversies could be owed to differences in the used diets composition, strain of mice and their sex and age of starting the diet. Major differences with our study are that we use young mice, starting the DIO at 4 weeks of age, which become obese and prediabetic. The mechanisms involved in the alteration of the sensory modalities in obese mice are not understood. We believe that our study is one of the first studies to show the particular role of LPC and the modulation of ASIC3 in the hyperexcitability of peripheral nociceptive fibers, and the hypersensitivity to heat in obese mice fed with HFD.

The induction of inflammatory mediators in the adipose tissue in response to metabolic stress caused by the consumption of HFD, and the establishment of a low grade inflammation is well described and reviewed in (Gregor and Hotamisligil, 2011). This is accompanied by increased infiltration of immune cells in the adipose tissue and inflammation in the hypothalamus (Weisberg et al., 2003; Xu et al., 2003). It was interesting to investigate the levels of inflammatory markers in DRGs and spinal cord. Our preliminary results obtained by qPCR showed that some inflammatory markers (mRNA for Ilβ, TNFα, CCL2/MCP-1 and GFAP) were increased in the DRG or the spinal cord after 8 and 12 weeks of HFD compared to ND (some of the data not shown). Because astrocytes and microglia are activated during inflammation and disease, we performed IHC to observe their activation. After 12 weeks of diet, we observed that both types of glial cells showed morphological changes that are characteristics of their activation in the CNS. The main glial cells in the peripheral nervous system are satellite cells that wrap neuron cell bodies and Schwann cells. Both cell types

were also reported to have an increased activity during inflammation (Farina et al., 2007; Kim and de Vellis, 2005; Sofroniew and Vinters, 2010). We are thus investigating their morphology and distribution in lumbar DRG neurons (L4-L6) by using GFAP and glutamine synthase (GS) antibodies that were described to stain satellite cells (Nascimento et al., 2014; Siemionow et al., 2009). GFAP also stains Schwann cells. Preliminary observations show swelling of the satellite glial cells and increase GS surface staining in HFD DRGs. This of course would need to be completed and further investigated. Interestingly the experiment done by injecting low doses of LPC in young mice five weeks on ND or HFD showed that the HFD mice are more prone to inflammatory pain. This could be owed to that HFD mice already had low-grade systemic inflammation described above and any further increase in levels of inflammation would lead to the induction of pain in these mice. Indeed further investigations is required to complete this part.

# Annexes

During my PhD, I helped Prof. Jacques NOEL in four projects done in frames of collaborations. My role included conducting nerve skin experiments, analyzing them, present results and discussing them.

First project is a collaboration with Dr. Emmanuel DEVAL to study the activation of ASIC3 channel by cold. (Under progress)

Second is a collaboration with Dr. Sylvie DIOCHOT to characterize the role of a toxin (THA903) on ion channels and in nociception. (Under progress)

Third project is a study on the role of CCL5 in the development of obesity. I helped in conducting behavioral experiments and other experiments not including nerve skin. (Under progress)

Last project was a collaboration with Prof.  Xavier Gasull. This work was just submitted to bio-archives (bioRxiv) and Journal of Pain title "TRESK background $K^+$ channel deletion selectively uncovers enhanced mechanical and cold sensitivity".

# TRESK background $K^+$ channel deletion selectively uncovers enhanced mechanical and cold sensitivity

Aida Castellanos[1,2], Anna Pujol-Coma[1,2], Alba Andres-Bilbe[1,2], Ahmed Negm[3,4], Gerard Callejo[1], David Soto[1,2], Jacques Noël[3,4], Nuria Comes[1,2] and Xavier Gasull[1,2]

[1] Neurophysiology Laboratory, Department of Biomedicine, Medical School, Institute of Neurosciences, Universitat de Barcelona, 08036 Barcelona, Spain
[2] Institut d'Investigacions Biomèdiques August Pi i Sunyer (IDIBAPS), 08036 Barcelona, Spain
[3]Université Côte d'Azur, CNRS UMR 7275, Institut de Pharmacologie Moléculaire et Cellulaire, Valbonne, France
[4]LabEx Ion Channel Science and Therapeutics, Valbonne, France.

Abbreviated title: TRESK modulation of mechanical and cold sensitivity

Corresponding author:

Xavier Gasull, Ph.D.

Dept. Biomedicina-Fisiologia

Facultat de Medicina

Universitat de Barcelona

Casanova 143

E-08036 Barcelona

Spain

Tel: (+34) 934.024.519

E-mail: xgasull@ub.edu

Num. of pages: 52

6 Figures, 1 Suppl. Figure, 1 Suppl. Table

## Abstract

Changes in TRESK $K^+$ channel expression/function enhance sensory neurons excitability, but its role in somatosensory perception and nociception is poorly understood. We show that TRESK regulates the sensitivity to mechanical and cold stimuli but not the perception of heat. TRESK knockout mice nociceptive neurons present an enhanced excitability; skin nociceptive C-fibers show an increased activation by lower intensity cold or mechanical stimulation and mice lacking TRESK present mechanical and cold hypersensitivity. TRESK is also involved in osmotic pain and in early phases of formalin-induced inflammatory pain, but not in the development of mechanical and heat hyperalgesia during chronic pain. In contrast, mice lacking TRESK present cold allodynia that is not further enhanced by oxaliplatin. In summary, genetic removal of TRESK uncovers enhanced mechanical and cold sensitivity, indicating that it regulates the excitability of specific neuronal subpopulations involved in mechanosensitivity and cold-sensing, acting as a brake to prevent activation by low-intensity stimuli.

## Introduction

Sensory perception is triggered by excitation of sensory neurons terminals in the periphery and generation of action potentials that carries sensory information towards the central nervous system. The combined activation of different ion channels and membrane receptors determine the likelihood of excitation and generation of action potentials in specific subtypes of sensory neurons such as thermoreceptors, mechanoreceptors or nociceptors. Two-pore domain potassium channels ($K_{2P}$) are expressed in different subpopulations of sensory neurons, including nociceptors where they carry most of the "leak" or background current [1]. Their electrophysiological properties allow them to carry $K^+$ currents over a wide range of membrane potentials and hence they are key determinants of neuronal excitability, decreasing the probability of depolarizing stimuli to achieve action potential threshold, as well as shaping the neuron firing response [1]. TRESK, TREK-1, TREK-2 and TRAAK channels make the major contribution to leak currents in trigeminal (TG) and dorsal root ganglion (DRG) neurons [2-6], where they have been implicated in perception of pain induced by mechanical, thermal and chemical stimuli, as well as in neuropathic and inflammatory pain [4,7-11]. Depending on the specific expression and properties of each one of the $K_{2P}$ channels in different subpopulations of sensory neurons they fine-tune the sensitivity of neuronal subpopulations to noxious stimuli. In this regard, deletion of one of the $K_{2P}$ channels enhances the specific sensitivity to certain external stimuli but not others, rather than acting as a general effect on neuronal excitability due to the removal of hyperpolarization by $K^+$ currents. TRESK shows a high expression in DRG and TG sensory neurons in human,

rat and mouse and is particularly enriched in sensory ganglia compared to other neural and non-neural tissues [3,5,10,12-16]. Single-cell RNA sequencing data has provided further insight on the potential role of TRESK in sensory neurons, since the channel is predominantly expressed in non-peptidergic nociceptors (NP1-NP3) as well as in a subpopulation of low-threshold mechanoreceptors, while its expression is lower in peptidergic nociceptors [15,16]. Interestingly, TRESK expression in DRG neurons is downregulated in different pain conditions, comprising sciatic nerve axotomy [4], spared nerve injury [17] and chronic inflammation [10], which contributes to the enhancement of neuronal excitability. In contrast, different experimental manipulations to increase TRESK expression resulted in a decrease in neuronal excitability and amelioration of painful behaviors [17-19]. In the same line of evidence, sensory neurons from a functional TRESK[G339R] knockout mice showed a significant reduction of outward $K^+$ current, increased excitability and reduced rheobase [3]. Also, a frameshift mutation leading to the truncation of the channel has been associated with familial migraine with aura, thus involving the channel in the enhanced activation of the trigeminovascular system and the release of inflammatory neuropeptides (CGRP/substance P) in the meninges and cerebral vessels triggering pain associated to migraine [20]. Recent studies show that, to trigger migraine pain, not only TRESK malfunction is needed but also the combined down-regulation of TREK-1/2 induced by the heteromerization with truncated TRESK proteins that prevent membrane channel expression [21].

Despite the fact that TRESK shares some functional properties with other $K_{2P}$ channels, its high expression in sensory ganglia and its selective expression in specific subsets of sensory neurons points to a relevant role of this channel in sensory perception and pain that is not yet well understood. Here, we report that removal of TRESK uncovers enhanced cold and mechanical sensitivity without affecting thermal sensitivity to warmth or hot temperatures.

## Results

### *TRESK deletion reduces total background current and enhances neuronal excitability*

TRESK channels have been detected in small- and medium-sized sensory neurons, together with other members of the $K_{2P}$ family of background $K^+$ channels [5,15,16]. To confirm the elimination of TRESK expression in homozygous knockout animals and to assess possible effects on the expression of other $K_{2P}$ channels induced by knocking out TRESK, we first studied the mRNA expression in DRGs by real-time quantitative PCR. TRESK mRNA was undetected in KO mice while a significant expression was found in wild-type (WT) animals (Fig 1A). Since removal of TRESK could potentially induce compensatory effects on other $K_{2P}$ channels involved in pain perception, the expression of TREK-1, TREK-2 and TRAAK was determined (the more expressed $K_{2P}$s in sensory neurons, together with TWIK1, which is unclear if it forms functional membrane channel). Analogously to what has been reported in a previous study [22], mRNA for these channels were present in WT and KO mice at similar levels, thus excluding a compensation effect on the expression of these $K_{2P}$ channels in KO mice. Interestingly, the expression of TRPA1 and TRPV1, two channels highly expressed in nociceptors, was not significantly changed.

To assess whether removal of TRESK modifies $K^+$ background currents, we next recorded total $K^+$ current from small diameter DRG neurons, that are usually assumed to be nociceptive neurons (soma size <30 µm; capacitance

<30pF). For this, as previously described [3,4,23,24], we measured the current density at -25 mV followed by a voltage ramp to -135 mV (Fig 1B). Wild-type sensory neurons presented a significantly larger current density compared to KO neurons both at -25 mV (for WT, 15.3±1.5; n=31; Cm=21.7±1.8 pF; for KO, 9.7±1.2 pA/pF; n=50; Cm=22.1±1.0 pF; unpaired t-test p=0.004), and -135 mV (for WT, -11.1±1.6 pA/pF; for KO, -8.5±1.2 pA/pF; unpaired t-test p=0.038), indicating that the absence of TRESK has a significant functional consequence in the membrane current. In a second batch of recordings from small-sized DRG neurons, we investigated the functional effects of TRESK removal on neuronal excitability by measuring their resting membrane potential and action potential properties (Fig 2A and B). Wild-type and TRESK KO sensory neurons did not present significant changes in resting membrane potential (RMP: -58.3±3.9 vs. -56.2±1.5 mV, respectively. Unpaired t-test p=0.540; Fig 2B), suggesting that TRESK might have a minor role in setting the RMP and other $K^+$ channels are possibly more important in setting the RMP in the cell body. This is in agreement with previous data where RMP was not significantly modified after TRESK down-regulation or deletion [3,4]. Interestingly, injected current threshold to action potential firing in current-clamp configuration was significantly decreased in TRESK KO neurons (Fig 2B, p=0.0013 unpaired t-test) compared to neurons from WT littermates. This effect is likely a consequence of the increased membrane resistance found in TRESK KO neurons (1262.8±133.8MΩ) compared to controls (Wild-type: 792.7±186.9MΩ; p=0.045 unpaired t-test; Fig 2B). As expected, action potential amplitude was not significantly altered (p=0.406, unpaired t-test) since this parameter is more

dependent on voltage-dependent sodium channels ($Na_v$) activity. However, action potentials were significantly wider in neurons from TRESK KO, likely reflecting the consequence of the decrease in total $K^+$ current (50% AP width TRESK KO 4.03±0.5 s; n=27 neurons; Wild-type: 2.38±0.5 s; n=13; p=0.041; Fig 2B). To investigate if these changes affect the excitability of sensory neurons, we injected a current ramp (0 to 500 pA, 1s) in current-clamp configuration and counted the number of action potentials fired for each genotype. As shown in Fig 2C, TRESK KO neurons fired on average more spikes (9.0±1.3 spikes) than wild-type neurons (5.5±1.1 spikes; p=0.036), indicating that removal of TRESK increased the excitability of sensory neurons.

To further characterize the responsiveness of sensory neurons in TRESK KO mice, we measured the intracellular $Ca^{2+}$ signals ($[Ca^{2+}]$) of cultured DRG neurons from WT and KO mice in response to capsaicin (1 µM; TRPV1 agonist) and AITC (100 µM; TRPA1 agonist), two markers of nociceptive neurons, and menthol (100 µM; TRPM8 agonist), a marker of cold sensory neurons. Among wild-type DRG neurons (total number of neurons analyzed = 1124), 49.2% responded to capsaicin, 40.4% to AITC and 7.0% to menthol. Responses to both capsaicin and AITC were seen in 17.9% of the neurons (Fig 3A and B). A percentage of neurons did not respond to any of the agonists tested (246 neurons, 21.9%). Responses to capsaicin (45.7%) and menthol (9.1%) were not different in neurons from TRESK KO mice (n=1228) but, the percentage of neurons activated by AITC was significantly lower (24.7%, p=0.009). Neurons non-responding to any agonists were 446 (36.3%). The diameters of sensory

neurons responding to the different agonists between WT and KO animals were not different which means that they represent identical populations of DRG neurons (mean soma diameter WT: 20.2±0.19 µm; KO: 20.3±0.23 µm). In parallel experiments, the response of cultured trigeminal neurons was assessed. These showed no significant differences for the response to the different agonists (data not shown) between genotypes. Therefore, the diminished response to AITC is restricted to DRG neurons.

We next assessed if the reduced response to AITC of DRG neurons from TRESK KO mice had a behavioral correlate by injecting AITC (100 µM) into the mouse hind paw. In agreement with the previous observation, nocifensive behavior measured as the time spent licking or shaking the paw significantly diminished in KO compared to WT mice (TRESK KO: 9.0±2.4 s; WT: 18.1±3.6 s; p=0.039; n=13 for each group; Fig 3C). In contrast, painful behavioral responses to capsaicin injection did not differ between KO and WT mice (40.0±8.6s vs. 28.8±4.5s, respectively; p=0.236; Fig 3C). Injection of vehicles for each compound did not produce significant behavioral effects (data not shown). To further investigate to what extend chemical nociception was altered by the absence of TRESK, we used the formalin test [25,26], which is characterized by an initial phase (phase I; 0-5 min) due to direct nociceptor activation [27] and a second phase (phase II; 15-50 min) that is attributed to a combined nociceptive input together with central spinal sensitization [26]. The phase I nocifensive response has been directly linked to the activation of TRPA1 [27] although high concentrations of formalin are still able to induce

some pain in TRPA1 KO mice [28]. Interestingly, animals lacking TRESK showed a diminished response to formalin injection in phase I (30.8±6.1s; p=0.002; Fig 3D) compared to control WT animals (69.9±7.2s). The decreased response in phase I of TRESK KO animals is in agreement with the decreased nocifensive response observed after AITC injection (Fig 3C) which corroborates the decreased fraction of AITC sensitive DRG neurons from TRESK KO in culture. All these observations confirm that TRPA1 activation is decreased in TRESK KO animals. Phase II of the formalin test can be further split in phase IIa (15-25 min) and IIb (25-50 min), where IIa has a higher nociceptive input than IIb. TRESK KO animals showed a decreased licking time during phase IIa (107.7±16.3s) compared to wild-type animals (154.8±18.9s; p=0.048); which probably reflects a decreased nociceptors activation as found in phase I. In contrast, phase IIb of the formalin test did not show significant differences and licking behavior was similar between groups (p=0.421, Fig 3D). Injection of hypertonic saline stimulates primary afferent nociceptors and produce pain in humans [29,30]. This response can be further enhanced by sensitization of nociceptors with $PGE_2$. Injection of hypotonic stimuli did not induce significant nocifensive behavior in resting conditions (p=0.146, Fig 3E) but, as previously described [7,30], nocifensive responses were enhanced after sensitization with $PGE_2$ in wild-type mice but not in TRESK KO mice (p=0.019, unpaired t-test WT vs. KO). Nocifensive responses to mild hypertonic saline were diminished in TRESK KO animals both, in resting conditions (2% or 10% NaCl, p=0.049 and p=0.002) or after sensitization with $PGE_2$ (p=0.002; Fig 3E). Again, these effects are similar to the one reported after knocking out TREK-1 and TREK-2, but not

in the single TRAAK knockout mice [7-9], thus implying that TREK-1, TREK-2 and TRESK are involved in the sensitivity to hypertonic stimuli and their absence prevents sensitization by $PGE_2$.

***Mice lacking TRESK present mechanical allodynia and normal heat perception***

Since TRESK knockout enhances nociceptive sensory neuron excitability, we next analyzed the sensitivity of nerve fibers from TRESK KO mice to different types of stimuli and whether the activation of sensory fibers was correlated to behavioral responses to these stimuli. Saphenous nerve C-fibers from WT (n=14) and TRESK KO mice (n=22) were recorded with the nerve-skin preparation. Mechanical thresholds were determined with calibrated von Frey filaments applied on the receptive fields of C-fibers. TRESK KO mice presented an enhanced sensitivity to mechanical stimuli. Mean threshold value for the whole population was not significantly different in KO animals (27.6±5.2 mN) compared to WT mice (33.2±6.2 mN; p=0.268 unpaired t-test), but threshold values from KO mice presented a wider distribution and a significant shift towards lower values (Fig 4A). Further analysis showed that KO mice presented a significant percentage of fibers with lower thresholds (<12 mN; 40.9%) compared to fibers from WT animals (0%; p=0.006; Fisher's exact test). This suggests that TRESK function prevents C-fiber activation by low intensity mechanical stimuli and therefore deletion of the channel reveals mechanical sensitivity with low threshold values in a fraction of C-fibers (Fig 4A). We then compared the mechanical sensitivity of TRESK KO to WT mice with the von

Frey up and down method. Hind paw mechanical sensitivity was significantly higher in TRESK KO mice compared to WT ($p<0.0001$ for males and females; Fig 4D), thus showing that lower C-fibers thresholds values produce mechanical allodynia in behaving mice. Measures of mechanical sensitivity with the dynamic plantar aesthesiometer also confirmed significant differences to pressure application between WT (5.06±0.12 g; n=27) and KO animals (4.66±0.17 g; n=22; t-test p=0.027; Fig 4D).

Other channels of the $K_{2P}$ family have been involved in thermosensation and pain perception in response to hot or cold stimuli [7-9]. TRESK activity is not modulated by changes in temperature in the physiological range [5]. Responses of C-fibers activated by heat-ramp applied on their receptive fields in the skin from TRESK KO and WT mice did not show significant differences in heat thresholds for the activation of C-fibers (37.6±0.46ºC, n=35 C-fibers for WT; 38.1±0.64ºC, n=37 C-fibers for KO; p=0.502 t-test; Fig 4B), nor the distribution of these thresholds in a range of temperatures, nor the number of spikes fired by heat sensitive C-fibers during heat-ramps (32.6±4.4 spikes WT; 34.8±4.4 spikes TRESK KO; p=0.720 t-test; Fig 4C), indicating that TRESK does not seem to have a major role in the detection of warm or hot temperatures by C-fibers. We then tested heat sensitivity of mice with Hargreaves and hot plate tests. Heat sensitivity was unaltered in TRESK KO mice compared to WT in the radiant heat Hargreaves test (p=0.08 males; p=0.603 females, Fig 4E), which measures the threshold sensitivity to heat confirming the observations made in C-fibers recordings. To further evaluate a possible implication of TRESK in heat

pain, we evaluated the sensitivity to more extreme temperatures in the hot plate test at 52 and 56ºC, but no significant differences were detected (Fig 4E). This indicates that the extreme heat sensitivity is conserved in TRESK KO mice. The dynamic hot plate with a ramp of temperature has been proposed as a valuable method to differentiate between thermal allodynia and hyperalgesia [31]. The number of jumps of the mice on a hot plate when the plate temperature is increased from 39 to 50 ºC did not show any difference between TRESK KO and WT, neither for the total number of jumps nor the temperature at which animals elicited their first jump (Suppl. Fig 1). Only a small difference was found for TRESK KO and WT female mice at the high temperature of 49ºC, where KO animals seem less sensitive, but not at 48 or 50ºC. Both recordings of C-fiber activity and behavioral tests discard a significant contribution of TRESK in heat sensitivity.

***Elevated perception of cold temperatures in the absence of TRESK channel***

Thermosensitivity to cold temperatures is governed by different mechanisms and by distinct neuronal subpopulations than warm/hot perception [32]. We evaluated the role of TRESK in the cold sensitivity of C-fibers by recording fibers activity with the saphenous nerve preparation upon cooling their receptive fields in the skin from 30 to 10ºC over 90 s (Fig 5A-D). C-fiber recordings from TRESK KO mice showed a significant change in the fractions of mechano-cold and mechano-heat and cold sensitivity of polymodal C-fibers compared to WT mice. TRESK KO increased the fraction of mechano-cold C-fibres compared to

WT mice (37% and 20% C-MC, respectively; Fig 5A). This was accompanied by a reduction of the percentage of mechano-heat-cold C-fibers (C-MHC) in KO mice (29%) compared to WT (38%; $p<0.01$; Chi-square test; Fig 5A). Nevertheless, the total number of cold sensitive fibers did not differ significantly between genotypes (KO: 66% of C-fibers; WT: 58%). The distribution of cold C-fibers thresholds showed a clear shift towards warmer temperatures, between 26 and 28ºC, in the TRESK KO, while fiber thresholds from WT animals were more uniformly distributed at different temperature segments (Fig 5B and 5C). Despite mean cold thresholds were not different ($p=0.388$, Fig 5C), we could observe a tendency to have more fibers activated at higher temperatures above 25ºC in knockout animals (58%) compared to WT (42%), although this difference did not reach significant statistical power (Fisher's exact test; $p=0.099$). The total response of TRESK KO fibers to the cooling of 90 s (33.1±5.1 spikes) was similar to WT (34.1±5.8 spikes; $p=0.90$ unpaired t-test), however, the distribution of the activity upon cooling was higher at temperatures between 25 and 19ºC for TRESK KO fibers (Fig 5D). The baseline activity between 30-31ºC was also higher in TRESK KO than WT fibers (0.3 spikes/s for TRESK KO and 0.1 spikes/s for WT; $n=36$ and $n=31$ respectively; $p<0.001$, t-test). These experiments indicate that the temperature for activation of cold-sensitive C-fibers was increased in TRESK KO, but also that the overall fiber activity in response to cooling did not depend drastically on the presence of TRESK.

In good agreement with observations in C-fibers, behavioral responses to cold were also altered in animals lacking TRESK. Sensitivity to noxious cold (2ºC; cold plate test) was enhanced in knockout animals from both sexes, with shorter latency times to elicit a nocifensive behavior ($p=0.006$ males; $p=0.041$ females, Fig 5E). In addition, cold sensitivity to more moderate temperatures assessed with the cold plantar assay was significantly higher in TRESK KO mice ($p<0.0001$ males, $p=0.008$ females, Fig 5F). Finally, we assessed whether changes in cold sensitivity modified the aptitude of mice to discriminate cool and cold temperatures in a test of thermal preference between plates at different temperatures. TRESK KO animals spent more time on the reference plate (at 30ºC) than on the experimental plate at 20ºC ($p=0.022$, Fig 5G) compared to wild-type animals, further supporting previous evidence from cold sensitive C-fibers recordings and cold sensitivity assays. In contrast, place preference assays at other temperatures (10, 15, 30, 40, 50ºC) did not show significant alterations between mice genotypes, corroborating the non-involvement of TRESK in heat and warmth perception (Fig 4).

### *Mice lacking TRESK show selective changes in persistent inflammatory and neuropathic pain*

To assess the contribution of TRESK in chronic pain conditions, the behavior of TRESK KO and WT mice was measured after CFA injection into the mice hind paw, a model of persistent inflammatory pain. Both genotypes developed mechanical and thermal hypersensitivity in the injected hind paw beginning 1h after injection and lasting up to 16 days (Fig 6A). Despite the initial difference in

basal mechanical thresholds (p=0.047), the extent of mechanical hyperalgesia in response to tactile stimuli was similar between WT and KO animals 1h after CFA injection and during the entire 16 days observation period. The development of thermal hyperalgesia was similar between both genotypes, thus showing that TRESK does not contribute significantly to peripheral sensitization of nociceptors due to inflammation. The sciatic nerve cuff-model was used to evaluate TRESK contribution in persistent neuropathic pain. Mechanical hypersensitivity developed in KO animals 5 and 7 days after sciatic nerve cuffing was significantly higher compared to WT (p=0.046 and p=0.047, respectively; Fig 6B). Sham surgery did not show significant effects on this parameter in any genotype (data not shown). Nevertheless, when the percentage of threshold decrease (difference vs. basal value) was compared between WT and KO animals, this showed similar values (at 5 days, KO: -45.1±17.4%; WT: -37.9±12.1%; p=0.742; at 7 days, KO: -47.3±16.9%; WT: -45.0±19.3%; p=0.931), indicating that nerve injury exerted a similar effect in both genotypes but, since KO had a lower mechanical threshold to begin with, animals reached lower mechanical thresholds at days 5 and 7. Mechanical hypersensitivity was undistinguishable between groups at later stages, at 14 and 21days post-injury. Heat sensitivity showed a similar level of hyperalgesia after neuropathy, akin to the lack of implication of TRESK in mechanical perception. Surprisingly withdrawal latencies from KO animals recovered baseline values faster than WT group after 14 and 21 days. Finally, we evaluated chemo-induced neuropathic pain with the anti-cancer drug oxaliplatin that induces cold allodynia in a majority of patients under therapy, to evaluate

whether the development of cold hyperalgesia after oxaliplatin treatment was modified in TRESK KO. As expected, wild-type mice showed an enhanced cold sensitivity 90h after the oxaliplatin injection. Both, cold plantar assay ($p=0.0002$) and thermal place preference test (30/20ºC; $p=0.0045$) showed significant differences compared to pre-injection values, indicating a higher sensitivity to cold stimuli in neuropathic mice (Fig 6C). In contrast, when TRESK KO animals were tested in the cold plantar assay, we did not observe any further decrease in paw withdrawal latency compared to the baseline value ($p=0.912$), which was already lower than that of WT animals. Again, thermal place preference between 20 and 30ºC did not show significant differences after oxaliplatin treatment ($p=0.770$), suggesting that the enhanced cold sensitivity due to TRESK removal cannot be further increased by neuropathy induced by oxaliplatin.

## Discussion

TRESK is a leak $K^+$ channel highly expressed in human and rodent sensory neurons both in DRGs and TG [3-5,12,13,33-35]. Recent single-cell sequencing data indicates that in DRG and TG neurons, TRESK expression is restricted to some subtypes of sensory neurons, mainly, non-peptidergic medium/small diameter neurons involved in nociception [15,35-37]. In addition, TRESK is also present in a population of low-threshold mechanoreceptors (expressing high levels of TRKB and Piezo2) involved in touch sensation. TRESK main role has been attributed to preventing neuronal depolarization [1], and reduction of its expression after nerve injury or inflammation contribute to neuronal hyperexcitability [3,4,10]. Mutations in this channel have been linked to the enhanced nociceptor excitability that occurs during familial migraine with aura [20,21]. In the present study, we propose that TRESK balances the effects of depolarizing stimuli, acting as a brake to prevent the activation of specific subpopulations of sensory neurons expressing the channel. We found that TRESK channel prevents mechanical and cold hypersensitivity in mice, while the sensitivity to other stimulus modalities remains unaffected.

Small diameter nociceptive sensory neurons lacking TRESK presented a significant diminution in the amplitude of $K^+$ current, an increase in membrane input resistance, and an increase in action potential duration, which are evidence of a major contribution of TRESK channel to $K^+$ current in small diameter, presumably nociceptive, DRG neurons, in agreement with previous reports [5]. Resting membrane potentials were not different between TRESK

KO and WT DRG neurons, which is in agreement with previous studies [3]. In contrast to other channels [11], it is likely that TRESK does not contribute significantly in setting this parameter but it has a major impact over the range of membrane potentials between the resting membrane potential and the action potential threshold. Indeed, other $K^+$ channels from $K_{2P}$ and other $K^+$ channel families have been proposed to control membrane polarization at rest [38]. Although we cannot completely discard a compensatory effect due to other channels not analyzed (e.g. HCN, KCNQ), TRESK removal does not seem to significantly modify the expression of other leak channels expressed in sensory neurons that have a major contribution to the $K^+$ background current (TREK-1, TREK-2, TRAAK) [5]. Therefore, the effects observed in excitability appear to be mainly attributable to the specific removal of TRESK. Nociceptive DRG neurons from TRESK KO mice showed higher excitability, with a decreased injected current threshold for action potential firing and an increased firing response to a depolarizing ramp, which is also consistent with a significant decrease of a potassium conductance in KO mice. Despite finding significant differences in these parameters, these effects could be underestimated by the fact that TRESK is not expressed in all types of nociceptive sensory neurons. Therefore, it is possible that studying specific subpopulations of sensory neurons (mainly non-peptidergic) genetically labeled with specific markers might render larger effects in excitability after TRESK deletion. Studies in this line are underway to unveil particular effects in different types of sensory neurons. Similar findings on neuronal excitability to these found in the present study have been reported after a decreased TRESK expression, such as in a functional

TRESK[G339R] knockout mice [3,23], after sciatic nerve axotomy [4] or in a model of cancer-associated pain [24]. This is in agreement with the neuronal activation observed by compounds blocking TRESK [4,33,39]. Conversely, opposite consequences on excitability were found when overexpressing TRESK channel [18,24], thus indicating that the regulation of TRESK expression is an important factor to control sensory neuron excitability.

Recordings from C-fibers showed that detection of mechanical and cold stimuli, but no heat, were enhanced in the KO mice. The effects of TRESK KO were specific to some properties of these modalities and did not enhance neurons excitability over the whole range of stimulation. This indicates that removal of TRESK channel does not produce a general increase in excitability but a selective effect on certain types of fibers/sensory neuron subtypes affecting specific sensory modalities. This is similar to what occurs for other $K_{2P}$ or $K^+$ channels: genetic deletion of TREK-1 modifies mechanical, heat and cold pain perception [7] but when TRAAK is deleted, cold sensitivity remains unaffected and animals only present an enhanced heat sensitivity. Interestingly, deleting both channels (TREK-1/TRAAK double KO mice) potentiates the effects on cold sensitivity compared to TREK-1 alone [9]. Besides, the role of TREK-2 in thermosensation is different from that of TREK-1 and TRAAK channels and deletion of the channel enhances thermal sensitivity to non-aversive warm temperatures but not to cold stimuli [8]. Besides, knocking down the $BK_{Ca}$ potassium channel does not modify acute nociceptive or neuropathic pain, but KO mice show an increased nociceptive behavior in models of persistent

inflammatory pain [40], highlighting its specific participation during inflammation-induced hyperalgesia. Our data shows that the lack of TRESK enhances cold sensitivity by increasing the percentage of C-fibers activated at moderate cold temperatures, which is translated at the behavioral level by an enhanced sensitivity to cold stimuli. The bigger fraction of cold sensitive C-MC fibers (37%) in KO animals compared to wild-types (20%) suggests that TRESK normally silences a population of neurons that would be only activated at low temperatures in normal conditions. This is combined with a decrease in the fractions of C-MHC and C-MH fibers. These observations are consistent with a possible role of TRESK in preventing cold allodynia, acting as a brake to avoid C-fiber activation at moderate cool temperatures. In fact, knocking out TRESK mimics cold allodynia and oxaliplatin injection is not able to further enhance cold sensitivity. Cold allodynia induced by the anti-cancer drug oxaliplatin has been attributed to a combined remodeling of ion channels in subsets of sensory neurons, including down-regulation of TREK-1, TREK-2, TRAAK, $K_v1.1$ and $K_v1.2$, coupled with up-regulation of TRPA1, $Na_v1.8$ and HCN1, while other channels involved, such as TRPM8, are not significantly modified [8,41]. It has been proposed that a reduced activity of $K_{2P}$ channels when temperature decreases is responsible of releasing the excitability brake exerted by these channels, and thus, combined with depolarizing thermo-TRP channels activation, trigger sensory neurons activity when they sense cold temperature stimuli [5,8,9]. TRESK activity is not significantly modified by temperature between 20-37ºC [5]. Since we show that DRG neurons from TRESK KO have lower action potential threshold and increase firing upon membrane

depolarization, it is possible that the channel prevents the activation of a subpopulation of C-fibers by cold-activated excitatory depolarizing channels even if lower temperature does not modify its activity, at least, in a moderate range. Moreover, we show an increase in input membrane resistance in TRESK KO DRG neurons. Low temperatures increase the membrane resistance, which potentiates voltage change by membrane currents and enhance excitability. This effect has been shown previously to contribute to cold sensation [42].

TRPA1 was initially proposed to be involved in noxious cold sensing [43] but recent reports have questioned its role. It has been hypothesized that it might be regulating cold sensitivity indirectly, rather than acting as a cold-sensing receptor [32,44]. We observed a reduced response to TRPA1 agonists (Fig 3) but no change in its mRNA expression in DRGs. Whether the enhanced cold sensitivity in TRESK KO animals being dependent on TRPA1 expression remains a possibility, recent studies have shown that TRPA1-expressing neurons are unresponsive to noxious cold stimuli [44]. $K_v$ channels can blunt cold responses by opposing to depolarizing stimuli in $TRPA1^+$ and $TRPM8^+$ neurons [45,46]. It is possible that TRESK might exert a similar effect, hence silencing cold responses in normal conditions. Neurons lacking TRESK or down-regulation of the channel might release this excitability brake, uncovering an enhanced cold sensation. Even if this is the case, it remains to be examined in greater depth. Moreover, changes observed in the sensitivity to AITC might result from post-transcriptional regulation of protein expression levels or other intracellular signaling mechanisms altered in TRESK KO cellular background

such as phosphorylation of the receptor due to the enhanced excitability of TRESK KO neurons.

In addition to cold, mechanical sensitivity is also enhanced in TRESK KO animals, which present a higher number of C-fibers with low mechanical thresholds (<12 mN) and an increased response to von Frey hairs application. Similar results were previously reported after knocking down TRESK expression or after injecting TRESK blockers, where animals showed mechanical allodynia [4,24,39]. Likewise, trigeminal expression of a mutated form of TRESK linked to migraine results in facial mechanical allodynia [21]. Similar to cold, mechanical sensitivity is enhanced by decreasing the threshold of activation of a population of sensory fibers, and therefore, a higher number of fibers are activated by low intensity mechanical stimulation. This effect was not linked to gender, since both male and female animals showed similar responses. Piezo2 channel is involved in the detection of both innocuous touch and high threshold noxious mechanical stimuli due to its expression in low threshold mechanoreceptors (LTMR) and nociceptors [47-50], and has been proposed to play a crucial role in the generation of mechanical allodynia during inflammation and neuropathic pain states [47]. TRESK is also highly expressed in these populations of sensory neurons involved in mechanical hypersensitivity [15]. We can hypothesize that when these neuronal populations lack TRESK, they are more sensitive to mechanical stimuli activating Piezo2 or other mechanosensitive channels such as the recently identified TACAN [51], that would depolarize sensory neurons more effectively. We have not evaluated whether LTMR

lacking TRESK are more excitable and if other touch modalities such as light touch (brush stroke) are also enhanced by TRESK deletion, but mechanical allodynia present in these animals suggests that they might also be affected. TRESK is notably expressed in MrgprD$^{+}$ neurons [15] and deletion of this subpopulation of neurons abolishes mechanical but not thermal pain [52]. Here, the opposite effect is found after TRESK deletion and that will likely enhance the excitability of MrgprD$^{+}$ neurons. In contrast, mechanical sensitization that occurs after inflammation does not seem to be further enhanced by the absence of TRESK whereas mechanical hypersensitivity after nerve injury seems to reach lower values compared to wild-type animals. Nevertheless, this effect appears to be related to the lower mechanical threshold present in TRESK KO animals since the mechanical threshold decrease is similar in both WT and KO groups. Our data suggests that the molecular effect of injury, down-regulating TRESK expression [4], has already been achieved by genetic removal of TRESK, thus any further decrease in mechanical threshold observed is likely due to other mechanisms sensitizing nociceptors or derived from central effects.

In our study, TRESK KO mice did not display relevant differences in heat sensitivity to the tested temperatures. Only a significant difference on the thermal place preference test was observed between 20/30ºC that seems to reflect the observed enhancement of cold sensitivity rather than any effect on the warm/heat sensitivity. In agreement, TRESK KO C-fibers recorded did not show any specific effects upon temperature increase compared to WT. No significant alterations on heat sensitivity were either observed after CFA-

induced inflammation, and only a slightly higher effect on heat sensitivity was observed in the neuropathic pain model of mice lacking TRESK. All together it seems that the role of TRESK in neurons detecting warm or hot stimuli is not relevant, in contrast to other channels of the TRP and $K_{2P}$ family that play a major role [7-9,44,53,54]. Chemical sensitivity was altered for some stimuli (AITC, osmosensitivity) but not for others (capsaicin, menthol). Besides the altered sensitivity to AITC as previously discussed, removal of TRESK produced a decreased response to pain induced by osmotic stimuli. Whether TRESK is involved in detecting this type of stimuli is unknown, although we previously described that hypertonic and hypotonic stimuli are able to modify TRESK currents [55]. Interestingly, similar results in osmotic pain have been reported in animals lacking channels of the TREK subfamily [7-9] and in TRPV4 KO animals [29]. Similarly to TREK-1/2 KO mice but not TRAAK KO, $PGE_2$ was unable to sensitize nociceptors to osmotic stimuli in TRESK KO animals. It has been proposed that the negative regulation of TREK-1/2 channels by cAMP/PKA downstream of the G-coupled $PGE_2$ receptor might be involved in the lack of $PGE_2$-mediated nociceptor sensitization. PKA is known to phosphorylate TRESK and keep it in a resting state where the channel is less active but a direct link between PKA activation, TRESK activity and osmotic sensing is still unknown. In fact, neurons activated by radial stretch and hypotonic stimuli seem to express TRESK, as they are sensitive to hydroxy-$\alpha$-sanshool, a TRESK blocker [56]. These neurons were initially classified as LTMR or non-peptidergic nociceptors, which is in agreement with the TRESK expression pattern obtained from single-cell mRNA sequencing [15].

In summary, we describe that genetic removal of TRESK enhances mechanical and cold sensitivity in mice; consequently TRESK function is important to regulate the excitability in specific subpopulations of sensory neurons involved in mechanosensitivity and cold sensing. Because mice lacking TRESK display mechanical hypersensitivity as well as enhanced cold perception similar to the reported cold allodynia induced by oxaliplatin treatment, activators of the channel would be expected to improve these conditions during neuropathic pain. The development of specific channel openers/activators would be worthwhile and due to the rather restricted expression of TRESK in sensory ganglia (DRG and TG) will avoid undesired side effects in other tissues.

## Methods

*Animals*

All behavioral and experimental procedures were carried out in accordance with the recommendations of the International Association for the Study of Pain (IASP) and were reviewed and approved by the Animal Care Committee of the University of Barcelona and by the Department of the Environment of the *Generalitat de Catalunya*, Catalonia, Spain (#8466, 8468, 8548, 6869, 9876). Female and male C57BL/6N mice between 8 and 15 weeks old were used in all experimental procedures (RNA extraction and qPCR, cell cultures, electrophysiology, calcium imaging, nerve fiber recording and behavior) unless differentially indicated. Mice were housed at 22ºC with free access to food and water in an alternating 12h light and dark cycle.

TRESK (Kcnk18/K2P18.1) knockout mice and wild-type (WT) littermates were obtained from the KOMP Repository (Mouse Biology Program, University of California, Davis, CA). The TRESK knockout (KO) mouse was generated by replacing the complete Kcnk18 gene by a ZEN-UB1 cassette according to the VelociGene's KOMP Definitive Null Allele Design. At 3 weeks of age, WT or KO newborn mice were weaned, separated, and identified by ear punching. Genomic DNA was isolated from tail snip samples with Maxwell® Mouse Tail DNA Purification Kit (Promega, Madison, WI). Polymerase chain reaction (PCR) was performed with primers to detect the Kcnk18 gene: forward 5'-ACCAACACCAAGCTGTCTTGTTTCTC-3' and reverse 5'-AGACAGATGGACGGACAGACATAGATG-3' or the inserted cassette in the KO

mice: forward (REG-Neo-F) 5'-GCAGCCTCTGTTCCACATACACTTCA-3' and reverse (gene-specific) 5'-AGACTTCTCCCAGGTAACAACTCTGC-3'. The PCR mixture contained 1 µl DNA sample, 2.5 µl PCR buffer (10x concentration), 2 µl dNTP mixture (2.5 mM), 0.5 µl (20 µM) forward and reverse primers, 0.2 µl Taq DNA polymerase (5 U/µl), 1.7 µl $MgCl_2$ (25 mM), 6.5 µl Betaine (5 M), 0.325 µl DMSO and 9.7 µl water (final volume of 25 µl). PCR amplifications were carried out with 31 cycles in a programmable thermal cycler (Eppendorf AG, Hamburg, Germany). The program used was: 94ºC for 5 min and cycles of 94ºC for 15 s, 60ºC for 30 s, 72ºC for 40 s, with a final extension at 72ºC for 5 min. PCR products were analyzed by electrophoresis in 1% agarose gels. Once identified, genotyped animals were used as breeders for colony expansion and their offspring were used in all experimental procedures in which mice were required.

*Behavioral studies*

Female and male wild-type or TRESK KO mice between 8 and 15 weeks of age were used in all behavioral studies. To avoid stress-induced variability in the results, mice were habituated to the experimental room and the experimental setup prior testing. Behavioral measurements were done in a quiet room, taking great care to minimize or avoid discomfort of the animals.

*Mouse mechanical sensitivity*

Mechanical sensitivity of wild-type and TRESK KO mice was assessed using the ‘up and down’ method by the application of calibrated von Frey filaments (North Coast Medical, Inc. Morgan Hill, CA) as previously described [4,39]. The

von Frey filaments [size: 2.44, 2.83, 3.22, 3.61, 3.84, 4.08, 4.17, 4.31, 4.56; equivalent to (in grams) 0.04, 0.07, 0.16, 0.4, 0.6, 1, 1.4, 2 and 4] were applied perpendicularly to the plantar surface of the hind paw and gently pushed to the bending point for 5 s. The 50% withdrawal threshold was determined using the up and down method [57]. A brisk hind paw lift in response to von Frey filament stimulation was regarded as a withdrawal response. Dynamic plantar aesthesiometer (Ugo Basile, Italy) was also used to assess mechanical sensitivity. A von Frey-type 0.5 mm filament was applied with a 10 s ramp (0 to 7.5 g) and the hind paw withdrawal threshold of mice was recorded.

*Mouse thermal sensitivity*

*Hot plate and cold plate test*

After habituation, the cold/hot plate apparatus (Ugo Basile, Italy) was set to 2ºC, 52ºC or 56ºC and animals were individually placed in the center of the plate. Latency time to elicit a nocifensive behavior (a jump or a paw lick/lift) was counted with the apparatus stopwatch and the average of three separately trials was used as a measurement. Since the temperatures tested are in the noxious range, a cut-off time of 25 seconds was established to avoid tissue damage.

*Dynamic hot plate test*

In contrast to the conventional hot plate, the dynamic hot plate allows the testing of a wide range of temperatures. Before testing, animals were habituated and later placed individually to the hot/cold plate apparatus where the plate temperature increased from 30ºC to 50ºC at a 1ºC/min rate. To

determine the temperature that is perceived as noxious for mice and quantify pain-related behaviors, the number of jumps at each temperature was scored.

*Radiant heat test*

The heat sensitivity of mice was assessed by measuring hind paw withdrawal latency from a radiant infrared source (Hargreaves' method) using the Ugo Basile (Italy) Model 37370 Plantar test. Each measurement was the mean of 3 trials spaced 15 min apart. For all experiments, infrared intensity was set to 30% and a cut-off time of 20 seconds was established to avoid skin burn damage.

*Thermal place preference test*

The thermal place preference test is a test of better comfort temperature rather than an indicator of temperature aversion. The hot/cold plate apparatus was placed side by side with a complementary plate and a small divider platform was situated between them to connect the two devices (Ugo Basile, Italy). The reference plate was always set at 30ºC and the test plate was set at 50, 40, 30, 20, 15 or 10ºC. Animals were habituated at the experience room for 30 minutes before testing and then they were allowed to investigate the testing setup for 10 minutes or until animals crossed homogeneously from one plate to the other. Mice were then placed individually to the center of the platform and once they crossed to a plate the cumulative time they spent on each plate for a total of 5 minutes was then counted. Only animals that performed properly when both plates were set to 30ºC were used for the study (50% of the time at each plate

and more than 2 crossings). To exclude the possibility that animals could be learning which one the reference plate was, the position of the reference and the test plate was switched randomly between trials.

*Cold plantar assay*

To complement the cold plate test, we studied noxious cold sensitivity of TRESK KO mice using the cold plantar assay [58]. This assay produces an unambiguous nocifensive response that is easily identified when compared to the cold plate test. Animals were placed on top of a 1/8'' thick glass plate and were enclosed in transparent boxes separated by opaque dividers to prevent animals to see each other. The cold probe consisted of a modified 3 mL syringe filled with freshly powdered dry ice. This powder was then packed into a pellet and its surface was flattened. Using a mirror to target the mouse hind paw, we applied the dry ice pellet below the glass, making sure that the paw was completely in contact with it. This delivers a cooling ramp to the mice paw and a few seconds later withdrawal responses occur. The withdrawal latency time was measured with a stopwatch and the final withdrawal latency time for each animal was the average of 3 trials, which were tested at intervals of at least 15 minutes. A cut-off time of 20 seconds was used to prevent tissue damage.

*Evaluation of nocifensive behavior*

Using a 30g needle, 10 µl of a solution containing 100 µM AITC (10%), capsaicin (1µg/10µl) or their vehicle solutions were administered intradermally into the plantar surface of the hind paw. Mice behavior was observed and the

number of flinches and lickings of the paw were counted for a 5-minute period starting immediately after the injection. On the day previous to testing, animals were habituated to the testing room and to the handling procedure. The flinching and licking test was also used to examine the painful response of mice to different osmolality solutions, both in naive and sensitized conditions. 10 µl of the following solutions were administered in the hind paw to different groups of male mice: NaCl -33% (hypotonic, 100 $mOsm \cdot Kg^{-1}$), NaCl 2% (hypertonic, 622 $mOsm \cdot Kg^{-1}$), NaCl 10% (hypertonic, 3157 $mOsm \cdot Kg^{-1}$) and PBS (Isotonic, 298 $mOsm \cdot Kg^{-1}$). A different group of animals was used to study osmotic pain under inflammatory conditions. A 5 µl injection of prostaglandin $E_2$ ($PGE_2$; 10 µM) was injected into the hind paw of each mouse and 30 minutes after, 10 µl of NaCl -33% or NaCl 2% were injected into the sensitized paw. After the injection of different osmolality solutions, nocifensive behaviors of paw licking and shaking were manually counted for 5 minutes.

*CFA model of inflammatory pain*

After baseline measurements and under brief isoflurane anesthesia, Complete Freund's Adjuvant (CFA, Sigma-Aldrich; 20 µl; 1mg/ml) was injected subcutaneously (glabrous skin) in the hind paw of mice to induce a local inflammation. Mechanical von Frey threshold and heat withdrawal latency (radiant heat test) was examined at different time points after the injection (1h, 5h, 1d, 3d, 7d and 16d).

*Formalin test*

After habituation, mouse hind paw was subcutaneously injected with formalin (10 µl of a 5% formaldehyde solution) and nocifensive behaviors were measured for 50 minutes after the injection. The cumulative time spent shaking and licking the injected paw was counted with a stopwatch in 5 min periods.

*Oxaliplatin-induced cold hypersensitivity*

Prior to oxaliplatin injection, naive thermal preference was measured with the thermal place preference test set at 20ºC vs. 30ºC. Thirty min later, paw withdrawal latency to cold stimuli was determined using the cold plantar assay. A single intraperiotoneal injection of oxaliplatin (6 mg/Kg in PBS with 5% glucose) was delivered to mice. Cold preference and cold sensitivity were re-evaluated 90 h after oxaliplatin injection, a time point that is known to correlate with the peak of oxaliplatin-induced cold hyperalgesia [41].

*Cuff-induced neuropathic pain model*

The sciatic nerve cuffing model was used to induce mechanical and thermal hyperalgesia in the hind paw of mice, as described in [59]. Mice were housed individually to avoid stress derived from the surgery and to prevent injury. Cardboard rolls were placed into their home cages to provide shelter and additional stimulation after the surgery. All surgeries were done under aseptic conditions using intraperitoneal ketamine/xylazyne anesthesia. The left leg of mice was shaved from the hip to the knee and the surgical field was disinfected. A 0.5 cm incision parallel to the femur was made to expose the common branch of the sciatic nerve, which appeared after separating the muscles close to the

femur. A drop of sterile physiological saline was applied to prevent the nerve from dehydrating and this concluded the procedure for the sham group. The 'cuff' consisted of a 2 mm-long piece of polyethylene tubing (PE-20) with an inner diameter of 0.38 mm and an outer diameter of 1.09 mm, opened by one of its sides. For the cuff group, the sciatic nerve was gently straightened with two sterile sticks and the 'cuff' was inserted around the main branch of the nerve and closed by applying moderate pressure with surgical forceps. To ensure that the 'cuff' was correctly positioned and closed, it was turned gently around the nerve. Both sham and cuff surgeries ended by suturing the incision with surgical knots. After the procedure, animals were placed in their respective home cages laying on their right side and were under constant supervision until they were completely awakened. Mechanical and heat sensitivity of mice were determined with the von Frey and the radiant heat tests as previously described, before surgery and 5, 7, 14 and 21 days after surgery.

*Skin-nerve preparation and single fiber recordings*

The isolated skin-saphenous nerve preparation for single C-fiber recording was used as previously described [9]. The hind paw skin of male mice 10 to 20 weeks of age was isolated with the saphenous nerve. The skin was pinned corium side up in a perfusion chamber with the nerve being pulled in a recording chamber filled with paraffin oil. The skin was perfused with warm (~30-31°C) synthetic interstitial fluid (SIF), in mM : 120 NaCl, 3.5 KCl, 5 $NaHCO_3$, 1.7 $NaH_2PO_4$, 2 $CaCl_2$, 0.7 $MgSO_4$, 9.5 Na-Gluconate, 5.5 glucose, 7.5 sucrose, and 10 HEPES, pH 7.4 adjusted with NaOH, saturated with $O_2/CO_2$ 95%/5%.

Isolated nerve fibers were placed on a gold recording electrode connected to a DAM-80 AC differential amplifier (WPI), Digidata 1322A (Axon Instruments) and Spike2 software (CED) to record extracellular potentials. The skin was probed with mechanical stimulation with a glass rod and calibrated von Frey filaments to characterize the mechanical sensitivity of nerve fibers. The C-fibers were classified according to their conduction velocity of less than 1.2 m/s measured by electrical stimulation (Stimulus Isolator A385, WPI). The skin receptive field of C-fibers was isolated from the surrounding bath chamber with a stainless steel ring 0.8 cm in diameter, an internal volume of 400 µl, and a hot or cold temperature-controlled SIF was infused into the ring through a bipolar temperature controller CL-100 (Warner instrument). Electrical recordings were amplified (x10 000), band-pass filtered between 10 Hz and 10 kHz and stored on computer at 20 kHz. The action potentials were detected and analyzed offline with the principal component analysis extension of the Spike2 software (CED).

*RNA extraction and Quantitative real-time PCR*

Mouse tissue samples were obtained from dorsal root ganglia, kept in RNAlater solution (Ambion) and stored at -80°C until use. Total RNA was isolated using the Nucleospin RNA (Macherey-Nagel) and first-strand cDNA was then transcribed using the SuperScript IV Reverse Transcriptase (Invitrogen, ThermoFisher Scientific) according to the manufacturer's instructions. Quantitative real-time PCR was performed in an ABI Prism 7300 using the Fast SYBR Green Master mix (Applied Biosystems) and primers detailed in Suppl.

Table 1; obtained from Invitrogen (ThermoFisher Scientific). Amplification of Glyceraldehyde 3-phosphate dehydrogenase (GAPDH) transcripts was used as a standard for normalization of all qPCR experiments and gene-fold expression was assessed using the $\Delta C_T$ method. All reactions were performed in triplicate. After amplification, melting curves were obtained and evaluated to confirm correct transcript amplification.

*Culture of dorsal root ganglion neurons*

Mice were euthanized by decapitation under anesthesia (isoflurane) and thoracic, lumbar and cervical dorsal root ganglia (DRG) were removed for neuronal culture as previously described [4,55]. Briefly, DRGs were collected and maintained in cold (4–5°C) $Ca^{2+}$ - and $Mg^{2+}$ -free Phosphate Buffered Saline solution (PBS) supplemented with 10 mM glucose, 10 mM Hepes, 100 U.I./mL penicillin and 100 µg/mL streptomycin until dissociation. Subsequently, ganglia were incubated in 2 ml HAM F-12 with collagenase CLS I (1 mg/ml; Biochrome AG, Berlin) and Bovine Serum Albumin (BSA, 1 mg/ml) for 1 h 45 min at 37°C followed by 15 min trypsin treatment (0.25%). Ganglia were then resuspended in Dulbecco's Modified Eagle medium (DMEM) supplemented with 10% FBS, penicillin/streptomycin (100 µg/ml) and L-glutamine (100 mg/ml) and mechanical dissociation was conducted with fire-polished glass Pasteur pipettes of decreasing diameters. Neurons were centrifuged at 1000 rpm for 5 min and re-suspended in culture medium [DMEM + 10% FBS, 100 µg/ml penicillin/streptomycin, 100 mg/mL L-glutamine]. Cell suspensions were transferred to 12 mm-diameter glass coverslips pre-treated with poly-L-

lysine/laminin and incubated at 37°C in humidified 5% $CO_2$ atmosphere for up to 1 day, before being used for patch-clamp electrophysiological recordings or calcium imaging experiments. Nerve Growth Factor or other growth factors were not added.

*Calcium imaging*

Cultured DRG neurons from wild-type and TRESK KO mice were loaded with 5 µM fura-2/AM (Invitrogen, Carlsbad, CA) for 45-60 min at 37ºC in culture medium. Coverslips with fura-2 loaded cells were transferred into an open flow chamber (0.5 ml) mounted on the stage of an inverted Olympus IX70 microscope equipped with a TILL monochromator as a source of illumination. Pictures were acquired with an attached cooled CCD camera (Orca II-ER, Hamamatsu Photonics, Japan) and stored and analyzed on a PC computer using Aquacosmos software (Hamamatsu Photonics, Shizuoka, Japan). After a stabilization period, pairs of images were obtained every 4 s at excitation wavelengths of 340 (λ1) or 380 nm (λ2; 10 nm bandwidth filters) in order to excite the $Ca^{2+}$ bound or $Ca^{2+}$ free forms of the fura-2 dye, respectively. The emission wavelength was 510 nm (12-nm bandwidth filter). Typically, 20-40 cells were present in the microscope field. $[Ca^{2+}]_i$ values were calculated and analyzed individually for each single cell from the 340- to 380-nm fluorescence ratios at each time point. Only neurons that produced a response >10% of the baseline value and that, at the end of the experiment, produced a $Ca^{2+}$ response to KCl-induced depolarization (50 mM) were included in the analysis. Several experiments with cells from different primary cultures and different

animals were used in all the groups assayed. The extracellular (bath) solution used was 140 mM NaCl, 4.3 mM KCl, 1.3 mM $CaCl_2$, 1 mM $MgCl_2$, 10 mM glucose, 10 mM HEPES, at pH 7.4 with NaOH. Experiments were performed at room temperature.

*Electrophysiological recording*

Electrophysiological recordings in DRG sensory neurons were performed as previously described [39,55,60]. Briefly, recordings were performed with a patch-clamp amplifier (Axopatch 200B, Molecular Devices, Union City, CA) and restricted to small size DRG neurons (<30 µm soma diameter), which largely correspond to nociceptive neurons [61]. Patch electrodes were fabricated in a Flaming/Brown micropipette puller P-97 (Sutter instruments, Novato, CA). Electrodes had a resistance between 2-4 MΩ when filled with intracellular solution (in mM): 140 KCl, 2.1 $CaCl_2$, 2.5 $MgCl_2$, 5 EGTA, 10 HEPES, 2 ATP at pH 7.3. Bath solution (in mM): 145 NaCl, 5 KCl, 2 $CaCl_2$, 2 $MgCl_2$, 10 HEPES, 5 glucose at pH 7.4. The osmolality of the isotonic solution was 310.6±1.8 mOsm/Kg. Membrane currents were recorded in the whole-cell patch-clamp configuration, filtered at 2 kHz, digitized at 10 kHz and acquired with pClamp 10 software. Data was analyzed with Clampfit 10 (Molecular Devices) and Prism 7 (GraphPad Software, Inc., La Jolla, CA). Series resistance was always kept below 15 MΩ and compensated at 70-80%. All recordings were done at room temperature (22-23ºC), 18-24h after dissociation. To study sensory neuron excitability, after achieving the whole-cell configuration in the patch clamp technique, the amplifier was switched to current-clamp bridge mode. Only

neurons with a resting membrane voltage below -50 mV were considered for the study. To study neuronal excitability, we examined the resting membrane potential (RMP); action potential (AP) current threshold elicited by 400 ms depolarizing current pulses in 10 pA increments; whole-cell input resistance ($R_{in}$) was calculated on the basis of the steady-state I-V relationship during a series of 400 ms hyperpolarizing currents delivered in steps of 10 pA from -50 to -10 pA; AP amplitude was measured from RMP to AP peak and AP duration was measured at 50% of AP amplitude.

*Drugs*

All reagents and culture media were obtained from Sigma-Aldrich (Madrid, Spain) unless otherwise indicated. Menthol (100 µM), allyl isothiocyanate (AITC; 100 µM) and capsaicin (1 µM) were also purchased from Sigma (Madrid, Spain).

*Data analysis*

Data are presented as mean ± SEM. Statistical differences between different sets of data were assessed by performing paired or unpaired Student's t-tests or Wilcoxon matched pairs test, Chi-square test or Fisher's exact test, as indicated. The significance level was set at $p<0.05$ in all statistical analyses. Data analysis was performed using GraphPad Prism 7 software and GraphPad QuickCalcs online tools (GraphPad Software, Inc., La Jolla, CA)

## Acknowledgements

Supported by grants from Ministerio de Economia y Competitividad and Instituto de Salud Carlos III/FEDER of Spain FIS PI14/00141 (XG), FIS PI17/00296 (XG), RETICs Oftared RD16/0008/0014 (XG), Generalitat de Catalunya 2017SGR737 (XG) and Ministerio de Economia, Industria y Competitividad, Spain (BFU2017-83317-P (DS).

## Competing interests

The authors declare no competing financial interests

## Authors' contributions

Authors AC, AAB and GC performed electrophysiological recordings in neurons and calcium imaging. AC, APC and AAB performed behavioral experiments. AC, AAB carried out primary cell cultures. AC, GC, APC and NC performed qPCR experiments. AN and JN performed skin-nerve recordings. AC, DS, JN, NC and XG participated in the design of the study and performed the statistical analysis. XG conceived the study, oversaw the research and prepared the manuscript with help from all others. All authors read and approved the final manuscript.

## References

1. Enyedi P, Czirják G. Molecular background of leak K+ currents: two-pore domain potassium channels. Physiological Reviews. 2010 Apr;90(2):559–605.

2. Yamamoto Y, Hatakeyama T, Taniguchi K. Immunohistochemical colocalization of TREK-1, TREK-2 and TRAAK with TRP channels in the trigeminal ganglion cells. Neurosci Lett. 2009 Apr 24;454(2):129–33.

3. Dobler T, Springauf A, Tovornik S, Weber M, Schmitt A, Sedlmeier R, Wischmeyer E, Döring F. TRESK two-pore-domain K+ channels constitute a significant component of background potassium currents in murine dorsal root ganglion neurones. J Physiol (Lond). 2007 Dec 15;585(Pt 3):867–79.

4. Tulleuda A, Cokic B, Callejo G, Saiani B, Serra J, Gasull X. TRESK channel contribution to nociceptive sensory neurons excitability: modulation by nerve injury. Mol Pain. 2011;7(1):30.

5. Kang D, Kim D. TREK-2 (K2P10.1) and TRESK (K2P18.1) are major background K+ channels in dorsal root ganglion neurons. Am J Physiol, Cell Physiol. 2006 Jul;291(1):C138–46.

6. Patel AJ, Honoré E, Maingret F, Lesage F, Fink M, Duprat F, Lazdunski M. A mammalian two pore domain mechano-gated S-like K+ channel. EMBO J. 1998 Aug 3;17(15):4283–90.

7. Alloui A, Zimmermann K, Mamet J, Duprat F, Noël J, Chemin J, Guy N, Blondeau N, Voilley N, Rubat-Coudert C, Borsotto M, Romey G, Heurteaux C, Reeh P, Eschalier A, Lazdunski M. TREK-1, a K+ channel involved in polymodal pain perception. EMBO J. 2006 Jun 7;25(11):2368–76.

8. Pereira V, Busserolles J, Christin M, Devilliers M, Poupon L, Legha W, Alloui A, Aissouni Y, Bourinet E, Lesage F, Eschalier A, Lazdunski M, Noel J. Role of the TREK2 potassium channel in cold and warm thermosensation and in pain perception. Pain. 2014 Dec;155(12):2534–44.

9. Noël J, Zimmermann K, Busserolles J, Deval E, Alloui A, Diochot S, Guy N, Borsotto M, Reeh P, Eschalier A, Lazdunski M. The mechano-activated K+ channels TRAAK and TREK-1 control both warm and cold perception. EMBO J. 2009 May 6;28(9):1308–18.

10. Marsh B, Acosta C, Djouhri L, Lawson SN. Leak $K^+$ channel mRNAs in dorsal root ganglia: relation to inflammation and spontaneous pain behaviour. Molecular and cellular neurosciences. 2012 Mar;49(3):375–86.

11. Acosta C, Djouhri L, Watkins R, Berry C, Bromage K, Lawson SN. TREK2

Expressed Selectively in IB4-Binding C-Fiber Nociceptors Hyperpolarizes Their Membrane Potentials and Limits Spontaneous Pain. J Neurosci. Society for Neuroscience; 2014 Jan 22;34(4):1494–509.

12. Manteniotis S, Lehmann R, Flegel C, Vogel F, Hofreuter A, Schreiner BSP, Altmüller J, Becker C, Schöbel N, Hatt H, Gisselmann G. Comprehensive RNA-Seq Expression Analysis of Sensory Ganglia with a Focus on Ion Channels and GPCRs in Trigeminal Ganglia. Zhang Z, editor. PLoS ONE. Public Library of Science; 2013 Nov 8;8(11):e79523.

13. Ray P, Torck A, Quigley L, Wangzhou A, Neiman M, Rao C, Lam T, Kim J-Y, Kim TH, Zhang MQ, Dussor G, Price TJ. Comparative transcriptome profiling of the human and mouse dorsal root ganglia: an RNA-seq-based resource for pain and sensory neuroscience research. Pain. 2018 Jul;159(7):1325–45.

14. Flegel C, Schöbel N, Altmüller J, Becker C, Tannapfel A, Hatt H, Gisselmann G. RNA-Seq Analysis of Human Trigeminal and Dorsal Root Ganglia with a Focus on Chemoreceptors. PLoS ONE. 2015;10(6):e0128951.

15. Usoskin D, Furlan A, Islam S, Abdo H, Lönnerberg P, Lou D, Hjerling-Leffler J, Haeggström J, Kharchenko O, Kharchenko PV, Linnarsson S, Ernfors P. Unbiased classification of sensory neuron types by large-scale single-cell RNA sequencing. Nat Neurosci. 2015 Jan;18(1):145–53.

16. Zeisel A, Hochgerner H, Lönnerberg P, Johnsson A, Memic F, van der Zwan J, Häring M, Braun E, Borm LE, La Manno G, Codeluppi S, Furlan A, Lee K, Skene N, Harris KD, Hjerling-Leffler J, Arenas E, Ernfors P, Marklund U, Linnarsson S. Molecular Architecture of the Mouse Nervous System. Cell. 2018 Aug 9;174(4):999–1014.e22.

17. Zhou J, Yang C-X, Zhong J-Y, Wang H-B. Intrathecal TRESK gene recombinant adenovirus attenuates spared nerve injury-induced neuropathic pain in rats. Neuroreport. 2013 Feb;24(3):131–6.

18. Guo Z, Cao Y-Q. Over-expression of TRESK K(+) channels reduces the excitability of trigeminal ganglion nociceptors. PLoS ONE. 2014;9(1):e87029.

19. Zhou J, Yao S-L, Yang C-X, Zhong J-Y, Wang H-B, Zhang Y. TRESK gene recombinant adenovirus vector inhibits capsaicin-mediated substance P release from cultured rat dorsal root ganglion neurons. Mol Med Report. 2012 Apr;5(4):1049–52.

20. Lafrenière RG, Cader MZ, Poulin J-F, Andres-Enguix I, Simoneau M, Gupta N, Boisvert K, Lafrenière F, Mclaughlan S, Dubé M-P, Marcinkiewicz MM, Ramagopalan S, Ansorge O, Brais B, Sequeiros J, Pereira-Monteiro JM, Griffiths LR, Tucker SJ, Ebers G, Rouleau GA. A dominant-negative mutation in the TRESK potassium channel is linked to

familial migraine with aura. Nat Med. 2010 Oct;16(10):1157–60.

21. Royal P, Andres-Bilbe A, Ávalos Prado P, Verkest C, Wdziekonski B, Schaub S, Baron A, Lesage F, Gasull X, Levitz J, Sandoz G. Migraine-Associated TRESK Mutations Increase Neuronal Excitability through Alternative Translation Initiation and Inhibition of TREK. Neuron. 2019 Jan 16;101(2):232–6.

22. Chae YJ, Zhang J, Au P, Sabbadini M, Xie G-X, Yost CS. Discrete change in volatile anesthetic sensitivity in mice with inactivated tandem pore potassium ion channel TRESK. Anesthesiology. 2010 Dec;113(6):1326–37.

23. Kollert S, Dombert B, Döring F, Wischmeyer E. Activation of TRESK channels by the inflammatory mediator lysophosphatidic acid balances nociceptive signalling. Sci Rep. 2015;5:12548.

24. Yang Y, Li S, Jin Z-R, Jing H-B, Zhao H-Y, Liu B-H, Liang Y-J, Liu L-Y, Cai J, Wan Y, Xing G-G. Decreased abundance of TRESK two-pore domain potassium channels in sensory neurons underlies the pain associated with bone metastasis. Sci Signal. American Association for the Advancement of Science; 2018 Oct 16;11(552):eaao5150.

25. Abbott FV, Franklin KB, Westbrook RF. The formalin test: scoring properties of the first and second phases of the pain response in rats. Pain. 1995 Jan;60(1):91–102.

26. Tjølsen A, Berge OG, Hunskaar S, Rosland JH, Hole K. The formalin test: an evaluation of the method. Pain. 1992 Oct;51(1):5–17.

27. McNamara CR, Mandel-Brehm J, Bautista DM, Siemens J, Deranian KL, Zhao M, Hayward NJ, Chong JA, Julius D, Moran MM, Fanger CM. TRPA1 mediates formalin-induced pain. Proc Natl Acad Sci USA. 2007 Aug 14;104(33):13525–30.

28. Fischer M, Carli G, Raboisson P, Reeh P. The interphase of the formalin test. Pain. 2013 Nov 27;155(3):511–21.

29. Alessandri-Haber N, Joseph E, Dina OA, Liedtke W, Levine JD. TRPV4 mediates pain-related behavior induced by mild hypertonic stimuli in the presence of inflammatory mediator. Pain. 2005 Nov;118(1-2):70–9.

30. Alessandri-Haber N, Yeh JJ, Boyd AE, Parada CA, Chen X, Reichling DB, Levine JD. Hypotonicity induces TRPV4-mediated nociception in rat. Neuron. 2003 Jul 31;39(3):497–511.

31. Yalcin I, Charlet A, Freund-Mercier M-J, Barrot M, Poisbeau P. Differentiating Thermal Allodynia and Hyperalgesia Using Dynamic Hot and Cold Plate in Rodents. The Journal of Pain. 2009 Jul;10(7):767–73.

32. Lolignier S, Gkika D, Andersson D, Leipold E, Vetter I, Viana F, Noël J, Busserolles J. New Insight in Cold Pain: Role of Ion Channels, Modulation, and Clinical Perspectives. J Neurosci. 2016 Nov 9;36(45):11435–9.

33. Bautista DM, Sigal YM, Milstein AD, Garrison JL, Zorn JA, Tsuruda PR, Nicoll RA, Julius D. Pungent agents from Szechuan peppers excite sensory neurons by inhibiting two-pore potassium channels. Nat Neurosci. 2008 Jul;11(7):772–9.

34. LaPaglia DM, Sapio MR, Burbelo PD, Thierry-Mieg J, Thierry-Mieg D, Raithel SJ, Ramsden CE, Iadarola MJ, Mannes AJ. RNA-Seq investigations of human post-mortem trigeminal ganglia. Cephalalgia. 2018 Apr;38(5):912–32.

35. Nguyen MQ, Wu Y, Bonilla LS, Buchholtz von LJ, Ryba NJP. Diversity amongst trigeminal neurons revealed by high throughput single cell sequencing. Obukhov AG, editor. PLoS ONE. Public Library of Science; 2017 Sep 28;12(9):e0185543–22.

36. Chiu IM, Barrett LB, Williams EK, Strochlic DE, Lee S, Weyer AD, Lou S, Bryman G, Roberson DP, Ghasemlou N, Piccoli C, Ahat E, Wang V, Cobos EJ, Stucky CL, Ma Q, Liberles SD, Woolf C. Transcriptional profiling at whole population and single cell levels reveals somatosensory neuron molecular diversity. Elife. 2014 Dec 19;3:e04660.

37. Li C-L, Li K-C, Wu D, Chen Y, Luo H, Zhao J-R, Wang S-S, Sun M-M, Lu Y-J, Zhong Y-Q, Hu X-Y, Hou R, Zhou B-B, Bao L, Xiao H-S, Zhang X. Somatosensory neuron types identified by high-coverage single-cell RNA-sequencing and functional heterogeneity. Cell Res. 2016 Jan;26(1):83–102.

38. Du X, Gao H, Jaffe D, Zhang H, Gamper N. M-type K +channels in peripheral nociceptive pathways. British Journal of Pharmacology. John Wiley & Sons, Ltd (10.1111); 2018;175(12):2158–72.

39. Castellanos A, Andres-Bilbe A, Bernal L, Callejo G, Comes N, Gual A, Giblin JP, Roza C, Gasull X. Pyrethroids inhibit K2P channels and activate sensory neurons. Pain. 2018 Jan;159(1):92–105.

40. Lu R, Lukowski R, Sausbier M, Zhang DD, Sisignano M, Schuh C-D, Kuner R, Ruth P, Geisslinger G, Schmidtko A. BKCa channels expressed in sensory neurons modulate inflammatory pain in mice. Pain. 2013 Dec 11;155(3):556–65.

41. Descoeur J, Pereira V, Pizzoccaro A, Francois A, Ling B, Maffre V, Couette B, Busserolles J, Courteix C, Noël J, Lazdunski M, Eschalier A, Authier N, Bourinet E. Oxaliplatin-induced cold hypersensitivity is due to remodelling of ion channel expression in nociceptors. EMBO Mol Med. 2011 May;3(5):266–78.

42. Zimmermann K, Leffler A, Babes A, Cendan CM, Carr RW, Kobayashi J-I, Nau C, Wood JN, Reeh PW. Sensory neuron sodium channel Nav1.8 is essential for pain at low temperatures. Nature. 2007 Jun 14;447(7146):855–8.

43. Story GM, Peier AM, Reeve AJ, Eid SR, Mosbacher J, Hricik TR, Earley TJ, Hergarden AC, Andersson DA, Hwang SW, McIntyre P, Jegla T, Bevan S, Patapoutian A. ANKTM1, a TRP-like channel expressed in nociceptive neurons, is activated by cold temperatures. Cell. 2003 Mar 21;112(6):819–29.

44. Yarmolinsky DA, Peng Y, Pogorzala LA, Rutlin M, Hoon MA, Zuker CS. Coding and Plasticity in the Mammalian Thermosensory System. Neuron. Elsevier; 2016 Dec 7;92(5):1079–92.

45. Memon T, Chase K, Leavitt LS, Olivera BM, Teichert RW. TRPA1 expression levels and excitability brake by KV channels influence cold sensitivity of TRPA1-expressing neurons. Neuroscience. 2017 Jun 14;353:76–86.

46. Madrid R, la Peña de E, Donovan-Rodriguez T, Belmonte C, Viana F. Variable threshold of trigeminal cold-thermosensitive neurons is determined by a balance between TRPM8 and Kv1 potassium channels. J Neurosci. 2009 Mar 11;29(10):3120–31.

47. Murthy SE, Loud MC, Daou I, Marshall KL, Schwaller F, Kühnemund J, Francisco AG, Keenan WT, Dubin AE, Lewin GR, Patapoutian A. The mechanosensitive ion channel Piezo2 mediates sensitivity to mechanical pain in mice. Sci Transl Med. American Association for the Advancement of Science; 2018 Oct 10;10(462):eaat9897.

48. Szczot M, Liljencrantz J, Ghitani N, Barik A, Lam R, Thompson JH, Bharucha-Goebel D, Saade D, Necaise A, Donkervoort S, Foley AR, Gordon T, Case L, Bushnell MC, Bönnemann CG, Chesler AT. PIEZO2 mediates injury-induced tactile pain in mice and humans. Sci Transl Med. American Association for the Advancement of Science; 2018 Oct 10;10(462):eaat9892.

49. Dhandapani R, Arokiaraj CM, Taberner FJ, Pacifico P, Raja S, Nocchi L, Portulano C, Franciosa F, Maffei M, Hussain AF, de Castro Reis F, Reymond L, Perlas E, Garcovich S, Barth S, Johnsson K, Lechner SG, Heppenstall PA. Control of mechanical pain hypersensitivity in mice through ligand-targeted photoablation of TrkB-positive sensory neurons. Nature Communications. Nature Publishing Group; 2018 Apr 24;9(1):1640.

50. Ranade SS, Woo S-H, Dubin AE, Moshourab RA, Wetzel C, Petrus M, Mathur J, Bégay V, Coste B, Mainquist J, Wilson AJ, Francisco AG, Reddy K, Qiu Z, Wood JN, Lewin GR, Patapoutian A. Piezo2 is the major transducer of mechanical forces for touch sensation in mice. Nature. 2014

Dec 4;516(7529):121–5.

51. Beaulieu-Laroche L, Christin M, Donoghue A, Agosti F, Yousefpour N, Petitjean H, Davidova A, Stanton C, Khan U, Dietz C, Faure E, Fatima T, MacPherson A, Ribeiro-da-Silva A, Bourinet E, Blunck R, Sharif-Naeini R. TACAN is an essential component of the mechanosensitive ion channel responsible for pain sensing. bioRxiv. 2018 Jan 1;:338673.

52. Cavanaugh DJ, Lee H, Lo L, Shields SD, Zylka MJ, Basbaum AI, Anderson DJ. Distinct subsets of unmyelinated primary sensory fibers mediate behavioral responses to noxious thermal and mechanical stimuli. Proc Natl Acad Sci U S A. 2009 Jun 2;106(22):9075–80.

53. Vriens J, Nilius B, Voets T. Peripheral thermosensation in mammals. Nat Rev Neurosci. 2014 Jul 23;15(9):573–89.

54. Julius D. TRP channels and pain. Annu Rev Cell Dev Biol. 2013;29:355–84.

55. Callejo G, Giblin JP, Gasull X. Modulation of TRESK background K+ channel by membrane stretch. Ceña V, editor. PLoS ONE. 2013;8(5):e64471.

56. Bhattacharya MRC, Bautista DM, Wu K, Haeberle H, Lumpkin EA, Julius D. Radial stretch reveals distinct populations of mechanosensitive mammalian somatosensory neurons. Proc Natl Acad Sci U S A. 2008 Dec 16;105(50):20015–20.

57. Chaplan SR, Bach FW, Pogrel JW, Chung JM, Yaksh TL. Quantitative assessment of tactile allodynia in the rat paw. J Neurosci Methods. 1994 Jul;53(1):55–63.

58. Brenner DS, Golden JP, Gereau RW IV. A novel behavioral assay for measuring cold sensation in mice. PLoS ONE. Public Library of Science; 2012;7(6):e39765.

59. Yalcin I, Megat S, Barthas F, Waltisperger E, Kremer M, Salvat E, Barrot M. The sciatic nerve cuffing model of neuropathic pain in mice. J Vis Exp. 2014 Jul 16;(89).

60. Callejo G, Castellanos A, Castany M, Gual A, Luna C, Acosta MC, Gallar J, Giblin JP, Gasull X. Acid-sensing ion channels detect moderate acidifications to induce ocular pain. Pain. 2015 Mar;156(3):483–95.

61. Le Pichon CE, Chesler AT. The functional and anatomical dissection of somatosensory subpopulations using mouse genetics. Front Neuroanat. Frontiers; 2014;8:21.

## Figure Legends

### Figure 1: Nociceptive sensory neurons lacking TRESK have a decreased standing outward current.

**A.** Expression profile of $K_{2P}$ channels, TRPA1 and TRPV1 in mouse sensory neurons from wild-type and TRESK knockout mice. mRNA expression obtained by quantitative PCR shows no significant differences between WT and KO animals after genetic deletion of TRESK. Y-axis shows the ΔCt (number of cycles target - number of cycles GADPH) for the different mRNAs. Notice that the Y-axis has been inverted to visually show that lower ΔCt numbers are indicative of a higher expression. Each dot represents a single animal (wild-type n=6; TRESK knockout n=7). **B.** Top: Representative recordings of whole-cell currents from small-sized DRG sensory neurons using a protocol to minimize activation of voltage-gated transient $K^+$ outward currents (holding voltage -60mV). Bottom: quantification of currents at the end of the pulse at -25 mV (a) and at the end of the ramp (-135 mV; b) showed significant differences among groups (*p<0.05; **p<0.01 unpaired t-test. wild-type n=31; TRESK KO n=50).

### Figure 2: Nociceptive sensory neurons lacking TRESK present a higher excitability

**A.** Representative whole-cell current-clamp recordings from wild-type and TRESK knockout nociceptive sensory neurons elicited by hyperpolarizing or depolarizing 400 ms current pulses in 10 pA increments. *Right*: mean membrane capacitance ($C_m$) from neurons studied is shown. **B.** Quantification of the electrophysiological parameters analyzed in wild-type (black bars, n=13)

and TRESK KO (red bars, n=27) sensory neurons. RMP: resting membrane potential. Current threshold was measured using 400 ms depolarizing current pulses in 10 pA increments; $R_{in}$: whole-cell input resistance was calculated on the basis of the steady-state I-V relationship during a series of 400 ms hyperpolarizing currents delivered in steps of 10 pA from -50 to -10 pA. AP amplitude was measured from the RMP to the AP peak. AP duration/width was measured at 50% of the AP amplitude. Statistical differences between groups are shown (*p<0.05, **p<0.01 unpaired t-test). **C.** Examples and quantification of neuronal excitability as the number of action potentials fired in response to a depolarizing current ramp (0 to 500 pA, 1s) form a holding voltage of -60 mV (black, wild-type n=6; red, TRESK KO n=7). Statistical differences between groups are shown (*p<0.05; **p<0.01 unpaired t-test).

**Figure 3: TRESK KO mice present diminished responses to osmotic stimuli and TRPA1 activation.**

**A.** Venn diagrams showing the relative size and overlap between the population of neurons activated by menthol (100 µM), allyl isothiocyanate (AITC, 100 µM) and capsaicin (1 µM) using Fura-2 ratiometric intracellular calcium imaging. Number of total cells analyzed was 1124 (wild-type) and 1228 (knock-out). The number of responding cells in each subgroup is shown in parenthesis. Non-responding neurons to any of the agonists assayed was 246 (wild-type) and 446

(knock-out). **B.** Quantification of the percentage of neurons responding to each agonist in intracellular calcium recordings. Statistical differences between groups are shown (**p<0.01 unpaired t-test). **C.** Nocifensive behavior: quantification of the time the animals spent licking and shaking the paw after intradermal injection of AITC (10%) or capsaicin (1µg/10µl) in the hind paw for wild-type and TRESK knockout mice. The mean time spent showing nocifensive behaviors over a period of 5 min is shown (WT n=13; KO n=13 animals). **D.** Formalin-induced pain: *Top*. Time course of licking/shaking behavior directed to the formalin-injected hind paw. *Bottom*: quantification of cumulative time spent in phase I (0-10 min), IIa (11-30 min) and IIb (31 to 50 min). n= 5-6 animals per group. **E.** Osmotic pain: quantification of the time spent licking and shaking the paw after intradermal injection of hypotonic (-33%) or hypertonic (2% and 10%) stimuli in the hind paw of wild-type and TRESK knockout mice. The mean time spent showing nocifensive behaviors over a period of 5 min is shown. 6 to 11 animals were evaluated in each group. When indicated, a 5 µl-injection of prostaglandin $E_2$ ($PGE_2$) was injected in the hind paw of each mouse 30 min before the test to sensitize nociceptors. Statistical differences are shown as *p<0.05, **p<0.01 (Student's unpaired t-test) between WT and KO mice.

**Figure 4: TRESK-lacking mice present mechanical allodynia and normal heat sensitivity**

**A.** Mechanical threshold obtained with von Frey hairs from saphenous nerve C-fibers. *Left.* Distribution of von Frey thresholds. *Right*. Box and whiskers plot of the distribution of von Frey thresholds. Whiskers show the minimum and

maximum values obtained. Mean value is shown as an + and median as a straight line. Wild-type n=14, knock-out n=22. **B.** Distribution of heat thresholds from C-fibers recorded from wild-type (n=35) and TRESK KO mice (n=37), measured in skin-nerve experiments. **C.** Mean number of spikes fired by heat sensitive C-fibers during a heat-ramp from 30 to 50ºC. No significant differences were found. **D.** Mechanical sensitivity. *Left*: von Frey response thresholds obtained with the up and down method in male and female wild-type and TRESK knockout animals (male WT n=58, KO n=33; female WT n=18, KO n=19). *Right*: latency to hind paw withdrawal in the dynamic plantar test (male WT n=27; KO n=22). Statistical differences are shown as *p<0.05, ***p<0.001 (Student's unpaired t-test) between WT and KO mice. **E.** Heat sensitivity. *Left*: radiant heat (Hargreaves test) in male (WT n=39; KO n=38); and female animals (WT n=18; KO n=15). *Right*: Noxious heat sensitivity to 52 and 56ºC (Hot plate test) in male (WT n=8/9; KO n=13/11); and female animals (WT n=9/9; KO n=12/8).

**Figure 5: Cold allodynia in TRESK deleted mice**

**A.** Fractions of cold-sensitive C-fibers in WT (total number of C-fibers = 35) and TRESK KO (n=37 C-fibers), measured in skin-nerve experiments. Numbers in bars are the percentage of Mechano-Heat-Cold (C-MHC) and Mechano-Cold (C-MC) fibers. A significant difference in the distribution of cold fibers is shown (**p<0.01, Chi-square test). **B.** Distribution of the C-fibers activated by cold at different temperatures between WT and KO animals. **C.** Distribution of cold thresholds from fibers recorded (WT n=19; KO n=38). Mean and SEM are

shown. **D.** Representative experiments of C-fibers activated by a cold ramp. *Top*. Action potentials (Spikes) fired in response to a temperature decrease are shown for wild-type and a TRESK knockout cold C-fibers. The average action potential is presented on the right. A representative cold ramp from 30 to 10°C is shown below. *Bottom*: Histogram of mean responses to cooling, 5-second bin, of C-fibers from wild-type and TRESK KO mice. **E, F.** Cold sensitivity measured with the cold plate (2ºC) and cold plantar assays in male and female wild-type and TRESK knockout animals (n=11-19 animals per group). **G.** Cold avoidance measured in the thermal place preference test. The percentage of time spent at the reference plate (30ºC) at each experimental temperature is shown (n=8-14 male animals per group). Statistical differences are shown as *p<0.05, **p<0.01, ***p<0.001 (Student's unpaired t-test) between WT and KO mice.

**Figure 6: Changes in chronic pain in TRESK-deleted mice**

**A.** Mechanical and thermal sensitivity in the CFA-induced inflammatory pain model. Mechanical sensitivity was measured with von Frey filaments (up and down method) and thermal sensitivity was measured with the Hargreaves test (n=7 animals in each group) **B.** Mechanical and thermal sensitivity in the cuff-induced neuropathic pain model. Mechanical sensitivity was measured with von Frey filaments (up and down method) and thermal sensitivity was measured with the Hargreaves test (n=6 animals in each group). **C.** Oxaliplatin-induced cold sensitization model. *Left.* Paw withdrawal latency to the cold plantar assay before (baseline) and 90h after oxaliplatin injection in WT and TRESK KO animals (n=9 and 10 animals per group). *Right.* Cold avoidance measured in

the thermal place preference test. The percentage of time spent at the reference plate (30ºC) versus the experimental temperature (20ºC) is shown (n=6 and 8 animals per group). Statistical differences between WT and KO mice are shown as *p<0.05, **p<0.01, ***p<0.001 (Student's unpaired t-test).

**Supplementary Figure 1: Dynamic hot plate**

In contrast to the conventional hot plate, the dynamic hot plate allows the testing of a wide range of temperatures. Plate temperature was ramped from 30ºC to 50ºC at a 1ºC/min rate. To determine the temperature that is perceived as noxious for mice and quantify pain-related behaviors, the number of jumps at each temperature was scored. *Left*: number of jumps elicited at each temperature in male (top) and female (bottom) in wild-type and TRESK KO mice (n=11-15 animals per group). Only a significant difference was obtained at 49ºC (p<0.05, unpaired t-test) between wild-type and TRESK KO females. *Right, top*: mean temperature at which animals did the first jump (threshold). Right. bottom: Total number of jumps for male and female mice in the whole range of temperatures. Values for temperatures between 30 and 38ºC are not shown in the plots since were probably detected as non-noxious and did not produce any observable response.

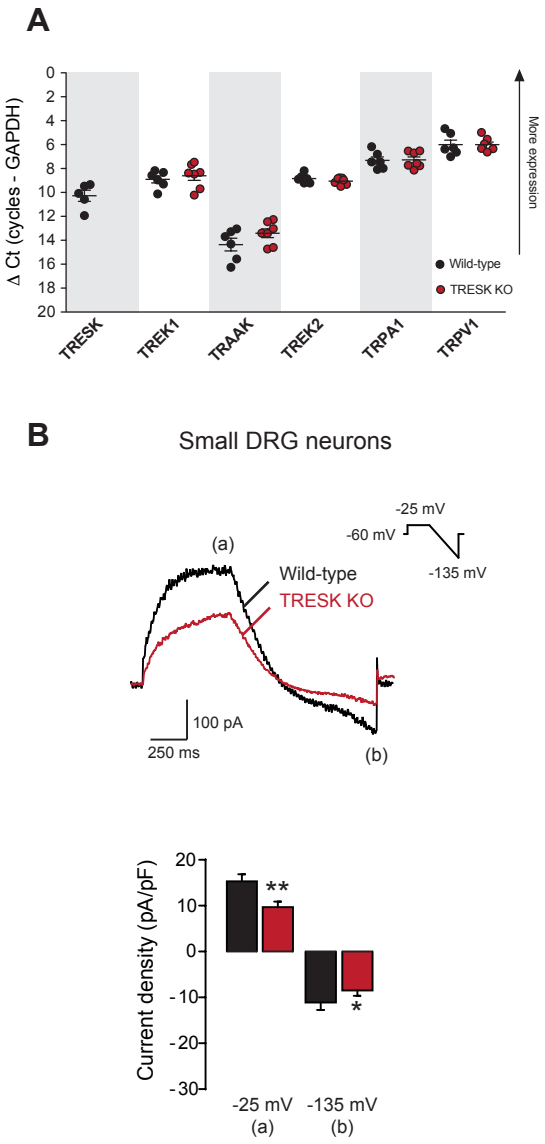


**Figure 1: Nociceptive sensory neurons lacking TRESK have a decreased standing outward current.** **A.** Expression profile of $K_{2P}$ channels, TRPA1 and TRPV1 in mouse sensory neurons from wild-type and TRESK knockout mice. mRNA expression obtained by quantitative PCR shows no significant differences between WT and KO animals after genetic deletion of TRESK. Y-axis shows the ΔCt (number of cycles target - number of cycles GADPH) for the different mRNAs. Notice that the Y-axis has been inverted to visually show that lower ΔCt numbers are indicative of a higher expression. Each dot represents a single animal (wild-type n=6; TRESK knockout n=7). **B.** Top: Representative recordings of whole-cell currents from small-sized DRG sensory neurons using a protocol to minimize activation of voltage-gated transient $K^+$ outward currents (holding voltage -60mV). Bottom: quantification of currents at the end of the pulse at -25 mV (a) and at the end of the ramp (-135 mV; b) showed significant differences among groups (*p<0.05; **p<0.01 unpaired t-test. wild-type n=31; TRESK KO n=50).

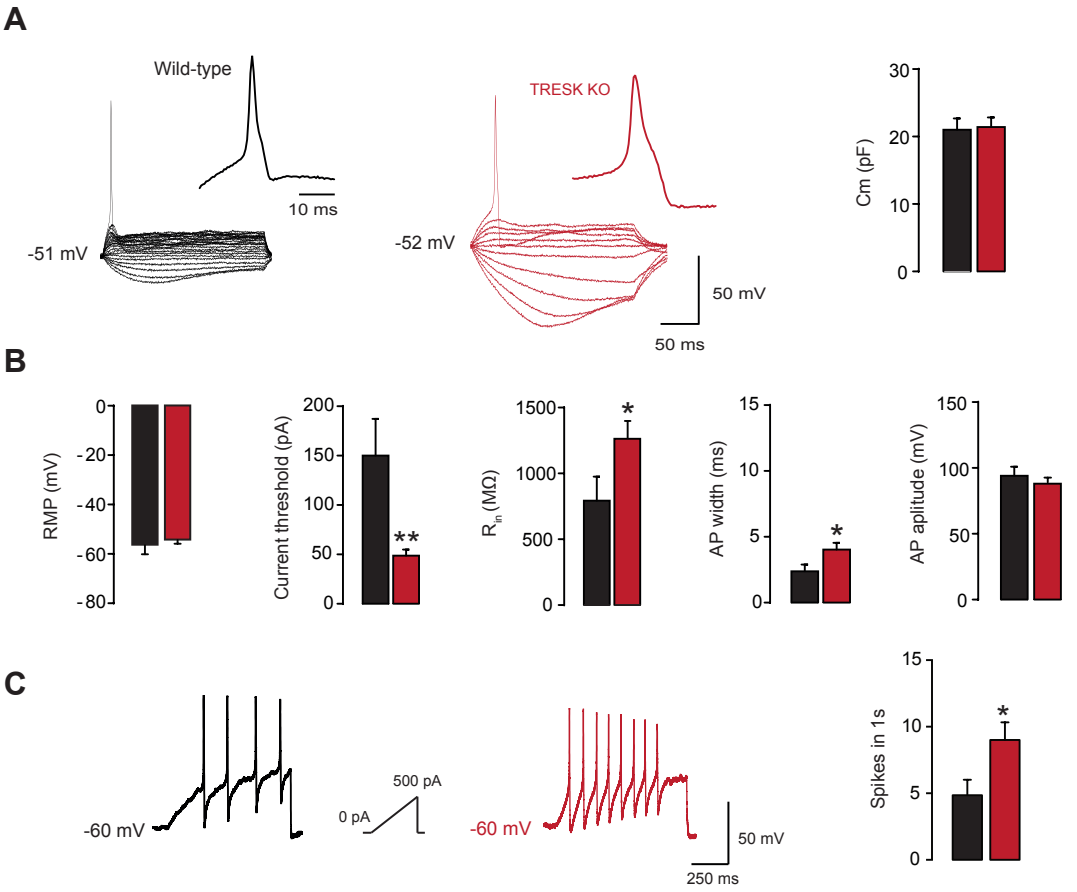


**Figure 2: Nociceptive sensory neurons lacking TRESK present a higher excitability**
**A.** Representative whole-cell current-clamp recordings from wild-type and TRESK knockout nociceptive sensory neurons elicited by hyperpolarizing or depolarizing 400 ms current pulses in 10 pA increments. Right: mean membrane capacitance ($C_m$) from neurons studied is shown. **B.** Quantification of the electrophysiological parameters analyzed in wild-type (black bars, n=13) and TRESK KO (red bars, n=27) sensory neurons. RMP: resting membrane potential. Current threshold was measured using 400 ms depolarizing current pulses in 10 pA increments; $R_{in}$: whole-cell input resistance was calculated on the basis of the steady-state I-V relationship during a series of 400 ms hyperpolarizing currents delivered in steps of 10 pA from -50 to -10 pA. AP amplitude was measured from the RMP to the AP peak. AP duration/width was measured at 50% of the AP amplitude. Statistical differences between groups are shown (*p<0.05, **p<0.01 unpaired t-test). **C.** Examples and quantification of neuronal excitability as the number of action potentials fired in response to a depolarizing current ramp (0 to 500 pA, 1s) form a holding voltage of -60 mV (black, wild-type n=6; red, TRESK KO n=7). Statistical differences between groups are shown (*p<0.05; **p<0.01 unpaired t-test).

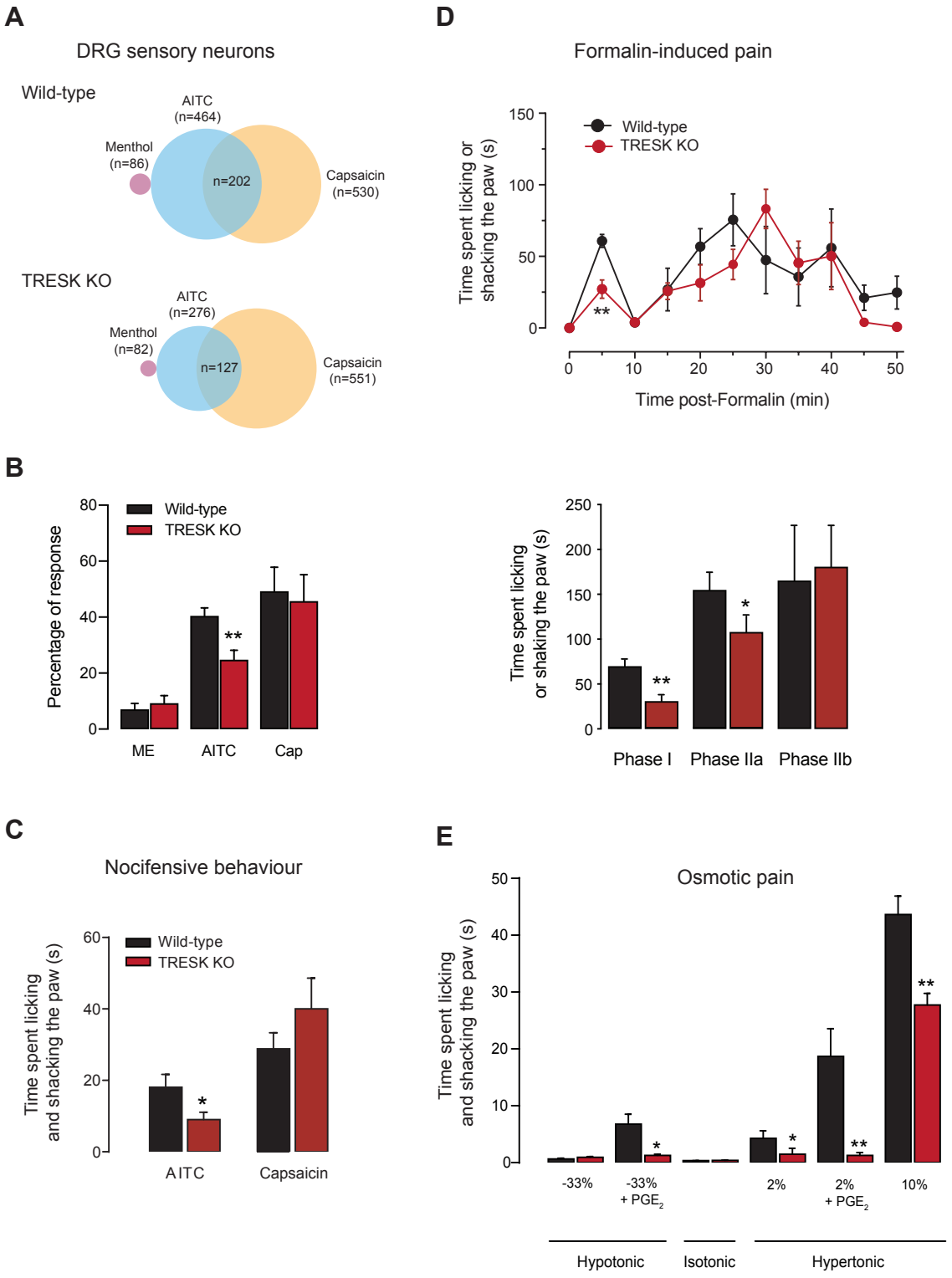


**Figure 3: TRESK KO mice present diminished responses to osmotic stimuli and TRPA1 activation.**
**A.** Venn diagrams showing the relative size and overlap between the population of neurons activated by menthol (100 µM), allyl isothiocyanate (AITC, 100 µM) and capsaicin (1 µM) using Fura-2 ratiometric intracellular calcium imaging. Number of total cells analyzed was 1124 (wild-type) and 1228 (knock-out). The number of responding cells in each subgroup is shown in parenthesis. Non-responding neurons to any of the agonists assayed was 246 (wild-type) and 446 (knock-out). **B.** Quantification of the percentage of neurons responding to each agonist in intracellular calcium recordings. Statistical differences between groups are shown (**p<0.01 unpaired t-test). **C.** Nocifensive behavior: quantification of the time the animals spent licking and shaking the paw after intradermal injection of AITC (10%) or capsaicin (1µg/10µl) in the hind paw for wild-type and TRESK knockout mice. The mean time spent showing nocifensive behaviors over a period of 5 min is shown (WT n=13; KO n=13 animals). **D.** Formalin-induced pain: *Top.* Time course of licking/shaking behavior directed to the formalin-injected hind paw. *Bottom:* quantification of cumulative time spent in phase I (0-10 min), IIa (11-30 min) and IIb (31 to 50 min). n= 5-6 animals per group. **E.** Osmotic pain: quantification of the time spent licking and shaking the paw after intradermal injection of hypotonic (-33%) or hypertonic (2% and 10%) stimuli in the hind paw of wild-type and TRESK knockout mice. The mean time spent showing nocifensive behaviors over a period of 5 min is shown. 6 to 11 animals were evaluated in each group. When indicated, a 5 µl-injection of prostaglandin E2 (PGE2) was injected in the hind paw of each mouse 30 min before the test to sensitize nociceptors. Statistical differences are shown as *p<0.05, **p<0.01 (Student's unpaired t-test) between WT and KO mice.

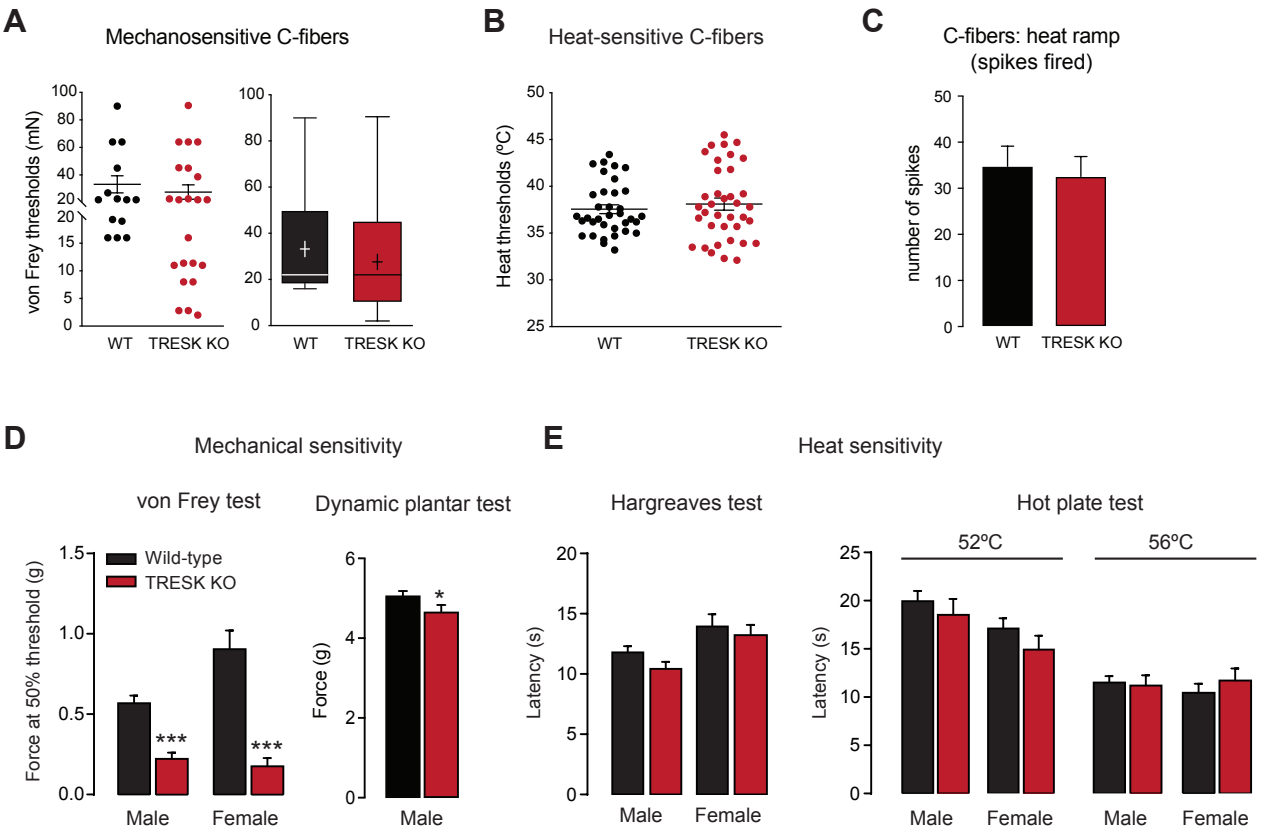


**Figure 4: TRESK-lacking mice present mechanical allodynia and normal heat sensitivity**
**A.** Mechanical threshold obtained with von Frey hairs from saphenous nerve C-fibers. *Left.* Distribution of von Frey thresholds. *Right.* Box and whiskers plot of the distribution of von Frey thresholds. Whiskers show the minimum and maximum values obtained. Mean value is shown as an + and median as a straight line. Wild-type n=14, knock-out n=22. **B.** Distribution of heat thresholds from C-fibers recorded from wild-type (n=35) and TRESK KO mice (n=37), measured in skin-nerve experiments. **C.** Mean number of spikes fired by heat sensitive C-fibers during a heat-ramp from 30 to 50ºC. No significant differences were found. **D.** Mechanical sensitivity. *Left:* von Frey response thresholds obtained with the up and down method in male and female wild-type and TRESK knockout animals (male WT n=58, KO n=33; female WT n=18, KO n=19). *Right:* latency to hind paw withdrawal in the dynamic plantar test (male WT n=27; KO n=22). Statistical differences are shown as *p<0.05, ***p<0.001 (Student's unpaired t-test) between WT and KO mice. **E.** Heat sensitivity. *Left:* radiant heat (Hargreaves test) in male (WT n=39; KO n=38); and female animals (WT n=18; KO n=15). *Right:* Noxious heat sensitivity to 52 and 56ºC (Hot plate test) in male (WT n=8/9; KO n=13/11); and female animals (WT n=9/9; KO n=12/8).

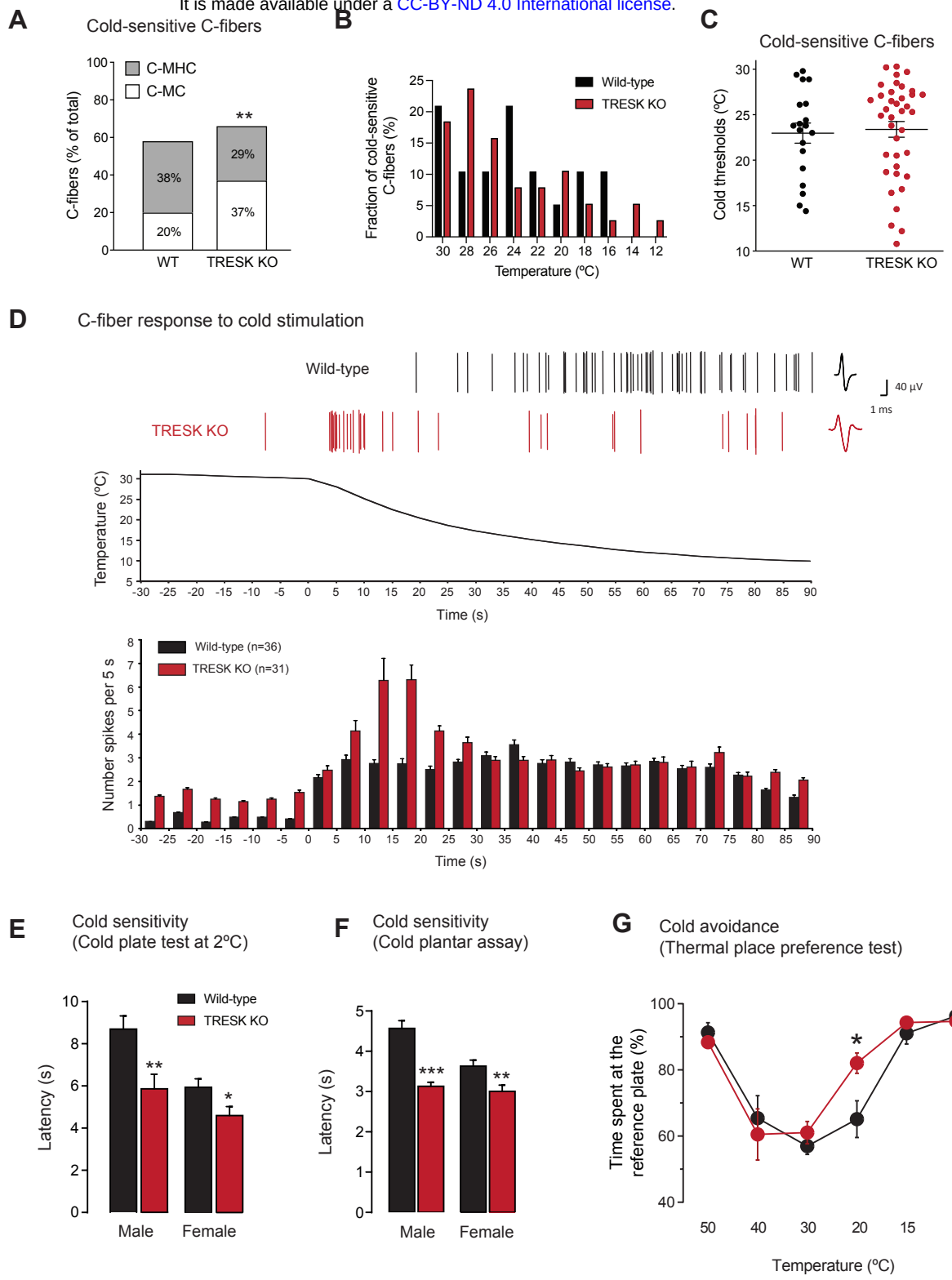


**Figure 5: Cold allodynia in TRESK deleted mice**

**A.** Fractions of cold-sensitive C-fibers in WT (total number of C-fibers = 35) and TRESK KO (n=37 C-fibers), measured in skin-nerve experiments. Numbers in bars are the percentage of Mechano-Heat-Cold (C-MHC) and Mechano-Cold (C-MC) fibers. A significant difference in the distribution of cold fibers is shown (**p<0.01, Chi-square test). **B.** Distribution of the C-fibers activated by cold at different temperatures between WT and KO animals. **C.** Distribution of cold thresholds from fibers recorded (WT n=19; KO n=38). Mean and SEM are shown. **D.** Representative experiments of C-fibers activated by a cold ramp. *Top.* Action potentials (Spikes) fired in response to a temperature decrease are shown for wild-type and a TRESK knockout cold C-fibers. The average action potential is presented on the right. A representative cold ramp from 30 to 10°C is shown below. *Bottom:* Histogram of mean responses to cooling, 5-second bin, of C-fibers from wild-type and TRESK KO mice. **E, F.** Cold sensitivity measured with the cold plate (2°C) and cold plantar assays in male and female wild-type and TRESK knockout animals (n=11-19 animals per group). **G.** Cold avoidance measured in the thermal place preference test. The percentage of time spent at the reference plate (30°C) at each experimental temperature is shown (n=8-14 male animals per group). Statistical differences are shown as *p<0.05, **p<0.01, ***p<0.001 (Student's unpaired t-test) between WT and KO mice.

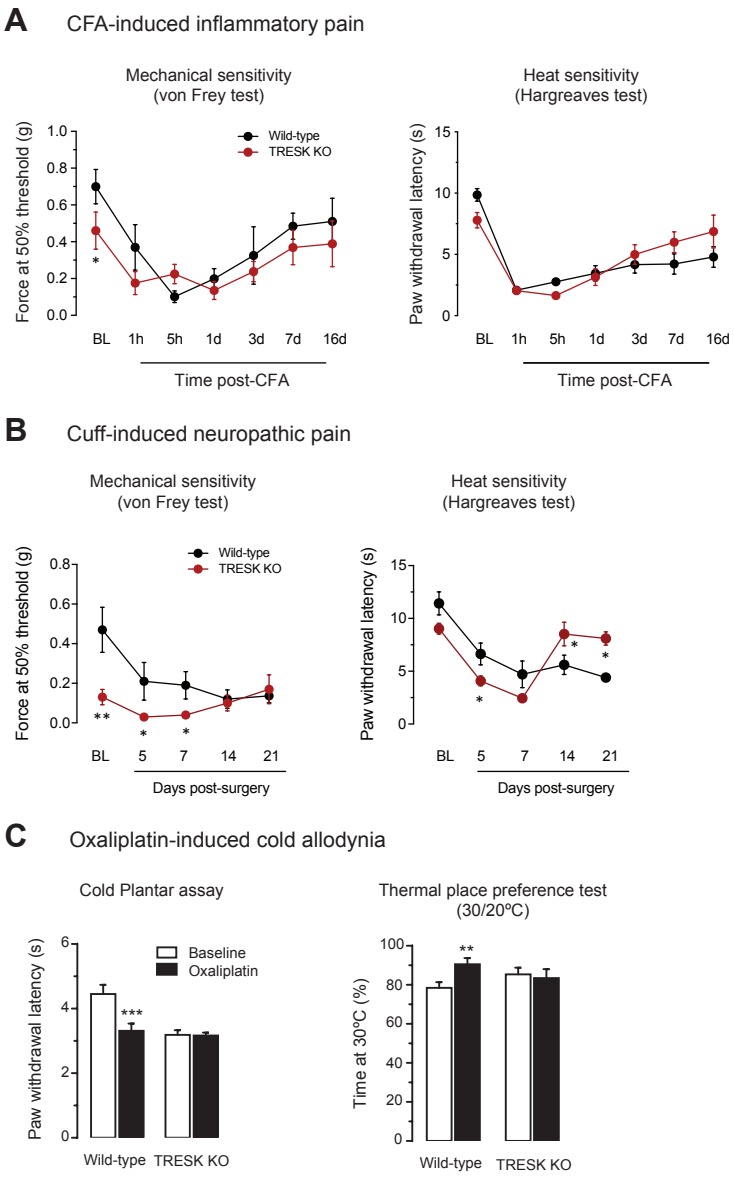


**Figure 6: Changes in chronic pain in TRESK-deleted mice**

**A.** Mechanical and thermal sensitivity in the CFA-induced inflammatory pain model. Mechanical sensitivity was measured with von Frey filaments (up and down method) and thermal sensitivity was measured with the Hargreaves test (n=7 animals in each group) **B.** Mechanical and thermal sensitivity in the cuff-induced neuropathic pain model. Mechanical sensitivity was measured with von Frey filaments (up and down method) and thermal sensitivity was measured with the Hargreaves test (n=6 animals in each group). **C.** Oxaliplatin-induced cold sensitization model. *Left.* Paw withdrawal latency to the cold plantar assay before (baseline) and 90h after oxaliplatin injection in WT and TRESK KO animals (n=9 and 10 animals per group). *Right.* Cold avoidance measured in the thermal place preference test. The percentage of time spent at the reference plate (30°C) versus the experimental temperature (20°C) is shown (n=6 and 8 animals per group). Statistical differences between WT and KO mice are shown as *p<0.05, **p<0.01, ***p<0.001 (Student's unpaired t-test).

# References

Acosta, C., Djouhri, L., Watkins, R., Berry, C., Bromage, K., and Lawson, S.N. (2014). TREK2 expressed selectively in IB4-binding C-fiber nociceptors hyperpolarizes their membrane potentials and limits spontaneous pain. J. Neurosci. Off. J. Soc. Neurosci. *34*, 1494–1509.

Aich, A., Afrin, L.B., and Gupta, K. (2015). Mast Cell-Mediated Mechanisms of Nociception. Int. J. Mol. Sci. *16*, 29069–29092.

Akopian, A.N., Souslova, V., England, S., Okuse, K., Ogata, N., Ure, J., Smith, A., Kerr, B.J., McMahon, S.B., Boyce, S., et al. (1999). The tetrodotoxin-resistant sodium channel SNS has a specialized function in pain pathways. Nat. Neurosci. *2*, 541–548.

Akopian, A.N., Chen, C.C., Ding, Y., Cesare, P., and Wood, J.N. (2000). A new member of the acid-sensing ion channel family. Neuroreport *11*, 2217–2222.

Alessandri-Haber, N., Dina, O.A., Chen, X., and Levine, J.D. (2009). TRPC1 and TRPC6 channels cooperate with TRPV4 to mediate mechanical hyperalgesia and nociceptor sensitization. J. Neurosci. Off. J. Soc. Neurosci. *29*, 6217–6228.

Aley, K.O., and Levine, J.D. (1999). Role of Protein Kinase A in the Maintenance of Inflammatory Pain. J. Neurosci. *19*, 2181–2186.

Aley, K.O., Messing, R.O., Mochly-Rosen, D., and Levine, J.D. (2000). Chronic Hypersensitivity For Inflammatory Nociceptor Sensitization Mediated by the ε Isozyme of Protein Kinase C. J. Neurosci. *20*, 4680–4685.

Alijevic, O., and Kellenberger, S. (2012). Subtype-specific modulation of acid-sensing ion channel (ASIC) function by 2-guanidine-4-methylquinazoline. J. Biol. Chem. *287*, 36059–36070.

Allan, S.M., and Rothwell, N.J. (2003). Inflammation in central nervous system injury. Philos. Trans. R. Soc. Lond. B. Biol. Sci. *358*, 1669–1677.

Allen, N.J., and Attwell, D. (2002). Modulation of ASIC channels in rat cerebellar Purkinje neurons by ischaemia-related signals. J. Physiol. *543*, 521–529.

Alloui, A., Zimmermann, K., Mamet, J., Duprat, F., Noël, J., Chemin, J., Guy, N., Blondeau, N., Voilley, N., Rubat-Coudert, C., et al. (2006). TREK-1, a K+ channel involved in polymodal pain perception. EMBO J. *25*, 2368–2376.

Amaya, F., Wang, H., Costigan, M., Allchorne, A.J., Hatcher, J.P., Egerton, J., Stean, T., Morisset, V., Grose, D., Gunthorpe, M.J., et al. (2006). The voltage-gated sodium channel Na(v)1.9 is an effector of peripheral inflammatory pain hypersensitivity. J. Neurosci. Off. J. Soc. Neurosci. *26*, 12852–12860.

Andersson, D.A., Nash, M., and Bevan, S. (2007). Modulation of the Cold-Activated Channel TRPM8 by Lysophospholipids and Polyunsaturated Fatty Acids. J. Neurosci. Off. J. Soc. Neurosci. *27*, 3347–3355.

Andersson, D.A., Gentry, C., Moss, S., and Bevan, S. (2008). Transient Receptor Potential A1 Is a Sensory Receptor for Multiple Products of Oxidative Stress. J. Neurosci. *28*, 2485–2494.

Andersson, D.A., Gentry, C., Light, E., Vastani, N., Vallortigara, J., Bierhaus, A., Fleming, T., and Bevan, S. (2013). Methylglyoxal Evokes Pain by Stimulating TRPA1. PLOS ONE *8*, e77986.

Anzai, N., Deval, E., Schaefer, L., Friend, V., Lazdunski, M., and Lingueglia, E. (2002). The Multivalent PDZ Domain-containing Protein CIPP Is a Partner of Acid-sensing Ion Channel 3 in Sensory Neurons. J. Biol. Chem. *277*, 16655–16661.

Apfel, S.C., Asbury, A.K., Bril, V., Burns, T.M., Campbell, J.N., Chalk, C.H., Dyck, P.J., Dyck, P.J., Feldman, E.L., Fields, H.L., et al. (2001). Positive neuropathic sensory symptoms as endpoints in diabetic neuropathy trials. J. Neurol. Sci. *189*, 3–5.

Ashwell, M., Mayhew, L., Richardson, J., and Rickayzen, B. (2014). Waist-to-Height Ratio Is More Predictive of Years of Life Lost than Body Mass Index. PLOS ONE *9*, e103483.

Askwith, C.C., Cheng, C., Ikuma, M., Benson, C., Price, M.P., and Welsh, M.J. (2000). Neuropeptide FF and FMRFamide potentiate acid-evoked currents from sensory neurons and proton-gated DEG/ENaC channels. Neuron *26*, 133–141.

Askwith, C.C., Benson, C.J., Welsh, M.J., and Snyder, P.M. (2001). DEG/ENaC ion channels involved in sensory transduction are modulated by cold temperature. Proc. Natl. Acad. Sci. U. S. A. *98*, 6459–6463.

Babinski, K., Lê, K.T., and Séguéla, P. (1999). Molecular cloning and regional distribution of a human proton receptor subunit with biphasic functional properties. J. Neurochem. *72*, 51–57.

Bandell, M., Story, G.M., Hwang, S.W., Viswanath, V., Eid, S.R., Petrus, M.J., Earley, T.J., and Patapoutian, A. (2004). Noxious cold ion channel TRPA1 is activated by pungent compounds and bradykinin. Neuron *41*, 849–857.

Barker, B.S., Young, G.T., Soubrane, C.H., Stephens, G.J., Stevens, E.B., and Patel, M.K. (2017). Ion Channels. In Conn's Translational Neuroscience, (Elsevier), pp. 11–43.

Baron, R., and Maier, C. (1995). Painful neuropathy: C-nociceptor activity may not be necessary to maintain central mechanisms accounting for dynamic mechanical allodynia. Clin. J. Pain *11*, 63–69.

Baron, A., Schaefer, L., Lingueglia, E., Champigny, G., and Lazdunski, M. (2001). Zn2+ and H+ are coactivators of acid-sensing ion channels. J. Biol. Chem. *276*, 35361–35367.

Baron, A., Waldmann, R., and Lazdunski, M. (2002a). ASIC-like, proton-activated currents in rat hippocampal neurons. J. Physiol. *539*, 485–494.

Baron, A., Deval, E., Salinas, M., Lingueglia, E., Voilley, N., and Lazdunski, M. (2002b). Protein kinase C stimulates the acid-sensing ion channel ASIC2a via the PDZ domain-containing protein PICK1. J. Biol. Chem. *277*, 50463–50468.

Baron, A., Voilley, N., Lazdunski, M., and Lingueglia, E. (2008). Acid sensing ion channels in dorsal spinal cord neurons. J. Neurosci. Off. J. Soc. Neurosci. *28*, 1498–1508.

Basbaum, A., and Jessell, T. (2013). Pain. In Principles of Neural Science, (United States of America: The McGraw-Hill Companies), pp. 530–555.

Basbaum, A.I., Bautista, D.M., Scherrer, G., and Julius, D. (2009). Cellular and Molecular Mechanisms of Pain. Cell *139*, 267–284.

Baumgärtner, U., Magerl, W., Klein, T., Hopf, H.C., and Treede, R.-D. (2002). Neurogenic hyperalgesia versus painful hypoalgesia: two distinct mechanisms of neuropathic pain. Pain *96*, 141–151.

Bautista, D.M., Sigal, Y.M., Milstein, A.D., Garrison, J.L., Zorn, J.A., Tsuruda, P.R., Nicoll, R.A., and Julius, D. (2008). Pungent agents from Szechuan peppers excite sensory neurons by inhibiting two-pore potassium channels. Nat. Neurosci. *11*, 772–779.

Bee, L., and Dickenson, A. (2009). Descending Modulation of Pain. In Synaptic Plasticity in Pain, M. Malcangio, ed. (New York, NY: Springer New York), pp. 307–335.

Benarroch, E.E. (2013). HCN channels: function and clinical implications. Neurology *80*, 304–310.

Bennasar-Veny, M., Lopez-Gonzalez, A.A., Tauler, P., Cespedes, M.L., Vicente-Herrero, T., Yañez, A., Tomas-Salva, M., and Aguilo, A. (2013). Body Adiposity Index and Cardiovascular Health Risk Factors in Caucasians: A Comparison with the Body Mass Index and Others. PLOS ONE *8*, e63999.

Bennett, D.L.H., and Woods, C.G. (2014). Painful and painless channelopathies. Lancet Neurol. *13*, 587–599.

Berg, A.H., and Scherer, P.E. (2005). Adipose tissue, inflammation, and cardiovascular disease. Circ. Res. *96*, 939–949.

Bergman, R.N., Stefanovski, D., Buchanan, T.A., Sumner, A.E., Reynolds, J.C., Sebring, N.G., Xiang, A.H., and Watanabe, R.M. (2011). A Better Index of Body Adiposity. Obesity *19*, 1083–1089.

Berridge, M.J., Lipp, P., and Bootman, M.D. (2000). The versatility and universality of calcium signalling. Nat. Rev. Mol. Cell Biol. *1*, 11–21.

Bhangoo, S., Ren, D., Miller, R.J., Henry, K.J., Lineswala, J., Hamdouchi, C., Li, B., Monahan, P.E., Chan, D.M., Ripsch, M.S., et al. (2007). Delayed functional expression of neuronal chemokine receptors following focal nerve demyelination in the rat: a mechanism for the development of chronic sensitization of peripheral nociceptors. Mol. Pain *3*, 38.

Bibiloni, M.D.M., Pons, A., and Tur, J.A. (2013). Prevalence of overweight and obesity in adolescents: a systematic review. ISRN Obes. *2013*, 392747.

Bierhaus, A., Fleming, T., Stoyanov, S., Leffler, A., Babes, A., Neacsu, C., Sauer, S.K., Eberhardt, M., Schnölzer, M., Lasitschka, F., et al. (2012). Methylglyoxal modification of Nav1.8 facilitates nociceptive neuron firing and causes hyperalgesia in diabetic neuropathy. Nat. Med. *18*, 926–933.

Birdsong, W.T., Fierro, L., Williams, F.G., Spelta, V., Naves, L.A., Knowles, M., Marsh-Haffner, J., Adelman, J.P., Almers, W., Elde, R.P., et al. (2010). Sensing Muscle Ischemia: Coincident Detection of Acid and ATP via Interplay of Two Ion Channels. Neuron *68*, 739–749.

Björntorp, P. (1993). Visceral obesity: a "civilization syndrome." Obes. Res. *1*, 206–222.

Błachnio-Zabielska, A.U., Pułka, M., Baranowski, M., Nikołajuk, A., Zabielski, P., Górska, M., and Górski, J. (2012). Ceramide metabolism is affected by obesity and diabetes in human adipose tissue. J. Cell. Physiol. *227*, 550–557.

Black, J.A., Cummins, T.R., Plumpton, C., Chen, Y.H., Hormuzdiar, W., Clare, J.J., and Waxman, S.G. (1999). Upregulation of a Silent Sodium Channel After Peripheral, but not Central, Nerve Injury in DRG Neurons. J. Neurophysiol. *82*, 2776–2785.

Blanchard, M.G., Rash, L.D., and Kellenberger, S. (2012). Inhibition of voltage-gated Na(+) currents in sensory neurones by the sea anemone toxin APETx2. Br. J. Pharmacol. *165*, 2167–2177.

Bligh, E.G., and Dyer, W.J. (1959). A rapid method of total lipid extraction and purification. Can. J. Biochem. Physiol. *37*, 911–917.

Block, R.C., Duff, R., Lawrence, P., Kakinami, L., Brenna, J.T., Shearer, G.C., Meednu, N., Mousa, S., Friedman, A., Harris, W.S., et al. (2010). The Effects of EPA, DHA, and Aspirin Ingestion on Plasma Lysophospholipids and Autotaxin. Prostaglandins Leukot. Essent. Fatty Acids *82*, 87–95.

Bohlen, C.J., Chesler, A.T., Sharif-Naeini, R., Medzihradszky, K.F., Zhou, S., King, D., Sánchez, E.E., Burlingame, A.L., Basbaum, A.I., and Julius, D. (2011). A heteromeric Texas coral snake toxin targets acid-sensing ion channels to produce pain. Nature *479*, 410–414.

Boulton, A.J.M., Malik, R.A., Arezzo, J.C., and Sosenko, J.M. (2004). Diabetic somatic neuropathies. Diabetes Care *27*, 1458–1486.

Bourinet, E., Alloui, A., Monteil, A., Barrère, C., Couette, B., Poirot, O., Pages, A., McRory, J., Snutch, T.P., Eschalier, A., et al. (2005). Silencing of the Cav3.2 T-type calcium channel gene in sensory neurons demonstrates its major role in nociception. EMBO J. *24*, 315–324.

Bourinet, E., Altier, C., Hildebrand, M.E., Trang, T., Salter, M.W., and Zamponi, G.W. (2014). Calcium-Permeable Ion Channels in Pain Signaling. Physiol. Rev. *94*, 81–140.

Buckley, C.D., Gilroy, D.W., and Serhan, C.N. (2014). Proresolving lipid mediators and mechanisms in the resolution of acute inflammation. Immunity *40*, 315–327.

Bushnell, M.C., Čeko, M., and Low, L.A. (2013). Cognitive and emotional control of pain and its disruption in chronic pain. Nat. Rev. Neurosci. *14*, 502–511.

Busserolles, J., Tsantoulas, C., Eschalier, A., and López García, J.A. (2016). Potassium channels in neuropathic pain: advances, challenges, and emerging ideas. PAIN *157*, S7.

Cadiou, H., Studer, M., Jones, N.G., Smith, E.S.J., Ballard, A., McMahon, S.B., and McNaughton, P.A. (2007). Modulation of Acid-Sensing Ion Channel Activity by Nitric Oxide. J. Neurosci. *27*, 13251–13260.

Cai, D., Yuan, M., Frantz, D.F., Melendez, P.A., Hansen, L., Lee, J., and Shoelson, S.E. (2005). Local and systemic insulin resistance resulting from hepatic activation of IKK-beta and NF-kappaB. Nat. Med. *11*, 183–190.

Callaghan, B.C., Little, A.A., Feldman, E.L., and Hughes, R.A. (2012a). Enhanced glucose control for preventing and treating diabetic neuropathy. Cochrane Database Syst. Rev. *6*, CD007543.

Callaghan, B.C., Hur, J., and Feldman, E.L. (2012b). Diabetic Neuropathy: One disease or two? Curr. Opin. Neurol. *25*, 536–541.

Callejo, G., Giblin, J.P., and Gasull, X. (2013). Modulation of TRESK background K+ channel by membrane stretch. PloS One *8*, e64471.

Canessa, C.M., Schild, L., Buell, G., Thorens, B., Gautschi, I., Horisberger, J.-D., and Rossier, B.C. (1994). Amiloride-sensitive epithelial Na + channel is made of three homologous subunits. Nature *367*, 463.

Cani, P.D., Amar, J., Iglesias, M.A., Poggi, M., Knauf, C., Bastelica, D., Neyrinck, A.M., Fava, F., Tuohy, K.M., Chabo, C., et al. (2007). Metabolic endotoxemia initiates obesity and insulin resistance. Diabetes *56*, 1761–1772.

Cao, E., Cordero-Morales, J.F., Liu, B., Qin, F., and Julius, D. (2013). TRPV1 channels are intrinsically heat sensitive and negatively regulated by phosphoinositide lipids. Neuron *77*, 667–679.

Carroll, L., Voisey, J., and Van Daal, A. (2004). Mouse models of obesity. Clin. Dermatol. *22*, 345–349.

Caterina, M.J., Schumacher, M.A., Tominaga, M., Rosen, T.A., Levine, J.D., and Julius, D. (1997). The capsaicin receptor: a heat-activated ion channel in the pain pathway. Nature *389*, 816.

Caterina, M.J., Rosen, T.A., Tominaga, M., Brake, A.J., and Julius, D. (1999). A capsaicin-receptor homologue with a high threshold for noxious heat. Nature *398*, 436–441.

Caterina, M.J., Leffler, A., Malmberg, A.B., Martin, W.J., Trafton, J., Petersen-Zeitz, K.R., Koltzenburg, M., Basbaum, A.I., and Julius, D. (2000). Impaired nociception and pain sensation in mice lacking the capsaicin receptor. Science *288*, 306–313.

Catterall, W.A. (2017). Forty Years of Sodium Channels: Structure, Function, Pharmacology, and Epilepsy. Neurochem. Res. *42*, 2495–2504.

CDC, C. for D.C. and (2011). National diabetes fact sheet: national estimates and general information on diabetes and prediabetes in the United States, 2011. Atlanta GA US Dep. Health Hum. Serv. Cent. Dis. Control Prev. *201*, 2568–2569.

Chahine, M., Ziane, R., Vijayaragavan, K., and Okamura, Y. (2005). Regulation of Na v channels in sensory neurons. Trends Pharmacol. Sci. *26*, 496–502.

Chaplan, S.R., Bach, F.W., Pogrel, J.W., Chung, J.M., and Yaksh, T.L. (1994). Quantitative assessment of tactile allodynia in the rat paw. J. Neurosci. Methods *53*, 55–63.

Chaurasia, B., and Summers, S.A. (2015). Ceramides - Lipotoxic Inducers of Metabolic Disorders. Trends Endocrinol. Metab. TEM *26*, 538–550.

Chemin, J., Patel, A., Duprat, F., Zanzouri, M., Lazdunski, M., and Honoré, E. (2005). Lysophosphatidic acid-operated K+ channels. J. Biol. Chem. *280*, 4415–4421.

Chen, C.-C., England, S., Akopian, A.N., and Wood, J.N. (1998). A sensory neuron-specific, proton-gated ion channel. Proc. Natl. Acad. Sci. *95*, 10240–10245.

Chen, C.-C., Zimmer, A., Sun, W.-H., Hall, J., Brownstein, M.J., and Zimmer, A. (2002). A role for ASIC3 in the modulation of high-intensity pain stimuli. Proc. Natl. Acad. Sci. *99*, 8992–8997.

Chen, G., Koyama, K., Yuan, X., Lee, Y., Zhou, Y.-T., O'Doherty, R., Newgard, C.B., and Unger, R.H. (1996). Disappearance of body fat in normal rats induced by adenovirus-mediated leptin gene therapy. Proc. Natl. Acad. Sci. *93*, 14795–14799.

Chen, X., Kalbacher, H., and Gründer, S. (2006). Interaction of acid-sensing ion channel (ASIC) 1 with the tarantula toxin psalmotoxin 1 is state dependent. J. Gen. Physiol. *127*, 267–276.

Cheng, H.T. (2010). Spinal Cord Mechanisms of Chronic Pain and Clinical Implications. Curr. Pain Headache Rep. *14*, 213–220.

Chiu, I.M., Pinho-Ribeiro, F.A., and Woolf, C.J. (2016). Pain and infection: pathogen detection by nociceptors. Pain *157*, 1192–1193.

Chiurchiù, V., Leuti, A., and Maccarrone, M. (2018). Bioactive Lipids and Chronic Inflammation: Managing the Fire Within. Front. Immunol. *9*.

Cho, H., Yang, Y.D., Lee, J., Lee, B., Kim, T., Jang, Y., Back, S.K., Na, H.S., Harfe, B.D., Wang, F., et al. (2012). The calcium-activated chloride channel anoctamin 1 acts as a heat sensor in nociceptive neurons. Nat. Neurosci. *15*, 1015–1021.

Chomczynski, P., and Sacchi, N. (2006). The single-step method of RNA isolation by acid guanidinium thiocyanate-phenol-chloroform extraction: twenty-something years on. Nat. Protoc. *1*, 581–585.

Chu, X.-P., and Xiong, Z.-G. (2013). Acid-sensing ion channels in pathological conditions. Adv. Exp. Med. Biol. *961*, 419–431.

Clément, K., Vaisse, C., Lahlou, N., Cabrol, S., Pelloux, V., Cassuto, D., Gourmelen, M., Dina, C., Chambaz, J., Lacorte, J.-M., et al. (1998). A mutation in the human leptin receptor gene causes obesity and pituitary dysfunction. Nature *392*, 398.

Coetzee, W.A., Amarillo, Y., Chiu, J., Chow, A., Lau, D., McCormack, T., Moreno, H., Nadal, M.S., Ozaita, A., Pountney, D., et al. (1999). Molecular diversity of K+ channels. Ann. N. Y. Acad. Sci. *868*, 233–285.

Cohen, A., Sagron, R., Somech, E., Segal-Hayoun, Y., and Zilberberg, N. (2009). Pain-associated signals, acidosis and lysophosphatidic acid, modulate the neuronal K(2P)2.1 channel. Mol. Cell. Neurosci. *40*, 382–389.

Coleman, D.L. (1978). Obese and diabetes: Two mutant genes causing diabetes-obesity syndromes in mice. Diabetologia *14*, 141–148.

Colloca, L., Ludman, T., Bouhassira, D., Baron, R., Dickenson, A.H., Yarnitsky, D., Freeman, R., Truini, A., Attal, N., Finnerup, N.B., et al. (2017). Neuropathic pain. Nat. Rev. Dis. Primer *3*, 17002.

Considine, R.V., Sinha, M.K., Heiman, M.L., Kriauciunas, A., Stephens, T.W., Nyce, M.R., Ohannesian, J.P., Marco, C.C., McKee, L.J., and Bauer, T.L. (1996). Serum immunoreactive-leptin concentrations in normal-weight and obese humans. N. Engl. J. Med. *334*, 292–295.

Coppey, L., Davidson, E., Lu, B., Gerard, C., and Yorek, M. (2011). Vasopeptidase Inhibitor Ilepatril (AVE7688) Prevents Obesity- and Diabetes-induced Neuropathy in C57Bl/6J Mice. Neuropharmacology *60*, 259–266.

Coste, B., Mathur, J., Schmidt, M., Earley, T.J., Ranade, S., Petrus, M.J., Dubin, A.E., and Patapoutian, A. (2010). Piezo1 and Piezo2 Are Essential Components of Distinct Mechanically Activated Cation Channels. Science *330*, 55–60.

Coste, B., Xiao, B., Santos, J.S., Syeda, R., Grandl, J., Spencer, K.S., Kim, S.E., Schmidt, M., Mathur, J., Dubin, A.E., et al. (2012). Piezo proteins are pore-forming subunits of mechanically activated channels. Nature *483*, 176–181.

Couture, R., Harrisson, M., Vianna, R.M., and Cloutier, F. (2001). Kinin receptors in pain and inflammation. Eur. J. Pharmacol. *429*, 161–176.

Cristofori-Armstrong, B., and Rash, L.D. (2017). Acid-sensing ion channel (ASIC) structure and function: Insights from spider, snake and sea anemone venoms. Neuropharmacology *127*, 173–184.

Dabelea, D., and Harrod, C.S. (2013). Role of developmental overnutrition in pediatric obesity and type 2 diabetes. Nutr. Rev. *71 Suppl 1*, S62-67.

Dai, S.-P., Huang, Y.-H., Chang, C.-J., Huang, Y.-F., Hsieh, W.-S., Tabata, Y., Ishii, S., and Sun, W.-H. (2017). TDAG8 involved in initiating inflammatory hyperalgesia and establishing hyperalgesic priming in mice. Sci. Rep. *7*.

Daniels, R.L., Takashima, Y., and McKemy, D.D. (2009). Activity of the neuronal cold sensor TRPM8 is regulated by phospholipase C via the phospholipid phosphoinositol 4,5-bisphosphate. J. Biol. Chem. *284*, 1570–1582.

Dauch, J.R., Bender, D.E., Luna-Wong, L.A., Hsieh, W., Yanik, B.M., Kelly, Z.A., and Cheng, H.T. (2013). Neurogenic factor-induced Langerhans cell activation in diabetic mice with mechanical allodynia. J. Neuroinflammation *10*, 64.

Davis, J.B., Gray, J., Gunthorpe, M.J., Hatcher, J.P., Davey, P.T., Overend, P., Harries, M.H., Latcham, J., Clapham, C., Atkinson, K., et al. (2000). Vanilloid receptor-1 is essential for inflammatory thermal hyperalgesia. Nature *405*, 183–187.

De Souza, C.T., Araujo, E.P., Bordin, S., Ashimine, R., Zollner, R.L., Boschero, A.C., Saad, M.J.A., and Velloso, L.A. (2005). Consumption of a fat-rich diet activates a proinflammatory response and induces insulin resistance in the hypothalamus. Endocrinology *146*, 4192–4199.

Delmas, P., and Brown, D.A. (2005). Pathways modulating neural KCNQ/M (Kv7) potassium channels. Nat. Rev. Neurosci. *6*, 850–862.

Delmas, P., Hao, J., and Rodat-Despoix, L. (2011). Molecular mechanisms of mechanotransduction in mammalian sensory neurons. Nat. Rev. Neurosci. *12*, 139–153.

Dennis, E.A., and Norris, P.C. (2015). Eicosanoid storm in infection and inflammation. Nat. Rev. Immunol. *15*, 511–523.

Deval, E., and Lingueglia, E. (2015). Acid-Sensing Ion Channels and nociception in the peripheral and central nervous systems. Neuropharmacology *94*, 49–57.

Deval, E., Baron, A., Lingueglia, E., Mazarguil, H., Zajac, J.-M., and Lazdunski, M. (2003). Effects of neuropeptide SF and related peptides on acid sensing ion channel 3 and sensory neuron excitability. Neuropharmacology *44*, 662–671.

Deval, E., Salinas, M., Baron, A., Lingueglia, E., and Lazdunski, M. (2004). ASIC2b-dependent regulation of ASIC3, an essential acid-sensing ion channel subunit in sensory neurons via the partner protein PICK-1. J. Biol. Chem. *279*, 19531–19539.

Deval, E., Noël, J., Lay, N., Alloui, A., Diochot, S., Friend, V., Jodar, M., Lazdunski, M., and Lingueglia, E. (2008). ASIC3, a sensor of acidic and primary inflammatory pain. EMBO J. *27*, 3047–3055.

Deval, E., Gasull, X., Noël, J., Salinas, M., Baron, A., Diochot, S., and Lingueglia, E. (2010). Acid-sensing ion channels (ASICs): pharmacology and implication in pain. Pharmacol. Ther. *128*, 549–558.

Deval, E., Noël, J., Gasull, X., Delaunay, A., Alloui, A., Friend, V., Eschalier, A., Lazdunski, M., and Lingueglia, E. (2011). Acid-sensing ion channels in postoperative pain. J. Neurosci. Off. J. Soc. Neurosci. *31*, 6059–6066.

Dib-Hajj, S.D., Cummins, T.R., Black, J.A., and Waxman, S.G. (2010). Sodium channels in normal and pathological pain. Annu. Rev. Neurosci. *33*, 325–347.

Diochot, S., Baron, A., Rash, L.D., Deval, E., Escoubas, P., Scarzello, S., Salinas, M., and Lazdunski, M. (2004). A new sea anemone peptide, APETx2, inhibits ASIC3, a major acid-sensitive channel in sensory neurons. EMBO J. *23*, 1516–1525.

Diochot, S., Baron, A., Salinas, M., Douguet, D., Scarzello, S., Dabert-Gay, A.-S., Debayle, D., Friend, V., Alloui, A., Lazdunski, M., et al. (2012). Black mamba venom peptides target acid-sensing ion channels to abolish pain. Nature *490*, 552–555.

Dixon, J.B., Zimmet, P., Alberti, K.G., and Rubino, F. (2011). Bariatric surgery: an IDF statement for obese Type 2 diabetes. Diabet. Med. *28*, 628–642.

Dolphin, A.C. (2016). Voltage-gated calcium channels and their auxiliary subunits: physiology and pathophysiology and pharmacology. J. Physiol. *594*, 5369–5390.

Duan, B., Wu, L.-J., Yu, Y.-Q., Ding, Y., Jing, L., Xu, L., Chen, J., and Xu, T.-L. (2007). Upregulation of acid-sensing ion channel ASIC1a in spinal dorsal horn neurons contributes to inflammatory pain hypersensitivity. J. Neurosci. Off. J. Soc. Neurosci. *27*, 11139–11148.

Dubé, G.R., Lehto, S.G., Breese, N.M., Baker, S.J., Wang, X., Matulenko, M.A., Honoré, P., Stewart, A.O., Moreland, R.B., and Brioni, J.D. (2005). Electrophysiological and in vivo characterization of A-317567, a novel blocker of acid sensing ion channels. Pain *117*, 88–96.

Dubé, G.R., Elagoz, A., and Mangat, H. (2009). Acid sensing ion channels and acid nociception. Curr. Pharm. Des. *15*, 1750–1766.

Dubin, A.E., and Patapoutian, A. (2010). Nociceptors: the sensors of the pain pathway. J. Clin. Invest. *120*, 3760–3772.

Dubuisson, D., and Dennis, S.G. (1977). The formalin test: A quantitative study of the analgesic effects of morphine, meperidine, and brain stem stimulation in rats and cats. Pain *4*, 161–174.

Duggan, A., García-Añoveros, J., and Corey, D.P. (2002). The PDZ Domain Protein PICK1 and the Sodium Channel BNaC1 Interact and Localize at Mechanosensory Terminals of Dorsal Root Ganglion Neurons and Dendrites of Central Neurons. J. Biol. Chem. *277*, 5203–5208.

Ehses, J.A., Perren, A., Eppler, E., Ribaux, P., Pospisilik, J.A., Maor-Cahn, R., Gueripel, X., Ellingsgaard, H., Schneider, M.K.J., Biollaz, G., et al. (2007). Increased number of islet-associated macrophages in type 2 diabetes. Diabetes *56*, 2356–2370.

El Alwani, M., Wu, B.X., Obeid, L.M., and Hannun, Y.A. (2006). Bioactive sphingolipids in the modulation of the inflammatory response. Pharmacol. Ther. *112*, 171–183.

Elg, S., Marmigere, F., Mattsson, J.P., and Ernfors, P. (2007). Cellular subtype distribution and developmental regulation of TRPC channel members in the mouse dorsal root ganglion. J. Comp. Neurol. *503*, 35–46.

Emery, E.C., and Ernfors, P. (2018). Dorsal Root Ganglion Neuron Types and Their Functional Specialization. Oxf. Handb. Neurobiol. Pain.

Emery, E.C., and Wood, J.N. (2018). Gaining on Pain. N. Engl. J. Med. *379*, 485–487.

Emery, E.C., Young, G.T., Berrocoso, E.M., Chen, L., and McNaughton, P.A. (2011). HCN2 ion channels play a central role in inflammatory and neuropathic pain. Science *333*, 1462–1466.

Emery, E.C., Young, G.T., and McNaughton, P.A. (2012). HCN2 ion channels: an emerging role as the pacemakers of pain. Trends Pharmacol. Sci. *33*, 456–463.

Erlanger, J., and Blair, E.A. (1938). Comparative observations on motor and sensory fibers with special reference to repetitiousness. Am. J. Physiol.-Leg. Content *121*, 431–453.

Erridge, C., Attina, T., Spickett, C.M., and Webb, D.J. (2007). A high-fat meal induces low-grade endotoxemia: evidence of a novel mechanism of postprandial inflammation. Am. J. Clin. Nutr. *86*, 1286–1292.

Escoubas, P., De Weille, J.R., Lecoq, A., Diochot, S., Waldmann, R., Champigny, G., Moinier, D., Ménez, A., and Lazdunski, M. (2000). Isolation of a tarantula toxin specific for a class of proton-gated Na+ channels. J. Biol. Chem. *275*, 25116–25121.

Escribá, P.V., González-Ros, J.M., Goñi, F.M., Kinnunen, P.K.J., Vigh, L., Sánchez-Magraner, L., Fernández, A.M., Busquets, X., Horváth, I., and Barceló-Coblijn, G. (2008). Membranes: a meeting point for lipids, proteins and therapies. J. Cell. Mol. Med. *12*, 829–875.

Faber, C.G., Lauria, G., Merkies, I.S.J., Cheng, X., Han, C., Ahn, H.-S., Persson, A.-K., Hoeijmakers, J.G.J., Gerrits, M.M., Pierro, T., et al. (2012). Gain-of-function Nav1.8 mutations in painful neuropathy. Proc. Natl. Acad. Sci. U. S. A. *109*, 19444–19449.

Facer, P., Casula, M.A., Smith, G.D., Benham, C.D., Chessell, I.P., Bountra, C., Sinisi, M., Birch, R., and Anand, P. (2007). Differential expression of the capsaicin receptor TRPV1 and related novel receptors TRPV3, TRPV4 and TRPM8 in normal human tissues and changes in traumatic and diabetic neuropathy. BMC Neurol. *7*, 11.

Farina, C., Aloisi, F., and Meinl, E. (2007). Astrocytes are active players in cerebral innate immunity. Trends Immunol. *28*, 138–145.

Federico, L., Pamuklar, Z., Smyth, S.S., and Morris, A.J. (2008). Therapeutic Potential of Autotaxin/Lysophospholipase D Inhibitors. Curr. Drug Targets *9*, 698–708.

Feldman, E.L., Nave, K.-A., Jensen, T.S., and Bennett, D.L.H. (2017). New Horizons in Diabetic Neuropathy: Mechanisms, Bioenergetics, and Pain. Neuron *93*, 1296–1313.

Ferreira, I., Twisk, J.W., van Mechelen, W., Kemper, H.C., Seidell, J.C., and Stehouwer, C.D. (2004). Current and adolescent body fatness and fat distribution: relationships with carotid intima–media thickness and large artery stiffness at the age of 36 years. J. Hypertens. *22*, 145.

Finnerup, N.B., Haroutounian, S., Kamerman, P., Baron, R., Bennett, D.L.H., Bouhassira, D., Cruccu, G., Freeman, R., Hansson, P., Nurmikko, T., et al. (2016). Neuropathic pain: an updated grading system for research and clinical practice. Pain *157*, 1599–1606.

Flegel, C., Schöbel, N., Altmüller, J., Becker, C., Tannapfel, A., Hatt, H., and Gisselmann, G. (2015). RNA-Seq Analysis of Human Trigeminal and Dorsal Root Ganglia with a Focus on Chemoreceptors. PloS One *10*, e0128951.

Francois, A., Kerckhove, N., Meleine, M., Alloui, A., Barrere, C., Gelot, A., Uebele, V.N., Renger, J.J., Eschalier, A., Ardid, D., et al. (2013). State-dependent properties of a new T-type calcium channel blocker enhance Ca(V)3.2 selectivity and support analgesic effects. Pain *154*, 283–293.

Fredman, G., Hellmann, J., Proto, J.D., Kuriakose, G., Colas, R.A., Dorweiler, B., Connolly, E.S., Solomon, R., Jones, D.M., Heyer, E.J., et al. (2016). An imbalance between specialized pro-resolving lipid mediators and pro-inflammatory leukotrienes promotes instability of atherosclerotic plaques. Nat. Commun. *7*, 12859.

Fuchs, B., Muller, K., Paasch, U., and Schiller, J. (2012). Lysophospholipids: Potential Markers of Diseases and Infertility? Mini-Rev. Med. Chem. *12*, 74–86.

Fujimoto, W.Y., Abbate, S.L., Kahn, S.E., Hokanson, J.E., and Brunzell, J.D. (1994). The visceral adiposity syndrome in Japanese-American men. Obes. Res. *2*, 364–371.

Fukuoka, T., Tokunaga, A., Tachibana, T., Dai, Y., Yamanaka, H., and Noguchi, K. (2002). VR1, but not P2X(3), increases in the spared L4 DRG in rats with L5 spinal nerve ligation. Pain *99*, 111–120.

Gao, Y.-J., and Ji, R.-R. (2010). Chemokines, neuronal-glial interactions, and central processing of neuropathic pain. Pharmacol. Ther. *126*, 56–68.

Gao, J., Wu, L.-J., Xu, L., and Xu, T.-L. (2004). Properties of the proton-evoked currents and their modulation by Ca2+ and Zn2+ in the acutely dissociated hippocampus CA1 neurons. Brain Res. *1017*, 197–207.

Gao, J., Duan, B., Wang, D.-G., Deng, X.-H., Zhang, G.-Y., Xu, L., and Xu, T.-L. (2005). Coupling between NMDA Receptor and Acid-Sensing Ion Channel Contributes to Ischemic Neuronal Death. Neuron *48*, 635–646.

García-Añoveros, J., Derfler, B., Neville-Golden, J., Hyman, B.T., and Corey, D.P. (1997). BNaC1 and BNaC2 constitute a new family of human neuronal sodium channels related to degenerins and epithelial sodium channels. Proc. Natl. Acad. Sci. U. S. A. *94*, 1459–1464.

Garcia-Larrea, L., and Peyron, R. (2013). Pain matrices and neuropathic pain matrices: a review. Pain *154 Suppl 1*, S29-43.

Gardner, E.P., and Johnson, K.O. (2013). The Somatosensory System: Receptors and Central Pathways. In Principles of Neural Science, (United States of America: The McGraw-Hill Companies), pp. 475–497.

Gentry, C., Stoakley, N., Andersson, D.A., and Bevan, S. (2010). The roles of iPLA2, TRPM8 and TRPA1 in chemically induced cold hypersensitivity. Mol. Pain *6*, 4.

Ginter, E., and Simko, V. (2014a). Becoming overweight: is there a health risk? Bratisl. Lek. Listy *115*, 527–531.

Ginter, E., and Simko, V. (2014b). Recent data on obesity research: β-aminoisobutyric acid. Bratisl. Lek. Listy *115*, 492–493.

Goldberg, Y.P., MacFarlane, J., MacDonald, M.L., Thompson, J., Dube, M.-P., Mattice, M., Fraser, R., Young, C., Hossain, S., Pape, T., et al. (2007). Loss-of-function mutations in the Nav1.7 gene underlie congenital indifference to pain in multiple human populations. Clin. Genet. *71*, 311–319.

Gram, D.X., Holst, J.J., and Szallasi, A. (2017). TRPV1: A Potential Therapeutic Target in Type 2 Diabetes and Comorbidities? Trends Mol. Med. *23*, 1002–1013.

Green, A.Q., Krishnan, S., Finucane, F.M., and Rayman, G. (2010). Altered C-Fiber Function as an Indicator of Early Peripheral Neuropathy in Individuals With Impaired Glucose Tolerance. Diabetes Care *33*, 174–176.

Gregg, E.W., Sorlie, P., Paulose-Ram, R., Gu, Q., Eberhardt, M.S., Wolz, M., Burt, V., Curtin, L., Engelgau, M., and Geiss, L. (2004). Prevalence of Lower-Extremity Disease in the U.S. Adult Population ≥40 Years of Age With and Without Diabetes: 1999–2000 National Health and Nutrition Examination Survey. Diabetes Care *27*, 1591–1597.

Gregor, M.F., and Hotamisligil, G.S. (2011). Inflammatory Mechanisms in Obesity. Annu. Rev. Immunol. *29*, 415–445.

Gründer, S., and Pusch, M. (2015). Biophysical properties of acid-sensing ion channels (ASICs). Neuropharmacology *94*, 9–18.

Gründer, S., Geissler, H.S., Bässler, E.L., and Ruppersberg, J.P. (2000). A new member of acid-sensing ion channels from pituitary gland. Neuroreport *11*, 1607–1611.

Guilford, B.L., Ryals, J.M., and Wright, D.E. (2011). Phenotypic changes in diabetic neuropathy induced by a high-fat diet in diabetic C57BL/6 mice. Exp. Diabetes Res. *2011*, 848307.

Guo, Z., and Cao, Y.-Q. (2014). Over-expression of TRESK K(+) channels reduces the excitability of trigeminal ganglion nociceptors. PloS One *9*, e87029.

Guo, S.S., Wu, W., Chumlea, W.C., and Roche, A.F. (2002). Predicting overweight and obesity in adulthood from body mass index values in childhood and adolescence. Am. J. Clin. Nutr. *76*, 653–658.

Habib, A.M., Wood, J.N., and Cox, J.J. (2015). Sodium Channels and Pain. In Pain Control, H.-G. Schaible, ed. (Berlin, Heidelberg: Springer Berlin Heidelberg), pp. 39–56.

Hains, B.C., Klein, J.P., Saab, C.Y., Craner, M.J., Black, J.A., and Waxman, S.G. (2003). Upregulation of Sodium Channel Nav1.3 and Functional Involvement in Neuronal Hyperexcitability Associated with Central Neuropathic Pain after Spinal Cord Injury. J. Neurosci. *23*, 8881–8892.

Hansen, C.S., Jensen, T.M., Jensen, J.S., Nawroth, P., Fleming, T., Witte, D.R., Lauritzen, T., Sandbaek, A., Charles, M., Fleischer, J., et al. (2015). The role of serum methylglyoxal on diabetic peripheral and cardiovascular autonomic neuropathy: the ADDITION Denmark study. Diabet. Med. J. Br. Diabet. Assoc. *32*, 778–785.

Harding, S.D., Sharman, J.L., Faccenda, E., Southan, C., Pawson, A.J., Ireland, S., Gray, A.J.G., Bruce, L., Alexander, S.P.H., Anderton, S., et al. (2018). The IUPHAR/BPS Guide to PHARMACOLOGY in 2018: updates and expansion to encompass the new guide to IMMUNOPHARMACOLOGY. Nucleic Acids Res. *46*, D1091–D1106.

Haus, J.M., Kashyap, S.R., Kasumov, T., Zhang, R., Kelly, K.R., Defronzo, R.A., and Kirwan, J.P. (2009). Plasma ceramides are elevated in obese subjects with type 2 diabetes and correlate with the severity of insulin resistance. Diabetes *58*, 337–343.

Heimerl, S., Fischer, M., Baessler, A., Liebisch, G., Sigruener, A., Wallner, S., and Schmitz, G. (2014). Alterations of plasma lysophosphatidylcholine species in obesity and weight loss. PloS One *9*, e111348.

Hesselager, M., Timmermann, D.B., and Ahring, P.K. (2004). pH Dependency and Desensitization Kinetics of Heterologously Expressed Combinations of Acid-sensing Ion Channel Subunits. J. Biol. Chem. *279*, 11006–11015.

Heydemann, A. (2016). An Overview of Murine High Fat Diet as a Model for Type 2 Diabetes Mellitus.

Hirosumi, J., Tuncman, G., Chang, L., Görgün, C.Z., Uysal, K.T., Maeda, K., Karin, M., and Hotamisligil, G.S. (2002). A central role for JNK in obesity and insulin resistance. Nature *420*, 333–336.

Hoeijmakers, J.G.J., Faber, C.G., Merkies, I.S.J., and Waxman, S.G. (2014). Channelopathies, painful neuropathy, and diabetes: which way does the causal arrow point? Trends Mol. Med. *20*, 544–550.

Hökfelt, T., Kellerth, J.O., Nilsson, G., and Pernow, B. (1975). Substance p: localization in the central nervous system and in some primary sensory neurons. Science *190*, 889–890.

Hökfelt, T., Elde, R., Johansson, O., Luft, R., Nilsson, G., and Arimura, A. (1976). Immunohistochemical evidence for separate populations of somatostatin-containing and substance P-containing primary afferent neurons in the rat. Neuroscience *1*, 131–136.

Horch, K.W., Tuckett, R.P., and Burgess, P.R. (1977). A key to the classification of cutaneous mechanoreceptors. J. Invest. Dermatol. *69*, 75–82.

Hotamisligil, G.S., Murray, D.L., Choy, L.N., and Spiegelman, B.M. (1994). Tumor necrosis factor alpha inhibits signaling from the insulin receptor. Proc. Natl. Acad. Sci. U. S. A. *91*, 4854–4858.

Hruby, A., and Hu, F.B. (2015). The Epidemiology of Obesity: A Big Picture. PharmacoEconomics *33*, 673–689.

Hruska-Hageman, A.M., Wemmie, J.A., Price, M.P., and Welsh, M.J. (2002). Interaction of the synaptic protein PICK1 (protein interacting with C kinase 1) with the non-voltage gated sodium channels BNC1 (brain Na+ channel 1) and ASIC (acid-sensing ion channel). Biochem. J. *361*, 443–450.

Huang, J., Zhang, X., and McNaughton, P.A. (2006). Inflammatory Pain: The Cellular Basis of Heat Hyperalgesia. Curr. Neuropharmacol. *4*, 197–206.

Huang, S.-J., Yang, W.-S., Lin, Y.-W., Wang, H.-C., and Chen, C.-C. (2008). Increase of insulin sensitivity and reversal of age-dependent glucose intolerance with inhibition of ASIC3. Biochem. Biophys. Res. Commun. *371*, 729–734.

Huang, W.-Y., Dai, S.-P., Chang, Y.-C., and Sun, W.-H. (2015). Acidosis Mediates the Switching of Gs-PKA and Gi-PKCε Dependence in Prolonged Hyperalgesia Induced by Inflammation. PLOS ONE *10*, e0125022.

Huda, R., Pollema-Mays, S.L., Chang, Z., Alheid, G.F., McCrimmon, D.R., and Martina, M. (2012). Acid-sensing ion channels contribute to chemosensitivity of breathing-related neurons of the nucleus of the solitary tract: ASICs in neurons of the nucleus of the solitary tract. J. Physiol. *590*, 4761–4775.

Iftinca, M., Hamid, J., Chen, L., Varela, D., Tadayonnejad, R., Altier, C., Turner, R.W., and Zamponi, G.W. (2007). Regulation of T-type calcium channels by Rho-associated kinase. Nat. Neurosci. *10*, 854–860.

Ikemoto, S., Takahashi, M., Tsunoda, N., Maruyama, K., Itakura, H., and Ezaki, O. (1996). High-fat diet-induced hyperglycemia and obesity in mice: differential effects of dietary oils. Metabolism. *45*, 1539–1546.

Immke, D.C., and McCleskey, E.W. (2001). Lactate enhances the acid-sensing Na+ channel on ischemia-sensing neurons. Nat. Neurosci. *4*, 869–870.

Inoue, M., Rashid, M.H., Fujita, R., Contos, J.J.A., Chun, J., and Ueda, H. (2004). Initiation of neuropathic pain requires lysophosphatidic acid receptor signaling. Nat. Med. *10*, 712–718.

Inoue, M., Ma, L., Aoki, J., and Ueda, H. (2008a). Simultaneous stimulation of spinal NK1 and NMDA receptors produces LPC which undergoes ATX-mediated conversion to LPA, an initiator of neuropathic pain. J. Neurochem. *107*, 1556–1565.

Inoue, M., Xie, W., Matsushita, Y., Chun, J., Aoki, J., and Ueda, H. (2008b). Lysophosphatidylcholine induces neuropathic pain through an action of autotaxin to generate lysophosphatidic acid. Neuroscience *152*, 296–298.

Jang, E., Kim, J.-H., Lee, S., Kim, J.-H., Seo, J.-W., Jin, M., Lee, M.-G., Jang, I.-S., Lee, W.-H., and Suk, K. (2013). Phenotypic polarization of activated astrocytes: the critical role of lipocalin-2 in the classical inflammatory activation of astrocytes. J. Immunol. Baltim. Md 1950 *191*, 5204–5219.

Jarvis, M.F., Burgard, E.C., McGaraughty, S., Honore, P., Lynch, K., Brennan, T.J., Subieta, A., Biesen, T. van, Cartmell, J., Bianchi, B., et al. (2002). A-317491, a novel potent and selective non-nucleotide antagonist of P2X3 and P2X2/3 receptors, reduces chronic inflammatory and neuropathic pain in the rat. Proc. Natl. Acad. Sci. *99*, 17179–17184.

Jensen, T.S., and Finnerup, N.B. (2014). Allodynia and hyperalgesia in neuropathic pain: clinical manifestations and mechanisms. Lancet Neurol. *13*, 924–935.

Jensen, J.E., Mobli, M., Brust, A., Alewood, P.F., King, G.F., and Rash, L.D. (2012). Cyclisation increases the stability of the sea anemone peptide APETx2 but decreases its activity at acid-sensing ion channel 3. Mar. Drugs *10*, 1511–1527.

Joeres, N., Augustinowski, K., Neuhof, A., Assmann, M., and Gründer, S. (2016). Functional and pharmacological characterization of two different ASIC1a/2a heteromers reveals their sensitivity to the spider toxin PcTx1. Sci. Rep. *6*, 27647.

Jones, B.J., and Roberts, D.J. (1968). The quantitative measurement of motor inco-ordination in naive mice using an accelerating rotarod. J. Pharm. Pharmacol. *20*, 302–304.

Jones, N.G., Slater, R., Cadiou, H., McNaughton, P., and McMahon, S.B. (2004). Acid-Induced Pain and Its Modulation in Humans. J. Neurosci. *24*, 10974–10979.

Juárez-Contreras, R., Rosenbaum, T., and Morales-Lázaro, S.L. (2018). Lysophosphatidic Acid and Ion Channels as Molecular Mediators of Pain. Front. Mol. Neurosci. *11*.

Julius, D., and Basbaum, A.I. (2001). Molecular mechanisms of nociception. Nature *413*, 203.

K. Ryborg, B. Deleuran, H. Søgaard, A. (2000). Intracutaneous Injection of Lysophosphatidylcholine Induces Skin Inflammation and Accumulation of Leukocytes. Acta Derm. Venereol. *80*, 242–246.

Kahn, S.E., Prigeon, R.L., Schwartz, R.S., Fujimoto, W.Y., Knopp, R.H., Brunzell, J.D., and Porte, D. (2001). Obesity, body fat distribution, insulin sensitivity and Islet beta-cell function as explanations for metabolic diversity. J. Nutr. *131*, 354S-60S.

Kang, D., Choe, C., and Kim, D. (2005). Thermosensitivity of the two-pore domain K+ channels TREK-2 and TRAAK. J. Physiol. *564*, 103–116.

Kelesidis, T., Kelesidis, I., Chou, S., and Mantzoros, C.S. (2010). Narrative Review: The Role of Leptin in Human Physiology: Emerging Clinical Applications. Ann. Intern. Med. *152*, 93–100.

Kellenberger, S., and Schild, L. (2002). Epithelial sodium channel/degenerin family of ion channels: a variety of functions for a shared structure. Physiol. Rev. *82*, 735–767.

Kellenberger, S., and Schild, L. (2015). International union of basic and clinical pharmacology. XCI. structure, function, and pharmacology of acid-sensing ion channels and the epithelial Na+ channel. Pharmacol. Rev. *67*, 1–35.

Khan, G.M., Chen, S.-R., and Pan, H.-L. (2002). Role of primary afferent nerves in allodynia caused by diabetic neuropathy in rats. Neuroscience *114*, 291–299.

Khasar, S.G., Lin, Y.-H., Martin, A., Dadgar, J., McMahon, T., Wang, D., Hundle, B., Aley, K.O., Isenberg, W., McCarter, G., et al. (1999a). A Novel Nociceptor Signaling Pathway Revealed in Protein Kinase C ε Mutant Mice. Neuron *24*, 253–260.

Khasar, S.G., McCarter, G., and Levine, J.D. (1999b). Epinephrine Produces a β-Adrenergic Receptor-Mediated Mechanical Hyperalgesia and In Vitro Sensitization of Rat Nociceptors. J. Neurophysiol. *81*, 1104–1112.

Kihara, Y., Gupta, S., Maurya, M.R., Armando, A., Shah, I., Quehenberger, O., Glass, C.K., Dennis, E.A., and Subramaniam, S. (2014). Modeling of Eicosanoid Fluxes Reveals Functional Coupling between Cyclooxygenases and Terminal Synthases. Biophys. J. *106*, 966–975.

Kilpeläinen, T.O., Qi, L., Brage, S., Sharp, S.J., Sonestedt, E., Demerath, E., Ahmad, T., Mora, S., Kaakinen, M., Sandholt, C.H., et al. (2011). Physical activity attenuates the influence of FTO variants on obesity risk: a meta-analysis of 218,166 adults and 19,268 children. PLoS Med. *8*, e1001116.

Kim, S.U., and de Vellis, J. (2005). Microglia in health and disease. J. Neurosci. Res. *81*, 302–313.

Kittaka, H., Uchida, K., Fukuta, N., and Tominaga, M. (2017). Lysophosphatidic acid-induced itch is mediated by signalling of LPA5 receptor, phospholipase D and TRPA1/TRPV1. J. Physiol. *595*, 2681–2698.

Kobayashi, K., Fukuoka, T., Obata, K., Yamanaka, H., Dai, Y., Tokunaga, A., and Noguchi, K. (2005). Distinct expression of TRPM8, TRPA1, and TRPV1 mRNAs in rat primary afferent neurons with adelta/c-fibers and colocalization with trk receptors. J. Comp. Neurol. *493*, 596–606.

Kollert, S., Dombert, B., Döring, F., and Wischmeyer, E. (2015). Activation of TRESK channels by the inflammatory mediator lysophosphatidic acid balances nociceptive signalling. Sci. Rep. *5*, 12548.

Koltzenburg, M., and Lewin, G.R. (1997). Receptive Properties of Embryonic Chick Sensory Neurons Innervating Skin. J. Neurophysiol. *78*, 2560–2568.

Kooijman, E.E., Chupin, V., Kruijff, B. de, and Burger, K.N.J. (2003). Modulation of Membrane Curvature by Phosphatidic Acid and Lysophosphatidic Acid. Traffic *4*, 162–174.

Koppert, W., Martus, P., and Reeh, P.W. (2001). Interactions of histamine and bradykinin on polymodal C-fibres in isolated rat skin. Eur. J. Pain *5*, 97–106.

Krishtal, O.A., and Pidoplichko, V.I. (1980). A receptor for protons in the nerve cell membrane. Neuroscience *5*, 2325–2327.

Kusano, K.F., Allendoerfer, K.L., Munger, W., Pola, R., Bosch-Marce, M., Kirchmair, R., Yoon, Y., Curry, C., Silver, M., Kearney, M., et al. (2004). Sonic hedgehog induces arteriogenesis in diabetic vasa nervorum and restores function in diabetic neuropathy. Arterioscler. Thromb. Vasc. Biol. *24*, 2102–2107.

Lafrenière, R.G., Cader, M.Z., Poulin, J.-F., Andres-Enguix, I., Simoneau, M., Gupta, N., Boisvert, K., Lafrenière, F., McLaughlan, S., Dubé, M.-P., et al. (2010). A dominant-negative mutation in the TRESK potassium channel is linked to familial migraine with aura. Nat. Med. *16*, 1157–1160.

Latremoliere, A., and Woolf, C.J. (2009). Central Sensitization: A Generator of Pain Hypersensitivity by Central Neural Plasticity. J. Pain *10*, 895–926.

Lawson, S.N. (2002). Phenotype and function of somatic primary afferent nociceptive neurones with C-, Aδ- or Aα/β-fibres. Exp. Physiol. *87*, 239–244.

Lawson, S.N., McCarthy, P.W., and Prabhakar, E. (1996). Electrophysiological properties of neurones with CGRP-like immunoreactivity in rat dorsal root ganglia. J. Comp. Neurol. *365*, 355–366.

Le Thuc, O., Stobbe, K., Cansell, C., Nahon, J.-L., Blondeau, N., and Rovère, C. (2017). Hypothalamic Inflammation and Energy Balance Disruptions: Spotlight on Chemokines. Front. Endocrinol. *8*, 197.

Lee, S. (2013). Pharmacological Inhibition of Voltage-gated Ca2+ Channels for Chronic Pain Relief. Curr. Neuropharmacol. *11*, 606–620.

Lee, H., Liao, J.J., Graeler, M., Huang, M.C., and Goetzl, E.J. (2002). Lysophospholipid regulation of mononuclear phagocytes. Biochim. Biophys. Acta *1582*, 175–177.

Lee, W., Su Kim, H., and Lee, G.R. (2015). Leukotrienes induce the migration of Th17 cells. Immunol. Cell Biol. *93*, 472–479.

Leffler, A., Mönter, B., and Koltzenburg, M. (2006). The role of the capsaicin receptor TRPV1 and acid-sensing ion channels (ASICS) in proton sensitivity of subpopulations of primary nociceptive neurons in rats and mice. Neuroscience *139*, 699–709.

Leonard, A.S., Yermolaieva, O., Hruska-Hageman, A., Askwith, C.C., Price, M.P., Wemmie, J.A., and Welsh, M.J. (2003). cAMP-dependent protein kinase phosphorylation of the acid-sensing ion channel-1 regulates its binding to the protein interacting with C-kinase-1. Proc. Natl. Acad. Sci. *100*, 2029–2034.

Lesage, F., Terrenoire, C., Romey, G., and Lazdunski, M. (2000). Human TREK2, a 2P domain mechano-sensitive K+ channel with multiple regulations by polyunsaturated fatty acids, lysophospholipids, and Gs, Gi, and Gq protein-coupled receptors. J. Biol. Chem. *275*, 28398–28405.

Levy, D., and Zochodne, D.W. (2000). Increased mRNA expression of the B1 and B2 bradykinin receptors and antinociceptive effects of their antagonists in an animal model of neuropathic pain. Pain *86*, 265–271.

Li, Q.S., Cheng, P., Favis, R., Wickenden, A., Romano, G., and Wang, H. (2015). SCN9A Variants May be Implicated in Neuropathic Pain Associated With Diabetic Peripheral Neuropathy and Pain Severity. Clin. J. Pain *31*, 976–982.

Lin, S.-H., Chien, Y.-C., Chiang, W.-W., Liu, Y.-Z., Lien, C.-C., and Chen, C.-C. (2015a). Genetic mapping of ASIC4 and contrasting phenotype to ASIC1a in modulating innate fear and anxiety. Eur. J. Neurosci. *41*, 1553–1568.

Lin, S.-H., Sun, W.-H., and Chen, C.-C. (2015b). Genetic exploration of the role of acid-sensing ion channels. Neuropharmacology *94*, 99–118.

Lin, S.-Y., Chang, W.-J., Lin, C.-S., Huang, C.-Y., Wang, H.-F., and Sun, W.-H. (2011). Serotonin Receptor 5-HT2B Mediates Serotonin-Induced Mechanical Hyperalgesia. J. Neurosci. *31*, 1410–1418.

Lingueglia, E., de Weille, J.R., Bassilana, F., Heurteaux, C., Sakai, H., Waldmann, R., and Lazdunski, M. (1997). A modulatory subunit of acid sensing ion channels in brain and dorsal root ganglion cells. J. Biol. Chem. *272*, 29778–29783.

Liu, J., Divoux, A., Sun, J., Zhang, J., Clément, K., Glickman, J.N., Sukhova, G.K., Wolters, P.J., Du, J., Gorgun, C.Z., et al. (2009). Genetic deficiency and pharmacological stabilization of mast cells reduce diet-induced obesity and diabetes in mice. Nat. Med. *15*, 940–945.

Liu, P., Xiao, Z., Ren, F., Guo, Z., Chen, Z., Zhao, H., and Cao, Y.-Q. (2013). Functional analysis of a migraine-associated TRESK K+ channel mutation. J. Neurosci. Off. J. Soc. Neurosci. *33*, 12810–12824.

Lolignier, S., Bonnet, C., Gaudioso, C., Noël, J., Ruel, J., Amsalem, M., Ferrier, J., Rodat-Despoix, L., Bouvier, V., Aissouni, Y., et al. (2015). The Nav1.9 channel is a key determinant of cold pain sensation and cold allodynia. Cell Rep. *11*, 1067–1078.

Lu, H.-C., and Mackie, K. (2016). An introduction to the endogenous cannabinoid system. Biol. Psychiatry *79*, 516–525.

Maccarrone, M., Guzmán, M., Mackie, K., Doherty, P., and Harkany, T. (2014). Programming of neural cells by (endo)cannabinoids: from physiological rules to emerging therapies. Nat. Rev. Neurosci. *15*, 786–801.

Maingret, F., Patel, A.J., Lesage, F., Lazdunski, M., and Honoré, E. (1999). Mechano- or acid stimulation, two interactive modes of activation of the TREK-1 potassium channel. J. Biol. Chem. *274*, 26691–26696.

Maingret, F., Patel, A.J., Lesage, F., Lazdunski, M., and Honoré, E. (2000). Lysophospholipids open the two-pore domain mechano-gated K(+) channels TREK-1 and TRAAK. J. Biol. Chem. *275*, 10128–10133.

Malan, T.P., and Porreca, F. (2005). Lipid mediators regulating pain sensitivity. Prostaglandins Other Lipid Mediat. *77*, 123–130.

Malik, R.A., Tesfaye, S., Newrick, P.G., Walker, D., Rajbhandari, S.M., Siddique, I., Sharma, A.K., Boulton, A.J.M., King, R.H.M., Thomas, P.K., et al. (2005). Sural nerve pathology in diabetic patients with minimal but progressive neuropathy. Diabetologia *48*, 578–585.

Mamet, J., Baron, A., Lazdunski, M., and Voilley, N. (2002). ProInflammatory Mediators, Stimulators of Sensory Neuron Excitability via the Expression of Acid-Sensing Ion Channels. J. Neurosci. *22*, 10662–10670.

Mantzoros, C.S. (1999). The role of leptin in human obesity and disease: a review of current evidence. Ann. Intern. Med. *130*, 671–680.

Marger, F., Gelot, A., Alloui, A., Matricon, J., Ferrer, J.F.S., Barrère, C., Pizzoccaro, A., Muller, E., Nargeot, J., Snutch, T.P., et al. (2011). T-type calcium channels contribute to colonic hypersensitivity in a rat model of irritable bowel syndrome. Proc. Natl. Acad. Sci. U. S. A. *108*, 11268–11273.

Markiewicz, I., and Lukomska, B. (2006). The role of astrocytes in the physiology and pathology of the central nervous system. Acta Neurobiol. Exp. (Warsz.) *66*, 343–358.

Marra, S., Ferru-Clément, R., Breuil, V., Delaunay, A., Christin, M., Friend, V., Sebille, S., Cognard, C., Ferreira, T., Roux, C., et al. (2016). Non-acidic activation of pain-related Acid-Sensing Ion Channel 3 by lipids. EMBO J. *35*, 414–428.

Martinac, B. (2014). The ion channels to cytoskeleton connection as potential mechanism of mechanosensitivity. Biochim. Biophys. Acta *1838*, 682–691.

Matsuoka, H., Tanaka, H., Sayanagi, J., Iwahashi, T., Suzuki, K., Nishimoto, S., Okada, K., Murase, T., and Yoshikawa, H. (2018). Neurotropin® Accelerates the Differentiation of Schwann Cells and Remyelination in a Rat Lysophosphatidylcholine-Induced Demyelination Model. Int. J. Mol. Sci. *19*.

Mazzuca, M., Heurteaux, C., Alloui, A., Diochot, S., Baron, A., Voilley, N., Blondeau, N., Escoubas, P., Gélot, A., Cupo, A., et al. (2007). A tarantula peptide against pain via ASIC1a channels and opioid mechanisms. Nat. Neurosci. *10*, 943–945.

McCarthy, P.W., and Lawson, S.N. (1990). Cell type and conduction velocity of rat primary sensory neurons with calcitonin gene-related peptide-like immunoreactivity. Neuroscience *34*, 623–632.

McKemy, D.D., Neuhausser, W.M., and Julius, D. (2002). Identification of a cold receptor reveals a general role for TRP channels in thermosensation. Nature *416*, 52–58.

Medzhitov, R. (2010). Inflammation 2010: New Adventures of an Old Flame. Cell *140*, 771–776.

Melmer, A., Lamina, C., Tschoner, A., Ress, C., Kaser, S., Laimer, M., Sandhofer, A., Paulweber, B., and Ebenbichler, C.F. (2013). Body adiposity index and other indexes of body composition in the SAPHIR study: Association with cardiovascular risk factors. Obesity *21*, 775–781.

Melzack, R., and Wall, P.D. (1965). Pain mechanisms: a new theory. Science *150*, 971–979.

Messinger, R.B., Naik, A.K., Jagodic, M.M., Nelson, M.T., Lee, W.Y., Choe, W.J., Orestes, P., Latham, J.R., Todorovic, S.M., and Jevtovic-Todorovic, V. (2009). In vivo silencing of the CaV3.2 T-type

calcium channels in sensory neurons alleviates hyperalgesia in rats with streptozocin-induced diabetic neuropathy. PAIN® *145*, 184–195.

Millan, M.J. (1999). The induction of pain: an integrative review. Prog. Neurobiol. *57*, 1–164.

Mishra, S.K., Tisel, S.M., Orestes, P., Bhangoo, S.K., and Hoon, M.A. (2011). TRPV1-lineage neurons are required for thermal sensation. EMBO J. *30*, 582–593.

Mizisin, A.P. (2014). Chapter 27 - Mechanisms of diabetic neuropathy: Schwann cells. In Handbook of Clinical Neurology, D.W. Zochodne, and R.A. Malik, eds. (Elsevier), pp. 401–428.

Moayedi, M., and Davis, K.D. (2012). Theories of pain: from specificity to gate control. J. Neurophysiol. *109*, 5–12.

Moehring, F., Halder, P., Seal, R.P., and Stucky, C.L. (2018). Uncovering the Cells and Circuits of Touch in Normal and Pathological Settings. Neuron *100*, 349–360.

Mogil, J.S., Breese, N.M., Witty, M.-F., Ritchie, J., Rainville, M.-L., Ase, A., Abbadi, N., Stucky, C.L., and Séguéla, P. (2005). Transgenic Expression of a Dominant-Negative ASIC3 Subunit Leads to Increased Sensitivity to Mechanical and Inflammatory Stimuli. J. Neurosci. *25*, 9893–9901.

Mokdad, A.H., Marks, J.S., Stroup, D.F., and Gerberding, J.L. (2004). Actual causes of death in the United States, 2000. JAMA *291*, 1238–1245.

Monet, M., Gkika, D., Lehen'kyi, V., Pourtier, A., Vanden Abeele, F., Bidaux, G., Juvin, V., Rassendren, F., Humez, S., and Prevarsakaya, N. (2009). Lysophospholipids stimulate prostate cancer cell migration via TRPV2 channel activation. Biochim. Biophys. Acta *1793*, 528–539.

Montague, C.T., Farooqi, I.S., Whitehead, J.P., Soos, M.A., Rau, H., Wareham, N.J., Sewter, C.P., Digby, J.E., Mohammed, S.N., Hurst, J.A., et al. (1997). Congenital leptin deficiency is associated with severe early-onset obesity in humans. Nature *387*, 903.

Moon, H.-S., Dalamaga, M., Kim, S.-Y., Polyzos, S.A., Hamnvik, O.-P., Magkos, F., Paruthi, J., and Mantzoros, C.S. (2013). Leptin's role in lipodystrophic and nonlipodystrophic insulin-resistant and diabetic individuals. Endocr. Rev. *34*, 377–412.

Morales-Lázaro, S.L., Lemus, L., and Rosenbaum, T. (2016). Regulation of thermoTRPs by lipids. Temp. Multidiscip. Biomed. J. *4*, 24–40.

Moran, M.M., and Szallasi, A. (2018). Targeting nociceptive transient receptor potential channels to treat chronic pain: current state of the field. Br. J. Pharmacol. *175*, 2185–2203.

Moreno-Navarrete, J.M., Catalán, V., Whyte, L., Díaz-Arteaga, A., Vázquez-Martínez, R., Rotellar, F., Guzmán, R., Gómez-Ambrosi, J., Pulido, M.R., Russell, W.R., et al. (2012). The L-α-lysophosphatidylinositol/GPR55 system and its potential role in human obesity. Diabetes *61*, 281–291.

Muller, C., Morales, P., and Reggio, P.H. (2018). Cannabinoid Ligands Targeting TRP Channels. Front. Mol. Neurosci. *11*, 487.

Murakami, N., Yokomizo, T., Okuno, T., and Shimizu, T. (2004). G2A Is a Proton-sensing G-protein-coupled Receptor Antagonized by Lysophosphatidylcholine. J. Biol. Chem. *279*, 42484–42491.

Nagai, J., Uchida, H., Matsushita, Y., yano, R., Ueda, M., Niwa, M., Aoki, J., Chun, J., and Ueda, H. (2010). Autotaxin and lysophosphatidic acid1 receptor-mediated demyelination of dorsal root fibers by sciatic nerve injury and intrathecal lysophosphatidylcholine. Mol. Pain *6*, 78.

Nagy, J.I., and Hunt, S.P. (1982). Fluoride-resistant acid phosphatase-containing neurones in dorsal root ganglia are separate from those containing substance P or somatostatin. Neuroscience *7*, 89–97.

Nakamura, T., Furuhashi, M., Li, P., Cao, H., Tuncman, G., Sonenberg, N., Gorgun, C.Z., and Hotamisligil, G.S. (2010). Double-stranded RNA-dependent protein kinase links pathogen sensing with stress and metabolic homeostasis. Cell *140*, 338–348.

Nascimento, D.S.M., Castro-Lopes, J.M., and Moreira Neto, F.L. (2014). Satellite glial cells surrounding primary afferent neurons are activated and proliferate during monoarthritis in rats: is there a role for ATF3? PloS One *9*, e108152.

Neelands, T.R., Zhang, X.-F., McDonald, H., and Puttfarcken, P. (2010). Differential effects of temperature on acid-activated currents mediated by TRPV1 and ASIC channels in rat dorsal root ganglion neurons. Brain Res. *1329*, 55–66.

Ng, M., Fleming, T., Robinson, M., Thomson, B., Graetz, N., Margono, C., Mullany, E.C., Biryukov, S., Abbafati, C., Abera, S.F., et al. (2014). Global, regional and national prevalence of overweight and obesity in children and adults 1980-2013: A systematic analysis. Lancet Lond. Engl. *384*, 766–781.

Nieto-Posadas, A., Picazo-Juárez, G., Llorente, I., Jara-Oseguera, A., Morales-Lázaro, S., Escalante-Alcalde, D., Islas, L.D., and Rosenbaum, T. (2011). Lysophosphatidic acid directly activates TRPV1 through a C-terminal binding site. Nat. Chem. Biol. *8*, 78–85.

Nilius, B., Talavera, K., Owsianik, G., Prenen, J., Droogmans, G., and Voets, T. (2005). Gating of TRP channels: a voltage connection? J. Physiol. *567*, 35–44.

Noël, J., Zimmermann, K., Busserolles, J., Deval, E., Alloui, A., Diochot, S., Guy, N., Borsotto, M., Reeh, P., Eschalier, A., et al. (2009). The mechano-activated K+ channels TRAAK and TREK-1 control both warm and cold perception. EMBO J. *28*, 1308–1318.

Noël, J., Sandoz, G., and Lesage, F. (2011). Molecular regulations governing TREK and TRAAK channel functions. Channels Austin Tex *5*, 402–409.

Oates, P.J. (2008). Aldose Reductase, Still a Compelling Target for Diabetic Neuropathy.

O'Brien, P.D., Sakowski, S.A., and Feldman, E.L. (2014). Mouse models of diabetic neuropathy. ILAR J. Natl. Res. Counc. Inst. Lab. Anim. Resour. *54*, 259–272.

Obrosova, I.G., Ilnytska, O., Lyzogubov, V.V., Pavlov, I.A., Mashtalir, N., Nadler, J.L., and Drel, V.R. (2007). High-Fat Diet–Induced Neuropathy of Pre-Diabetes and Obesity: Effects of "Healthy" Diet and Aldose Reductase Inhibition. Diabetes *56*, 2598–2608.

Ohmura, K., Ishimori, N., Ohmura, Y., Tokuhara, S., Nozawa, A., Horii, S., Andoh, Y., Fujii, S., Iwabuchi, K., Onoé, K., et al. (2010). Natural killer T cells are involved in adipose tissues inflammation and glucose intolerance in diet-induced obese mice. Arterioscler. Thromb. Vasc. Biol. *30*, 193–199.

Ohta, T., Ikemi, Y., Murakami, M., Imagawa, T., Otsuguro, K., and Ito, S. (2006). Potentiation of transient receptor potential V1 functions by the activation of metabotropic 5-HT receptors in rat primary sensory neurons: 5-HT-induced potentiation of TRPV1 in DRG neurons. J. Physiol. *576*, 809–822.

Okifuji, A., and Hare, B.D. (2015). The association between chronic pain and obesity. J. Pain Res. *8*, 399–408.

Olefsky, J.M., and Glass, C.K. (2010). Macrophages, inflammation, and insulin resistance. Annu. Rev. Physiol. *72*, 219–246.

Orestes, P., Osuru, H.P., McIntire, W.E., Jacus, M.O., Salajegheh, R., Jagodic, M.M., Choe, W., Lee, J., Lee, S.-S., Rose, K.E., et al. (2013). Reversal of Neuropathic Pain in Diabetes by Targeting Glycosylation of Cav3.2 T-Type Calcium Channels. Diabetes *62*, 3828–3838.

Ossipov, M.H., Morimura, K., and Porreca, F. (2014). Descending pain modulation and chronification of pain. Curr. Opin. Support. Palliat. Care *8*, 143–151.

Page, A.J., Brierley, S.M., Martin, C.M., Martinez-Salgado, C., Wemmie, J.A., Brennan, T.J., Symonds, E., Omari, T., Lewin, G.R., Welsh, M.J., et al. (2004). The ion channel ASIC1 contributes to visceral but not cutaneous mechanoreceptor function. Gastroenterology *127*, 1739–1747.

Pan, H.-L., Liu, B.-L., Lin, W., and Zhang, Y.-Q. (2016). Modulation of Nav1.8 by Lysophosphatidic Acid in the Induction of Bone Cancer Pain. Neurosci. Bull. *32*, 445–454.

Park, H.-K., and Ahima, R.S. (2015). Physiology of leptin: energy homeostasis, neuroendocrine function and metabolism. Metabolism. *64*, 24–34.

Park, U., Vastani, N., Guan, Y., Raja, S.N., Koltzenburg, M., and Caterina, M.J. (2011). TRP vanilloid 2 knock-out mice are susceptible to perinatal lethality but display normal thermal and mechanical nociception. J. Neurosci. Off. J. Soc. Neurosci. *31*, 11425–11436.

Peier, A.M., Reeve, A.J., Andersson, D.A., Moqrich, A., Earley, T.J., Hergarden, A.C., Story, G.M., Colley, S., Hogenesch, J.B., McIntyre, P., et al. (2002a). A heat-sensitive TRP channel expressed in keratinocytes. Science *296*, 2046–2049.

Peier, A.M., Moqrich, A., Hergarden, A.C., Reeve, A.J., Andersson, D.A., Story, G.M., Earley, T.J., Dragoni, I., McIntyre, P., Bevan, S., et al. (2002b). A TRP channel that senses cold stimuli and menthol. Cell *108*, 705–715.

Peigneur, S., Béress, L., Möller, C., Marí, F., Forssmann, W.-G., and Tytgat, J. (2012). A natural point mutation changes both target selectivity and mechanism of action of sea anemone toxins. FASEB J. Off. Publ. Fed. Am. Soc. Exp. Biol. *26*, 5141–5151.

Peirs, C., and Seal, R.P. (2016). Neural circuits for pain: Recent advances and current views. Science *354*, 578–584.

Perea, G., Navarrete, M., and Araque, A. (2009). Tripartite synapses: astrocytes process and control synaptic information. Trends Neurosci. *32*, 421–431.

Petersen, M., Segond von Banchet, G., Heppelmann, B., and Koltzenburg, M. (1998). Nerve growth factor regulates the expression of bradykinin binding sites on adult sensory neurons via the neurotrophin receptor p75. Neuroscience *83*, 161–168.

Pinho-Ribeiro, F.A., Verri, W.A., and Chiu, I.M. (2017). Nociceptor Sensory Neuron-Immune Interactions in Pain and Inflammation. Trends Immunol. *38*, 5–19.

Piomelli, D., Hohmann, A.G., Seybold, V., and Hammock, B.D. (2014). A lipid gate for the peripheral control of pain. J. Neurosci. Off. J. Soc. Neurosci. *34*, 15184–15191.

Pop-Busui, R., Boulton, A.J.M., Feldman, E.L., Bril, V., Freeman, R., Malik, R.A., Sosenko, J.M., and Ziegler, D. (2017). Diabetic Neuropathy: A Position Statement by the American Diabetes Association. Diabetes Care *40*, 136–154.

Pouliot, M.C., Després, J.P., Nadeau, A., Moorjani, S., Prud'Homme, D., Lupien, P.J., Tremblay, A., and Bouchard, C. (1992). Visceral obesity in men. Associations with glucose tolerance, plasma insulin, and lipoprotein levels. Diabetes *41*, 826–834.

Price, M.P., Snyder, P.M., and Welsh, M.J. (1996). Cloning and expression of a novel human brain Na+ channel. J. Biol. Chem. *271*, 7879–7882.

Price, M.P., McIlwrath, S.L., Xie, J., Cheng, C., Qiao, J., Tarr, D.E., Sluka, K.A., Brennan, T.J., Lewin, G.R., and Welsh, M.J. (2001). The DRASIC Cation Channel Contributes to the Detection of Cutaneous Touch and Acid Stimuli in Mice. Neuron *32*, 1071–1083.

Priest, B.T., Murphy, B.A., Lindia, J.A., Diaz, C., Abbadie, C., Ritter, A.M., Liberator, P., Iyer, L.M., Kash, S.F., Kohler, M.G., et al. (2005). Contribution of the tetrodotoxin-resistant voltage-gated

sodium channel NaV1.9 to sensory transmission and nociceptive behavior. Proc. Natl. Acad. Sci. U. S. A. *102*, 9382–9387.

Primeaux, S.D., Blackmon, C., Barnes, M.J., Braymer, H.D., and Bray, G.A. (2008). Central administration of the RFamide peptides, QRFP-26 and QRFP-43, increases high fat food intake in rats. Peptides *29*, 1994–2000.

Qiu, F., Qiu, C.-Y., Liu, Y.-Q., Wu, D., Li, J.-D., and Hu, W.-P. (2012). Potentiation of acid-sensing ion channel activity by the activation of 5-HT2 receptors in rat dorsal root ganglion neurons. Neuropharmacology *63*, 494–500.

Qiu, F., Qiu, C.-Y., Cai, H., Liu, T.-T., Qu, Z.-W., Yang, Z., Li, J.-D., Zhou, Q.-Y., and Hu, W.-P. (2014). Oxytocin inhibits the activity of acid-sensing ion channels through the vasopressin, V1A receptor in primary sensory neurons. Br. J. Pharmacol. *171*, 3065–3076.

Quick, K., Zhao, J., Eijkelkamp, N., Linley, J.E., Rugiero, F., Cox, J.J., Raouf, R., Gringhuis, M., Sexton, J.E., Abramowitz, J., et al. (2012). TRPC3 and TRPC6 are essential for normal mechanotransduction in subsets of sensory neurons and cochlear hair cells. Open Biol. *2*, 120068.

Ramaswamy, S.S., MacLean, D.M., Gorfe, A.A., and Jayaraman, V. (2013). Proton-mediated conformational changes in an acid-sensing ion channel. J. Biol. Chem. *288*, 35896–35903.

Ranade, S.S., Woo, S.-H., Dubin, A.E., Moshourab, R.A., Wetzel, C., Petrus, M., Mathur, J., Bégay, V., Coste, B., Mainquist, J., et al. (2014). Piezo2 is the major transducer of mechanical forces for touch sensation in mice. Nature *516*, 121–125.

Ranade, S.S., Syeda, R., and Patapoutian, A. (2015). Mechanically Activated Ion Channels. Neuron *87*, 1162–1179.

Rash, L.D. (2017a). Chapter Two - Acid-Sensing Ion Channel Pharmacology, Past, Present, and Future …. In Advances in Pharmacology, D.P. Geraghty, and L.D. Rash, eds. (Academic Press), pp. 35–66.

Rash, L.D. (2017b). Acid-Sensing Ion Channel Pharmacology, Past, Present, and Future …. In Advances in Pharmacology, (Elsevier), pp. 35–66.

Reeh, P.W., and Steen, K.H. (1996). Tissue acidosis in nociception and pain. Prog. Brain Res. *113*, 143–151.

Renaud, J.F., Scanu, A.M., Kazazoglou, T., Lombet, A., Romey, G., and Lazdunski, M. (1982). Normal serum and lipoprotein-deficient serum give different expressions of excitability, corresponding to different stages of differentiation, in chicken cardiac cells in culture. Proc. Natl. Acad. Sci. *79*, 7768–7772.

Riaz, A., Huang, Y., and Johansson, S. (2016). G-Protein-Coupled Lysophosphatidic Acid Receptors and Their Regulation of AKT Signaling. Int. J. Mol. Sci. *17*.

Rivera, R., and Chun, J. (2008). Biological effects of lysophospholipids. Rev. Physiol. Biochem. Pharmacol. *160*, 25–46.

Rizzo, M.A., Kocsis, J.D., and Waxman, S.G. (1994). Slow sodium conductances of dorsal root ganglion neurons: intraneuronal homogeneity and interneuronal heterogeneity. J. Neurophysiol. *72*, 2796–2815.

Rocha-González, H.I., Herrejon-Abreu, E.B., López-Santillán, F.J., García-López, B.E., Murbartián, J., and Granados-Soto, V. (2009). Acid increases inflammatory pain in rats: Effect of local peripheral ASICs inhibitors. Eur. J. Pharmacol. *603*, 56–61.

Rosa, D.A. de la, Zhang, P., Shao, D., White, F., and Canessa, C.M. (2002). Functional implications of the localization and activity of acid-sensitive channels in rat peripheral nervous system. Proc. Natl. Acad. Sci. *99*, 2326–2331.

Rose, K.E., Lunardi, N., Boscolo, A., Dong, X., Erisir, A., Jevtovic-Todorovic, V., and Todorovic, S.M. (2013). Immunohistological demonstration of CaV3.2 T-type voltage-gated calcium channel expression in soma of dorsal root ganglion neurons and peripheral axons of rat and mouse. Neuroscience *250*, 263–274.

Royal, P., Andres-Bilbe, A., Ávalos Prado, P., Verkest, C., Wdziekonski, B., Schaub, S., Baron, A., Lesage, F., Gasull, X., Levitz, J., et al. (2019). Migraine-Associated TRESK Mutations Increase Neuronal Excitability through Alternative Translation Initiation and Inhibition of TREK. Neuron *101*, 232-245.e6.

Russo, A.F. (2017). Overview of neuropeptides: awakening the senses? Headache *57*, 37–46.

Saberi, M., Woods, N.-B., de Luca, C., Schenk, S., Lu, J.C., Bandyopadhyay, G., Verma, I.M., and Olefsky, J.M. (2009). Hematopoietic cell-specific deletion of toll-like receptor 4 ameliorates hepatic and adipose tissue insulin resistance in high-fat-fed mice. Cell Metab. *10*, 419–429.

Saghizadeh, M., Ong, J.M., Garvey, W.T., Henry, R.R., and Kern, P.A. (1996). The expression of TNF alpha by human muscle. Relationship to insulin resistance. J. Clin. Invest. *97*, 1111–1116.

Salinas, M., Lazdunski, M., and Lingueglia, E. (2009). Structural elements for the generation of sustained currents by the acid pain sensor ASIC3. J. Biol. Chem. *284*, 31851–31859.

Salvemini, D., Doyle, T., Kress, M., and Nicol, G. (2013). Therapeutic targeting of the ceramide-to-sphingosine 1-phosphate pathway in pain. Trends Pharmacol. Sci. *34*, 110–118.

Saugstad, J.A., Roberts, J.A., Dong, J., Zeitouni, S., and Evans, R.J. (2004). Analysis of the membrane topology of the acid-sensing ion channel 2a. J. Biol. Chem. *279*, 55514–55519.

Schaible, H.G. (2007). Peripheral and central mechanisms of pain generation. Handb. Exp. Pharmacol. 3–28.

Schroder, K., Zhou, R., and Tschopp, J. (2010). The NLRP3 inflammasome: a sensor for metabolic danger? Science *327*, 296–300.

Sekiguchi, F., Tsubota, M., and Kawabata, A. (2018). Involvement of Voltage-Gated Calcium Channels in Inflammation and Inflammatory Pain. Biol. Pharm. Bull. *41*, 1127–1134.

Serhan, C.N. (2014). Novel Pro-Resolving Lipid Mediators in Inflammation Are Leads for Resolution Physiology. Nature *510*, 92–101.

Seung Lee, W., Hong, M.-P., Hoon Kim, T., Kyoo Shin, Y., Soo Lee, C., Park, M., and Song, J.-H. (2005). Effects of lysophosphatidic acid on sodium currents in rat dorsal root ganglion neurons. Brain Res. *1035*, 100–104.

Sevastou, I., Kaffe, E., Mouratis, M.-A., and Aidinis, V. (2013). Lysoglycerophospholipids in chronic inflammatory disorders: the PLA(2)/LPC and ATX/LPA axes. Biochim. Biophys. Acta *1831*, 42–60.

Sexton, J.E., Vernon, J., and Wood, J.N. (2014). TRPs and Pain. In Mammalian Transient Receptor Potential (TRP) Cation Channels: Volume II, B. Nilius, and V. Flockerzi, eds. (Cham: Springer International Publishing), pp. 873–897.

Sherwood, T.W., Lee, K.G., Gormley, M.G., and Askwith, C.C. (2011). Heteromeric acid-sensing ion channels (ASICs) composed of ASIC2b and ASIC1a display novel channel properties and contribute to acidosis-induced neuronal death. J. Neurosci. Off. J. Soc. Neurosci. *31*, 9723–9734.

Shi, H., Kokoeva, M.V., Inouye, K., Tzameli, I., Yin, H., and Flier, J.S. (2006). TLR4 links innate immunity and fatty acid-induced insulin resistance. J. Clin. Invest. *116*, 3015–3025.

Shibasaki, K., Ishizaki, Y., and Mandadi, S. (2013). Astrocytes express functional TRPV2 ion channels. Biochem. Biophys. Res. Commun. *441*, 327–332.

Shindou, H., Hishikawa, D., Harayama, T., Eto, M., and Shimizu, T. (2013). Generation of membrane diversity by lysophospholipid acyltransferases. J. Biochem. (Tokyo) *154*, 21–28.

Shoelson, S.E., Lee, J., and Goldfine, A.B. (2006). Inflammation and insulin resistance. J. Clin. Invest. *116*, 1793–1801.

Shubayev, V.I., and Myers, R.R. (2001). Axonal transport of TNF-alpha in painful neuropathy: distribution of ligand tracer and TNF receptors. J. Neuroimmunol. *114*, 48–56.

Siemionow, K., Klimczak, A., Brzezicki, G., Siemionow, M., and McLain, R.F. (2009). The effects of inflammation on glial fibrillary acidic protein expression in satellite cells of the dorsal root ganglion. Spine *34*, 1631–1637.

Silverman, J.D., and Kruger, L. (1988). Lectin and neuropeptide labeling of separate populations of dorsal root ganglion neurons and associated “nociceptor” thin axons in rat testis and cornea whole-mount preparations. Somatosens. Res. *5*, 259–267.

Singleton, J.R., Smith, A.G., Russell, J., and Feldman, E.L. (2005). Polyneuropathy with Impaired Glucose Tolerance: Implications for Diagnosis and Therapy. Curr. Treat. Options Neurol. *7*, 33–42.

Smith, H.S. (2006). Arachidonic acid pathways in nociception. J. Support. Oncol. *4*, 277–287.

Smith, A.G., and Singleton, J.R. (2008). Impaired glucose tolerance and neuropathy. The Neurologist *14*, 23–29.

Smith, E.S., Cadiou, H., and McNaughton, P.A. (2007). Arachidonic acid potentiates acid-sensing ion channels in rat sensory neurons by a direct action. Neuroscience *145*, 686–698.

Smith, G.D., Gunthorpe, M.J., Kelsell, R.E., Hayes, P.D., Reilly, P., Facer, P., Wright, J.E., Jerman, J.C., Walhin, J.-P., Ooi, L., et al. (2002). TRPV3 is a temperature-sensitive vanilloid receptor-like protein. Nature *418*, 186–190.

Smith, W.L., DeWitt, D.L., and Garavito, R.M. (2000). Cyclooxygenases: structural, cellular, and molecular biology. Annu. Rev. Biochem. *69*, 145–182.

Sofroniew, M.V. (1983). Morphology of vasopressin and oxytocin neurones and their central and vascular projections. Prog. Brain Res. *60*, 101–114.

Sofroniew, M.V., and Vinters, H.V. (2010). Astrocytes: biology and pathology. Acta Neuropathol. (Berl.) *119*, 7–35.

Song, M.J., Kim, K.H., Yoon, J.M., and Kim, J.B. (2006). Activation of Toll-like receptor 4 is associated with insulin resistance in adipocytes. Biochem. Biophys. Res. Commun. *346*, 739–745.

Song, Z., Xie, W., Chen, S., Strong, J.A., Print, M.S., Wang, J.I., Shareef, A.F., Ulrich-Lai, Y.M., and Zhang, J.-M. (2017). High-fat diet increases pain behaviors in rats with or without obesity. Sci. Rep. *7*, 10350.

Speliotes, E.K., Willer, C.J., Berndt, S.I., Monda, K.L., Thorleifsson, G., Jackson, A.U., Lango Allen, H., Lindgren, C.M., Luan, J., Mägi, R., et al. (2010). Association analyses of 249,796 individuals reveal 18 new loci associated with body mass index. Nat. Genet. *42*, 937–948.

Spiegelman, B.M., and Flier, J.S. (2001). Obesity and the regulation of energy balance. Cell *104*, 531–543.

Stino, A.M., and Smith, A.G. (2017). Peripheral neuropathy in prediabetes and the metabolic syndrome. J. Diabetes Investig. *8*, 646–655.

Story, G.M., Peier, A.M., Reeve, A.J., Eid, S.R., Mosbacher, J., Hricik, T.R., Earley, T.J., Hergarden, A.C., Andersson, D.A., Hwang, S.W., et al. (2003). ANKTM1, a TRP-like channel expressed in nociceptive neurons, is activated by cold temperatures. Cell *112*, 819–829.

Strobel, A., Issad, T., Camoin, L., Ozata, M., and Strosberg, A.D. (1998). A leptin missense mutation associated with hypogonadism and morbid obesity. Nat. Genet. *18*, 213.

Sullivan, K.A., Hayes, J.M., Wiggin, T.D., Backus, C., Oh, S.S., Lentz, S.I., Brosius, F., and Feldman, E.L. (2007). Mouse Models of Diabetic Neuropathy. Neurobiol. Dis. *28*, 276–285.

Sun, W., Miao, B., Wang, X.-C., Duan, J.-H., Wang, W.-T., Kuang, F., Xie, R.-G., Xing, J.-L., Xu, H., Song, X.-J., et al. (2012). Reduced conduction failure of the main axon of polymodal nociceptive C-fibres contributes to painful diabetic neuropathy in rats. Brain *135*, 359–375.

Syvänne, M., and Taskinen, M.R. (1997). Lipids and lipoproteins as coronary risk factors in non-insulin-dependent diabetes mellitus. Lancet Lond. Engl. *350 Suppl 1*, SI20-23.

Takayama, Y., Uta, D., Furue, H., and Tominaga, M. (2015). Pain-enhancing mechanism through interaction between TRPV1 and anoctamin 1 in sensory neurons. Proc. Natl. Acad. Sci. *112*, 5213–5218.

Tan, C.-H., and McNaughton, P.A. (2016). The TRPM2 ion channel is required for sensitivity to warmth. Nature *536*, 460–463.

Tartaglia, L.A. (1997). The Leptin Receptor. J. Biol. Chem. *272*, 6093–6096.

Tesfaye, S., Boulton, A.J.M., Dyck, P.J., Freeman, R., Horowitz, M., Kempler, P., Lauria, G., Malik, R.A., Spallone, V., Vinik, A., et al. (2010). Diabetic Neuropathies: Update on Definitions, Diagnostic Criteria, Estimation of Severity, and Treatments. Diabetes Care *33*, 2285–2293.

Theile, J.W., and Cummins, T.R. (2011). Recent developments regarding voltage-gated sodium channel blockers for the treatment of inherited and acquired neuropathic pain syndromes. Front. Pharmacol. *2*, 54.

Themistocleous, A.C., Ramirez, J.D., Shillo, P.R., Lees, J.G., Selvarajah, D., Orengo, C., Tesfaye, S., Rice, A.S.C., and Bennett, D.L.H. (2016). The Pain in Neuropathy Study (PiNS): a cross-sectional observational study determining the somatosensory phenotype of painful and painless diabetic neuropathy. Pain *157*, 1132–1145.

Todorovic, S.M. (2016). Painful Diabetic Neuropathy. In International Review of Neurobiology, (Elsevier), pp. 211–225.

Tokunaga, A., Saika, M., and Senba, E. (1998). 5-HT2A receptor subtype is involved in the thermal hyperalgesic mechanism of serotonin in the periphery. Pain *76*, 349–355.

Tsantoulas, C., and McMahon, S.B. (2014). Opening paths to novel analgesics: the role of potassium channels in chronic pain. Trends Neurosci. *37*, 146–158.

Tsantoulas, C., Laínez, S., Wong, S., Mehta, I., Vilar, B., and McNaughton, P.A. (2017). Hyperpolarization-activated cyclic nucleotide-gated 2 (HCN2) ion channels drive pain in mouse models of diabetic neuropathy. Sci. Transl. Med. *9*, eaam6072.

Tulleuda, A., Cokic, B., Callejo, G., Saiani, B., Serra, J., and Gasull, X. (2011). TRESK channel contribution to nociceptive sensory neurons excitability: modulation by nerve injury. Mol. Pain *7*, 30.

Twells, L.K., Gregory, D.M., Reddigan, J., and Midodzi, W.K. (2014). Current and predicted prevalence of obesity in Canada: a trend analysis. CMAJ Open *2*, E18-26.

Ueda, H. (2008). Peripheral Mechanisms of Neuropathic Pain — Involvement of Lysophosphatidic Acid Receptor-Mediated Demyelination. Mol. Pain *4*, 1744-8069-4–11.

Ueda, H. (2011). Lysophosphatidic acid as the initiator of neuropathic pain. Biol. Pharm. Bull. *34*, 1154–1158.

Ugawa, S., Ueda, T., Ishida, Y., Nishigaki, M., Shibata, Y., and Shimada, S. (2002). Amiloride-blockable acid-sensing ion channels are leading acid sensors expressed in human nociceptors. J. Clin. Invest. *110*, 1185–1190.

Usoskin, D., Furlan, A., Islam, S., Abdo, H., Lönnerberg, P., Lou, D., Hjerling-Leffler, J., Haeggström, J., Kharchenko, O., Kharchenko, P.V., et al. (2015). Unbiased classification of sensory neuron types by large-scale single-cell RNA sequencing. Nat. Neurosci. *18*, 145–153.

Uysal, K.T., Wiesbrock, S.M., Marino, M.W., and Hotamisligil, G.S. (1997). Protection from obesity-induced insulin resistance in mice lacking TNF-alpha function. Nature *389*, 610–614.

Uysal, K.T., Wiesbrock, S.M., and Hotamisligil, G.S. (1998). Functional analysis of tumor necrosis factor (TNF) receptors in TNF-alpha-mediated insulin resistance in genetic obesity. Endocrinology *139*, 4832–4838.

Vandewauw, I., De Clercq, K., Mulier, M., Held, K., Pinto, S., Van Ranst, N., Segal, A., Voet, T., Vennekens, R., Zimmermann, K., et al. (2018). A TRP channel trio mediates acute noxious heat sensing. Nature *555*, 662–666.

Vane, J.R. (2002). Biomedicine. Back to an aspirin a day? Science *296*, 474–475.

Vareniuk, I., Pavlov, I.A., Drel, V.R., Lyzogubov, V.V., Ilnytska, O., Bell, S.R., Tibrewala, J., Groves, J.T., and Obrosova, I.G. (2007). Nitrosative stress and peripheral diabetic neuropathy in leptin-deficient (ob/ob) mice. Exp. Neurol. *205*, 425–436.

Verhaak, P.F.M., Kerssens, J.J., Dekker, J., Sorbi, M.J., and Bensing, J.M. (1998). Prevalence of chronic benign pain disorder among adults: a review of the literature. Pain *77*, 231–239.

Verkest, C., Piquet, E., Diochot, S., Dauvois, M., Lanteri-Minet, M., Lingueglia, E., and Baron, A. (2018). Effects of systemic inhibitors of acid-sensing ion channels 1 (ASIC1) against acute and chronic mechanical allodynia in a rodent model of migraine. Br. J. Pharmacol. *175*, 4154–4166.

Viero, C., Shibuya, I., Kitamura, N., Verkhratsky, A., Fujihara, H., Katoh, A., Ueta, Y., Zingg, H.H., Chvatal, A., Sykova, E., et al. (2010). REVIEW: Oxytocin: Crossing the bridge between basic science and pharmacotherapy. CNS Neurosci. Ther. *16*, e138-156.

Vincent, A.M., Hayes, J.M., McLean, L.L., Vivekanandan-Giri, A., Pennathur, S., and Feldman, E.L. (2009a). Dyslipidemia-Induced Neuropathy in Mice. Diabetes *58*, 2376–2385.

Vincent, A.M., Hinder, L.M., Pop-Busui, R., and Feldman, E.L. (2009b). Hyperlipidemia: a new therapeutic target for diabetic neuropathy. J. Peripher. Nerv. Syst. JPNS *14*, 257–267.

Voilley, N., Weille, J. de, Mamet, J., and Lazdunski, M. (2001). Nonsteroid Anti-Inflammatory Drugs Inhibit Both the Activity and the Inflammation-Induced Expression of Acid-Sensing Ion Channels in Nociceptors. J. Neurosci. *21*, 8026–8033.

Vriens, J., Owsianik, G., Hofmann, T., Philipp, S.E., Stab, J., Chen, X., Benoit, M., Xue, F., Janssens, A., Kerselaers, S., et al. (2011). TRPM3 Is a Nociceptor Channel Involved in the Detection of Noxious Heat. Neuron *70*, 482–494.

Vullo, S., and Kellenberger, S. (2019). A molecular view of the function and pharmacology of acid-sensing ion channels. Pharmacol. Res.

Walder, R.Y., Rasmussen, L.A., Rainier, J.D., Light, A.R., Wemmie, J.A., and Sluka, K.A. (2010). ASIC1 and ASIC3 Play Different Roles in the Development of Hyperalgesia After Inflammatory Muscle Injury. J. Pain *11*, 210–218.

Waldmann, R., Champigny, G., Voilley, N., Lauritzen, I., and Lazdunski, M. (1996). The mammalian degenerin MDEG, an amiloride-sensitive cation channel activated by mutations causing neurodegeneration in Caenorhabditis elegans. J. Biol. Chem. *271*, 10433–10436.

Waldmann, R., Champigny, G., Bassilana, F., Heurteaux, C., and Lazdunski, M. (1997a). A proton-gated cation channel involved in acid-sensing. Nature *386*, 173–177.

Waldmann, R., Bassilana, F., Weille, J. de, Champigny, G., Heurteaux, C., and Lazdunski, M. (1997b). Molecular Cloning of a Non-inactivating Proton-gated Na+ Channel Specific for Sensory Neurons. J. Biol. Chem. *272*, 20975–20978.

Wang, Y.-Z., and Xu, T.-L. (2011). Acidosis, Acid-Sensing Ion Channels, and Neuronal Cell Death. Mol. Neurobiol. *44*, 350–358.

Wang, F., Bélanger, E., Côté, S.L., Desrosiers, P., Prescott, S.A., Côté, D.C., and De Koninck, Y. (2018). Sensory Afferents Use Different Coding Strategies for Heat and Cold. Cell Rep. *23*, 2001–2013.

Wang, H., Storlien, L.H., and Huang, X.-F. (2002a). Effects of dietary fat types on body fatness, leptin, and ARC leptin receptor, NPY, and AgRP mRNA expression. Am. J. Physiol. Endocrinol. Metab. *282*, E1352-1359.

Wang, J.T., Medress, Z.A., and Barres, B.A. (2012). Axon degeneration: molecular mechanisms of a self-destruction pathway. J. Cell Biol. *196*, 7–18.

Wang, X., Li, W.-G., Yu, Y., Xiao, X., Cheng, J., Zeng, W.-Z., Peng, Z., Zhu, M.X., and Xu, T.-L. (2013). Serotonin Facilitates Peripheral Pain Sensitivity in a Manner That Depends on the Nonproton Ligand Sensing Domain of ASIC3 Channel. J. Neurosci. *33*, 4265–4279.

Wang, X.Y., Yan, W.W., Zhang, X.L., Liu, H., and Zhang, L.C. (2014). ASIC3 in the cerebrospinal fluid-contacting nucleus of brain parenchyma contributes to inflammatory pain in rats. Neurol. Res. *36*, 270–275.

Wang, Y., Miura, Y., Kaneko, T., Li, J., Qin, L.-Q., Wang, P.-Y., Matsui, H., and Sato, A. (2002b). Glucose intolerance induced by a high-fat/low-carbohydrate diet in rats effects of nonesterified fatty acids. Endocrine *17*, 185–191.

Warwick, Z.S. (1996). Probing the causes of high-fat diet hyperphagia: A mechanistic and behavioral dissection. Neurosci. Biobehav. Rev. *20*, 155–161.

Wei, H., Hämäläinen, M.M., Saarnilehto, M., Koivisto, A., and Pertovaara, A. (2009). Attenuation of Mechanical Hypersensitivity by an Antagonist of the TRPA1 Ion Channel in Diabetic Animals. Anesthesiol. J. Am. Soc. Anesthesiol. *111*, 147–154.

Weisberg, S.P., McCann, D., Desai, M., Rosenbaum, M., Leibel, R.L., and Ferrante, A.W. (2003). Obesity is associated with macrophage accumulation in adipose tissue. J. Clin. Invest. *112*, 1796–1808.

Wellen, K.E., Fucho, R., Gregor, M.F., Furuhashi, M., Morgan, C., Lindstad, T., Vaillancourt, E., Gorgun, C.Z., Saatcioglu, F., and Hotamisligil, G.S. (2007). Coordinated regulation of nutrient and inflammatory responses by STAMP2 is essential for metabolic homeostasis. Cell *129*, 537–548.

Wemmie, J.A., Chen, J., Askwith, C.C., Hruska-Hageman, A.M., Price, M.P., Nolan, B.C., Yoder, P.G., Lamani, E., Hoshi, T., Freeman, J.H., et al. (2002). The Acid-Activated Ion Channel ASIC Contributes to Synaptic Plasticity, Learning, and Memory. Neuron *34*, 463–477.

Wemmie, J.A., Askwith, C.C., Lamani, E., Cassell, M.D., Freeman, J.H., and Welsh, M.J. (2003). Acid-Sensing Ion Channel 1 Is Localized in Brain Regions with High Synaptic Density and Contributes to Fear Conditioning. J. Neurosci. *23*, 5496–5502.

Wiesenfeld-Hallin, Z., Hökfelt, T., Lundberg, J.M., Forssmann, W.G., Reinecke, M., Tschopp, F.A., and Fischer, J.A. (1984). Immunoreactive calcitonin gene-related peptide and substance P coexist in sensory neurons to the spinal cord and interact in spinal behavioral responses of the rat. Neurosci. Lett. *52*, 199–204.

Willis, W.D., and Westlund, K.N. (1997). Neuroanatomy of the Pain System and of the Pathways That Modulate Pain. J. Clin. Neurophysiol. *14*, 2.

Winzell, M.S., and Ahrén, B. (2004). The High-Fat Diet–Fed Mouse: A Model for Studying Mechanisms and Treatment of Impaired Glucose Tolerance and Type 2 Diabetes. Diabetes *53*, S215–S219.

Wood, J.N., Boorman, J.P., Okuse, K., and Baker, M.D. (2004). Voltage-gated sodium channels and pain pathways. J. Neurobiol. *61*, 55–71.

Woolf, C.J., Allchorne, A., Safieh-Garabedian, B., and Poole, S. (1997). Cytokines, nerve growth factor and inflammatory hyperalgesia: the contribution of tumour necrosis factor alpha. Br. J. Pharmacol. *121*, 417–424.

Wu, L.-J., Duan, B., Mei, Y.-D., Gao, J., Chen, J.-G., Zhuo, M., Xu, L., Wu, M., and Xu, T.-L. (2004). Characterization of Acid-sensing Ion Channels in Dorsal Horn Neurons of Rat Spinal Cord. J. Biol. Chem. *279*, 43716–43724.

Wu, W.-L., Lin, Y.-W., Min, M.-Y., and Chen, C.-C. (2010). Mice lacking Asic3 show reduced anxiety-like behavior on the elevated plus maze and reduced aggression. Genes Brain Behav. *9*, 603–614.

Wultsch, T., Painsipp, E., Shahbazian, A., Mitrovic, M., Edelsbrunner, M., Waldmann, R., Lazdunski, M., and Holzer, P. (2008). Deletion of the acid-sensing ion channel ASIC3 prevents gastritis-induced acid hyperresponsiveness of the stomach – brainstem axis. Pain *134*, 245–253.

Wyatt, S.B., Winters, K.P., and Dubbert, P.M. (2006). Overweight and Obesity: Prevalence, Consequences, and Causes of a Growing Public Health Problem. Am. J. Med. Sci. *331*, 166–174.

Xie, J., Price, M.P., Berger, A.L., and Welsh, M.J. (2002). DRASIC contributes to pH-gated currents in large dorsal root ganglion sensory neurons by forming heteromultimeric channels. J. Neurophysiol. *87*, 2835–2843.

Xu, S., and Xue, Y. (2016). Pediatric obesity: Causes, symptoms, prevention and treatment. Exp. Ther. Med. *11*, 15–20.

Xu, H., Barnes, G.T., Yang, Q., Tan, G., Yang, D., Chou, C.J., Sole, J., Nichols, A., Ross, J.S., Tartaglia, L.A., et al. (2003). Chronic inflammation in fat plays a crucial role in the development of obesity-related insulin resistance. J. Clin. Invest. *112*, 1821–1830.

Yen, Y.-T., Tu, P.-H., Chen, C.-J., Lin, Y.-W., Hsieh, S.-T., and Chen, C.-C. (2009). Role of acid-sensing ion channel 3 in sub-acute-phase inflammation. Mol. Pain *5*, 1.

Yu, S.Q., Lundeberg, T., and Yu, L.C. (2003). Involvement of oxytocin in spinal antinociception in rats with inflammation. Brain Res. *983*, 13–22.

Yu, Y., Chen, Z., Li, W.-G., Cao, H., Feng, E.-G., Yu, F., Liu, H., Jiang, H., and Xu, T.-L. (2010). A Nonproton Ligand Sensor in the Acid-Sensing Ion Channel. Neuron *68*, 61–72.

Yung, Y.C., Stoddard, N.C., Mirendil, H., and Chun, J. (2015). Lysophosphatidic Acid signaling in the nervous system. Neuron *85*, 669–682.

Zamponi, G.W., Lewis, R.J., Todorovic, S.M., Arneric, S.P., and Snutch, T.P. (2009). Role of voltage-gated calcium channels in ascending pain pathways. Brain Res. Rev. *60*, 84–89.

Zeisel, A., Hochgerner, H., Lönnerberg, P., Johnsson, A., Memic, F., van der Zwan, J., Häring, M., Braun, E., Borm, L.E., La Manno, G., et al. (2018). Molecular Architecture of the Mouse Nervous System. Cell *174*, 999-1014.e22.

Zeng, W.-Z., Liu, D.-S., Liu, L., She, L., Wu, L.-J., and Xu, T.-L. (2015). Activation of acid-sensing ion channels by localized proton transient reveals their role in proton signaling. Sci. Rep. *5*, 14125.

Zhao, Y., Hong, N., Liu, X., Wu, B., Tang, S., Yang, J., Hu, C., and Jia, W. (2014). A Novel Mutation in Leptin Gene Is Associated with Severe Obesity in Chinese Individuals.

Zhu, K., Baudhuin, L.M., Hong, G., Williams, F.S., Cristina, K.L., Kabarowski, J.H.S., Witte, O.N., and Xu, Y. (2001). Sphingosylphosphorylcholine and Lysophosphatidylcholine Are Ligands for the G Protein-coupled Receptor GPR4. J. Biol. Chem. *276*, 41325–41335.

Ziegler, D., Rathmann, W., Dickhaus, T., Meisinger, C., and Mielck, A. (2009). Neuropathic Pain in Diabetes, Prediabetes and Normal Glucose Tolerance: The MONICA/KORA Augsburg Surveys S2 and S3. Pain Med. *10*, 393–400.

Ziemann, A.E., Allen, J.E., Dahdaleh, N.S., Drebot, I.I., Coryell, M.W., Wunsch, A.M., Lynch, C.M., Faraci, F.M., Howard, M.A., Welsh, M.J., et al. (2009). The Amygdala Is a Chemosensor that Detects Carbon Dioxide and Acidosis to Elicit Fear Behavior. Cell *139*, 1012–1021.

Zimmermann, M. (1983). Ethical guidelines for investigations of experimental pain in conscious animals. PAIN *16*, 109.

Zimmermann, K., Leffler, A., Babes, A., Cendan, C.M., Carr, R.W., Kobayashi, J., Nau, C., Wood, J.N., and Reeh, P.W. (2007). Sensory neuron sodium channel Nav1.8 is essential for pain at low temperatures. Nature *447*, 855–858.

Zygmunt, P.M., Petersson, J., Andersson, D.A., Chuang, H., Sørgård, M., Di Marzo, V., Julius, D., and Högestätt, E.D. (1999). Vanilloid receptors on sensory nerves mediate the vasodilator action of anandamide. Nature *400*, 452–457.

(2013). PRINCIPLES OF NEUR AL SCIENCE (United States of America: The McGraw-Hill Companies).

WHO | Obesity.

SAFE.

National Diabetes Fact Sheet, 2011. 12.